# An Investigation of Mitochondrial Dynamics and Networks Observed within Human Undifferentiated and Differentiated Cell Lines.

A dissertation submitted in fulfilment of the requirement for the degree of:

MASTER OF SCIENCE

Of

RHODES UNIVERSITY

By:

Pascalené Shannon Houseman

APRIL, 2017

# i. Declaration

I declare that this thesis is my own, unaided work. It is being submitted for the degree of Master of Science of Rhodes University. It has not been submitted before for any degree or examination at any other university.

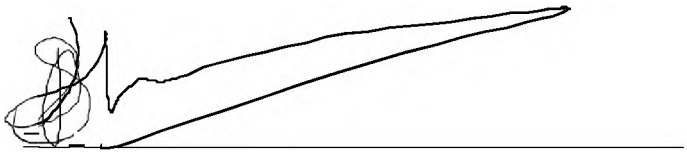

PASCALENE S. HOUSEMAN

## ii. Abstract

Mitochondrial dynamics refers to a series of constant division and fusion cycles that form interconnecting networks within healthy cells. Reactive oxygen species (ROS) are the by-products of cellular redox reactions, and, when in excess, have been linked to degenerative diseases and aging. Mesenchymal stem cells (MSCs) require a niche that presents with low levels of ROS; this enables the stem cell to maintain its "stemness", the stem cell population, as well as the ability to adhere, migrate, and proliferate. If ROS levels increase within the MSC niche, inhibition of cellular adhesion and migration occurs. In contrast, neural stem cells require a niche that presents with a high level of ROS, aiding in their proliferative, self-renewing capacities. Investigations into what constitutes a healthy mitochondrial network versus the disease state of the network are required in order to determine what promotes degeneration and aging within stem cells. It was hypothesized that increased levels of ROS would stunt the ability of MSCs to attach and migrate, and hinder their abilities of proliferation and differentiation. In contrast, neuronal differentiation would present with an increased proliferation. This led to the investigation into the effects of ROS and oxidative stress, and the resulting mitochondrial dynamics, have on undifferentiated and differentiated mesenchymal stem and SH-SY5Y cells. Upon the addition of non-lethal S3I-201 (STAT3 has been linked to a reduction in ROS) to MSCs, an increase in ROS was observed. Higher concentrations of STAT3 inhibitor resulted in a decrease in MSC attachment and proliferation. When exposed to similar conditions, the SH-SY5Y cells underwent an increased proliferation; due to multiple restrictions, they were not used any further within the study. Mitochondrial dynamics were observed using a fusion promoter (M1) and a fission inhibitor (Mdivi-1); the MSCs were dosed with varying concentrations in order to determine the effects that mitochondrial dysfunction may have on the established networks, and cell survival. The mitochondria within MSCs migrated to the extensions of the cell, and displayed an alteration in morphology, or were clustered around the nucleus and/or the lipid deposits. These high density clusters correlated with a high intensity of fluorescence using 2',7'-dichlorofluorescein diacetate. In conclusion, varying concentrations of ROS have different effects on MSCs in terms of overall maintenance and function; mitochondrial dynamics play an important role in cell survivability and the fate of stem cell differentiation. Further investigation into the mitochondrial dynamics and networks of these cell lines and their differentiated progeny is required.

## iii. Acknowledgements

I would like to take this opportunity to thank the Biotechnology Innovation Centre for the help and support given throughout the course of my post-graduate career at Rhodes University. In addition, I would like to thank the National Research Foundation, the department of Science and Technology, for their continuous funding.

I would also like to acknowledge my fellow colleagues of Lab 129c. Thank you for always being there through the tough times and the good times, and always helping out with a little bit of a laugh. It was great to work around such wonderful, generous, and light-hearted people that most certainly became good friends to cherish.

Lastly, a huge thank you should be mentioned to my supervisor, Dr. E. Prinsloo, for his ongoing support, wisdom, and patience, and exceptional guidance throughout this entire process.

# iv. Outputs

## iv-a. Journal Article:

Kramer, A.H., Kadye, R., Houseman, P.S., and Prinsloo, E. (2015). Mitochondrial STAT3 and Reactive Oxygen Species: A Fulcrum of Adipogenesis?, JAK-STAT. 4: 1 – 10

# Table of Contents

# List of Figures

Figure 5-3. Resulting ROS observed for adipogenic differentiating hMSC-ad cells with Mdivi1, mitochondrial fission inhibitor, treatment for a total period of 21 days.

# List of Tables

# List of Abbreviations

| | |
|---|---|
| AD | Alzheimer's Disease |
| ad-MSC | Adipose Derived Mesenchymal Stem/Stromal Cell |
| $AT_1R$ | Angiotensin II type 1 Receptor |
| BM | Bone Marrow |
| BSA | Bovine Serum Albumin |
| CDK | Cyclin-Dependent Kinase |
| CI | Cell Index |
| CMT2A | Charcot-Marie-Tooth type 2A |
| CNS | Central Nervous System |
| DCF-DA | 2'-7'-Dichlolrofluorescin Diacetate |
| DEX | Dexamethasone |
| $ddH_2O$ | Distilled Sterile Water |
| DMEM | Dulbecco's Modified Eagle Medium |
| DMSO | Dimethyl Sulphoxide |
| DOA | Dominant Optic Atrophy |
| DPBS | Dulbecco's Phosphate Buffered Saline |
| ESC | Embryonic Stem Cell |
| ETC | Electron Transport Chain |
| FBS | Foetal Bovine Serum |
| FCS | Foetal Calf Serum |
| FFA | Free Fatty Acid |
| $H_2O_2$ | Hydrogen Peroxide |
| hMSC-ad | Human Adipose-Derived Mesenchymal Stromal Cells |
| HSC | Hematopoietic Stem Cell |
| IBMX | 3-isobutyl-1-methylxanthine |
| ICAM-1 | Intracellular Adhesion Molecule 1 |
| INS | Insulin |
| JAK | Janus Kinase |
| MOMP | Mitochondrial Outer Membrane Permeabilization |
| MSC | Mesenchymal Stem/Stromal Cell |
| MSCM | Mesenchymal Stem Cell Medium |

| | |
|---|---|
| mtDNA | Mitochondrial DNA |
| NAC | N-Acetyl-L-Cysteine |
| NSC | Neural Stem Cell |
| PBS | Phosphate Buffered Saline |
| PBST | Phosphate Buffered Saline with Triton X-100 |
| PD | Parkinson's Disease |
| P/S | Penicillin/Streptomycin |
| PSA | Penicillin/Streptomycin/Amphotericin |
| PTP | Permeability Transition Pore |
| RA | Retinoic Acid |
| RNS | Reactive Nitrogen Species |
| ROS | Reactive Oxygen Species |
| ROSI | Rosiglitazone |
| STAT | Signal Transducers and Activators of Transcription |
| SVZ | Sub-Ventricular Zone |
| T2DM | Type 2 Diabetes Mellitus |
| TAG | Triacylglycerol |
| UCP | Uncoupling Protein |
| VCAM-1 | Vascular Cell Adhesion Molecule 1 |
| VLA-4 | Integrin Alpha-4 |

# List of Symbols

| | |
|---|---|
| α | Alpha |
| β | Beta |
| µ | Micro |
| ≥ | Greater than or equal to |
| % | Percent |
| γ | Gamma |
| ± | Plus, minus |

# Chapter 1:

# 1: Background Literature

Stem cells are becoming an increasingly popular topic of discussion due to their suggested therapeutic applications in regenerative medicine. Embryonic stem cells (ESC) held great promise for cell therapies, as these cells have the potential to differentiate into an array of cell types; however, great ethical controversy arose with the cultivation of human ESC. Research showed that adult mesenchymal stem cells (MSCs) could be used as an alternative to ESC, due to their capabilities of a multi-lineage potential of differentiation (Caplan., 1991; Minguell et al., 2001; Pittenger et al., 2001), thereby, increasing their popularity for use in therapeutic applications as well as research models.

Within the stem cell niche, there are various factors that are responsible for maintaining stem cells within their quiescent state. This includes adhesion molecules, cytokines and growth factors, as well as the local environment (Wilson et al., 2006; Matsumoto et al., 2011). For example, oxygen is one of the major constituents responsible for disrupting the stem cell niche, as its levels are directly correlated to the production of reactive oxygen species (ROS). In order for stem cells to maintain their self-renewal capacity and high proliferation, they require a hypoxic environment where the production of ROS is minimal. Should a higher level of ROS be introduced into the microenvironment, premature differentiation, and, thus, the exhaustion of the self-renewing stem cell population may occur (Jones et al., 2004; Wilson et al., 2006; Terskikh et al., 2007; Matsumoto et al., 2011;).

Reactive oxygen species (ROS) were viewed as toxic, harmful products that produced only damaging effects on various tissues within the human body; however, recently it has been shown that not only do ROS have an 'aging' effect on cells, but they may also be extremely viable as second messengers important for cell-to-cell communication and regulation of all cell function, in particular that experienced within the mitochondria (Forman et al., 2004; Finkel, 2011; Chan, 2001; Khacho et al., 2016). Recently, a link has been made between the production of reactive oxygen species and superoxides within the mitochondria and mitochondrial dysfunction located within the central nervous system, and the concept of degeneration leading to diseases, such as Parkinson's Disease and Alzheimer's Disease (Turrens, 2003; Winklhofer et al., 2010). So, in conclusion, one may deduce that while ROS are harmful in excess, they are also extremely important to maintain a healthy cell function,

in particular, within the stem cell niche. Neural stem cell niches seem to possess slightly elevated levels of ROS in comparison to other niches, such as that belonging to hematopoietic stem cells.

## 1-1. Cellular Models of Differentiation

### 1-1-1. Stem Cells and their Characteristics

The stem cell may be defined as an undifferentiated cell that does not bear mature tissue specific characteristics and presents with the capacity of self-renewal that is long lasting and unlimited (Watt et al., 2000; Reva et al., 2001). Self-renewal is a process that refers to the cycles of division that repeatedly generate one daughter cell that is the equivalent to the mother cell; whereas the second daughter cell produced demonstrates a different cell fate determined by various stimuli present within the cell niche (Watt et al., 2000; Reva et al., 2001; Kolf et al., 2007). This is known as asymmetric division. Stem cells will continue to undergo proliferation in accordance to varying stimuli that enable the cells to create suitable generations of progenitor cells capable of differentiating into various cell types (Watt et al., 2000; Krabbe et al., 2005).

Stem cells may be characterized according to their location, as well as their ability to undergo self-renewal and differentiation along the numerous lineages available to them. The ability of multi-lineage differentiation can be referred to as the cell potency (Krabbe et al., 2005; Gimble et al., 2007). This can further be defined as the different commitment options available to the cell (as shown in Figure 1-1) (Smith, 2006). Pluripotency refers to the stem cell's ability to differentiate into a wide variety of cell lineages, such as the endoderm, mesoderm, or ectoderm (Smith, 2006; Mitalipov, et al., 2009; Panchision, 2011). Multipotency results in the formation of multiple cell lineages; this may be noted in progenitor cells that differentiation to form a limited number of cell fates. Smith (2006) has further described oligopotency as the capability of the cell to form two or more lineages within a specific tissue, such as neural stem cells. Unipotent stem cells are capable of forming only one linages. As a stem cell matures and ages, or is subject to differentiation, it loses a level of potency.

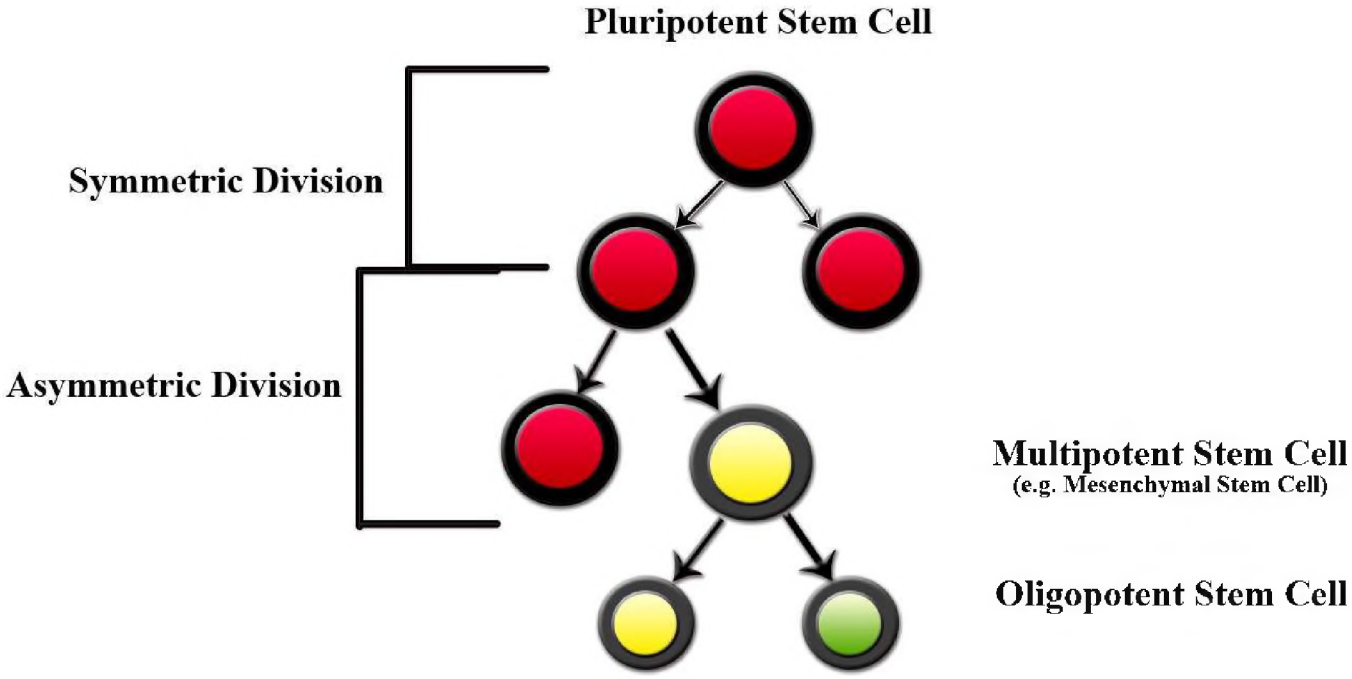


**Figure 1-1. The capabilities of stem cell differentiation and division.** Symmetric stem cell division produces two daughter cells that have an equivalent fate, and display an identical phenotype to that of the mother cell. Asymmetric stem cell division produces two daughter cells, one of which is identical to that of the mother cell, thus displaying the potential for self-renewal (the same phenotype is maintained). Whereas, the other daughter cell gains a different phenotype that allows for differentiation. Upon differentiation, the stem cell will lose a level of its potency.

Cell division occurs when two daughter cells have been produced of which either are capable of retaining the stem cell properties. Symmetric division is said to occur when either both or neither of the daughter cells retains the properties of the parent cell; in other words, both of the daughter cells have to be self-renewing or differentiate (Panchision, 2011). Asymmetric division, as previously mentioned, occurs when only one daughter cell retains the self-renewing properties of the parent cell, while the other undergoes differentiation or cell death

(Panchision, 2011; Katajisto et al., 2015). Furthermore, the process of aging may provide adverse effects on the asymmetrical division of stem cells due to the accumulation of damage over time; this may result in the exhaustion of the stem cell population, which may negatively impact the resulting functions of tissues (Katajisto et al., 2015). However, stem cells have a mechanism to overcome these damaging effects; the damaged subcellular components are separated away from the new daughter stem cell. Katajisto and colleagues (2015) demonstrated this principle with the use of 'stem-like' human mammary epithelial cells. Their study revealed a combination of 'young' and 'old' mitochondria present within the parent cell; however, the newly formed mitochondria were kept separate from the old mitochondria, whereby, the new mitochondria were preferentially apportioned to the P2 daughter cell. The P1 daughter cell contained a mixture of both old and young mitochondria. Furthermore, Katajisto and colleagues (2015) exploited the mitochondrial mechanisms responsible for removing damaged components from the mitochondrial network with the addition of Mdivi-1, a mitochondrial fission inhibitor responsible for the inhibition of dynamin related protein 1 (Drp1) through the prevention of Drp1 self-assembly (Kim et al., 2016).

Dynamin related protein, or Drp1, is an essential GTPase protein required for mitochondrial fission, alongside F-actin (Smirnoya et al., 2001; Lee et al., 2004; De Vos et al., 2005; Kim et al., 2016). De Vos and colleagues (2005) reviewed that generation of elongated mitochondria within the networks are the result of an impairment of mitochondrial fission due to the loss of Drp1. Furthermore, Drp1 also plays an important role in apoptosis, where Drp1 allows mitochondrial fragmentation to occur during cell death; an inhibition of Drp1 disrupts this ability to fragment, thereby decreasing the rate of cell death (Lee et al., 2004). Smirnoya and colleagues (2001), have also reported that mutations in Drp1 result in the breakdown of the mitochondria to form perinuclear clusters, which indicates that Drp1 plays significant part in the maintenance of mitochondrial morphology.

A deficit of stem cell-like properties is exhibited with the inhibition of Drp1-mediated mitochondrial fission (Kim et al., 2016). Therefore, it can be concluded that stem cells require this asymmetrical division of old and new mitochondria in order to maintain their stem-like properties and functions.

### 1-1-2. The Stem Cell Niche

In order for tissue homeostasis to be maintained, the stem cells need to be able to undergo self-renewal as well as generate daughter cells capable of differentiation. Stem cells ensure that a supply of adequately differentiated cells is constantly being maintained. This ensures that the short-lived, yet highly differentiated cells (such as the blood, skin, and sperm), are quickly and easily replenished and organ function is maintained (Jones et al., 2004; Matsumoto et al., 2011). The processes of self-renewal and differentiation are both extremely controlled; this ensures that the stem cell population is not depleted (if there are too many daughter cells differentiating) and that the formation of secondary mutations, such as the formation of tumours, is kept to a minimum (if the stem cells constantly undergo self-renewal, this leads to an abnormal expansion and proliferation of the cell line, as well as partially differentiated cells) (Jones et al., 2004). Stem cells reside in "niches" which can be defined as specific areas located within each organ; the purpose of these niches is to maintain stem cell function (Matsumoto et al., 2011).

Two mechanisms have been identified that are responsible for the daughter cells pursuing different cell fates. Firstly, asymmetric division, as shown in Figure 1-1, leads to the production of two daughter cells that have different cell fates, albeit, the two daughter cells remain in the same microenvironment (Jones et al., 2004). The second mechanism refers to the orientation of the plane of division, whereby two daughter cells may be placed in different microenvironments, or stem cell niches. During this mechanism, the different cell fate choices are specified through intercellular signalling (Jones et al., 2004). It can, therefore, be concluded that a combination of intrinsic factors and extrinsic signals, generated by the niche, are responsible for the regulation of stem cell numbers, self-renewal capabilities, division, and pathways of differentiation (Jones et al., 2004).

The concept of the stem cell niche was brought about by observations of adult stem cells (namely hematopoietic stem cells) losing their potential for continuous self-renewal once removed from their normal cellular environment, in combination with the concept of different cellular fates being adopted by daughter cells through the different signals generated in specific microenvironments (Jones et al., 2004; Yin et al., 2006; Terskikh et al., 2007). This generated the stem cell niche hypothesis, whereby stem cell self-renewal is achieved by signals from the local microenvironment; limited availability of space within the

microenvironment may result in one of the daughter cells being removed from said microenvironment and placed into another, which causes the initiation of differentiation; and availability of space within the niche, or an empty adjacent niche is present, both daughter cells produced will retain original identity (Jones et al., 2004; Terskikh et al., 2007). Jones and colleagues (2004) have stated that the stem cell niche hypothesis, therefore, can predict that the number of stem cells is restricted to the availability of the niches that possess the required signals for self-renewal and survival. Therefore, the niche regulates and limits the number of stem cells produced, using the aforementioned mechanisms. It also controls this definite number by causing the excess stem cells to undergo apoptosis if not in the presence of differentiating signals (Terskikh et al., 2007). Within mammals, the hematopoietic niche has overshadowed the study of the other niches; and as such, has become one of the most recognized models regarding the insight into stem cell niches.

Matsumoto and colleagues (2011) have stated that there are two different types of hematopoietic stem cells (HSCs) present within a niche: the quiescent (or 'dormant') HSCs (which maintain the ability of self-renewal and prevent stem cell depletion) and the cycling HSCs. When these stem cells experience a loss of p21 (which is a G1 checkpoint regulator and cyclin-dependent (CDK) inhibitor), HSCs exit the quiescent stage and the initiation of the cell cycle process is promoted. This leads to self-renewal impairment. (Wilson et al., 2006; Matsomoto et al., 2011) Therefore, it can be said that the main purpose of the HSC niche located within the bone marrow (BM) is to maintain this state of quiescence until differentiation is required. The niche possesses multiple cytokines, growth factors, adhesion molecules (which anchor the hematopoietic stem cells to the endosteum) and other environmental factors that aid in the maintenance of the quiescent state, as shown in Figure 1-2 (Yin et al., 2006; Matsumoto et al., 2011). This coincided with and expanded on Wilson and colleagues (2006) study centred on the characterisation haematopoietic stem cell niche.

There are two different known niches which the HSCs make use of during quiescence and cell cycling; the osteoblastic (quiescent) niche is located on the surface of the endosteum. The quiescent cells are maintained here during homeostasis; albeit, movement into the perivascular niche sometimes occurs, particularly when the cells need to be activated due to extrinsic stimuli, causing them to enter the cell cycle (Yin et al., 2006; Matsumoto et al., 2011). Here, the cycling hematopoietic stem cells undergo division and produce the peripheral

blood with mature cells. When these mature cells are no longer desired, they return to the osteoblastic niche before moving into a quiescent state once again (Matsumoto et al., 2011).

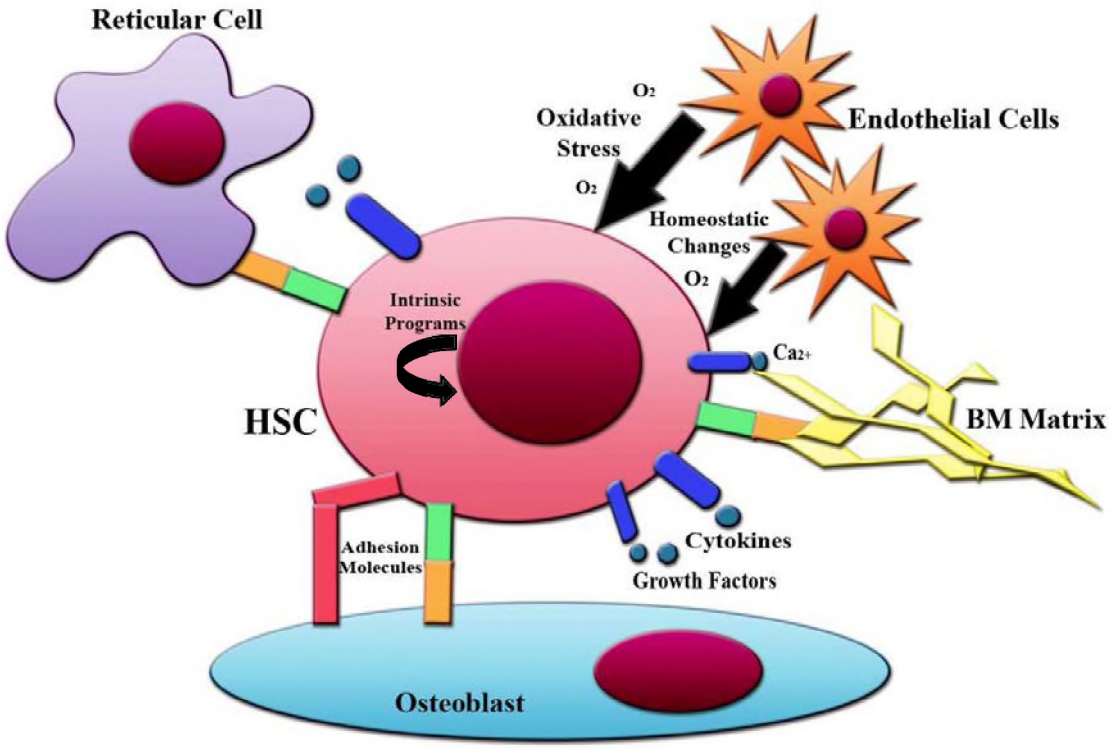


**Figure 1-2. The hematopoietic stem cell (HSC) niche found in bone marrow.** Intrinsic and extrinsic factors maintain and regulate the hematopoietic stem cells. Adhesion molecules attach the HSCs to the bone marrow (BM) matrix and surrounding "supporter" cells, which may aid in stimulating signals for HSC maintenance. Cytokines and growth factors, such as Wnt, MPL, and CXCL12, are secreted from the neighbouring bone marrow cells. Calcium is found in abundance within the BM. This aids in the regulation of the HSCs. Certain transcription factors, such as Hox and Evi-1, may be found in specific intrinsic programs that, in turn, aid in HSC fate regulation. (Image modified from Matsumoto et al., 2011).

Adhesion molecules present within the niche provide the primary function of interacting with the stem cells. A variety of adhesion molecules are present within the stem cell niche, such as N-Cadherin which attach to the N-Cadherin located on the hematopoietic stem cell; intracellular adhesion molecule 1 (ICAM-1) expressed within the niche binds to integrin

alpha-L (LFA-1A) expressed on HSCs; and the vascular cell adhesion molecule 1 (VCAM-1) expressed within the niche attaches to the osteoblast-expressed integrin alpha-4 (VLA-4) (Yin et al., 2006; Matsumoto et al., 2011).

Certain cytokines and growth factors play an important role in the extrinsic signalling pathways (Wnt and Notch pathways), which are extremely vital for the regulation of HSCs within the microenvironment. However, these pathways need to be tightly controlled and regulated as they have the potential to cause harm to the cellular niche. An example of this is found within the Wnt pathway: it is generally responsible for the proliferation of HSCs and the regulation of the stem cell function; however, if the Wnt pathway is not deactivated, the long-term stem cell pool may be in jeopardy of depletion (Matsumoto et al., 2011). Albeit, within mammalian systems, studies have shown that these signalling pathways may work in unison, and should one signal undergo functional impairment, another will compensate for this. Additionally, environmental factors also affect the stem cell niche. Oxygen is one of the main contributing factors to the stem cell environment due to its active involvement with the generation of reactive oxygen species (ROS). Reactive oxygen species are free radicals that have been known to cause DNA damage; examples of ROS are hydrogen peroxide, the hydroxyl radical and the superoxide anion radical (Matsumoto et al., 2011). Stem cells are generally maintained within a hypoxic environment in order to maintain their quiescent state and promote their self-renewal capabilities; here they are protected against oxidative damage caused by ROS. Studies have shown that an increase in ROS levels within the stem cell niche may lead to premature differentiation of the stem cells, such as that observed for the *Drosophilia* HSCs, which differentiates into mature red blood cells once exposed to increased ROS levels (Matsumoto et al., 2011). This would ultimately lead to the exhaustion of stem cells present within the niche. In addition to this, it has been demonstrated that microenvironments containing lower intercellular levels of ROS have an increased self-renewal potential.

### 1-1-3. Mesenchymal Stem Cells

Due to their great potential for therapeutic and clinical applications, mesenchymal stem cells (MSCs) have become of a particular interest within the field of regenerative medicine. The MSC may be defined by three major characteristics, as stated by the Mesenchymal and Tissue Stem Cell Committee of ISCT (The International Society for Cellular Therapy) (Dominici et al., 2006); the MSC must demonstrate an adherence to plastic, express specific surface antigens (namely, CD105, CD73 and CD90), and, perhaps their greatest and most unique characteristic, is their ability to undergo a multi-lineage differentiation (Dominici et al., 2006; Sethe et al., 2006; Banas et al., 2007; Ma et al., 2014). In contrast to both embryonic and induced pluripotent stem cells, mesenchymal stem cells demonstrate certain qualities that make them more desirable to research and use in therapeutic applications; for example, there is not as much of an ethical and moral concern over the acquisition of the MSC, as these cells are isolated from adult tissues, such as the bone marrow and adipose tissue. Mesenchymal stem cells also display minimal teratoma-forming capabilities, which may lead to tumorigenesis and immunogenicity, as noted with the aforementioned cell lines (Pountos et al., 2005; Sethe et al., 2006; Ma et al., 2014).

Originally, these cells were obtained from bone marrow; however, as research has progressed it has been found that MSCs may be isolated from a variety of sources, such as adipose tissue, nervous tissue, amniotic fluid, umbilical cord blood, as well as dental pulps, and expanded *in vitro* (Pountos et al., 2005; Sethe et al., 2006; Ma et al., 2014). These multipotent, fibroblast-like stem cells hold, not only the ability of self-renewal, but, if exposed to certain environmental and physiological stimuli/conditions, may differentiate into a multitude of cell types, including that of osteoblasts, myoblasts, chondrocytes, adipocytes, and early progenitors of neural cells (Pountos et al., 2005; Sethe et al., 2006; Ma et al., 2014). Within the human body, MSCs are known to be reparative cells that do not hold any tissue-specific characteristics. Certain stimuli, such as the damage of tissues due to trauma, fracture, or inflammation, cause mesenchymal stem cells to migrate to the sites of damage where they will be induced to differentiate into the needed cells in order to begin repairing the affected area. A process known as chemotaxis, which can be defined as the movement of cells due to chemical signals, durotaxis (migration in accordance with gradients generated by the

extracellular matrix structural properties), as well as the local microenvironment help to determine the fate of the MSC.

Adipose derived mesenchymal stem cells (ad-MSC) are isolated from adipose tissue (fat) which makes them an ideal source of cells due to the relative ease of procurement of these cells, via liposuction. This has led to these cells being identified as an alternate source of multipotent adult stem cells and bone-marrow derived stem cells. Thus, ad-MSCs have become a primary source for research and therapeutic applications such as the repair of nerves that would otherwise have to be repaired using limited techniques of nerve grafting or neurorrhaphy (the surgical process of joining two nerve ends together), both of which provide unpredictable results and success rates (Tocci et al., 2003; Pountas et al., 2005; Gimble et al., 2007; Mizuno et al., 2009; Ma et al., 2014).

## 1-2. Somatic Cell Models

### 1-2-1. SH-SY5Y Neuroblastoma Cell line

The SH-SY5Y neuroblastoma cell line is the third sub-clone of the original cell line, SK-NSH, which was originally isolated from a bone marrow biopsy from a neuroblastoma patient (Encinas et al., 2000). The SH-SY5Y cell line possesses characteristics that resemble dopaminergic neurons; they express tyrosine hydroxylase and dopamine-beta-hydroxylase, and dopamine transporter, thus, making it a popular model for Parkinson's Disease research (Xie et al., 2010). The neuroblastoma is a tumour that originates from neural crest neuroectodermal cells; however, these isolated cells still have the potential to be differentiated in vitro (López-Carballo et al., 2002).

SH-SY5Y cells may easily be differentiated into a neuronal-like phenotype after exposure to varying growth factors and/or an appropriate concentrations of retinoic acid (RA), which makes this cell line an extremely useful model for the study of the beginning phases of neuronal differentiation and other systems that encourage the use of a neuronal model. A variety of compounds may be used to initiate differentiation of SH-SY5Y cells, such as RA, which provides a cholinergic neuronal phenotype that demonstrates an increased

susceptibility to neurotoxins and neuroprotective agents; and RA in addition to phorbol ester 12-Otetradecanoylphorbol-13-acetate, which, after differentiation, provides a dopaminergic neuronal-like phenotype that presents with a decreased susceptibility to neurotoxins and neuroprotective agents (López-Carballo et al., 2002; Xie et al., 2010).

When these cells undergo differentiation, proliferation is halted and the cells maintain a continuous cell number as differentiation occurs. Encinas, and colleagues (2000), have suggested that approximately half of the neurons generated will undergo either a naturally occurring or induced apoptosis. This programmed cell death generally occurs when individual neurons are unable to utilize the neurotrophic factors, which are released in restricted amounts within varying target tissues or glial cells. (Encinas et al., 2000; Xie et al., 2010).

## 1-3. Reactive Oxygen Species

Reactive oxygen species (ROS) were once viewed as harmful by-products generated through cellular redox reactions; however, recent studies and a greater understanding of these small molecules have helped to create a more positive outlook as ROS were identified to be the physiological signalling molecules that are believed to play an important role in the fate of stem cells (Khacho et al., 2016). These small, easily diffusing, unique species may be defined as an ionic species that presents with one or more unpaired electrons, which is produced via interactions with molecular oxygen (which consists of two unpaired electrons in the outer shell) (Halliwell, 1992; Turrens, 2003; Forman et al., 2004). They are involved in several signal transduction pathways and cell-to-cell communications (Forman et al., 2004).

Second messengers are created during the period in which receptor activation occurs, and are generally considered to be 'short-lived'. Forman and colleagues (2004) stated that second messengers act on certain effectors to transiently change their activity. Generally, the specificity of the action that ROS and RNS demonstrate is difficult to calculate, with the exception of NO, which is known to bind to heme of guanylate cyclase, which causes its activation.

Reactive oxygen species and superoxide radicals are generally produced through ligand-receptor interactions where they function as targeted second messengers in the multiple signalling cascades present within proliferation and differentiation of a cell (Sauer et al.,

2001). Originally it was assumed that both reactive oxygen species as well as reactive nitrogen species were responsible for only damaging results on tissues and cells (Chan, 2001; Forman et al., 2004; Finkel, 2011). Initially, it was discovered that NO is produced endogenously within mammalian systems, and that it is capable of easy diffusion, leading to its participation in signal transduction pathways throughout the mammalian system. Research was further extended from NO to other reactive nitrogen species (RNS), and eventually led to reactive oxygen species (ROS), in particular, hydrogen peroxide ($H_2O_2$).

Reactive oxygen species, in particular, $^{\cdot}OH$, are known to react with any molecule and, therefore, do not demonstrate any specificity; however, when looking at the other ROS ($H_2O_2$ and superoxide - $O_2^{-}$) it is shown that these species are not as reactive as hydroxide. ROS are generally produced intracellularly by various sources, such as the mitochondria (Simon et al., 2000; Sauer et al., 2001; Forman et al., 2004). Hydrogen peroxide is produced endogenously by multiple receptor-mediated mechanisms in various cell types, and is enzymatically metabolized. It is considered to be a highly diffusible molecule that has established credibility as a second messenger, albeit Forman and colleagues (2004) have suggested that its targets have not yet been fully defined. The mode of action that ROS experiences involves a direct interaction with particular receptors and/or the 'redox activation of members of the signalling pathways, such as protein kinases, protein phosphatases, and transcription factors' (Sauer et al., 2001). According to Sauer and colleagues (2001), ROS act in conjunction in signalling pathways involving intracellular calcium, which are responsible for the maintenance of cell proliferation, cell cycle arrest and cell death. From the above information, it has been speculated that there is an intracellular relationship present between oxidizing and reducing agents, which permits ROS the ability to function as second messengers that play an important role in the control of cell proliferation and differentiation (Sauer et al., 2001).

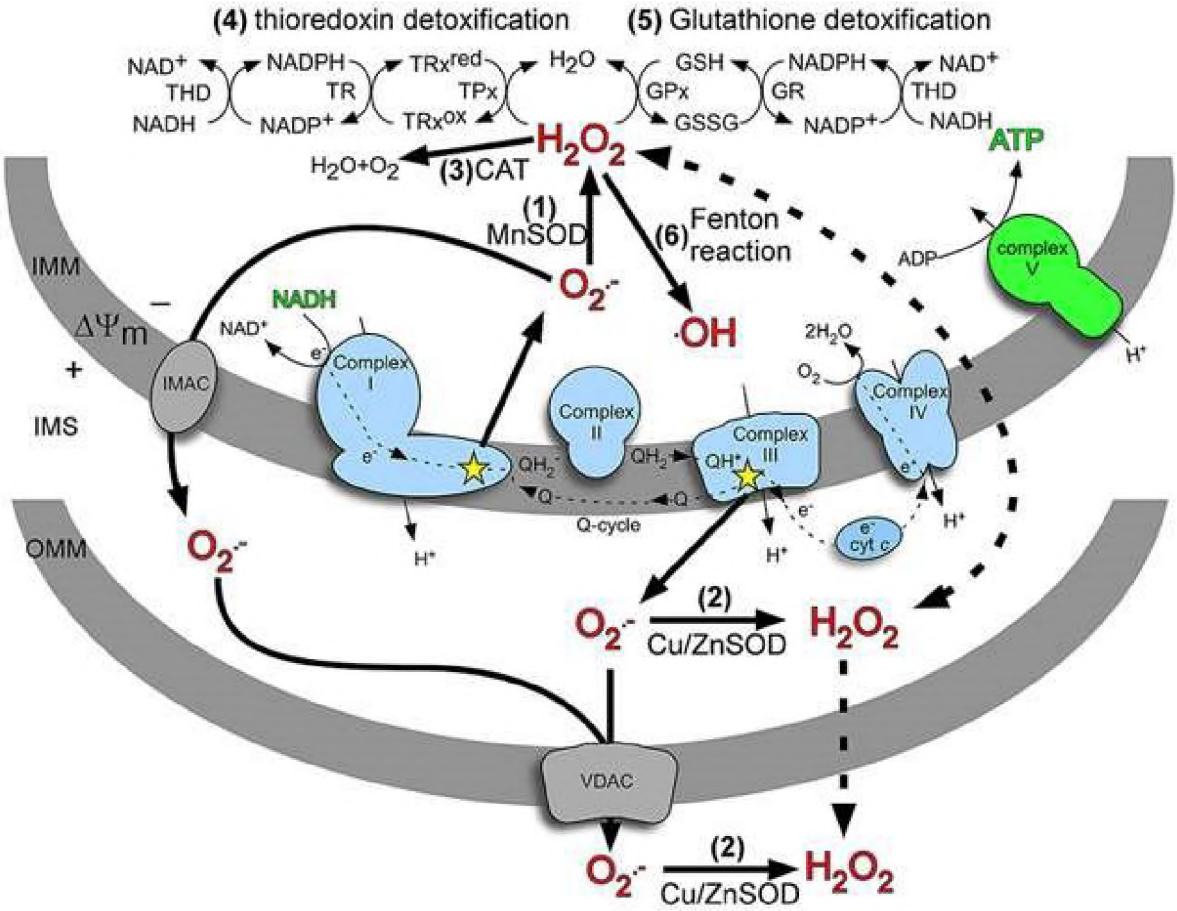


**Figure 1-3. A representation of the mitochondrial production of ROS and its defences.** Superoxide species are created via the respiratory chain and are released into the matrix at complex I and at complex II. These superoxide species are naturally capable of simultaneously producing hydrogen peroxide ($H_2O_2$) or they can be enzymatically oxidized and reduced simultaneously by matrix MnSOD or Cu/ZnSOD in the cytosol or intermembrane space. Hydrogen peroxide is detoxified in the matrix by three possible mechanisms: (1) catalase, (2) the thioredoxin/thioredoxin peroxidase system, (3) the glutathione/glutathione peroxidase system. Hydrogen peroxide may also interact with metal ions to create highly reactive hydroxyl radicals via Fenton reactions. Super-oxides are generally not membrane permeable; however, they are able to pass through ion channels, whereas hydrogen peroxide may pass freely through the membranes. (Image adapted from: Batty and colleagues (2009)).

### 1-3-1. The Effects of ROS on Different Cellular Models.

Investigations into the production of reactive oxygen species (ROS) in the mitochondria and mitochondrial dysfunction in the central nervous system (CNS) have been linked to the process of aging as well as neurodegenerative conditions, such as Parkinson's Disease (PD) and Alzheimer's Disease (AD) (Chan, 2001; Tsatmali et al., 2005). Oxidative stress has been identified as an important factor responsible in redox regulation which involves both reactive oxygen species (ROS) and reactive nitrogen species (RNS) (Emerit et al., 2004). Oxidative stress can further be defined as the different harmful processes that occur when an excessive amount of ROS and/or RNS are produced and the cellular antioxidant defences are unable to adjust to the increased levels (Turrens, 2003).

Reactive oxygen species (ROS) were generally thought to be maintained in low levels, within stem cells, as a protective agent used against cellular toxicity and premature differentiation (Le Belle et al., 2011); however, it has been suggested that ROS may also act as messengers where they activate normal cellular processes (Winklhofer et al., 2010; Hamanaka et al., 2010; Le Belle et al., 2011). Recently, studies have shown that multipotent neural progenitor stem cells, displaying phenotypic characteristics of neural stem cells, present with high ROS levels and are extremely responsive to stimulation by reactive oxygen species, which aids in the proliferative, self-renewing mechanisms involved (Le Belle et al., 2011). Le Belle and colleagues (2011) have further indicated that the PI3K/Akt signalling pathway plays an important role in the ROS-mediated processes involved in self-renewal and neurogenesis. It was suggested that if cellular ROS levels were to decrease, neural stem cell/multipotent progenitor cell function may be negatively altered. This leads to the belief that the central nervous system is particularly sensitive to alterations in ROS levels and oxidative stress. In contrast, stem cells present in the hematopoietic system possess a niche that contains a low endogenous cellular ROS state linked to maintaining the order of hematopoietic stem cells, in comparison to the higher demanding ROS status associated with a greater proliferation that may often lead to 'premature exhaustions of self-renewal' in such cells (Le Belle et al., 2011). This can be associated with the concept of ageing.

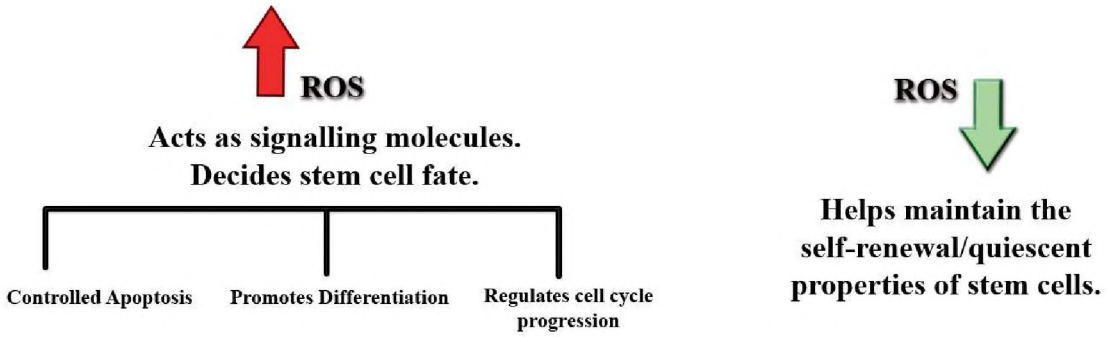


**Figure 1-4. High ROS vs low ROS within the general stem cell system.** Moderate levels of ROS are not always harmful for stem cells. Low ROS levels are required to maintain the self-renewal/quiescent state of stem cells. The hypoxic niche requires minimal oxidative stress. High ROS levels aid in the activation of certain proteins that may change mechanisms that regulate the cell cycle progression, apoptosis, or cellular differentiation. An increase in ROS results in a decrease in self-renewing properties and quiescence (Bigarella et al., 2014). This model is applicable to controlled increases/decreases in ROS, and not excessively damaging levels of ROS.

It is believed that within the general stem cell niche, low levels of ROS may be present, and are found to be of significant value for stem cell 'stemness' and the stem cell population. However, it is suggested that the neurogenic niche of the brain differs somewhat from normal stem cell niches (for example that present for the hematopoietic stem cells). Within the neurogenic niche, ROS levels are slightly elevated, albeit the reason for this is not truly understood nor is the effect that they might have on the stem cell population. However, it has been hypothesized that the increased ROS levels within the neural stem cell niche present within the sub-ventricular zone (SVZ) of the brain plays an important role in the maintenance of proliferation of progenitor cells (Le Belle et al., 2011). In order to regulate proliferation, a strong anti-oxidation process must be activated in order to lower the endogenous ROS levels to prevent further division. When endogenous ROS levels are decreased, SVZ proliferation and neurogenesis is reduced. From this, it can be deduced that neural stem cells must be able to undergo an increase of ROS required for cell division, yet be able to reduce this ROS level when entering a more quiescent state.

When ROS is introduced into a mesenchymal stem cell niche, the effects observed are generally quite dire. Studies performed by Kanada and colleagues (2011), and Song and colleagues (2010) suggest that intracellular ROS and superoxide species have an important role in the regulation of cell adhesions, migration and proliferation; albeit it was discovered that the antioxidant N-acetyl-L-cysteine (NAC) blocked the differentiation pathways of adipocytes in mesenchymal stem cells (MSCs). Song and colleagues (2010) treated MSCs with hydrogen peroxide in which they received results that demonstrated an inhibition of adhesion and migration of the cells. The process of detachment was increased; however, these effects could be rescued by the free radical scavenger NAC delivered at a 1 mM concentration. This indicates that reactive oxygen species and superoxide radicals inhibit the cellular adhesion of engrafted MSCs, providing evidence that improving the survival of engrafted MSCs may lay in the elimination of ROS (Song et al., 2010).

When used within a SH-SY5Y neuroblastoma cell line, reactive oxygen species are known to aid in the regulation of cell death. (Liu et al., 2009).

### 1-3-2. Mitochondrial Production of ROS, Oxidative Stress, and its role on Neurodegeneration

The mitochondria have been found to be the greatest producers of ROS within the cellular system. ROS is an important aspect of redox signalling which occurs from the mitochondrion to entire remaining cell. Murphy (2009) has stated that upon the isolation of mitochondria, increased levels of $H_2O_2$ were observed, which originated from the simultaneous oxidation and reduction (dismutation) of the superoxide that was produced within the mitochondria. Production of ROS within the mitochondria can have extremely detrimental effects on the organelle as it may cause oxidative damage to the mitochondrial proteins, DNA, and membranes, as well as it adversely affects the mitochondrial ability to synthesise ATP and perform the variety of important metabolic processes to ensure the cell's survival. These processes include the tricarboxylic acid cycle, fatty acid oxidation, amino acid metabolism, haem synthesis, and the urea cycle (Murphy, 2009). This oxidative damage may also cause the mitochondria to unnecessarily release intermembrane space proteins, such as cytochrome c, into the cytosol via mitochondrial outer membrane permeabilization (MOMP), thus, causing the cell to undergo apoptosis. The mitochondria permeability transition pore (PTP) may also become activated, which allows the inner membrane of the mitochondria to be

permeated by small molecules during events like ischaemia (Murphy, 2009). However, mitochondrial production of reactive oxygen species does not only cause damaging effects upon the cell; in fact, ROS also acts as the secondary messenger which aids in the modulation of redox signalling.

The mitochondrial production of ROS is a strictly controlled process that plays a significant role in the maintenance of cellular oxidative homeostasis and propagation of cellular signalling pathways (Hamanaka et al., 2010; Vieria et al., 2011). The mitochondria act as the primary source of cellular ROS, which is produced during oxidative metabolism through the one electron reduction of molecular oxygen to form a superoxide anion (Winklhofer et al., 2010; Hamanaka et al., 2010). A significant increase or decrease of mitochondrial ROS may result in oxidative damage to mitochondrial DNA (mtDNA), lipids and proteins, as well as the redox signalling pathways (Winklhofer et al., 2010). A link has, thus, been established between an impairment of mitochondrial function and the resulting cellular damage, which leads to neurodegeneration, particularly Parkinson's phenotypes (Turrens, 2003; Winklhofer et al., 2010). Ischaemia may be caused by an increase of iron availability within the brain, which causes free radical reactions to accelerate as the brain is known to be rich in iron ions. If the rate of free radical reactions is increased, the cerebrospinal fluid may not be able to bind to the released iron ions as a consequence (Halliwell, 1992). However, oxidative stress inflicted on nervous tissue may also be damaged through additional mechanisms that involve the increase of intracellular free calcium ions and the subsequent release of excitatory amino acids (Halliwell, 1992).

It has been suggested that protective stress response pathways may be activated with a slight increase of ROS (Winklhofer et al., 2010). Neural stem cells (NSCs) have recently demonstrated a high response to ROS stimulation. In the central nervous system, stress factors, such as excitotoxic damage and hypoxia reperfusion, have been known to lead to an increase in the production of superoxides and hydrogen peroxide (Tsatmali et al., 2005). Reactive oxygen species are also found at increased levels in the neurons of the hippocampal region during the induction of LTP and in response to glutamate agonists (Tsatmali et al., 2005). Mesenchymal stem cells may undergo neuronal differentiation by elevating ROS levels, which causes the promotion of NADPH oxidase activity (Wang et al., 2009; Hamanaka et al., 2010).

Thus, a high level of ROS aids in the regulation of normal self-renewal and differentiation (Vieria et al., 2011; Le Belle et al., 2011).

## 1-4. The Mitochondria: Energy Powerhouses of the Cell

Mitochondria are known to be the energy powerhouses of the cell. These important organelles are central to the contribution of energy used in metabolism; they are also responsible for other vital functions within a cell, including cell death as well as signalling pathways. In order for cells to maintain their function and tissue homeostasis, both mitochondrial dynamics and mitochondrial morphology must be maintained through the regulated cycles of fission and fusion (Khacho et al., 2016). These two key processes are responsible for the continuous production and regulation of functional mitochondria, which aids cells in coping with environmental and/or metabolic stress factors (Youle et al., 2012). Fission and fusion are dynamic processes that are controlled by guanosine triphosphatases (GTPases) and dynamin family members: Mfn1 and Mfn2 are crucial for mitochondrial outer membrane fusion, while Opa1 operates in the intermembrane space and maintains mitochondrial inner membrane fusion (Twig et al., 2008; Chen et al., 2009; Youle et al., 2012; Westermann, 2012). Whereas, cytosolic dynamin Drp1 is one of the primary proteins associated with fission, and is key to the formation of 'spirals around the mitochondria', that, as a result, separate the inner and outer membranes of the mitochondria (Youle et al., 2012).

The dynamic process of fusion is a vital component in the generation and maintenance of mitochondrial networks. Fusion has become largely established as the mechanism through which the complementation of mitochondria occurs; this mechanism allows for healthy mitochondria to share solutes, metabolites, electrochemical gradients, lipids, and proteins with mitochondria that have undergone damage and/or mutation due to environmental or other stress factors (Twig et al., 2008; Youle et al., 2012; Westermann, 2012). This process of complementation allows the mitochondria to maintain and recover activity which promotes efficient energy production (Twig et al., 2008). Alongside complementation, fusion also involves the recruitment of dysfunctional mitochondria into a pool, whereby depolarized

mitochondria are targeted for destruction through a mechanism known as autophagy, or more specifically: mitophagy. Mitophagy may be defined as the selective process of elimination of mitochondria through an autophagic mechanism (Twig et al., 2008; Youle et al., 2012).
Fission, on the other hand, is closely linked to mitochondrial fusion whereby it has been speculated that fission is triggered by fusion, and is essential for autophagy to occur (Twig et al., 2008). However, it is widely acknowledged that fission plays a key role in the growth and division of cells, as it is primarily responsible for populating the cell with a sufficient number of mitochondria to ensure effective metabolism occurs (Youle et al., 2012).

All aerobic organisms require oxygen in order to produce sufficient energy and additional nutrients for their systems. Eukaryotic cells produce energy in the form of ATP via unique organelles called the mitochondria. These energy powerhouses possess two membranes: the outer membrane and the inner membrane, where the respiratory chain occurs (Kim et al., 2008).

During ATP production, two predominant pathways are utilized: NADH or $FADH_2$ oxidation and ADP phosphorylation to produce ATP (otherwise known as oxidative phosphorylation). These two major steps occur within the mitochondria, where oxidative phosphorylation is considered to be an extremely efficient and 'energy-saving' method of generating energy (Kim et al., 2008).
Generation of NADH (or $FADH_2$) occurs during glucose metabolism using the glycolysis and tricarboxylic acid cycle or the β-oxidation of fatty acids. Oxidation of NADH or $FADH_2$ produces $NAD^+$ or $FAD^+$, respectively, during which protons are pushed into the inter-mitochondrial membrane through the complexes I, III, and IV. The transferal of electrons from NADH/$FADH_2$ to the respiratory chain complexes then occurs, with the resulting formation of oxygen ($O_2$), which is then used to generate water ($H_2O$) (Kim et al., 2008). The proton gradient formed across the mitochondrial membrane drives the reaction of ATP synthase to produce ATP from ADP; the ATP is then transported to the cytosol in exchange for ADP via the adenine nucleotide translocator (Kim et al., 2008).

Throughout the process of energy production, heat may be generated via the mitochondria in a mechanism known as the 'proton leak'. Heat is produced when the proton leak undergoes uncoupling from the intermembrane space to the matrix; this, in turn, causes a reduction in

the 'proton-motive force'. However, uncoupling proteins (UCP) are known to have a vital role in the reduction of the proton gradient. UCP1 is produced only within brown adipose tissue and is responsible for the regulation of adaptive thermogenesis. UCP2 is known to be expressed throughout the tissues, whereas UCP3 is generated within the skeletal muscle. Both UCP2 and UCP3 are not able to regulate thermogenesis; however, studies have shown that the overexpression of these two proteins results in a decrease of ROS production and the stimulation of the metabolic rate (Kim et al., 2008). UCP2 and UCP3 have also been linked to the regulation of weight gain and insulin resistance; this was demonstrated using UCP3 knockout in mice, which resulted in the increase of oxidative damage observed. Therefore, it can be concluded that the uncoupling proteins are extremely vital for the maintenance of mitochondrial function as they aid in the regulation of heat and ROS production (Kim et al., 2008).

### 1-4-1. Mitochondrial Dynamics: What Makes It Dynamic?

Within healthy cells, the mitochondria are known to undergo constant division and fusion to form a dynamic interconnecting three-dimensional network. This indicates that mitochondria are dynamic organelles due to their ability to undergo constant, repeated cycles of fusion and fission, be actively transported to sub-cellular locations, such as axons and dendrites of neurons, and their ability to maintain the quality of the mitochondrial population through mitophagy (Detmer et al., 2007; Suen et al., 2008; Tanaka et al., 2008; Chen et al., 2009; Liesa et al., 2009). The dynamic processes aid in the regulation of mitochondrial function, which, in turn, maintains the integrity of various cells.

Mitochondrial fission is an important process that must be maintained to ensure appropriate cell function. This process is regulated using a dynamin-like protein, Drp1. This protein is recruited into the mitochondria during fission. Additionally, a tail-anchored protein (Mff) is also involved in the process of mitochondrial fission (Chen et al., 2009). It can be said that mitochondrial fission helps facilitate equal separation of the mitochondria along the cytoskeletal tracks, and also aids in the isolation of damaged segments of mitochondria, thus

promoting autophagy. If these protective mechanisms are inhibited in some way, mitochondrial fission may also promote cell apoptosis (Chen et al., 2009).

Mitochondrial motility is especially vital for cells of a high polarity that require mitochondria at various sites that are distant from the main cell body, such as seen in neurons. (Suen et al., 2008; Chen et al., 2009). Mitochondrial motility may be inhibited/decreased for a variety of reasons, including disruptions in both fusion and fission mechanisms. Mitochondria susceptible to deficient fusion mechanisms may present with a loss of directed movement and may adopt a"hovering" motion similar to that observed in the Brownian motion (Chen et al., 2009). Chen and colleagues (2009) have reviewed that neurons lacking functioning mitochondria capable of fusion demonstrate an increased mitochondrial diameter caused by the swelling or expansion of the mitochondrial body. This alteration in size prevents mitochondria from passing through into the axons and dendrites of neural cells, which eventually leads to poorly developed neurons and/or gradual neurodegeneration (Chen et al., 2009). In mammalian cells, mitochondrial transport is based on microtubules whereby kinesin-1 motor protein interacts with the mitochondria via the outer membrane proteins, Miro1 and Miro2, in order to achieve an anterograde like movement (Chen et al., 2009). This motion is restricted by elevated concentrations of calcium, causing the mitochondria to be held at locations where ATP production is required. Should this Miro-dependent transport system be perturbed in any manner within neurons, axons and dendrites may become deprived of mitochondria, which, thus, leads to defects in neurotransmission. Mitochondrial shape may be affected with the manipulation of the Miro proteins; this may cause an interference in the dynein function, which is required for retrograde transport of the mitochondria, which, as a result, seizes Drp1 in the cytoplasm causing elongated mitochondria to form (Chen et al, 2009).

### 1-4-2. Mitochondrial Dysfunction and the Resulting Effects

If mitochondrial dynamics are disrupted, cellular dysfunction will occur; this is seen when mitochondrial fusion is hampered with the result being the loss of inner mitochondrial membrane electro-chemical potential (Tanaka et al., 2008). While all cells are reliant on mitochondrial function, neurons are particularly dependent on mitochondrial dynamic

properties. Multiple neurodegenerative diseases, such as Parkinson's disease and Alzheimer's disease (linked to disruption of mitochondrial dynamics), and Charcot-Marie-Tooth type 2A (CMT2A) and dominant optic atrophy (DOA) (resulting from a deficiency in mitochondrial fusion), have been linked to various forms of irregularities associated with the mitochondria (Chen et al., 2009; Khacho et al., 2016).

Charcot-Marie-Tooth type 2A pertains to a peripheral neuropathy, which affects both sensory and motor neurons located in the distal extremities. This disease is believed to be caused by a mutation in the Mfn2 outer membrane protein. Dominant optic atrophy is a degenerative disease that causes optic nerve atrophy through the deterioration of the retinal ganglia cells (Chen et al., 2009). It is generally associated with a mutation in OPA1, a protein responsible for the inner membrane fusion within the mitochondrion. Chen and colleagues (2009) have further reviewed that the mutations in either OPA1 or Mfn2 affect a vast array of tissues that go beyond the optic and peripheral nerves, which leads to symptoms that may 'overlap' between the two diseases, thus affecting specific tissues in a related manner, and that the participation of the central nervous system and myopathies are reminiscent of mitochondrial DNA mutation syndromes.

As mentioned, mitochondrial morphology is essential in tissue development and homeostasis; however, their exact function within stem cells still remains unclear. Within stem cells, for example neural stem cells, if mitochondrial dynamics are adversely affected, this may have a negative impact on the mitochondrial structure, which, in turn, affects the cell fate decisions (Khacho et al., 2016). After neural stem cells experienced a loss of MFN1/2, severe mitochondrial fragmentation was observed within the majority of cell populations present within the developing cortex. This mitochondrial fragmentation led to the increase of the number of dividing cells that displayed a horizontal cleavage plane in relation to the ventricular surface, which thus affected the cleavage angle of $Sox^{2+}$ cells. In addition to this, the loss of MFN 1 and 2 within the stem cells hampered the cells' ability to form neurospheres when in culture. Further experiments performed by Khacho and colleagues (2016) indicated that when DRP1 levels decreased within neural stem cells, excessive mitochondrial elongation occurred, as well as a general increase in the number of neurospheres formed when in culture. In order to alter the mitochondrial inner membrane fusion protein, OPA1, RNAi was used. A decrease in the primary and secondary neurospheres formed was observed.

From the information provided, it is believed that neuronal function will be heavily impacted should a disruption in mitochondrial fusion, fission, motility, and turnover occur, thus leading to the degradation of overall function. However, not only are the inhibition of the aforementioned processes responsible for degeneration, a fault in the mitophagy process may also impair neuronal function (Chen et al., 2009). Mitophagy is much like the process of autophagy whereby the various components of a cell are broken down via autophagosomes, which possess the necessary hydrolytic enzymes needed to degrade cellular material. This mechanism generally targets defective mitochondria, thereby if mitophagy is disrupted in any manner, a build-up of oxidized proteins may occur accompanied with the decrease of cellular respiration and insulin secretion, as defective mitochondria are not 'dealt with' accordingly (Chen et al., 2009).

Mitochondria play an important role regarding the maintenance of healthy neurons. However, in the cases where dysfunction occurs, neurodegenerative diseases are generally always the result. Alzheimer's disease (AD) has been classed as the most common neurodegenerative disorder present within humans. Typically, it is characterized by a loss of memory and cognitive dysfunction attributed to neuronal death within the cerebral cortex of the brain. Patients that present with AD generally demonstrate intracellular neurofibrillary tangles and extracellular amyloid plaques generated from beta-amyloid, as reviewed by Chen and colleagues (2009).

Parkinson's disease (PD) is, perhaps, the second most common neurodegenerative disorder to affect humans; it is characterized by the progressive loss of dopaminergic neurons located within the substantia nigra of the brain, and presents with symptoms that include: a resting tremor, bradykinesia, rigidity, and an unsteady pace. It has been suggested that mitochondrial dysfunction may play an important role in the cause of this disorder. Chen and colleagues (2009) have reviewed that PD like symptoms may occur with the inhibition of complex I in the electron transport chain (ETC); however, it may also be attributed to an inheritance of PD genes for Pink1 and Parkin proteins, which are both significant in regulating mitochondrial integrity. Pink1 is a serine/threonine kinase that presents with an N-terminal mitochondrial targeting sequence that is localized to the mitochondria and the cytosol. The protein Parkin is a cytosolic E3 ubiquitin ligase that presents with two RING fingers: a cysteine containing

protein motif and a histidine containing protein motif responsible for organizing zinc ions (Chen et al., 2009). If a decrease in Pink1 within dopaminergic neurons occurs, the mitochondrial morphology is affected in such a manner that it promotes abnormally swollen mitochondria.

Obesity is becoming an increasingly common disease throughout the world, and has been linked to a variety of different pathologies, such as type 2 diabetes and various components of cardiometabolic syndrome (such as hypertension and dyslipidaemia). These have been linked to insulin resistance, which may be defined as a decrease in the insulin metabolic actions that regulate glucose homeostasis by encouraging the uptake of glucose in skeletal muscle and suppressing glucose generation within the liver (Morino et al., 2006; Kim et al., 2008).

The mitochondria are responsible for glucose and lipid metabolism, which, in turn, produces the required energy for cellular function; therefore, the production of unwanted superoxide anions (ROS) occurs when the nutrient oxidation does not suffice and an imbalance in the ratio of ATP generation to the amount of oxygen used occurs.

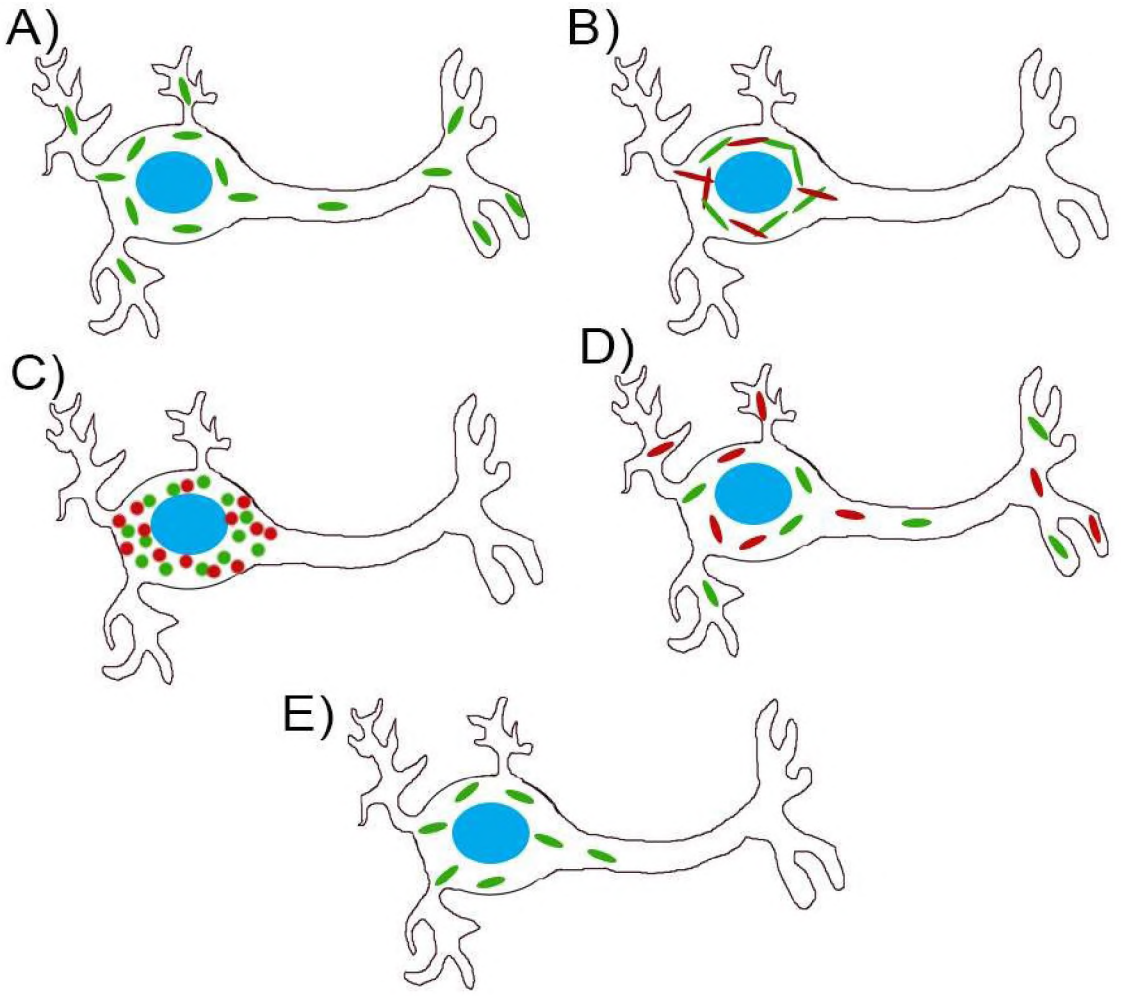


**Figure 1-5. Mitochondrial dynamics need to be maintained to prevent mitochondrial dysfunction in all cell types**. (A) A wild-type neuron that possesses mitochondria in various sites of the axons, dendrites, and cell body. The mitochondria aid in ATP production and calcium homeostasis. (B) If fission is hindered, the mitochondrial demonstrate an elongated morphology and often overlap/interconnect with one another. It is demonstrated that a lack of mitochondria is available within the distal sites of the axons and dendrites. (C) When the mechanism of fusion is prevented, ultra-structural dysfunction and defects may be observed as the mitochondria fragment. Distribution to the distal sites of the cell are inhibited. (D) Abnormal, defective mitochondria can build up within the cell if regulation via mitophagy is not maintained. (E) Mitochondrial motility defects prevent appropriate distribution of the mitochondria to distal sites of the neuron. The healthy mitochondria are represented by the green shapes. The morphed/unhealthy mitochondria are represented in red. (Chen et al., 2009).

Angiotensin II is a protein expressed in tissues, and may be stimulated using the angiotensin II type 1 receptor ($AT_1R$); overexpression of this protein has demonstrated abnormalities within mitochondrial function and morphology within the liver, cardiovascular tissue and skeletal muscle (Morino et al., 2006; Kim et al., 2008). Kim and colleagues (2008) have further demonstrated that when $AT_1R$ is inhibited, a reduction in oxidative stress occurs.

Mitochondrial dysfunction has been associated with the development of type 2 diabetes mellitus (T2DM) and insulin resistance due to aging. An array of factors, such as genetic components, oxidative stress, aging, and mitochondrial biogenesis, influence the overall health and function of the mitochondria; should this undergo disruption, disease will be the result (Morino et al., 2006; Kim et al., 2008)

From this, it may be concluded that mitochondrial dynamics and morphology, maintained through the regulated fission and fusion cycles, play an important role in terms of the general characteristics that form the "stem cells", such as their ability to self-renew and their ability to differentiate through the regulation of complex-I-mediated reactive oxygen species levels, which determines the cell commitment (Khacho et al., 2016). Mitochondrial dynamics have a variety of functions that extend past the associated ATP generation, and are responsible for, in conjunction with mediated ROS levels, developmental and physiological processes.

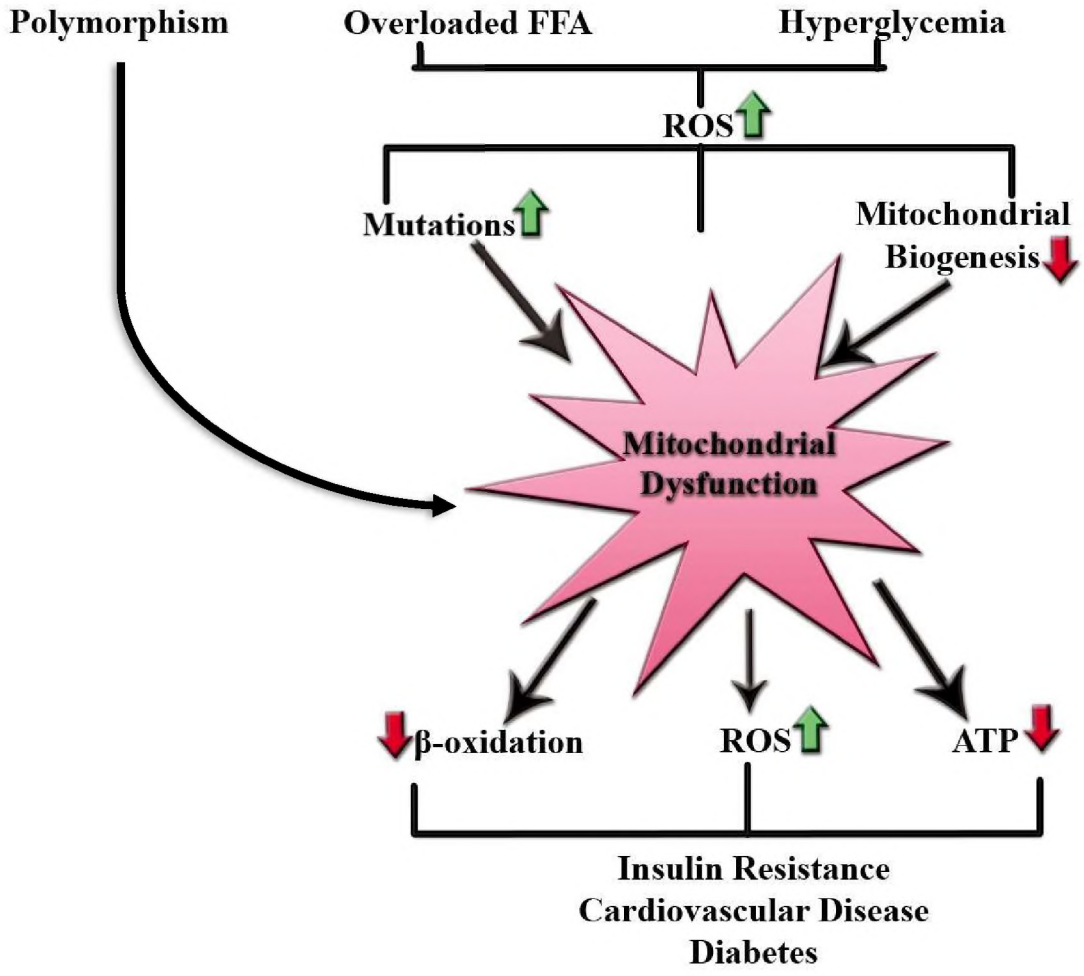


**Figure 1-6. Mitochondrial dysfunction mechanisms relating to insulin resistance**. Excess nutrients are taken up, including excess free fatty acids (Overloaded FFA) and a hyperglycemic environment, which causes the production of ROS, thus, decreasing the potential of mitochondrial biogenesis. Mitochondrial dysfunction occurs. A decrease in β-oxidation and the production of ATP is observed, alongside the increase of ROS produced. These factors may result in pathological diseases, including insulin resistance, cardiovascular diseases, and diabetes. (Image adapted from Kim et al., 2008).

## 1-5. Signal Transducers and Activators of Transcription Proteins: How ROS may affect them.

Signal transducers and activators of transcription (STAT) proteins are transcription factors that may be activated via the phosphorylation of a tyrosine residue, and may also operate as signalling molecules (Bromberg et al., 1999; Boengler et al., 2010). STAT3 has been identified in mitochondria and has been linked to the reduction of ROS, which could be problematic to neural stem cells, for example, that depend on higher levels of ROS (Boengler et al., 2010). An example of the role of STAT3 in the CNS may be found in astrocytes, which are responsible for the regulation of blood flow, play a role in synaptic function and plasticity, as well as provide energy metabolites to the neurons and are the first to respond to CNS trauma, infection, neurodegenerative disease and ischemia (Sarafian et al., 2010). STAT3 has been identified as an important regulator of the activity of astrocytes, and when depleted, causes an increase in the production of superoxides and reactive oxygen species and the decrease of mitochondrial function (Sarafian et al., 2010).

### 1-5-1. The function of STAT3 in Adipose Tissue

Adipose tissue provides an important source of energy required for tissue homeostasis within mammalian organisms. However, if produced in excess (when the uptake of energy surpasses the consumption), an increase of adipose tissue mass may occur, resulting in obesity. This health concern is typical characterized by the increase of adipocyte size caused by the storage of excess energy, or triacylglycerol (TAG), as well as the increase in the number of adipocytes produced via the differentiation of pre-adipocyte progenitor cells to mature adipocytes (Cernkovich et al., 2008; Wang et al., 2010).

Adipogenesis can be defined as the process involving the formation of “fat cells”. This mechanism is activated via a series of extrinsic factors that result in the activation of multiple transcription factors, of which STAT3 is included (Cernkovich et al., 2008). Studies have indicated that freshly isolated human pre-adipocytes contain STAT1, STAT3, STAT5, and STAT6; however, they lack STAT2 and STAT4. STAT1 and STAT5 have both been linked to adipogenesis, whereas STAT3 played a notable role in tumorigenesis, angiogenesis,

epithelial-to-mesenchymal stem cell transition, and apoptosis (Wang et al., 2010). Upon induction of the adipogenic differentiation media, a decrease in the levels of STAT1 and an increase in the levels of STAT3 and STAT5 were observed. There was no significant alteration of the levels of STAT6 produced (Harp et al., 2001). The activation of STAT3 is initiated by the phosphorylation of Tyr705, stimulated by the Janus Kinases (JAKs) and additional receptor and non-receptor tyrosine kinases (Wang et al., 2010; Kramer et al., 2015). The resulting phosphorylated STAT3 protein is then subjected to homodimerization, followed by the movement to the nucleus, where it is able to attach to DNA, permitting the regulation of the transcription factors for various specific genes.

Abundant expression and activation of STAT3 is observed within adipocytes and pre-adipocytes (Cernkovich et al., 2008; Wang et al., 2010; Kramer et al., 2015). Cernkovich and colleagues (2008), and Kramer and colleagues (2015) have suggested that the inhibition of STAT3 expression may result in a significant decrease in the proliferation of pre-adipocytes, as well as the levels of STAT3 are constantly altered during adipogenesis. STAT3 has also been associated with the maintenance of the adipocyte size via its role in the activation of the ligands: leptin (IL-6) and ciliary neurotrophic factor (CNTF). For example, leptin stimulates white adipose tissue lipolysis which is responsible for halting lipogenesis and promoting the oxidation of fatty acids.

From the above, it can be concluded that STAT3 plays a role in the regulation of adipogenesis, and should this protein be inhibited, an increase in adipogenesis may occur, resulting in a greater body weight (Cernkovich et al., 2008; Kramer et al., 2015).

## 1-6. The Problem Statement

Neurodegenerative diseases, such as Parkinson's disease and Alzheimer's disease, and other chronic diseases, such as obesity caused by insulin resistance, have been linked to mitochondrial dysfunction and impairments, as well as the production of reactive oxygen species (ROS). Healthy mitochondria are essential to maintain cellular function in both stem and differentiated cells. Investigations into the mitochondrial networks of human adipose-

derived mesenchymal stem cells, and their differentiated progeny of adipocytes, and a neuronal-like cellular model (SH-SY5Y cells and their differentiated progeny) will need to be conducted to identify the molecular mechanisms that regulate the formation of mitochondrial fission and fusion; and the effects that certain mitochondrial impairing small molecules and ROS may have on these different networks.

## 1-7. Research Question

What resulting effect will the induction of differentiation have on both mitochondrial dynamics and the mitochondrial networks observed in undifferentiated and differentiated human cellular models? What role does mitochondrial dynamics play during these processes?

## 1-8. The Hypothesis

Mitochondrial networks vary within differentiated and undifferentiated cell populations, where cellular function is dependent on the health of the mitochondria. Reactive oxygen species levels increase when the cells are driven into differentiation, and are maintained in low levels when mesenchymal stem cells are in their quiescent or self-renewal state. SH-SY5Y cells display an increased proliferation rate when exposed to slightly increased, yet undamaging, levels of ROS. Fragmentation of the mitochondria may be observed if fusion is inhibited, and elongation of mitochondria is the result of the inhibition of fission.

## 1-9. Aims and Objectives

### 1-9-1. Aims

1. To investigate and compare the resulting ROS and oxidative stress generated before and after differentiation.
2. To investigate the role mitochondrial dynamics and dysfunction has on the mitochondrial networks of undifferentiated and differentiated cells.
3. To investigate the two-dimensional mitochondrial networks present within undifferentiated and differentiated cells.

### 1-9-2. Objectives

1. Culture both the SH-SY5Y human neuroblastoma and human adipose-derived mesenchymal stromal cell lines.
2. To successfully induce differentiation into both cell lines (adipogenesis for the mesenchymal stem cells, and neuronal differentiation for SH-SY5Y cells).
3. To monitor the exposure of both differentiated and undifferentiated cell lines to multiple compounds and small molecules that may affect mitochondrial ROS and mitochondrial dynamics/morphology.
4. Observe the effects that certain small molecules (S3I-201, cobalt chloride, M1, and Mdivi-1) may have on the mitochondrial networks and the cell survival during differentiation.
5. Attempt to create a 2D portrayal of the mitochondrial networks using the Zeiss LSM780 Confocal microscope and the Zeiss AxioVert.A1 FL-LED inverted microscope.

# Chapter 2:

# 2: Materials and Methods

## 2-1. Materials

The various reagents required for the completion of the aforementioned experiments, are listed below. All reagents used were a standard high grade and purity, unless otherwise stated.

### 2-1-1. Materials used for Cell Culture:

| Product | Lot #, Cat # | Company |
|---|---|---|
| Mesenchymal Stem Cell Medium (MSCM) | 18848, 7501 | ScienCell |
| Foetal Bovine Serum (FBS) | 19233, 0025 | ScienCell |
| Foetal Bovine Serum (FBS) | S1300 / S1820 | Biowest |
| Penicillin/Streptomycin (100X) | 19273, 0503 | ScienCell |
| MSCGS | 19094, 7552 | ScienCell |
| Dulbecco's Modified Eagle Medium Ham's F-12 (1:1 MIX) with 15 mM Hepes and L-Glutamine | 5MB038, BE12-719F | Lonza |
| Dulbecco's Modified Eagle Medium with 4.5 g/l Glucose and L-Glutamine (DMEM) | 6MB071, BE12-604F | Lonza |
| Minimum Essential Eagle Medium (Alpha modification with sodium bicarbonate, without L-Glutamine, ribonucleosides and deoxyribonucleosides) (α-MEM) | RNBF5088, M4526 | Sigma Aldrich |
| Poly-L-Lysine (PLL) (10 mg/ml) | 1858, 0413 | Sigma Aldrich |

| | | |
|---|---|---|
| Trypsin/EDTA (0.25 mg/ml) | 0000500810, CC-5012 | Lonza |
| Dulbecco's Phosphate Buffered Saline (PBS) | RNBF3923, D8662 | Sigma Aldrich |

### 2-1-2. Materials Used during Differentiation:

| **Product** | **Lot #, CAS #** | **Company** |
|---|---|---|
| Insulin (10 mg/ml) | 91077C, 11061-68-0 | Sigma Aldrich |
| Dexamethasone ≥ 97 % | D4902-100 mg, 50-4 | Sigma Aldrich |
| 3-Isobutyl-1-methylxanthine ≥ 99 % (HPLC) | I5879, 2882-58-4 | Sigma Aldrich |
| Retinoic Acid ≥ 98 % (HPLC) | R2625, 302-79-4 | Sigma Aldrich |

### 2-1-3. Inhibitors and Small Molecule Chemical Compounds Utilized:

| Product | Lot #, Cat # | Company |
|---|---|---|
| S3I-201, SML0330 (5 mg) | 045M4731V | Sigma Aldrich |
| Cobalt Chloride ($CoCL_2.6H_2O$) (MW: 237.93) | | Saarchem; Merck Laboratory Supplies (PTY) Ltd |
| Mdivi-1 ≥ 98 % (HPLC) | M0199-25MG, 338967-87-6 | Sigma Aldrich |
| Mitochondrial Fusion Promoter M1 ≥ 95 % (HPLC) | SML0629-25MG, 219315-22-7 | Sigma Aldrich |

### 2-1-4. Antibodies and Fluorescent Dyes:

| Product | Cat #, Lot # | Company |
|---|---|---|
| ATP5B (c-20) goat polyclonal IgG (200 µg/ml) | sc-16690, D2214 | Santa Cruz Biotechnology |
| STAT3 (H-190) rabbit polyclonal IgG (200 µg/ml) | sc-7179, B1014 | Santa Cruz Biotechnology |
| Alexa Fluor 488 chicken anti-rabbit IgG (H + L) | 1304742 | Life Technologies |
| 2'-7'-Dichlorofluorescin diacetate (DCF-DA) | 064M4008V | Sigma Aldrich |
| Neurite Outgrowth Staining Kit | 1596811, A15001 | Molecular Probes, Life Technologies |
| CytoPainter Mitochondrial Staining Kit – Orange Fluorescence | ab112144, GR213686 | Abcam |
| JC-1 | T4069, 3520-43-2 | Sigma Aldrich |
| Oil Red O (MW 408.49 g/mol) | O0625-25G, 031M0143V | Sigma Aldrich |

| | | |
|---|---|---|
| Nile Red | N3013, 7385-67-3 | Sigma Aldrich |
| Prohibitin (H-80) rabbit polyclonal IgG | sc-28259, H1911 | Santa Cruz Biotechnology |

## 2-2. Mesenchymal Stem Cell Culture

### 2-2-1. Preparation of HMSC-ad culture

The human adipose-derived mesenchymal stromal cells (hMSC-ad) were received firstly at passage 2 and then passage 3, both as a kind donation from the University of Pretoria (Prof. Michael Pepper). To ensure hMSC-ad cells adhered to the plastic culture vessel, the vessel was pre-coated using 1 mg/ml poly-l-lysine [Sigma Aldrich, Cat. # M4526; stock solution, 10 mg/ml] in sterile milliQ water and for a minimum of 3 hours to incubate within a 5 % $CO_2$ humidified atmosphere at 37 °C. Once the minimal time had passed, the culture vessel was rinsed at least twice using dd$H_2O$ before the required medium was added to the culture vessel.

### 2-2-2. Initiation/Maintenance of HMSC-ad culture

Mesenchymal Stem Cell Media (MSCM) was required for the successful maintenance of the HMSC-ad cells. This medium was comprised of the basal medium (Mesenchymal stem cell medium) supplemented with 5 % (v/v) Foetal Bovine Serum (FBS) and 1 % (v/v) penicillin/streptomycin (P/S). Initially, the HMSC-ad stock was placed in a humidified incubator of 37 °C with a 5 % $CO_2$ atmosphere for a minimum of 24 hours to allow the cells to settle and adhere to the T-25 culture flask, whereby the recommended volume of medium used was approximately 5 ml. Following the 24 hours, the MSCM was changed to remove residual dimethyl sulphoxide (DMSO) and floating cell debris/dead cells. A media change occurred every 4 days until 70 % confluence was determined using light microscopy, after which the media was changed every 2 days until sub-culture was necessary at approximately 90 % confluence.

### 2-2-3. Sub-culturing of HMSC-ad

The HMSC-ad cells were sub-cultured once they reached approximately 90 % confluence. Prior to the initiation of sub-culture, all components required were warmed to 37 °C. The media was aspirated and the cells were washed using sterile $Ca^{2+}$ and $Mg^{2+}$ free Phosphate Buffered Saline (PBS) solution. Following the wash, an average volume of 4 ml PBS was added to the culture vessel followed by no more than 500 µl of 0.25 mg/ml trypsin/EDTA solution (500 µl of trypsin in 3 ml PBS for a T75 flask). The resulting combination was incubated at 37 °C in a 5 % $CO_2$ humidified atmosphere for approximately 2 – 5 minutes, or until all cells observed beneath a light microscope were rounded. The trypsin/PBS solution was transferred to a sterile 15 ml centrifuge tube containing approximately 5 ml MSCM to deactivate the trypsin. The remaining culture vessel was then incubated for a further 2 minutes before MSCM was added and then transferred into the allocated sterile centrifuge tube containing the previous trypsin/PBS solution. The centrifuge tube was then centrifuged at 1 000 rpm for approximately 5 – 6 minutes. The supernatant was carefully discarded, and the remaining pellet was re-suspended in complete media. This was, in turn, added to the relevant culture vessel (in most cases a T-75 flask with an average volume of 10 ml of MSCM), which had been prepared prior to sub culture with poly-l-lysine coating.

A cell count using 0.4 % trypan blue was performed in order to determine that a minimum of 5000 cells/ml was added to the appropriate culture vessel.

### 2-2-4. Cryopreservation of HMSC-ad

HMSC-ad cells underwent the process of sub-culturing; however, the resulting pellet formed underwent resuspension in 900 µl of complete MSCM to which 10 % (v/v) DMSO was added to make up 1 ml of cell suspension/DMSO within the cryo-vial. The cryo-vial was kept on ice for approximately 15 – 30 minutes before the cryo-vial was stored at -80 °C.

### 2-2-5. Differentiation of HMSC-ad to adipocytes

The media used for differentiation contained basal medium (Dulbecco's Modified Eagle Medium - DMEM) supplemented with 10 µg/ml insulin (INS), 2 µM rosiglitazone (ROSI), 0.5 mM 3-Isobutyl 1-methylxanthine (IBMX), and 0.25 µM dexamethasone (DEX). IBMX and dexamethasone were dissolved using ethanol, whereas the rosiglitazone was dissolved using DMSO.

HMSC-ad cells were grown to the desired confluence (90 – 100%) after which they were prepared for differentiation. Due to the nature of mesenchymal stem cell media (MSCM) regarding its ability to maintain the multipotent stem cell state, the MSCM was washed from the cells using Dulbecco's Phosphate Buffered Saline (PBS) solution (pH 7.4). Following the initial wash stage, the supplemented basal medium, as described above, was added to the cells.

A further two days after the induction of differentiation, the differentiation media (DMEM with INS/ROSI/DEX/IBMX) was aspirated and the cells were washed using sterile PBS. A maintenance medium (DMEM supplemented with 10 µg/ml insulin) was utilized throughout the remainder of the differentiation and maintenance stages of the maturing adipocytes.

## 2-3. SH-SY5Y Cell Culture

### 2-3-1. Preparation/Maintenance of SH-SY5Y culture

Recent stocks of SH-SY5Y (p3) cells acquired were a kind donation from Prof. Sonya Bardien-Kruger and Dr. William Haylett of the Department of Biomedical Sciences, Faculty of Medicine and Health Sciences at Stellenbosch University.

Dulbecco's Modified Eagle Medium (DMEM) Nutrient Mixture: F-12 Ham (ratio 1:1) with L-glutamine, supplemented with 1 % (v/v) penicillin/streptomycin/amphotericin (PSA) and 10 % (v/v) Foetal Calf Serum (FCS) was required for the effective maintenance of the SH-SY5Y cells. The culture medium was warmed to 37 °C prior to its use. Initially, the SH-SY5Y stock was placed into a T-25 culture flask (with approximately 5 ml of the DMEM F-12 Ham medium) within a humidified 37 °C, 5 % $CO_2$ atmosphere for a minimum of 24 hours to allow for the cells to settle and adhere to the culture vessel. Following this initial 24 hours, the DMEM F-12 Ham was replaced in order to remove the residual DMSO and the floating cell debris/dead cells present within the media. A medium change occurred every 4 to 7 days until sub-culture was necessary at approximately 80 % confluence, which was observed using a light microscope.

### 2-3-2. Sub-Culturing of SH-SY5Y cells

The SH-SY5Y cells were sub-cultured once an approximate confluence of 70 – 90 % had been reached. Prior to the commencement of sub-culturing, all components required were warmed to room temperature. The media was aspirated and the cells were washed using sterile $Ca^{2+}$ and $Mg^{2+}$ free Dulbecco's Phosphate Buffered Saline (DPBS) solution. Following the wash, an approximate volume of 2 ml DPBS was added to the culture vessel followed by no more than 500 µl of 0.25 mg/ml trypsin/EDTA solution (1 ml of trypsin in 4 ml PBS for a T75 flask). The resulting combination was incubated at 37 °C in a 5 % $CO_2$ humidified atmosphere for approximately 2 – 5 minutes, or until all cells observed beneath a light microscope were rounded. The trypsin/PBS solution was transferred to sterile centrifuge tube containing approximately 5 ml DMEM F-12 Ham to deactivate the trypsin. The remaining culture vessel was then incubated for a further 2 minutes before approximately 2 ml DMEM F-12 Ham was added and then transferred into the allocated centrifuge tube containing the previous trypsin/PBS solution. The centrifuge tube was then centrifuged at 2 000 rpm for approximately 5 – 6 minutes. The supernatant was carefully discarded, and the remaining pellet was re-suspended in complete media. This was, in turn, added to the relevant culture vessel.

A cell count using 0.4 % trypan blue was performed in order to determine that a minimum of 5000 cells/ml was added to the appropriate culture vessel.

### 2-3-3. Cryopreservation of SH-SY5Y cells

SH-SY5Y cells underwent the process of sub-culturing; however, the resulting pellet formed underwent resuspension in 900 µl of complete DMEM F-12 Ham to which 10 % (v/v) DMSO was added to make up 1 ml of cell suspension/DMSO within the cryo-vial. The cryo-vial was kept on ice for approximately 15 – 30 minutes before being stored at -80 °C.

### 2-3-4. Differentiation of SH-SY5Y cells to Neural-like cells

The media required for differentiation contained the general SH-SY5Y maintenance media (DMEM F-12 Ham) supplemented with 10 µM retinoic acid (RA).

SH-SY5Y cells were grown to the desired confluence (approximately 80 – 90 %) after which they were prepared for differentiation. Retinoic acid was diluted from 100 µM stock to 10 µM

working medium. The medium was aspirated and replaced with the differentiation medium (DMEM F-12 Ham supplemented with 10 % (v/v) FCS, 1 % (v/v) PSA, and 10 µM RA). Differentiation occurred over approximately 7 days. Every 3 – 4 days, the medium was replaced with fresh differentiation medium of 10 ml for a T-75 culture flask (3 ml was used for a 6-well plate), as described previously.

## 2-4. Mycoplasma Testing

Routine Mycoplasma checks were performed using Hoechst 33342 (1:1000 dilution in sterile water). The cells were seeded onto a sterile glass coverslip, or into a 24-well plate, and grown overnight at 37 °C, 5 % $CO_2$ atmosphere. The media was removed and the cells were washed once with sterile PBS. Ice cold methanol was used to fix the cells for approximately 5 minutes. The cells were washed once with Hoechst 33342 and then a second time with sterile PBS. The cover slip/culture vessel was left to dry before being mounted and viewed beneath the microscope.

In the presence of Mycoplasma, blue spots will appear around/within the cytoplasm in addition to the blue stained nuclei. In the absence of Mycoplasma only the blue-stained nuclei will be present.

## 2-5. Induction of STAT3 Inhibition

The STAT3 inhibitor (S3I-201) was initially dissolved in DMSO to make a stock solution of 6.85 M. The stock solution was aliquoted and stored at -80 °C for long term storage, whereas the remaining aliquots were kept at -20 °C for immediate use and short term storage. From the stock solution, an additional 'working stock' solution was generated; here the 6.85 M stock was diluted down to 100 mM for immediate use and extreme short term storage (approximately 7 days).

Varying concentrations, namely 6.25 µM, 12.5 µM, 25 µM, 50 µM, and 100 µM were made via a series of dilutions of the working stock solution using the cell culture medium to dilute. The medium was then added to the relevant cells in the desired concentrations at the desired

overall volumes (approximately 100 µl for a 96-well plate, 500 µl for a 24-well plate, 3 ml for a 6-well plate). General maintenance, regarding the change of medium, was performed; a medium change with the STAT3 inhibitor occurred every 4 – 7 days for the SH-SY5Y cells, and every 4 days for hMSC-ad cells until visualisation using either the Zeiss LSM780 Confocal microscope or the Zeiss AxioVert.A1 FL-LED inverted microscope could occur.

A negative control was established whereby the cells were not exposed to S3I-201 and, instead, remained cultured under normal conditions mentioned previously.

## 2-6. Induction of Mitochondrial Fission Inhibition using Mdivi-1

Mdivi-1, a mitochondrial fission inhibitor, was firstly dissolved in DMSO to provide a stock solution of 36.62 mM. The stock solution was aliquoted and stored at -80 °C for long term storage, whereas the remaining aliquots were kept at -20 °C for immediate use and short term storage.

From the stock solutions stored at -20 °C, varying concentrations, namely 10 µM, 25 µM, 50 µM, and 100 µM were made via a series of dilutions using the cell culture medium. The medium was then added to the relevant cells in the desired concentrations at the desired overall volumes (approximately 100 µl for a 96-well plate, 500 µl for a 24-well plate, 3 ml for a 6-well plate). General maintenance, regarding the change of medium, was performed; a medium change with Mdivi-1 occurred every 4 – 7 days for the SH-SY5Y cells, and every 4 days for hMSC-ad cells until visualisation using either the Zeiss LSM780 Confocal microscope or the Zeiss AxioVert.A1 FL-LED inverted microscope could occur.

A negative control was established whereby the cells were not exposed to Mdivi-1 and, instead, remained cultured under normal conditions mentioned previously.

## 2-7. Induction of Mitochondrial Fusion Promotion using M1

The mitochondrial fusion promoter, M1, was initially dissolved in DMSO to provide a stock solution of 27.47 mM. The stock solution was aliquoted and stored at -80 °C for long term

storage, whereas the remaining aliquots were kept at -20 °C for immediate use and short term storage.

From the stock solutions stored at -20 °C, varying concentrations, namely 10 µM, 25 µM, 50 µM, and 100 µM were made via a series of dilutions using the cell culture medium. The medium was then added to the relevant cells in the desired concentrations at the desired overall volumes (approximately 100 µl for a 96-well plate, 500 µl for a 24-well plate, 3 ml for a 6-well plate). General maintenance, regarding the change of medium, was performed; a medium change with the M1 mitochondrial fusion promoter occurred every 4 – 7 days for the SH-SY5Y cells, and every 4 days for hMSC-ad cells until visualisation using either the Zeiss LSM780 Confocal microscope or the Zeiss AxioVert.A1 FL-LED inverted microscope could occur.

A negative control was established whereby the cells were not exposed to the mitochondrial fusion promoter, M1, and, instead, remained cultured under normal conditions mentioned previously.

## 2-8. Induction of Hypoxic Conditions

Hypoxic conditions were induced within the cells by using cobalt chloride ($CoCl_2.6H_2O$).

A 1 M stock solution was initially prepared by dissolving the $CoCl_2.6H_2O$ in sterile water, from which a 100 µM working solution could be prepared. The 100 µM was prepared by the addition of the 1 M stock solution to the designated cell culture media required. The cells were incubated with the $CoCl_2.6H_2O$ containing media at 37 °C in a 5 % $CO_2$ atmosphere for approximately 24 hours.

A negative control was established whereby the cells were not exposed to the cobalt chloride and, instead, remained cultured under normal conditions mentioned previously.

## 2-9. Live-Staining Fluorescence Microscopy

### 2-9-1. Staining for Reactive Oxygen Species

The 102.6 mM stock solution was prepared by dissolving the 2',7'-Dichlorofluorescin diacetate (DCF-DA) powder in DMSO. The solution was aliquoted and stored at -80 °C for long term storage and -20 °C for short term storage. From the 102.6 mM stock solution prepared, a 100 µM working solution was required for staining; therefore, the stock solution was diluted in sterile PBS to make up 100 µM.

The following protocol was used for adherent cells.

The medium was first aspirated and the cells were washed using sterile PBS, after which the 100 µM working solution of DCF-DA was added. The cells were left to incubate at 37 °C for approximately 45 minutes – 2 hours. Bearing in mind that DCF-DA is light sensitive, the samples were kept protected from the light. After incubation, the cells were washed using sterile PBS. Hoechst 33342 (1:1000 diluted in PBS) was used in a flash-wash (approximately 30 seconds to 1 minute), after which the cells were washed once using sterile PBS. Hydrogen peroxide was added to one sample; $H_2O_2$ is a known producer of ROS, therefore this was essential as a positive control. The negative control included cells that remained unstained with DCF-DA. The results were visualised using either the Zeiss LSM780 Confocal microscope or the Zeiss AxioVert.A1 FL-LED inverted microscope. Replicates of 2 and 3 were performed for each small molecule concentration.

### 2-9-2. Staining of the Mitochondrial Networks and Integrity

In order to observe the mitochondrial networks located within the cells, as well as the overall integrity and health of the mitochondria, two different stains were used: CytoPainter (MitoOrange) and JC-1 and visualised using either the Zeiss LSM780 Confocal microscope or the Zeiss AxioVert.A1 FL-LED inverted microscope.

**CytoPainter Mitochondrial Stain**

The MitoOrange indicator (500X DMSO solution) provided by the staining kit was aliquoted and stored at – 20 °C. For the working solution preparation, the MitoOrange indicator stock was warmed to room temperature before 2.5 % (v/v) of the stock was diluted in 1.25 ml of the provided live staining buffer. This protocol was adapted using the protocol sheet provided by Abcam.

The cells were grown to the desired confluence (approximately 60 – 70 % for both cell lines). The cells were washed using sterile cold PBS before equal volumes of the working solution were added. The cells were incubated for approximately 30 minutes to 2 hours at 37 °C in a 5 % $CO_2$ atmosphere. After incubation, the sample was washed using sterile PBS, following a flash rinse, of approximately 30 – 60 seconds, using Hoechst 33342 (1:1000 dilution in PBS). The cells were rinsed once more with PBS before being replaced with warmed PBS or growth medium. The results were visualised using the aforementioned microscopes.

The established negative control consisted of a sample that was unstained for the MitoOrange indicator.

**JC-1 Mitochondrial Assay**

The JC-1 stock solution was prepared at 1 mg/ml in dimethylsulphoxide (DMSO) and stored at – 20 °C for long term storage until required for use. The working solution was prepared by diluting the 1 mg/ml stock solution in sterile PBS to acquire a 2 µg/ml dye concentration.

The cells were grown to their desired confluence (approximately 60 – 70 % for both cell lines) and treated as required. The cells were washed using sterile PBS after which the cells were treated with the diluted working solution of 2 µg/ml JC-1 stain. The samples were left to incubate for approximately 30 minutes to 1 hour at 37 °C in a 5 % $CO_2$ humidified atmosphere. After incubation, the cells were rinsed with sterile PBS. A flash rinse, or approximately 30 – 60 seconds, with Hoechst 33342 (1:1000 dilution in sterile PBS) was performed, after which an additional, final rinse with sterile PBS was performed. The PBS was aspirated and replaced with warmed PBS or growth medium, after which the cells were then visualised using the Zeiss AxioVert.A1 FL-LED inverted microscope or the Zeiss LSM780 Confocal microscope using emission/excitation wavelengths of 520/596 nm.

The established negative control consisted of a sample that was unstained for JC-1 indicator. Replicates of 2, 3, and 4 were performed for each small molecule concentration.

## 2-10. Immunofluorescence Microscopy

The cells were grown to the desired confluence. The media was aspirated and the cells were washed once with cold sterile PBS. Following this, the cells were fixed for 15 minutes using 4 % (v/v) paraformaldehyde at room temperature. After fixation, the cells were washed twice with cold PBS.

The cells were incubated for 10 minutes with 0.25 % (v/v) Triton X-100 (PBST), after which the cells were washed three times using sterile PBS. Cells were blocked using 1 % (w/v) Bovine Serum Albumin (BSA)/PBS for 45 minutes at room temperature with gentle rocking. The primary antibodies (1:500 dilutions in 1% (w/v) BSA/PBS) were added to the cells and left to incubate overnight at 4 °C, or if used in a 1:250 1 % (w/v) BSA/PBS dilution, the sample was left to incubate for approximately 1 hour at room temperature.

After incubation, the cells were washed three times in warmed PBS for 15 minutes each, followed by the incubation of the fluorescent tagged secondary antibodies (dilutions 1:1000 in 1 % (w/v) BSA/PBS) and incubated in the dark for approximately 1 hour at room temperature. The cells were washed 3 times in warmed PBS for approximately 15 minutes each wash.
Hoechst 33342 (1:1000 dilutions in sterile water) was used to flash-treat the cells in order to fluoresce the nuclei. A final wash with PBS was performed.

Mowiol mounting media was used to mount the cover slip onto the chamber slide. The chamber slide was allowed to dry before nail polish was used to seal the edges. The samples were observed using the Zeiss AxioVert.A1 FL-LED inverted microscope and the Zeiss LSM780 Confocal microscope.

## 2-11. Validation Staining

### 2-11-1. Oil Red O Staining

The 9 mM Oil Red O stock solution was prepared by dissolving the powder in 100 % isopropanol. The solution was left to stir overnight at room temperature, after which the solution was filtered using a 0.22 µm filter and stored at room temperature.

The 5.4 mM Oil Red O working solution was firstly prepared by diluting the 9 mM stock solution in sterile $ddH_2O$. The solution was left at room temperature for approximately 30 minutes, after which the solution was filtered using a 0.22 µm filter.

The cells were first washed using sterile PBS. The 4 % (v/v) paraformaldehyde was added to the cells and left to incubate at room temperature for approximately 10 minutes. The paraformaldehyde was discarded, after which fresh paraformaldehyde was added. This was incubated for approximately 1 hour at room temperature. The paraformaldehyde was then aspirated and the cells were washed twice using sterile $ddH_2O$. Following this, the cells were washed with 60 % isopropanol for approximately 5 minutes at room temperature. The cells were allowed to dry completely at room temperature.

The Oil Red O working solution was added and the cells were left to incubate at room temperature for approximately 20 - 30 minutes. The working solution was aspirated and $ddH_2O$ was added immediately after. The cells were washed 4 times using sterile $ddH_2O$. The resulting stain was visualised using bright-field microscopy on the Zeiss AxioVert.A1 FL-LED inverted microscope. Replicates of 2 and 3 were performed for the varying concentrations of S3I-201 and cobalt chloride.

### 2-11-2. Nile Red Staining

A 1 mM stock solution of Nile Red was prepared in anhydrous DMSO. The stock solution was aliquoted and stored at -20 °C.

From the stock solution previously prepared, a 200 nM working solution of 1 X Nile Red was prepared directly prior to use. The stock solution was diluted in sterile PBS (pH 7.4) and was mixed well.

Firstly, the media was aspirated from the cells before they were washed using cold sterile PBS. The 200 nM working solution of Nile Red was then added to the cells and left to incubate at 37 °C for approximately 30 minutes. Due to the light sensitivity of Nile Red, the solution was protected from light at all times. After incubation, the Nile Red solution was removed and the cells were washed with PBS. An additional wash with Hoechst 33342 (1:1000 dilution in PBS) was performed, after which the cells were washed once again with PBS. Additional PBS was added to the cells before visualisation could occur using the Zeiss AxioVert.A1 FL-LED inverted microscope. Green fluorescence (Em. = 488 nm) indicated neutral lipids, whereas a red fluorescence (Em. = 546 nm) indicated polar lipids.
Replicates of 2 and 3 were performed for each small molecule concentration.

### 2-11-3. The Neurite Outgrowth Kit

The Neurite Outgrowth Kit was used to stain the cell membranes of the cells (in this case, SHSY5Y and their differentiated progeny) which allowed for the measurement of neurite outgrowths to confirm if differentiation had occurred. The Neurite Outgrowth Kit also aided in the determination of the health of the cells. Three fluorescent dyes were present within the kit; these included the cell viability indicator (green fluorescence; excitation/emission: 495/515 nm), the cell membrane stain (orange fluorescence; excitation/emission: 555/565 nm), as well as a background suppression reagent.

The 1 X working solution was prepared as per the manual found in the Neurite Outgrowth Kit. The reagents were warmed to room temperature. The cell viability indicator (1000X) and the cell membrane stain (1000X) were diluted in Dulbecco's Phosphate Buffered Saline (DPBS) solution, containing $Ca^{2+}$ and $Mg^{2+}$ to provide 10X dilutions.

The media was aspirated and the cells were rinsed using sterile DPBS. Appropriate volumes of the 1 X working solution were added to the cells and left to incubate at 37 °C for approximately 10 – 20 minutes.

The 1 X working solution of the background suppression dye was prepared during incubation. This included a 100 X dilution in DPBS. After incubation, the stain was removed and rinsed using sterile DPBS. A flash wash, of approximately 30 – 60 seconds, was performed in which Hoechst 33342 was added to the cells, after which an additional rinse with PBS occurred. The 1 X background suppression dye working solution was added to the cells before visualisation occurred using the Zeiss Axiovert A1 FL-LED inverted microscope.

## 2-12. General Protocol Used for the xCELLigence System

The xCELLigence Real-Time Cell Analysis (RTCA) Single Plate (SP) reader was set up according to the ACEA, Bioscience, Inc. instructions.

Before the cells were seeded, approximately 100 µl of complete media was added to the 96well E-plate View 96 and was left to equilibrate at room temperature for approximately 30 minutes. The plate was then moved to the xCELLigence RTCA SP machine, which is stored within the 37 °C, 5 % $CO_2$ incubator. A background reading was established.
The HMSC-ad and SH-SY5Y cells were seeded at 5000 cells/well (for HMSC-ad) and 10 000 cells/well (for SH-SY5Y cells) using 0.4 % trypan blue during a cell count. The plate was placed within the cradle of the machine. The steps were setup to include the initial step, which calibrated the machine for approximately 30 seconds prior to the start. After this, the first step included a 24-hour period in which the cells were permitted to settle and adhere using normal maintenance media. Following the 24 hours, an additional step was generated over the course of 48 – 72 hours whereby the growth of the cells was monitored using electrical impedance measurements in the presence of the aforementioned small molecular compounds.

When used for differentiation, the standard differentiation procedure for both the HMSC-ad and SH-SY5Y cell lines were used as previously described. While the first step remained the same as that used for non-differentiating cell lines, the second step was generated over approximately 24 – 48 hours in which the cells were permitted to reach a confluency of 100 % and above. After this 24 - 48-hour period, the third step marked the initiation of differentiation in the presence of the small molecules. This occurred, for adipocytes and

neuronal-like differentiation, over a period of 72 – 96 hours. Adipocytes required a total minimal time of 12 days before being viewed, therefore, during this period multiple steps were set up to replenish the maintenance media containing the small molecules every 72 – 96 hours. The neuronal-like differentiation followed a similar time frame with the exception that the total minimal period for differentiation was 7 days. During these phases, the growth of the cells was monitored using the electrical impedance measurements.
Once the experiment had drawn to a close, the cells underwent live staining procedures as demonstrated in section 2-8: Live-Staining Fluorescence Microscopy.

Controls were maintained throughout these experiments; this included the addition of non-differentiating and differentiating cells that remained untreated with the small molecules. Non-differentiating cells were compared against differentiating cells. For non-differentiating cells, replicates of 3 per concentration were maintained; differentiating cells utilized replicates of either 3 or 12 per concentration of small molecule.

## 2-13. General Use of Mytoe Software and Statistical Analysis

### 2-13-1. Mytoe: Mitochondrial Analysis Software

From the acquired fluorescent images, Mytoe can segment the nucleus and cell membrane; it achieves segmentation of the mitochondria using two processes. The first step utilizes the concept of Koopman and colleagues' (2005) principle; albeit Lihavainen and colleagues (2012) opted for the method of morphological 'top-hat' (TH) instead of the linear filtering, whereby each image displaying mitochondria undergoes an initial 'denoising' process using a median filter. This is then followed by the enhancement of the separation of the mitochondria from the image background (otherwise known as the 'top-hat'). The resulting image obtained then undergoes median filtering, which eliminates the enhanced noise from the TH, after which the denoised image undergoes contrast stretching and binarized, resulting in the production of a mask (Lihavainen et al., 2012). Once this has been achieved, the second process of image analysis may begin, whereby the individual branches of the mitochondrial network are extracted. This is accomplished via the application of a two-iteration thinning procedure to the mask, after which a basic 'mitochondrial skeleton' is generated which allows for the location of the branch points.

### 2-13-2. Statistical representations

Due to the relatively small number of experimental replications performed in this study (with N = 2 being the minimum and N = 3 being the maximum of times the experiment was replicated in this study) it seemed unnecessary to calculate *P* values and a standard error of the mean (s.e.m). Vaux, 2012, has warned against the use of unnecessary statistical analysis for experimental scientists that do not possess large data sets, and has deemed it acceptable to incorporate the number of replications performed in the experimental system, generally N = 3, without having to involve 'sophisticated statistics'.

Standard errors and error bars were displayed for the outcome of information gathered from the Mytoe software, allowing for mean approximations to be established in addition to the calculation of the standard error; this was made possible due to the large number of mitochondria that were present within each of the cells that were screened through Mytoe.

# Chapter 3:

Specific Objectives:

1. The successful induction of differentiation in human adipose-derived mesenchymal stem cells and the SH-SY5Y neuroblastoma cell line.
2. The confirmation of differentiation using fluorescence and light microscopy techniques, such as Oil Red O and Nile Red staining for the adipogenesis of hMSC-ad cells and a neurite outgrowth kit for neuronal-like differentiation in SH-SY5Y cells.
3. The investigation of the effect that S3I-201 has on undifferentiated/differentiated cell lines.
4. The investigation of the effect that M1, a mitochondrial fusion promoter, has on undifferentiated/differentiated cell lines.
5. The investigation of the effect that Mdivi-1 has on undifferentiated/differentiated cell lines.

# 3: The validation of differentiation across multiple cell lineages in the presence/absence of small molecules.

## 3-1. Introduction

Obesity is becoming an increasingly prevalent health risk throughout the globe; with its rise comes an increase in the risk of cardiovascular diseases and type 2 diabetes (Wu et al., 1999; Bost et al., 2005; Sha et al., 2009). This prevalent disease is defined by its increased accumulation of adipose tissue.

Adipogenesis is induced by the activation and expression of various genes that promote differentiation, as well as induce insulin sensitivity (Wu et al., 1999). The peroxisome proliferator activated receptor (PPARγ) is activated during the early stages of adipogenesis, and exists in increased levels within pre-adipocyte and fibroblastic cells (Spiegelman et al., 1996). CCAAT/ enhancer-binding proteins (C/EBPs) have also been deemed as important regulators of adipogenesis; within the early stages of differentiation induction of C/EBPβ and C/EBPδ occurs, and has been linked to the activation of the expression of PPARγ (Wu et al., 1999). Once PPARγ has been activated, C/EBPα is induced; these two transcription factors provide a synergistic relationship and aid in the promotion of differentiation (Spiegelman et al., 1996; Wu et al., 1999).

Leptin and the leptin-receptor are considered to be an important hormone-receptor couple due to the role they play with regards to the development of obesity; when leptin is produced in deficit, obesity is the likely result (Spiegelman et al., 1996). Adipocytes secrete leptin as a signalling molecule that provides a function regulating food intake, and is believed to play a role in insulin resistance associated with obesity (Spiegelman et al., 1996; Wu et al., 1999).

Differentiation, in vitro, may be completed by exposing pre-adipocytes or mesenchymal stromal cells (MSCs) to certain conditions that may promote adipogenesis. Murine pre-adipocyte cells have been extensively used throughout various studies involving adipogenesis; human pre-adipocytes pose multiple differences and limitations in comparison. For example, Janderová and colleagues (2003) suggest that pre-adipocytes exhibit unipotency and cannot be utilized for studies that include the stages of early differentiation, such as the

formation of pre-adipocytes originating from the multipotent precursor cells. To induce differentiation in hMSC-ad cells, a concoction of insulin, dexamethasone, rosiglitazone, and IBMX was utilized; this protocol was adapted from that used previously by Kramer and colleagues (2015) for the differentiation of the murine pre-adipocytes: 3T3-L1.

Insulin is an important promoter of many processes, including adipogenesis, chondrogenesis, and the skeletal muscle growth; however, excessive exposure to insulin may result in a decreased or inhibited rate of adipogenesis (Janderová et al., 2003). Increased concentrations of insulin are generally associated with the activation of MAPK, which is vital for osteogenesis. Janderová and colleagues (2003) demonstrated that adipocyte differentiation was increased when the hMSC cells were not exposed to dexamethasone and IBMX for extended periods of time; therefore, this information aided in the adaption of the differentiation maintenance medium, which consisted only of DMEM, 5 % (v/v) FBS, 1 % (v/v) PSA, and 10 µg/ml insulin. The improved rate of differentiation was supported by Janderová and colleagues (2003) observations that suggested the lack of prolonged exposure to IBMX and dexamethasone resulted in increased levels of leptin mRNA; they later concluded that the initial hormonal concoction is a vital step required for the induction of differentiation, however, it is not necessary for the development of matured adipocytes.

Upon the induction of differentiation, the fibroblastic precursor cells partake in a morphological change whereby more rounded, circular cells are formed (Ramirez-Zacarias et al., 1992). Regarding size, adipocytes may vary; storage of triglycerides determine the overall size of the adipocyte (Spiegelman et al., 1996). White adipose cells may generally be identified by the formation of single, large lipid droplets (Frontini et al., 2010; Cedikova et al., 2016). White adipocytes possess a spherical morphology with a varying large size that can be between 25 – 200 µm. In comparison to the sizes of the white adipocytes, mesenchymal stem cells are quite notably smaller in size. Ranging from approximately 10 µm to 25 µm in diameter, the cell size is dependent on the cell cycle phase.

Adipocytes, in particular white adipose tissue, are responsible for the storage of excess energy in the form of triglycerides (Spiegelman et al., 1996; Boudina et al., 2014; De Pauw et al., 2009; Bost et al., 2005). This storage is often the result of energy expenditure being less than the overall intake.

### 3-1-1. Validation of Adipogenesis via Lipid Staining Techniques

Nile Red staining was first described by Smith (1907) as a method which provided the histochemical detection of tissue lipids. Albeit, a compound called Nile Blue, was originally used, it was later found that other comparable dyes of the phenoxazine family possessed the ability to simultaneously stain acid lipids blue, whereas the neutral lipids were stained red (Greenspan et al., 1985). Per Greenspan and colleagues (1985), the nile red staining method was considered as far superior when compared to other dyes, such as rhodamines and nitrobenzoxadiazol derivatives, which did not provide any distinguishable differences with the cytoplasmic lipid droplets.

Nile red can be defined as an uncharged heterocyclic molecule. It is not soluble in water, but is soluble in organic hydrocarbon solvents (such as heptone), more polar solvents (such as ethanol), as well as neutral lipids (such as triacylglycerols and cholesteryl esters) and phospholipids (such as phosphatidylcholine vesicles). Therefore, it acts as a hydrophobic probe that fluoresces per the level of hydrophobicity present within the environment (Fowler et al., 1985).

Alternatively, Oil Red O is a widely used staining technique whereby the amount of staining observed has been related to being directly proportional to the extent of cell differentiation and, thus, lipid accumulation (Ramirez-Zacarias et al., 1992).

## 3-2. Results and Discussion

### 3-2-1. The confirmation of the induction of adipogenesis with/without the presence of S3I-201.

**3-2-1. A. Morphological Changes Associated with Adipogenesis and Lipogenesis**

The result of the induction of adipogenesis was measured using light and fluorescence microscopy. At day 6, lipid accumulation was present within the differentiated hMSC-ad cells. This was easily identified by the observation of "fat" droplets (N = 3) as shown by the arrows highlighted in Figure 3-1. For the short period of time these cells were left to differentiate, there seemed to be a numerous collection of these lipid droplets present within the differentiating cells; however, there were only a select few that were easily visualized and identified, thus leading to the detection of adipogenesis by other means (Nile Red staining (N = 2) and Oil Red O staining (N = 3)).

Initially, undifferentiated human adipose-derived mesenchymal stromal cells (hMSC-ad) were subjected to S3I-201 treatment in order to determine any additional adverse effects that might result from exposure to the STAT3 inhibitor. The control referred to an untreated hMSC-ad sample, as shown in the relevant panel within Figure 3-2. Here, it was evident that the undifferentiated cells contained an equal visual ratio of polar lipids and neutral lipids, with no true "fat droplet" formation being present; in addition to this, the cells possessed a fibroblastic, fusiform, morphology and displayed long cellular extensions. Upon exposure to S3I-201, it was demonstrated within the listed panels 100 μM, 50 μM, 25 μM, 12.5 μM, and 6.25 μM that a definite decrease in neutral lipids stained; albeit, there was no true correlation between S3I201 concentration and the deficit neutral lipid stain exhibited.

Shortly after the induction medium was added (DMEM supplemented with 10 % (v/v) FBS, 1 % (v/v) PSA, 10 μg/ml insulin, 2 μM rosiglitazone, 0.5 mM IBMX, and 0.25 μM dexamethasone), a morphological change in the hMSC-ad cell lines was observed. While more confluent than what was established in Figure 3-2, the resulting hMSC-ad cells displayed early signs of adipogenesis. Using the control within Figure 3-3, it was evident that there was some lipid droplet formation and accumulation present, due to the fluorescence

observed within the panel titled "neutral lipids" for the control. The cells seemed to lose their original fibroblastic morphology and multiple cellular extensions to adopt a more classical rounded form that is commonly associated with differentiating adipocytes. The introduction of S3I-201 seemed to have little/no effect on the overall lipogenesis observed as there were multiple stains of neutral lipid droplets observed; in fact, they seemed to be greater than when compared to the control in Figure 3-3.

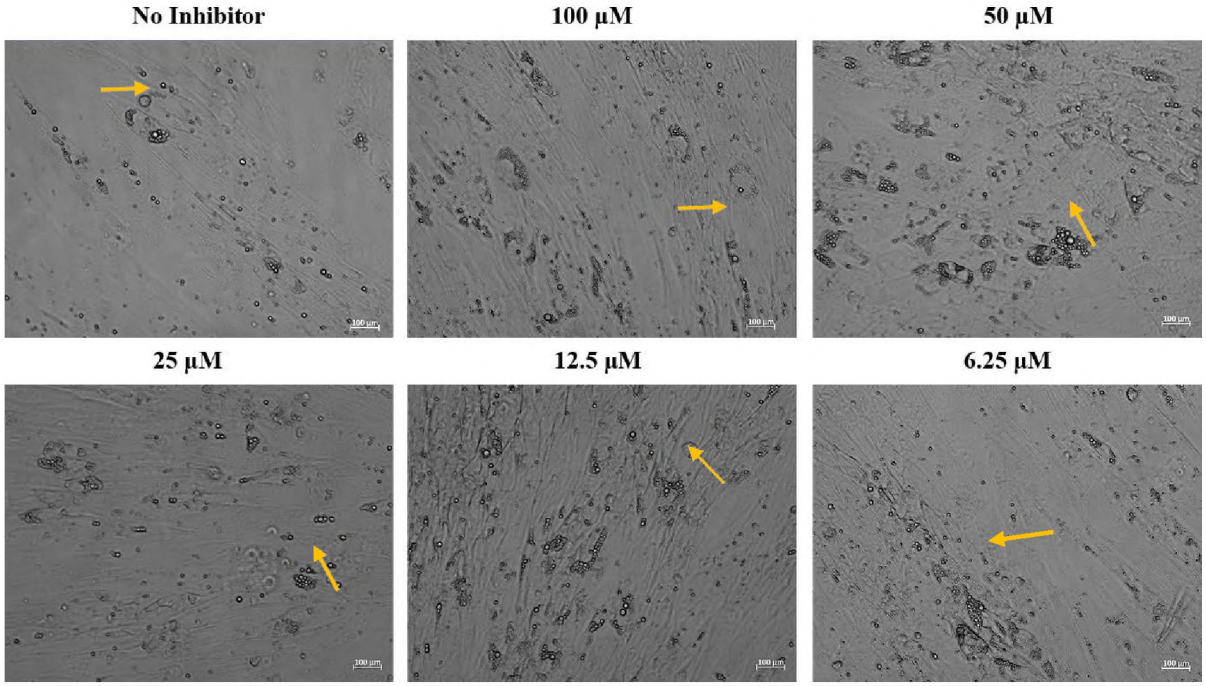


**Figure 3-1. Morphological changes observed during the induction of adipogenesis while in the presence of a STAT3 inhibitor.** Adipocyte differentiation was captured upon day 6 after adipogenesis was induced in combination with the presence/absence of varying concentrations of a STAT3 inhibitor (S3I-201). Arrows represent the areas of lipid formation and accumulation observed. Images were obtained using the phase contrast 2 filter on the Zeiss AxioVert.A1 FL-LED Fluorescence Microscope at 200x magnification. Scale bars = 20 µm. Images shown are representative of multiple images acquired (N = 3).

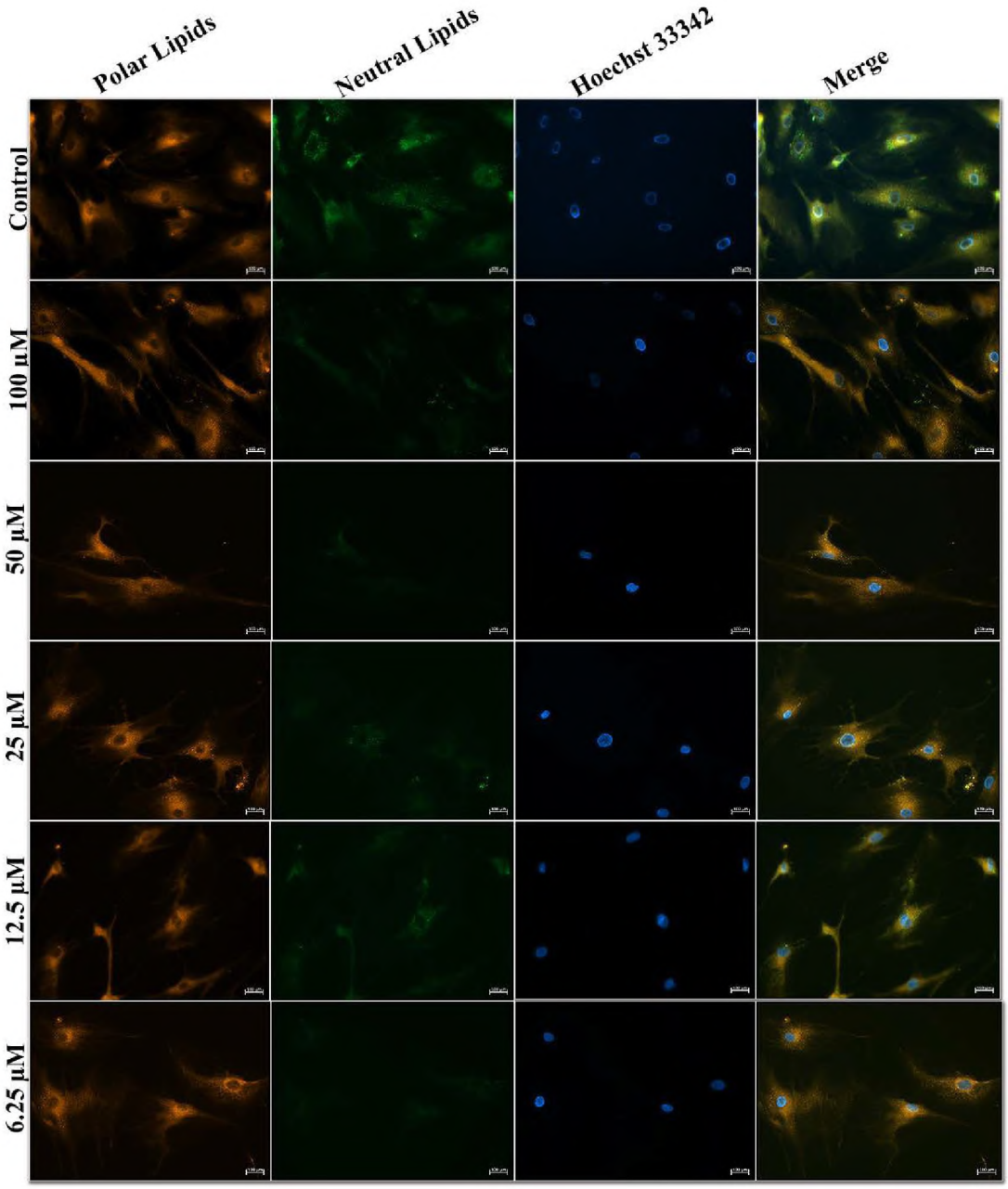


**Figure 3-2. Nile Red staining of human adipose-derived mesenchymal stem cells.** The hMSC-ad cells were stained after 48 hours of exposure to varying concentrations of S3I-201. Images were captured using the Zeiss AxioVert.A1 FL-LED fluorescence microscope at 200x magnification. Scale Bar = 20 µm. Images shown are representative of multiple images (N = 2).

Signal transducer and activator of transcription (STAT) proteins play an important role in aspects of cellular function, including the proliferative potential of the cells, as well as cell survival (Siddiquee et al., 2007). These proteins have been linked to numerous vascular diseases through the unwanted activation of angiotensin II type 1 receptors. STAT3 may undergo continuous activation via an abnormal upstream tyrosine kinase activity located within an array of cancer cell lines (Schust et al., 2007). During adipogenesis, levels of STAT3 and STAT5 have been reported to increase; Cernkovich and colleagues (2008) have suggested that when STAT3 is hindered in any manner, a decrease in the proliferation of pre-adipocytes may occur. In addition to the aforementioned, STAT3 has also been linked to the resulting size of the adipocytes formed. According to Cernkovich and colleagues (2008), if there is a deficit of STAT3, an increase in body weight and adiposity may occur; however, if inhibited, adipocyte differentiation is inhibited, thereby indicating that STAT3 is required for adipogenesis.

S3I-201 is a chemically produced inhibitor of STAT3 activity, which is said to restrict the growth of tumour cells that possess STAT3 that is being continuously activated, and result in an induced apoptosis (Siddiquee et al., 2007). This STAT3 inhibitor specifically halts the DNA-binding activity of STAT3, preventing activation, dimerization, and gene transcription, in vitro, displaying an $IC_{50}$ of 86 +/- 33 μM (Siddiquee et al., 2006; Johnson et al., 2013). S3I201 can be used as a protective agent against oxidative stress due to angiotensin II and hypertension (Johnson et al., 2013).

The images shown in Figure 3-2 represent an hMSC-ad population (N = 2) with images taken in a minimum of 4 random locations within the single well. The hMSC-ad cells were exposed to similar conditions to that of the differentiating adipocytes, in that they were cultured within a 37 °C, 5 % $CO_2$ environment and treated with the same concentrations of S3I-201, added after approximately 24 hours. The only difference between the two culturing conditions is the number of cells seeded onto the plates, and the level of confluency achieved before treatment and observations took place. The hMSC-ad cells were seeded at a density of 5 000 cell/well and left to settle for approximately 24 hours, after which the concentrations of S3I-201 were added. The cells were left to grow in the presence of S3I-201 for approximately 48 hours in

order to prevent the hMSC-ad cells from reaching a multi-layered confluency before results were generated.

Figure 3-2 represents the staining of hMSC-ad cells in order to gain insight into the effects of S3I-201 on non-differentiating hMSC-ad cells, performed in duplicate (N = 2), before exposure to adipocyte differentiation. The control provided evidence of the presence of neutral lipids naturally occurring within untreated, undifferentiated human adipose-derived mesenchymal stem cells; visually, there seemed to be an equal ratio of polar lipids to neutral lipids within the cell, which is indicative of lipogenesis, the formation of lipids. Jiang and colleagues (2009), have suggested that lipogenesis occurring within adipocytes is mediated by leptin using STAT3 independent fundamental mechanisms. Furthermore, their study provided evidence that leptin aided in the activation of STAT3 within white adipose tissue, providing the speculation that peripheral STAT3 activation may be necessary for the regulation of leptin and its role on promoting lipogenesis. Yang and colleagues (2010) provides evidence that supports the notion that STAT3 activation results in the inhibition of lipogenesis; STAT3 deficiency may result in the elevation of triglycerides present, in other words, lipogenesis is promoted. This is further supported by Miller and colleagues (2011), who report that the activation of interleukin-6 (IL6)/STAT3 causes the inhibition of the lipogenic gene (SREBP1c, ACC1, and FAS) expression.

The effect that S3I-201 had on the non-differentiating hMSC-ad cells (Figure 3-2) was unexpected, due to the fact that the inhibition of STAT3 should result in an increase of total lipid content found within the cells. This was not observed; as the S3I-201 concentrations increased, the lipid content observed within the panels titled 'neutral lipids' decreased. This may suggest that other forms of STAT3 may contribute to the formation of lipids, and may not be solely dependent on phosphorylated STAT3 present within the cell. Studies performed by Kramer and colleagues (2015) provided a similar result in that when STAT3 phosphorylation was inhibited, so too was the accumulation of lipids at an $IC_{50}$ of approximately 30 μM S3I-201. This decrease in lipid accumulation may be attributed to, perhaps, the effect that deficient levels of STAT3 pY705 may have on the cells; phosphorylated Y705 possesses the vital function of regulating the transcriptional activity of STAT3, as well as maintaining the significant properties of stem cells (Huang et al., 2014). Upon induction of differentiation, increased levels of phosphorylated STAT3 Y705

counteract the signals provided by fibroblast growth factor (FGF)/Erk pathways, which are believed to initiate cellular differentiation (Huang et al., 2014; Lanner et al., 2010). Furthermore, the decrease in neutral lipids could simply be the result of defective sampling and incorrect culturing methods.

Relative to the control, observed in Figure 3-2, fewer cells were observed within the random locations chosen for image capture (a total of 4 locations were chosen throughout); this may lead to the speculation that S3I-201 may have a slightly adverse effect on the proliferative capacity of the hMSC-ad cells. Before conclusions can be justified, additional experiments to monitor this proliferative ability would be required. Evidence of lipid formation remains due to the polar lipids stained within Figure 3-2, present throughout all panels (ranging from control to 6.25 μM S3I-201 treatment); however, the lipid droplet formation would appear to be significantly decreased.

Additional controls for this experiment, located within the attached appendix (Figure A.I.), include unstained cells, as well as those that were only stained for nuclear Hoechst 33342.

Confirmation of a successful adipogenic differentiation can be discussed in further detail regarding comparisons between the human adipose-derived mesenchymal stem cells (shown in Figure 3-2) and the adipogenic differentiation observed in Figure 3-3 (N = 2). An evident morphological transformation has occurred; the cells have lost their fibroblast-like appearance to adopt a more rounded or oval shape with clear evidence of lipid droplet formation demonstrated by the green fluorescence that indicates neutral lipids, which correlates to the orange stained polar lipids to form a golden colour when the image channels have been merged. An increase in cell confluency is required to induce adipogenesis as cell-cell communication and signalling helps promote this process; therefore, in order to induce adipogenesis, the hMSC-ad cells were required to reach 100 % confluency. Upon the induction of adipogenesis, proliferation ceased and the transformations started to occur. The Oil Red O stains (N = 3), shown in Figure 3-4, demonstrate, once again, successful differentiation, noted by the 'red' stained droplets of fat evident under light microscopy. Before the stain was performed, light microscopy images were captured to show the before and after events that may account for 'lost lipids' due to extensive rinsing cycles. It was clear

that some of the lipid droplets were washed from the cells; leaving less visual stain than originally hoped for.

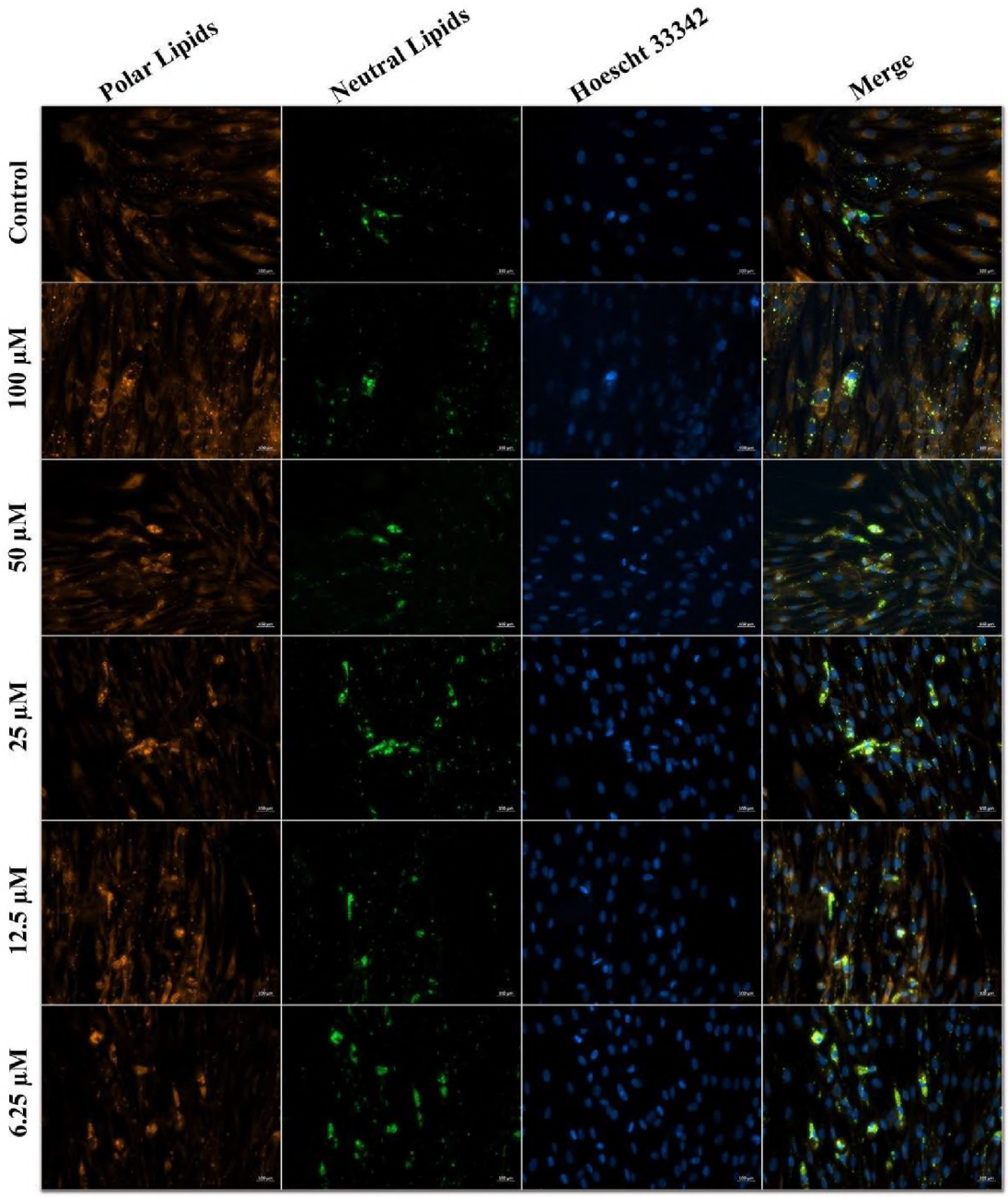


**Figure 3-3. Nile Red staining to confirm the induction of adipogenesis.** The cultures were stained on day 6 post induction in the presence/absence of varying concentrations of S3I-201. Images were captured using the Zeiss AxioVert.A1 FL-LED fluorescence microscope at 200x magnification. Scale Bar = 20 µm. Images shown are representative of multiple images (N = 2).

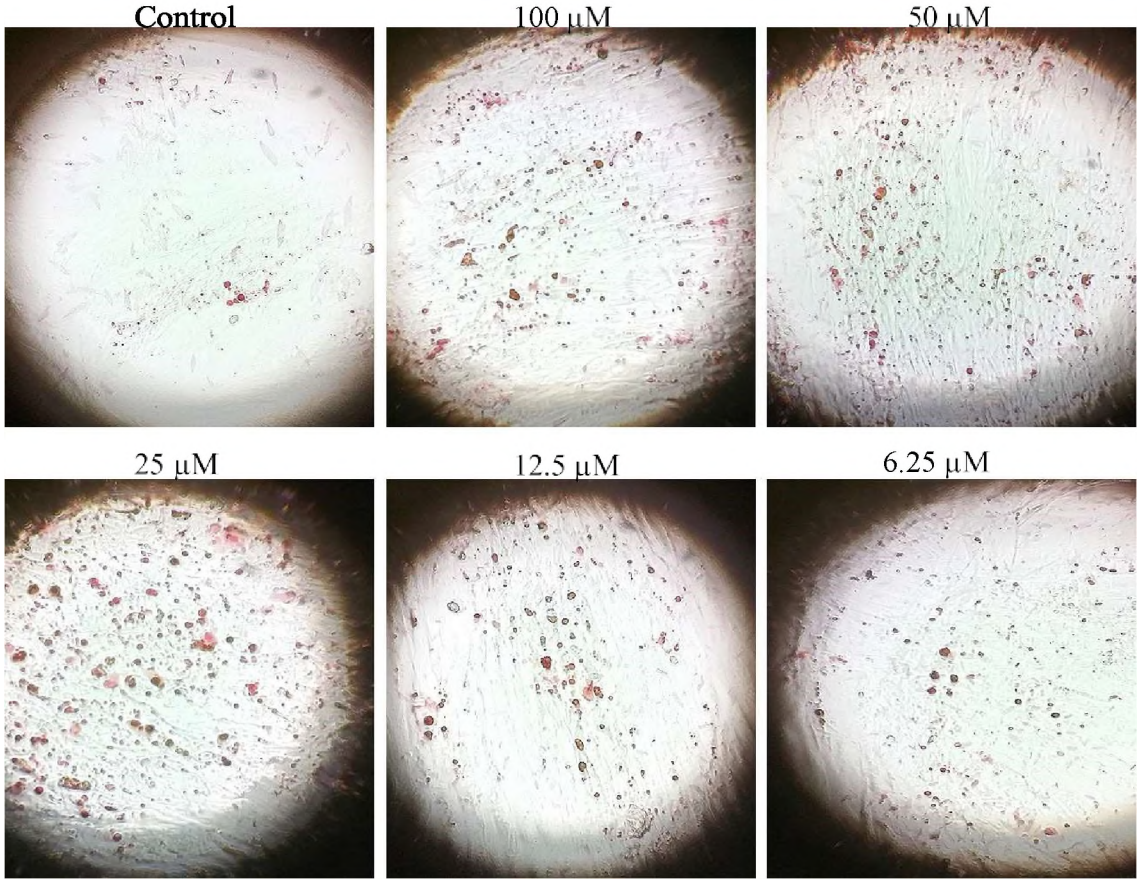


**Figure 3-4. Oil Red O staining to confirm the induction of adipogenesis.** The cultures were stained on day 6 post-induction in the presence/absence of the varying concentrations of STAT3 inhibitor (S3I-201). Images were captured using a Samsung Galaxy Note 4 camera with magnification 2x and the Zeiss AxioVert.A1 FL-LED Fluorescence Microscope at 200x magnification. Images shown are representative of multiple images acquired (N = 3).

The differentiation protocol utilized provided adipocytes that resembled those closely related to white adipose cells; they were larger in size, when compared to non-differentiating hMSC-ad cells, and considerably rounded with large, discernible lipid droplets present. This suggested that adipogenesis did, or was, in fact, occurring.

With the addition of the S3I-201, there seemed to be little/no evident visual effect on the formation of lipid droplets, and, thus, the process of adipogenic differentiation. In fact, there seemed to be almost a greater occurrence of lipid formation. The greatest number of lipid droplets seemed to occur between the ranges of 50 µM and 12.5 µM S3I-201; however, it

must also be noted that some of the lipid droplets may easily be washed from the cell, itself, during media changes or rinsing steps. This large amount of lipid formation was also evident within the Oil Red O stain (shown in Figure 3-4) whereby the red/pink colour represents the stained fat droplets. The formation of lipid droplets in the presence of S3I-201 could be explained by reasoning provided above.

From the results above, it can be concluded that the differentiation process was a success, and lipid formation is clearly seen after 6 days post-induction; adipogenesis was also able to occur within the presence of S3I-201, leading to the possible assumption that alternative pathways may have been activated to compensate for the defective levels of STAT3; as well as the concentrations of S3I-201 could have been less detrimental to the cell's ability to undergo adipogenesis than previously assumed. However, it may also be argued that, while lipogenesis generated the lipid droplets, as shown in Figures 3-1, 3-3, and 3-4, the differentiation of the hMSC-ad cells to adipocytes may have been hindered by S3I-201 treatment; therefore, additional experimentation using the ACEA xCELLigence RTCA system was necessary in order to generate a base line indicative of successful adipogenesis.

### 3-2-1. B. Use of ACEA xCELLigence RTCA system for monitoring the effects of S3I-201 on adipocyte differentiation.

XCELLigence RTCA protocols were optimized and utilized in order to determine CI growth curves that would validate the success of adipogenic differentiation, as well as the effects that various small molecules may have on the resulting cellular models. Using the hMSC-ad cell line, cells were seeded using normal hMSC-ad maintenance medium (MSCM) at a density of 5 000 cells/well. The cells were then left to settle for approximately 24 hours, after which a medium change occurred. An additional 48 hours was permitted, in which cells reached 100 %, and above, confluency in order to aid for a greater grounds for differentiation, due to the cell-to-cell contact. The induction medium was added, whereby S3I-201 was combined into this induction medium; after approximately 4 days of exposure to the induction medium, the adipocyte maintenance medium was utilized, in which fresh S3I-201 was added. This maintenance medium and fresh S3I-201 was provided to the cells approximately every 3 days. This process occurred throughout all adipocyte differentiation protocols.

In the case of non-differentiating hMSC-ad cells, which were used for comparative purposes to determine whether or not some form of differentiation was occurring, the control consisted of hMSC-ad cells that were left untreated for S3I-201. This aided in the acquisition of a guide, with respect to the CI growth curves obtained. The curve of the control, observed in Figure 35.A. included an initial peak, which is indicative of cells settling within the 96-well gold electrode plate; 24 hours was selected for the attachment of the cells to the surface of the culture vessel, which was exhibited via the point in which a plateau was reached. Following the 24 hours, a medium change (consisting of normal maintenance medium (MSCM or α-MEM)) occurred; this was shown by the slight drop in CI growth curve after the 24 hours. The following 48 hours demonstrated a gradual increase in CI value.

Addition of S3I-201 occurred during the first medium change after the 24 hour settling period; for S3I-201 concentrations 100 μM and 50 μM (Figures 3-5.B. and 3-5.C., respectively), a larger decline in CI peak was observed after this initial addition of S3I-201, in comparison to what was observed using the control in Figure 3-5.A. This decline is indicative of cell death, which would, ultimately, be expected due to the established $IC_{50}$ value of 30 μM, as previously mentioned. However, as it is shown, during the 48 hours after S3I-201 addition, there seems to be some compensation occurring whereby the cells are rectifying and adjusting to the STAT3 deficit, which may explain the resulting increase in the CI growth exhibited. In all cases demonstrated in Figure 3-5, there was an increase in CI growth curve after the initial addition of S3I-201; however, the general increasing trend was not as great as that observed for the control.

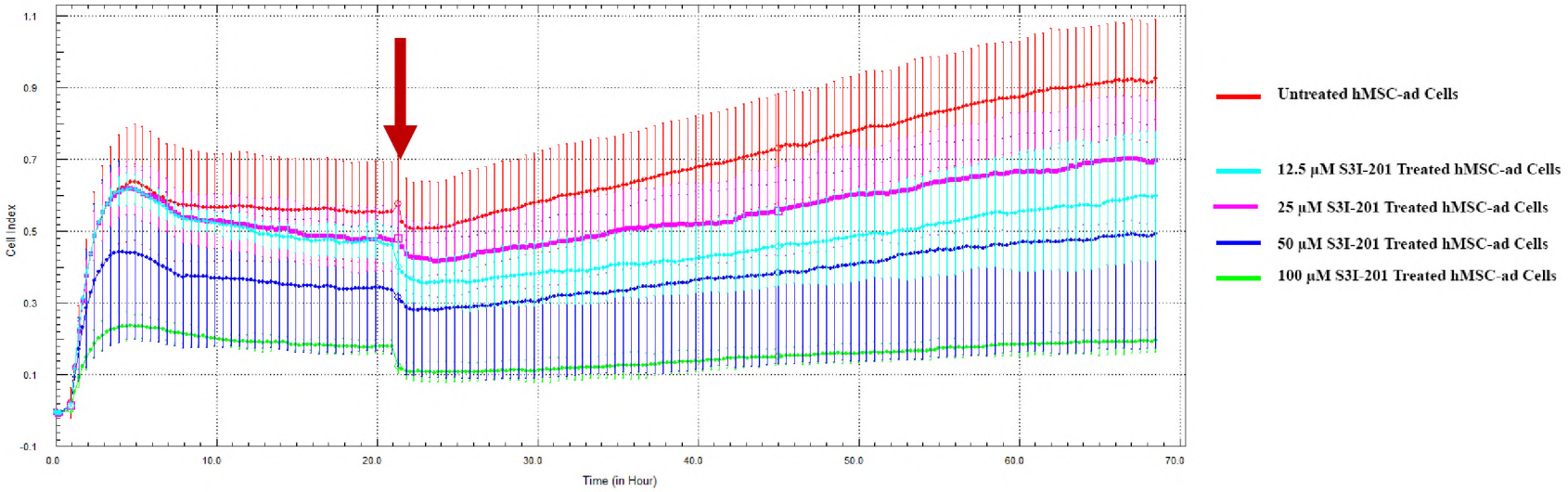


**Figure 3-5. Effects of S3I-201 on hMSC-ad cell growth after a period of 72 hours.** The cells were seeded onto the plate at a density of 5 000 cells/well, and allowed to settle for 24 hours in the general hMSC-ad cell maintenance medium (MSCM), after which a medium change occurred whereby S3I-201 was added at varying concentrations. The highlighted region indicates the point at which the medium was changed and the S3I-201 was added. All curves were plotted as an average of triplicate concentrations; graphs were constructed using the ACEA xCELLigence RTCA SP software provided. (N = 2).

In order to prepare for the induction of differentiation of the human adipose-derived mesenchymal stem cells, the cells were required to reach at least 100 % confluency. Usually, a CI of 1.0 is sufficient to begin differentiation; however, in order to ensure that sufficient cell-cell signalling was achieved, the cells were monitored using light microscopy as well as an extra 24 hours was allocated post-confluency to allow for addition proliferation before induction. However, just before the differentiation medium was added, a 'plateau' was observed whereby there is a minimal increase in the CI; this could be attributed to the fact that upon reaching 100 % confluency, mesenchymal stem cells form multiple layers, or sheets, of cells that do not come into contact with the gold electrodes used within the xCELLigence system. When the differentiation cocktail was added (IBMX/ROSI/DEX/INSULIN), a notable change in CI was observed, whereby an initial drop occurred before it was rectified; this indicated the addition of the differentiation medium followed by the maintenance media, both of which possessed the varying concentrations of S3I-201.

In comparison to the general upward climb of the human adipose-derived mesenchymal stromal cells, an extremely distinctive CI curve was generated that produced a significantly higher CI than what was found for the undifferentiated cells (as shown in Figure 3-5 and 3-6). This vast increase could be attributed to the morphological differences distinguished between undifferentiated mesenchymal stem cells and the differentiated adipocytes; MSCs are of a smaller size with a spindle/fibroblast-like shape, whereas, adipocytes may vary in size but are generally larger and rounder in size. Another reason for this vast difference in CI could be attributed to the symmetrical division of the hMSC-ad cell line; whereby proliferation simply generates the multi-layers of cells, whereas, the induced differentiated cells simply grow fatter and rounder as the lipid droplets accumulate within thecytoplasm.

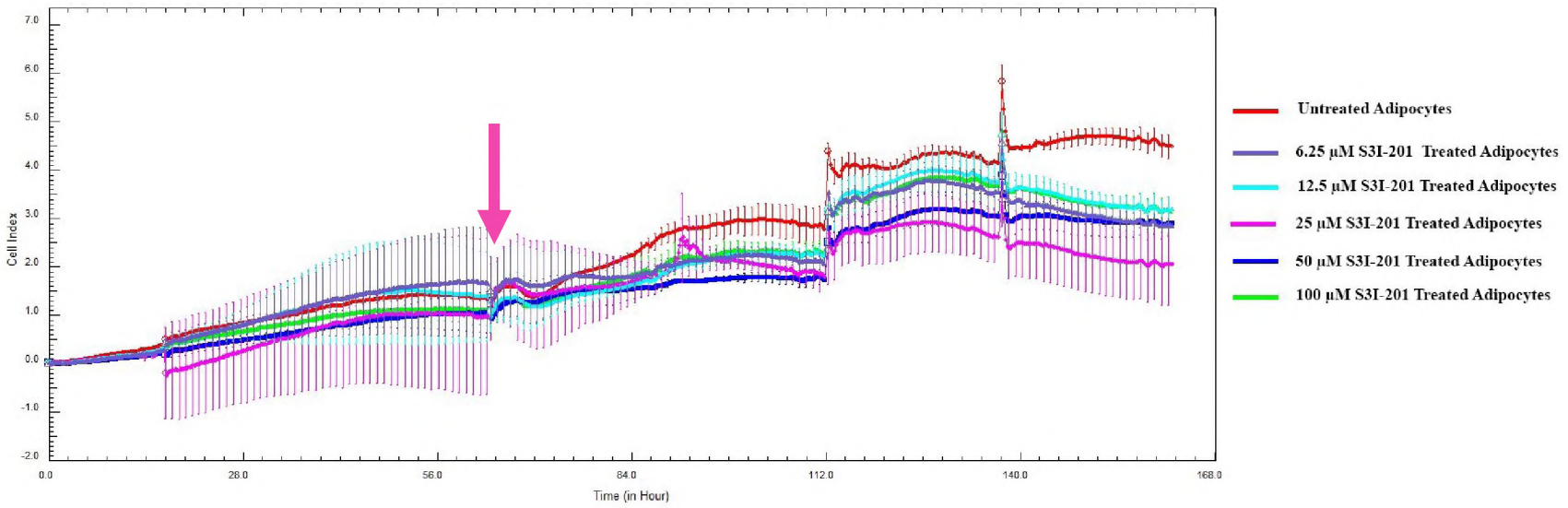


**Figure 3-6. Effects of S3I-201 on adipogenic differentiation hMSC-ad cell growth.** The cells were seeded onto the plate at a density of 5 000 cells/well, and allowed to settle for 24 hours in MSCM, after which a medium change occurred whereby S3I-201 was added at varying concentrations. The highlighted region indicates the point at which the cells were induced for adipogenesis with accompanying concentrations of S3I-201. All curves were plotted as an average of 12 treatments per concentration; graphs were constructed using the ACEA xCELLigence RTCA SP software provided. (N = 2).

With regards to overall differences observed upon the addition of S3I-201 to both the undifferentiated and differentiated hMSC-ad, Figures 3-5 and 3-6 respectively, there was a difference in CI observed between the controls (undifferentiated and differentiated hMSC-ad cells that did not contain any S3I-201) and the resulting average graphs plotted. A slight decrease in CI was observed amongst all concentrations of S3I-201; this may suggest several attributes: 1) Adipogenesis was adversely affected by the addition of S3I-201 but not inhibited altogether. The stimulation of other various proteins, including STAT1 and STAT5 could have compensated for the lack of STAT3; and 2) Cell growth/survival is generally affected by a defect of STAT3, indicating that it is essential to maintain optimal cellular health and function.

While the STAT3 inhibitor did not have as large an effect on the growth CI curves for both the undifferentiated and differentiated hMSC-ad cell lines, there was a slight change in CI curves generated between samples that did not contain S3I-201 (as shown in Figures 3-5 and 3-6) and those that possessed S3I-201 at the varying concentrations. There was no significant discrepancy between the CI curves generated for each of the S3I-201 concentrations; however, the graph depicting the 100 μM S3I-201 in Figure 3-5.B. depicts a generally decreased CI curve, regardless of the CI gradient remaining relatively similar to that of the control in Figure 3-5.A. This could be the result of an initially low CI caused by the lack of hMSC-ad binding to the surface of the gold-coated plate; this lack of hMSC-ad growth could have been caused by a discrepancy in hMSC-ad seeding or over-trypsinization of the hMSC-ad cells during subculture, leading to a decrease in cell survival rate. However, as previously mentioned, it must be acknowledged that when added at 100 μM S3I-201, this concentration is regarded as toxic; $IC_{50}$ values of approximately 30 μM were established for S3I-201. The graphs generated were the result of an average of a triplicate experiment set up.

In the case as shown in Figures 3-5 (D), (E), and (F), there was an irrelevant difference between the two initial CI values generated; however, upon the addition of the S3I-201 inhibitor, it was found that the 25 μM concentration seemed to have an increased CI in comparison to the 12.5 μM observed. This may provide a speculation that the cellular system may not necessarily require STAT3 for growth. The overall rate of growth and proliferation may be significantly decreased; however, the cell will not suffer death.

Further experiments may seek to involve looking at a STAT3 deficient undifferentiated hMSC-ad cell line, and, using the differentiating protocol, attempt to differentiate these cells into adipocytes, thereby confirming any fundamental properties that STAT3 may play in differentiation.

## 3-2-2. The confirmation of the induction of adipogenesis with/without the presence of the M1, mitochondrial fusion promoter.

### 3-2-2. A. Morphological Changes Associated with Adipogenesis and Lipogenesis

As per the S3I-201 protocol of observation, the results were viewed using microscopy methods. The mitochondrial fusion promoter, M1, provided results that demonstrated a significant amount of cell death after the allocated time provided in the S3I-201 protocol; therefore, light microscopy was utilized in order to determine whether or not M1 was responsible for cell death under 24 hours. Figures 3-7 and 3-8 demonstrate light microscopy images acquired after approximately 24 hours; the control throughout the M1 experiments consisted of an untreated sample in both undifferentiating and differentiating cell models. The control provides indication of healthy hMSC-ad differentiating cells. A clear fibroblastic morphology is present with little/no external interference present.

Upon the addition of the mitochondrial fusion promoter, background interference was observed; this interference increased as the concentration of M1 increased, as clearly shown in Figure 3-7 (N = 2). The sample containing 100 µM of M1 possessed the greatest indication of interference, whereas 10 µM contained the least. This 'interference' could be explained as the development of dark filamentous structures due to mitochondria undergoing vast levels of fusion; or, it may be attributed to the inclusion of the M1 crystals, demonstrated at an increased concentration of the small molecule compound, due to the fact that cells are present within the background. The speculation that the 'interference' may be due to crystalized M1 that is unable to dissolve within the medium may be reinforced by the preliminary $IC_{50}$ estimated through the acquisition of xCELLigence data. The estimated $IC_{50}$ was 5.4794 µM, which is significantly lower than the original concentrations used throughout the study.

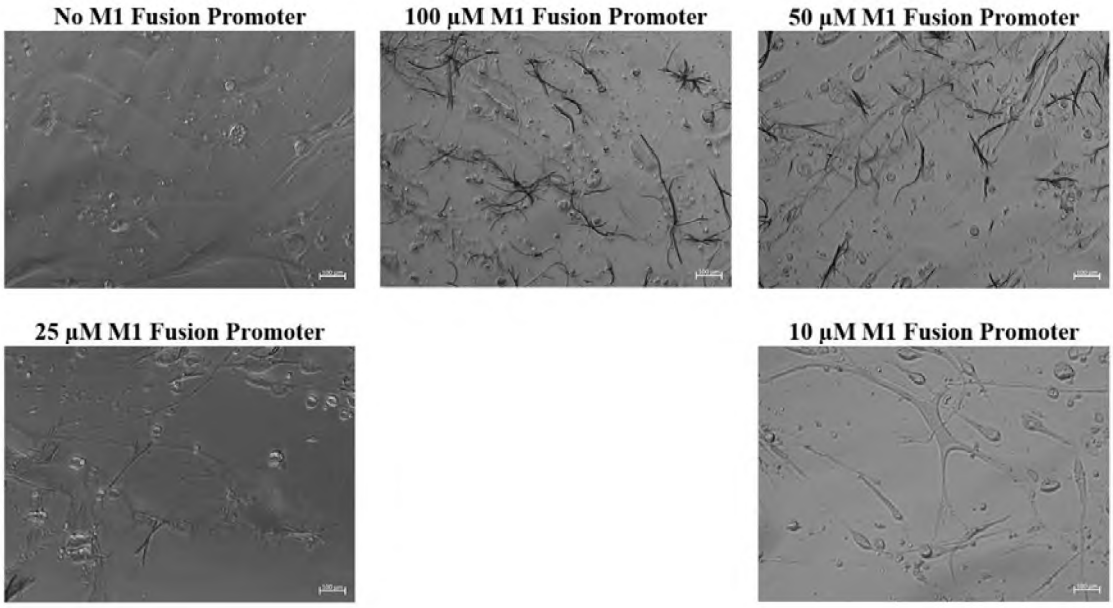


**Figure 3-7. The effects of mitochondrial fusion promoter, M1, on hMSC-ad cells after approximately 24 hours.** The hMSC-ad cells were seeded onto a plate and allowed to settle for approximately 24 hours, after which a medium change occurred. The cells were left to grow for an additional 24 hours without the presence of the M1 fusion promoter. The mitochondrial fusion promoter was then added at the aforementioned concentrations, and the effects were monitored after 24 hours using light microscopy. Images were captured using the Zeiss AxioVert.A1 FL-LED Fluorescence Microscope at 200X magnification. Images shown are a representative of multiple images acquired (N = 2) at random locations within the culture vessel. Scale bar = 20 µm.

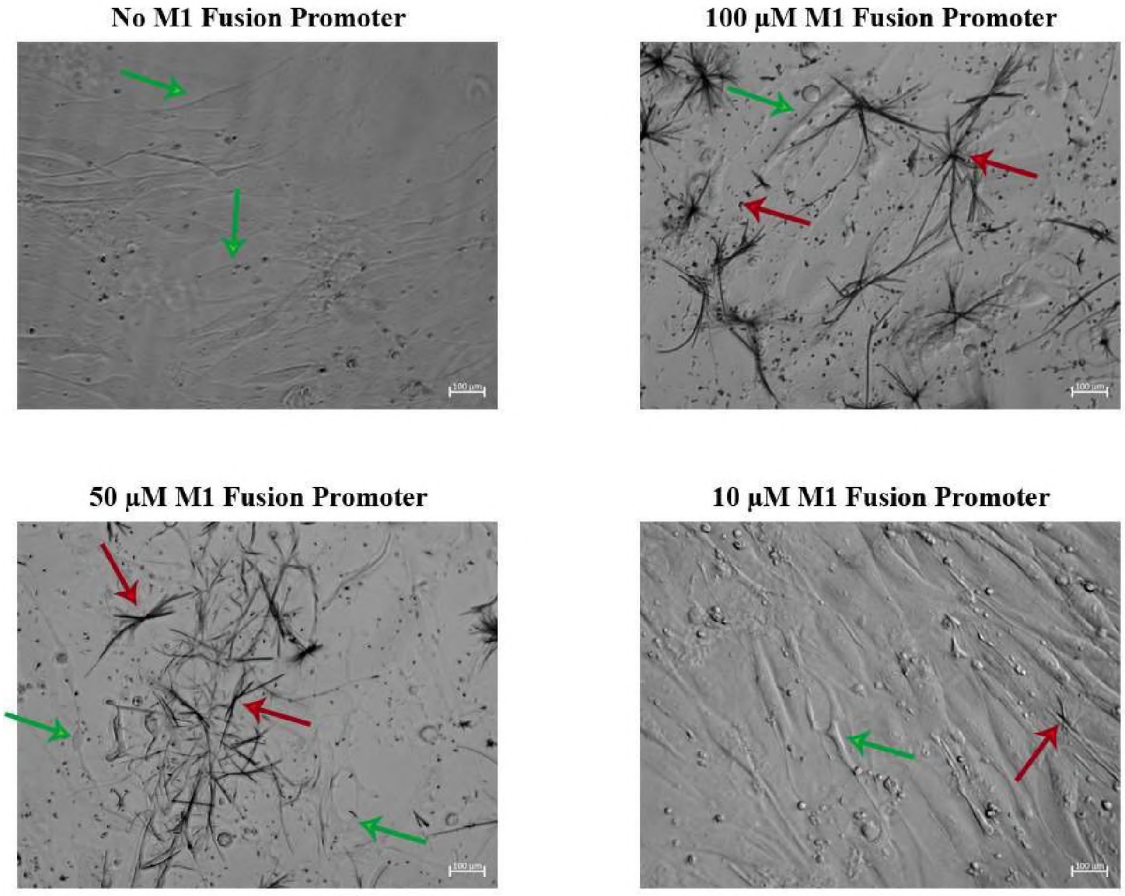


**Figure 3-8. Effects of the mitochondrial M1 fusion promoter on differentiating adipocytes after 24 hours.** The mitochondrial M1 fusion promoter was added alongside the cocktail of compounds used for the adipogenesis of hMSC-ad cells. The red arrows indicate the traces of filamentous/ellipsoidal 'crystal' morphologies, while the green arrows represent healthy differentiating hMSC-ad cells. Images were obtained using the Zeiss AxioVert.A1 FL-LED Fluorescence Microscope at 200x magnification. Images shown are representative of multiple images acquired (N= 3) at random locations within the culture vessel. Scale bar = 20 µm.

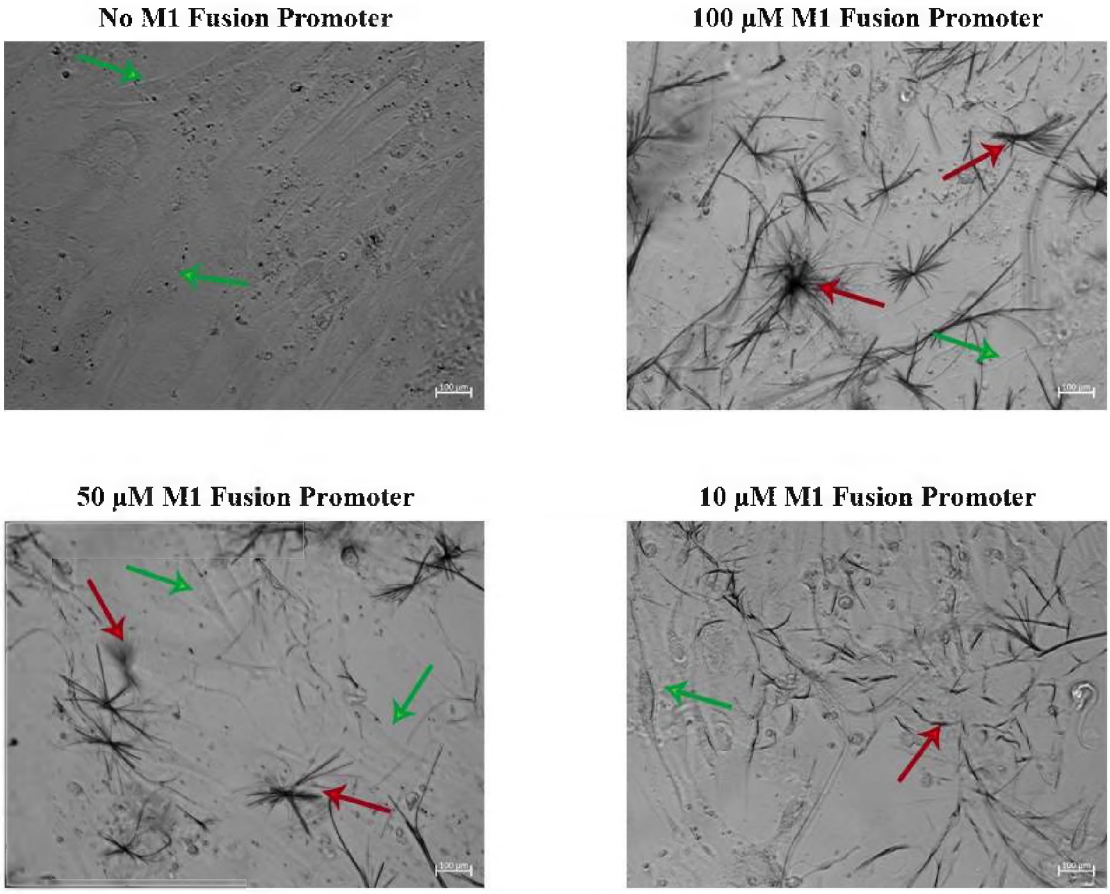


**Figure 3-9. Effects of the mitochondrial M1 fusion promoter on differentiating adipocytes after 72 hours.** The mitochondrial M1 fusion promoter was added alongside the cocktail of compounds used for the adipogenesis of hMSC-ad cells. The red arrows indicate the traces of filamentous/ellipsoidal 'crystal' morphologies, while the green arrows represent healthy differentiating hMSC-ad cells. Images were obtained using the Zeiss AxioVert.A1 FL-LED Fluorescence Microscope at 200x magnification. Images shown are representative of multiple images acquired (N = 3) at random locations within the culture vessel. Scale bar = 20 µm.

The actions of small molecules may occur within several hours after addition. The hMSC-ad cells were exposed to a combination of differentiation medium and the varying concentrations of M1, mitochondrial fusion promoter. The majority of the cells present within the 100 µM had most likely undergone apoptosis, leaving few live cells present after 24 hours. The dark filamentous 'crystal' structures remained adherent to the plastic surface; in

order to determine whether or not this crystalline structure was, in fact, the result of extensive mitochondrial fusion and a part of the cells, a variety of fluorescence markers, including nile red, and a cell membrane and viability stain, were utilized.

Upon Day 3 (Figure 3-9) of the induction of adipogenesis in the presence of the M1 mitochondrial fusion promoter, the extent of cell death was increased dramatically for concentrations 100 μM and 50 μM, with an increase of those filamentous and fragmented structures being present within the culture vessel; albeit there was some evidence of cell survival indicated by the green arrows. While there seemed to be some surviving cells within the 10 μM, an increase in filamentous/fragmented structures was observed; indicating that the possible mitochondrial disruption of the dynamic ability of fusion results in an altered morphology and/or apoptosis.

M1 is a phenyl-hydrazone able to penetrate the cell membrane; it is responsible for the restoration of the mitochondrial tubular network within cells that are defective of either the outer mitochondrial membrane mitofusins (Mfn1 or Mfn2), or MPP+ treated SH-SY5Y cells, but not MEF lacking Mfn1/2 nor OPA1 (the inner mitochondrial membrane fusion mediator). It provides a boost in the downregulated ATP5A and ATP5B protein levels in Mfn1/2 knockouts. M1 mitochondrial fusion promoter enhances mitochondrial fusion instead of causing the inhibition of fission and/or division. When Mfn1/2 is inhibited, fibroblasts are unable to undergo mitochondrial fusion, which, in turn, causes a decrease in cell growth, heterogeneity of the mitochondrial membrane potential, as well as respiration (Jheng et al., 2011).

In order to determine whether or not the cells were living and/or dead, as well as to further determine the morphological alterations, a cell membrane and viability stain was conducted using the neurite outgrowth staining kit. Generally used for the determination/validation of neuronal-like differentiation via the measurements of cellular extensions, this membrane and viability stain helped to determine the effects that the mitochondrial M1 fusion promoter had on hMSC-ad cells. The cellular membrane, or remnants of the outer membrane, were stained orange, whereas the cell-permeable viability stain provides a green fluorescence. The viability stain aided in the determination of the number of surviving cells after approximately 24 hours of staining, as well as whether or not the filamentous and fragmented structures,

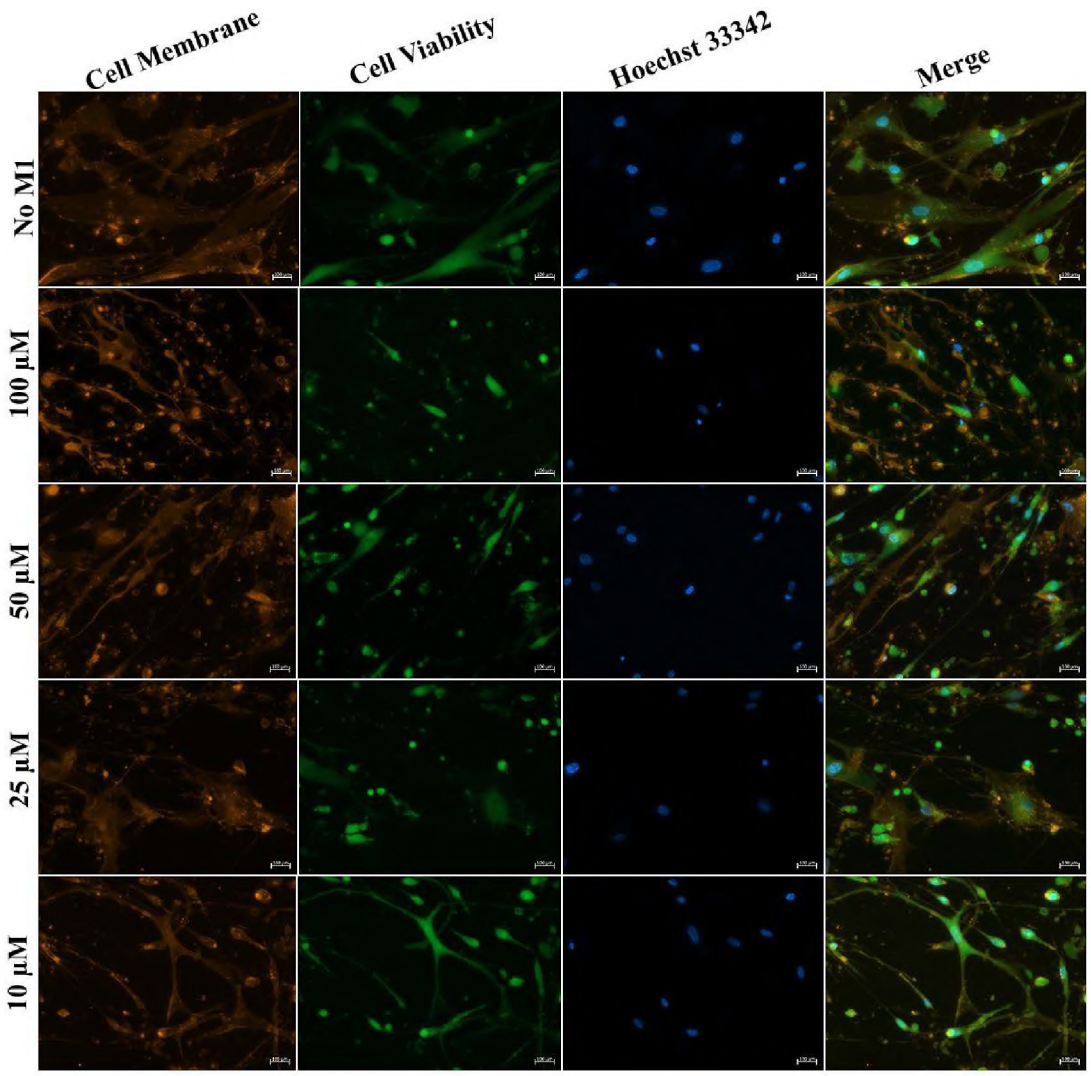


**Figure 3-10. The effects of mitochondrial M1 fusion promoter on hMSC-ad cells after 24 hours.** The hMSC-ad cells were seeded onto a plate and allowed to settle for 24 hours, after which a medium change occurred. The cells were left to grow for an additional 24 hours without the presence of the M1 fusion promoter. The fusion promoter was then added at the aforementioned concentrations, and the effects were monitored after 24 hours using a neurite outgrowth staining kit (cell membrane and viability staining). The control represents no mitochondrial M1 fusion promoter. Images were captured using the Zeiss AxioVert.A1 FLLED Fluorescence Microscope at 200x magnification. Images shown are representative of multiple images acquired (N = 2) at random locations within the culture vessel. Scale bar = 20 µm.

observed in the bright field images of Figures 3-7, 3-8, and 3-9, were a part of a transformed hMSC-ad cell.

As previously mentioned, the control consisted of hMSC-ad cells left untreated for the mitochondrial fusion promoter, M1. When stained with the cell membrane and viability fluorescent dyes, the untreated hMSC-ad cells displayed the typical fibroblastic morphology with a high cell viability, as shown by the green fluorescence relative to the number of Hoechst 33342 stained nuclei and orange fluorescent membranes. There was no evidence of filamentous 'crystalline' structures present within the control sample. The addition of 100 μM of M1 to the hMSC-ad maintenance medium displayed a decrease in cell viability; while the fluorescent stained membranes seemed quite prevalent within the cellular sample, the number that were alive did not correspond to cell membranes present; this was determined by visual inspection of cell viability and the amount of nuclei present within the cell culture vessel. Morphology wise, the cells were decreasing in size and undergoing a rounded alteration, indicative of apoptosis; few cells displayed a spindle-type morphology. This demonstrated that after 24 hours the cells were slowly dying in the presence of this excessively toxic concentration of M1. A similar scenario was exhibited regarding the addition of 50 μM of M1 to the hMSC-ad cells; however, a slightly increased cell viability was observed. The cells still displayed spindle-type, and rounded, morphologies. Cell viability improved significantly as the concentration of M1 decreased, with the concentration of 10 μM providing a viability similar to that expressed in the control of untreated hMSC-ad cells, which would be expected due to the preliminary $IC_{50}$ value of 5.479 μM established for hMSC-ad cells.

The filamentous and/or fragmented phenotypes did not seem to directly correlate with either the viability or the cell membrane stain shown in Figure 3-10 (N = 2). This indicates that the resulting structures are not comprised of the cell membrane nor do they correspond with viable cells; however, before the fragmented/filamentous structures can be definitively attributed to M1 crystals present within the medium, additional stains, including JC-1 mitochondrial fluorescent dyes, were performed.

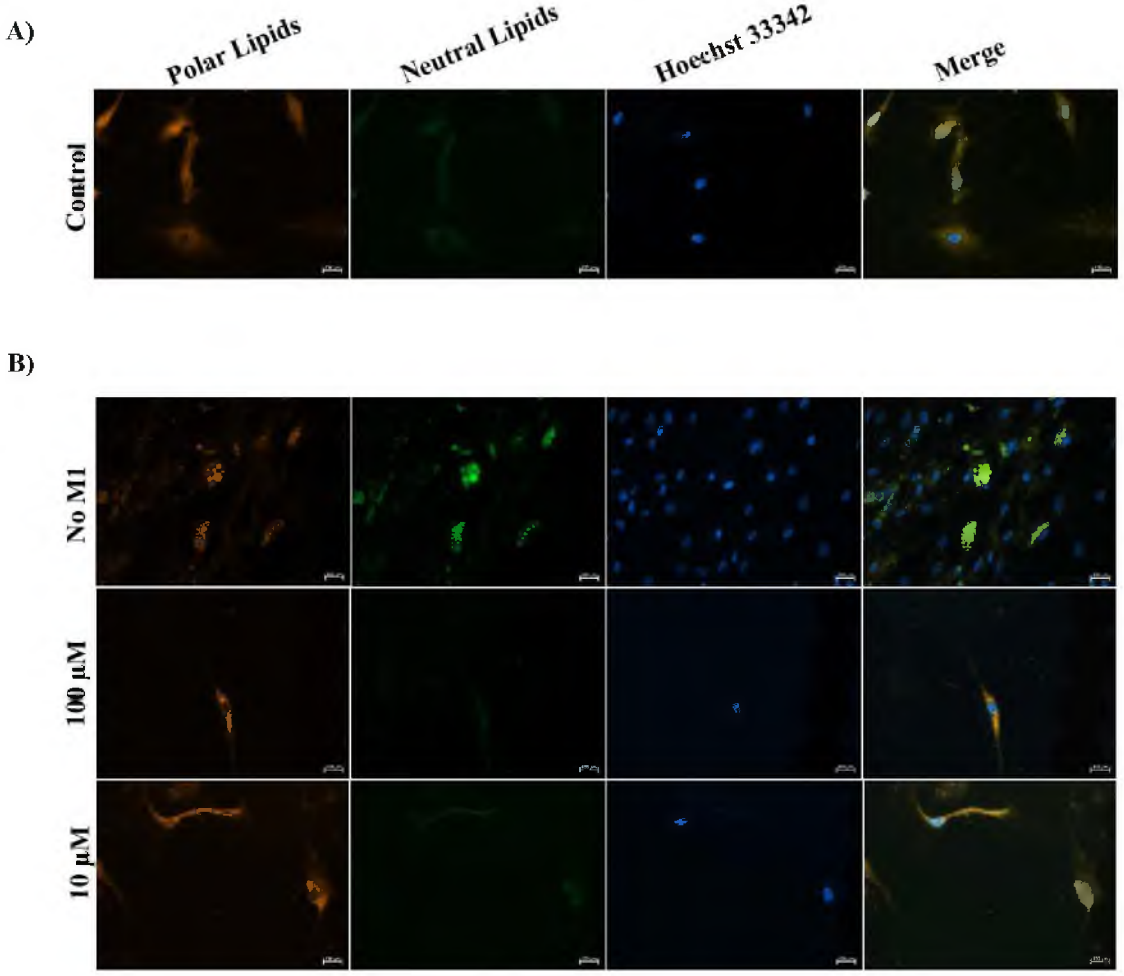


**Figure 3-11. The effects of the mitochondrial M1 fusion promoter throughout the course of adipogenesis.** HMSC-ad cells were seeded onto a plate and allowed to settle and reach confluency, after which adipogenesis was induced using the induction medium in combination with varying concentrations of the M1 fusion promoter. A) represents the undifferentiated hMSC-ad control, B) represents the course of adipogenesis which occurred over a total of 12 days within/without the presence of the M1 fusion promoter. Images were captured using the Zeiss AxioVert.A1 FL-LED Fluorescence Microscope at 200x magnification. Images shown are representative of multiple images acquired (N = 3) at random locations within the culture vessel. Scale bar = 100 µm.

In order to confirm a successful adipogenic differentiation, the cells were stained using Nile Red as it had provided with suitable recognition of, not only cellular morphology, but of the lipid droplets (as shown in Figure 3-11 where N = 3). The mitochondrial M1 fusion promoter was added to the undifferentiated hMSC-ad cells in addition to the adipogenic induction medium (INS/ROSI/DEX/IBMX), and the cells were left to differentiate in the presence of the M1 fusion promoter throughout the course of approximately 12 days, after which the results were observed using the Nile Red fluorescent stain. The control consisted of differentiating hMSC-ad cells left untreated for M1; these cells exhibited the successful differentiation into early adipocytes, indicative by the formation of multiple neutral lipid droplets highlighted within Figure 3-11.B. This was further reinforced by the acquisition of typical morphological traits, such as the rounded features, associated with adipocytes. This, therefore, indicated that both induction and maintenance media provided sufficient factors to push the hMSC-ad cells towards differentiation.

The treatment of M1 occurred throughout differentiation with fresh M1 being added every medium change; however, all concentrations exhibited an inhibition of neutral lipids, which is most likely, due to the inhibition of adipogenesis and lipogenesis. This was, again, reinforced by multiple factors, including the retention of the spindle-like, fusiform morphology previously seen during light microscopy, as well as the lack of neutral lipids formed. In addition to the inhibited differentiation, there was also a decreased cell survival whereby within a single well, which was once 100 % confluent with undifferentiated hMSC-ad cells, only a few single cells were observed. No cells were present within concentrations 50 μM and 25 μM, which may have been the result of excessive washing during the staining process, a lack of adherence caused by a disruption in mitochondrial dynamics, and/or induced apoptosis due to an increased mitochondrial fusion and/or stress rate.

### 3-2-2. B. Use of ACEA xCELLigence RTCA system for monitoring the effects of the mitochondrial M1 fusion promoter on adipocyte differentiation.

As per the xCELLigence RTCA protocols mentioned previously, this unique system was utilized in order to gain further insight into the effects that an over-stimulation of mitochondrial fusion may have on undifferentiated and differentiated hMSC-ad cell lines. The hMSC-ad cells were seeded using hMSC-ad maintenance medium (MSCM) at a density of 5 000 cells/well. Undifferentiating hMSC-ad cells were permitted to settle for 24 hours after a media change occurred in order to remove residual trypsin from previous sub culturing methods. The control was allocated a specific row in the system; this consisted of non-differentiating hMSC-ad cells that remained untreated for M1 throughout the course of the experiment. The initial curve that was presented was similar to that documented as the control sample for non-differentiating hMSC-ad cells seen in the previous S3I-201 studies. An initial increase in Cell Index (CI), followed by a plateau, was noted; this was indicative of the cells settling on the surface of the xCELLigence plate. Following the initial 24 hours allocated to allow cells to settle, a medium change occurred; this resulted in a slight drop in CI which was quickly rectified as the hMSC-ad cells continued to proliferate within the fresh medium. The experiment continued for approximate time period of 48 hours, in order for a sufficient allocation of time to be established for the exposure of M1 mitochondrial fusion promoter to the remaining samples.

The addition of the mitochondrial fusion promoter, shown in Figure 3-12, occurred in varying concentrations of 100 μM, 50 μM, 25 μM, and 10 μM. The resulting curves generated for 100 μM, 50 μM, and 25 μM were fairly conclusive in terms of cell death; when the cell index reached 0, it represents cell death or loss of adhesion. The curves for these concentrations initially followed a similar increase in CI when compared to that observed in the control; however, when M1 concentrations were added to the medium (as shown by the highlighted region in Figure 3-12), the cells were unable to recover and CI growth curves demonstrated a definite decrease. The sharpness of this decline was proportional to the concentrations used; 100 μM treatment demonstrated the most drastic decrease in CI with an almost instantaneous cell death observed, whereas 25 μM underwent a constant decline over a longer period of time.

The 10 μM sample also provided a general decline in cell survival; however, with this lower concentration, the cells did not undergo an almost instantaneous death. The observation of this drastic decline in cellular viability provided means to develop a preliminary $IC_{50}$ value to determine non-lethal concentrations of M1 required for the cells; this $IC_{50}$ value consisted of the 4 concentrations previously mentioned, and was calculated, as shown in Figure 3-13, to provide a value of 5.4794 μM. From this, it can be easily concluded that the aforementioned concentrations used here and throughout the study were extremely toxic to the cells, therefore, providing vast amounts of cell death. Future work would include the use of lower concentrations that may slightly exceed the $IC_{50}$ generated, and may be slightly decreased.

The cells were prepared for adipogenic differentiation as previously mentioned; however, instead of S3I-201, the mitochondrial M1 fusion promoter was used. When the differentiation cocktail was added to the hMSC-ad cells, an immediate change in overall growth was observed when compared to the curves generated for undifferentiated hMSC-ad cells. Figure 3-14 demonstrates the resulting graphs generated from the ACEA xCELLigence RTCA SP software; the red represents the control, which consists of differentiating hMSC-ad cells that were left untreated for M1. The typical growth curve, as noted in previous work by Kramer and colleagues (2015), was observed for adipocyte differentiation, with peaks indicative of change in medium (the first peak noted represents the change of the induction medium to the maintenance medium consisting of DMEM supplement with INS).

The mitochondrial fusion promoter was used throughout the course of adipogenesis, with fresh compound being added on each medium change, which occurred between 3 – 4 days. It was noted that the higher, toxic concentration (namely 100 μM M1, depicted using green) resulted in the expected cell death, similar to what was observed when added to the non-differentiating hMSC-ad cells found in Figure 3-12. Surprisingly, the mitochondrial fusion promoter, M1, displayed different results in terms of cell viability with respect to what was observed for the non-differentiating hMSC-ad cells. While the growth curves declined in CI,

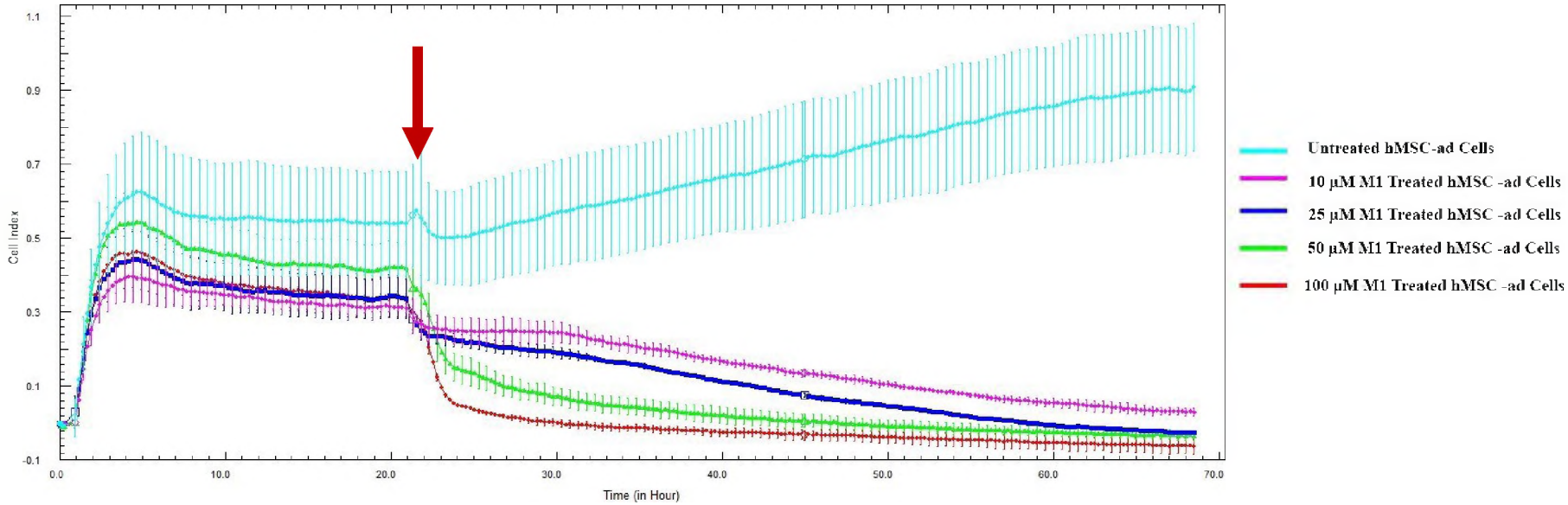


**Figure 3-12. Effects of varying concentrations of the M1 fusion promoter on hMSC-ad growth CI curves.** The cells were seeded onto the plate at a density of 5 000 cells/well, and allowed to settle for approximately 20 hours in MSCM, after which a medium change occurred whereby M1 fusion promoter was added at varying concentrations for a further approximate time of 44 hours. The highlighted region indicates the point at which the medium change, with the addition of M1, occurred. All curves were plotted as an average of 6 treatments per concentration; graphs were constructed using the ACEA xCELLigence RTCA SP software. (N = 2)

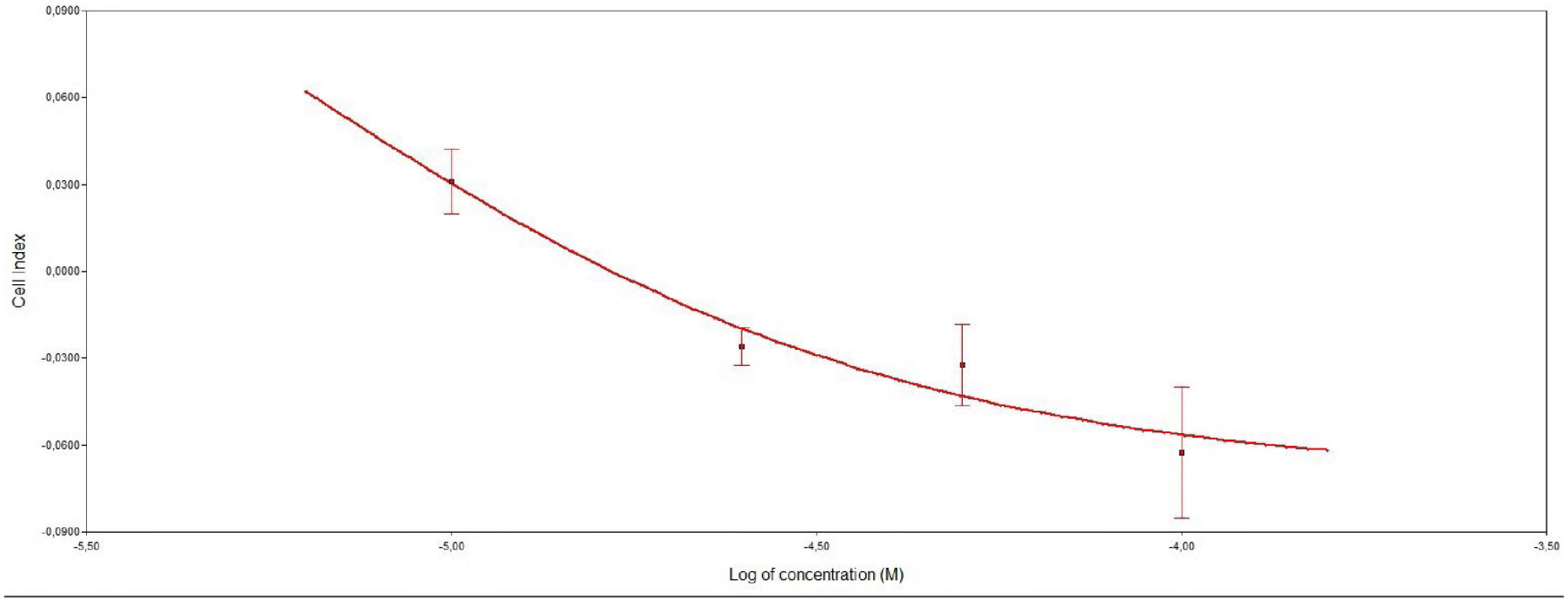


**Figure 3-13. The preliminary $IC_{50}$ values calculated for the addition of the mitochondrial fusion promoter, M1, to hMSC-ad cells.** Using the resulting data for the addition of mitochondrial fusion promoter, M1, at varying concentrations, a basic $IC_{50}$ could be established in order to better interpret the effects of M1 on non-differentiating and differentiating hMSC-ad cell lines. The $IC_{50}$ generated a value of 5.474 μM using the RTCA SP software provided by the ACEA xCELLigence.

compared to the control, for concentrations 25 μM and 10 μM, cell death was not the overall outcome. The cells were subjected to an overall decrease in numbers (CI), however, after approximately 217 hours when the medium was changed and fresh M1 was added, the cells seemed to experience a slight adjustment and formed a plateau with a very slight increase occurring around 280 hours of adipogenesis in the presence of M1. Another observation made, in contrast to the control, was the overall shape and trend of the graphs generated; while cell death did occur, the resulting graphs may suggest that the hMSC-ad cells did undergo some degree of differentiation or morphological changes; albeit, this may not have been exclusively evident using certain microscopy methods. It could be assumed that hMSC-ad cells adopted a different phenotype during the adipogenesis differentiation, or that a minimal population of cells did undergo adipogenesis but the majority were inhibited for differentiation. Further analysis is required in order to successfully determine the effects that the M1 fusion promoter may have on differentiating hMSC-ad cells, especially with regards to the mitochondrial networks established during differentiation.

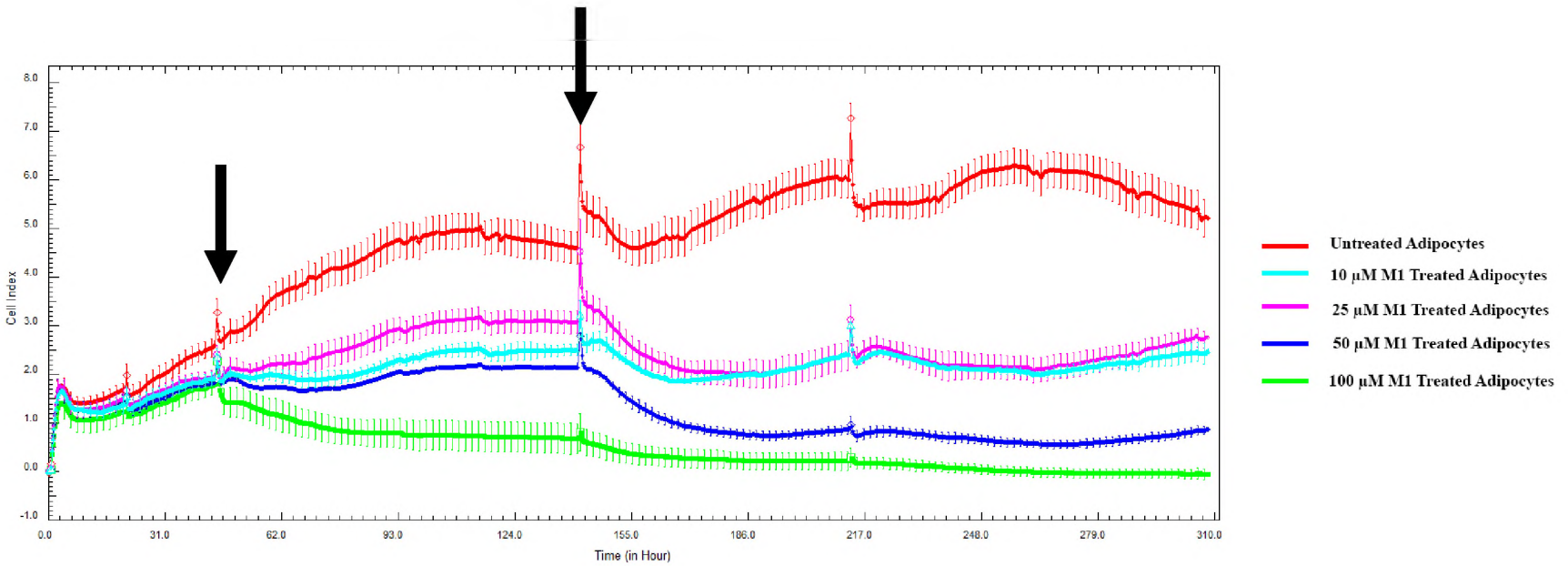


**Figure 3-14. Effects of varying concentrations of the mitochondrial M1 fusion promoter on adipogenic differentiating hMSC-ad growth CI curves.** The cells were seeded onto the plate at a density of 5 000 cells/well, and allowed to settle for 24 hours in MSCM, after which a medium change occurred whereby the mitochondrial fusion promoter, M1, was added at varying concentrations. The highlighted section demonstrates the point of time at which adipogenesis was induced and maintained with the addition of fresh M1 fusion promoter. All curves were plotted as an average of 6 treatments per concentration; graphs were constructed using the ACEA xCELLigence RTCA SP software. (N = 2)

## 3-2-3. The confirmation of the induction of adipogenesis with/without the presence of the mitochondrial fission inhibitor, Mdivi-1.

### 3-2-3. A. Morphological Changes Associated with Adipogenesis and Lipogenesis

The resulting effects on undifferentiating and differentiating hMSC-ad cells were observed using light and fluorescent microscopy. The differentiation induction and maintenance protocol was kept consistent throughout all experiments performed with the various small molecules; however, in this case, Mdivi-1, a mitochondrial fission inhibitor, was utilized and added into the induction medium and maintenance medium used throughout. The control consisted of adipocyte differentiating hMSC-ad cells that remained untreated for Mdivi-1; adipogenesis was initially maintained for a total of 12 days, as previously exhibited. The control (N = 2) provided successful indication, using basic light microscopy, of adipogenesis occurring due to the acquisition of cellular morphologies commonly associated with adipocytes; in addition to this, collections of lipid droplets were evident in the acquired images, as highlighted by the arrows present in Figure 3-15 for the "No Mdivi-1" panel. This provided a basic guideline as to the visual phenotypical traits required for differentiation to be met.

Upon the addition of Mdivi-1 to both induction and maintenance media, little/no deleterious effects were observed in contrast to the lethal effects observed when the cells were treated with M1, mitochondrial fusion promoter. For all concentrations, ranging from 100 μM to 10 μM, the accumulation of lipid droplets was observed in addition to morphological traits commonly associated with adipocytes. Albeit, for the 10 μM Mdivi-1 treatment, the lipid droplets were not as distinctive. This may have been the result of rough handling during medium changes.

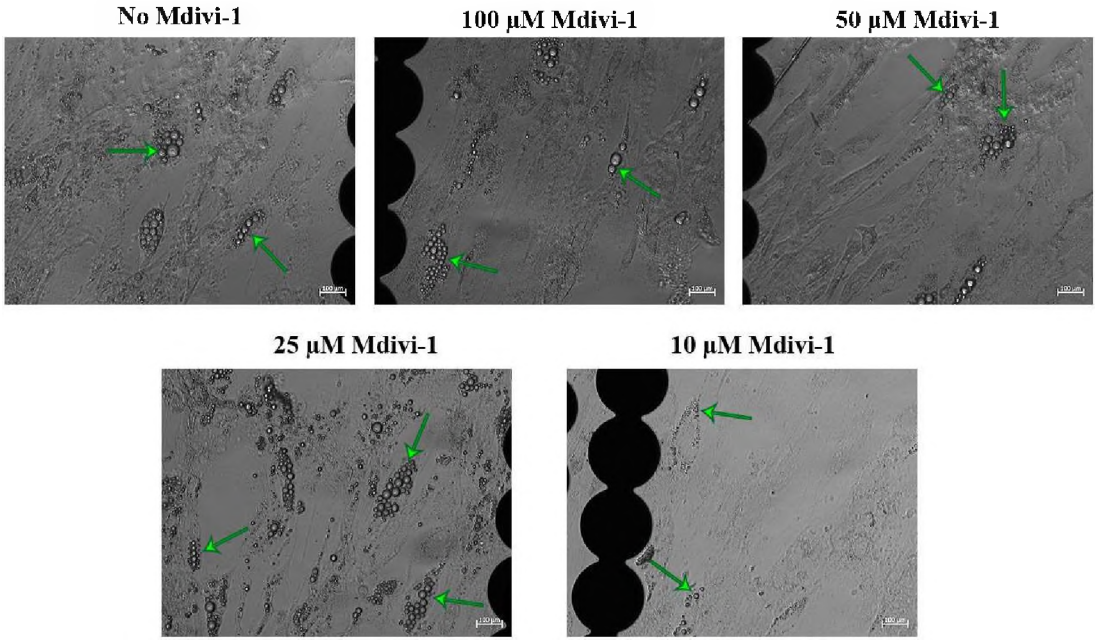


**Figure 3-15. Morphological effects of Mdivi-1, mitochondrial fission inhibitor, on adipogenesis after 12 days.** Adipocyte differentiation was captured upon day 12 after adipogenesis was induced in combination with the presence/absence of varying concentrations of a mitochondrial fission inhibitor, Mdivi-1. Arrows represent the areas of lipid formation and accumulation observed. Images were obtained using the bright field image capture on the Zeiss AxioVert.A1 FL-LED Fluorescence Microscope at 200x magnification. Scale bars = 20 µm. Images shown are representative of multiple images acquired (N = 2) captured at random locations within the culture vessel.

Mdivi-1 (a mitochondrial division inhibitor-1) is a chemical division inhibitor that specifically inhibits the Drp1 function through blocking GTPase activity, and, thus, halting Drp1 self-assembly into the ring-like structures around the mitochondria, which is used during the pinching of the membrane and mitochondrial fission during division (Kim et al., 2016; Cassidy-Stone et al., 2008; Jheng et al., 2012). It is believed that Mdivi-1 may have therapeutic advantages by the inhibition of excessive mitochondrial fragmentation (Kim et al., 2016). Mdivi-1 is also believed to be a neuroprotective agent, as demonstrated by Kim and colleagues (2016) whereby they determined that this fission inhibitor aided in decreased neuro-inflammation and neuronal death within the hippocampus of kainic acid-treatedmice.

Parkin is a ubiquitin-protein ligase responsible for the regulation of mitochondrial morphology, and may produce enlarged and/or swollen mitochondria if Drp1-mediated fission is blocked (Kim et al., 2016).

When treated with Mdivi-1 fission inhibitor, the mitochondrial inner and outer membranes were severely compromised, as well as the mitochondria were of all different sizes. It is known that when mitochondrial membranes are defective, impairments in mitochondrial membrane potential, as well as other mitochondrial functions, occur (Kim et al., 2016).

It was hypothesized that treatment with Mdivi-1 throughout the adipogenic process would subtly inhibit the formation of lipid droplets and differentiation into adipocytes, due to the deficiency of Drp1 action and, thus, the resulting lack of mitochondrial fission; an increase of mitochondria and mitochondrial energy is required for adipogenesis. However, upon the repeated treatments of Mdivi-1 (treatments occurred every 3 – 4 days with the maintenance media change) adipogenesis was not inhibited in any form; in fact, the inclusion of Mdivi-1 seemed to increase the rate of lipogenesis, as an increased amount of lipid accumulation was observed. However, this is not a definitive conclusion as the Mdivi-1 half-life must be taken into account under all circumstances. While the Mdivi-1 half-life experienced within human adipose-derived mesenchymal stromal cells has not been extensively studied; multiple cell lines have been used to determine the Mdivi-1 half-life. These cell lines included cardiomyocytes, vascular cells, neurons, skeletal myoblasts, and cancer cells (Rappold et al., 2014; Rosdah et al., 2016). From in vitro and in vivo experiments, it was demonstrated that Mdivi-1 presented with a half-life of approximately 8.9 hours within the brain, and ranged between 6 – 24 hours for in vitro cell lines. There have been few studies performed that demonstrate an accurate half-life for adipocytes and the hMSC-ad cell lines; however, it may be speculated that the half-life may fall within the in vitro range. With this information in mind, it may be further speculated that while it appeared that Mdivi-1 had little/no deleterious effect on the overall cell growth, mitochondrial compensation may have rectified the damage done in order to produce a healthy mitochondrial progeny once the effects of Mdivi-1 wore off.

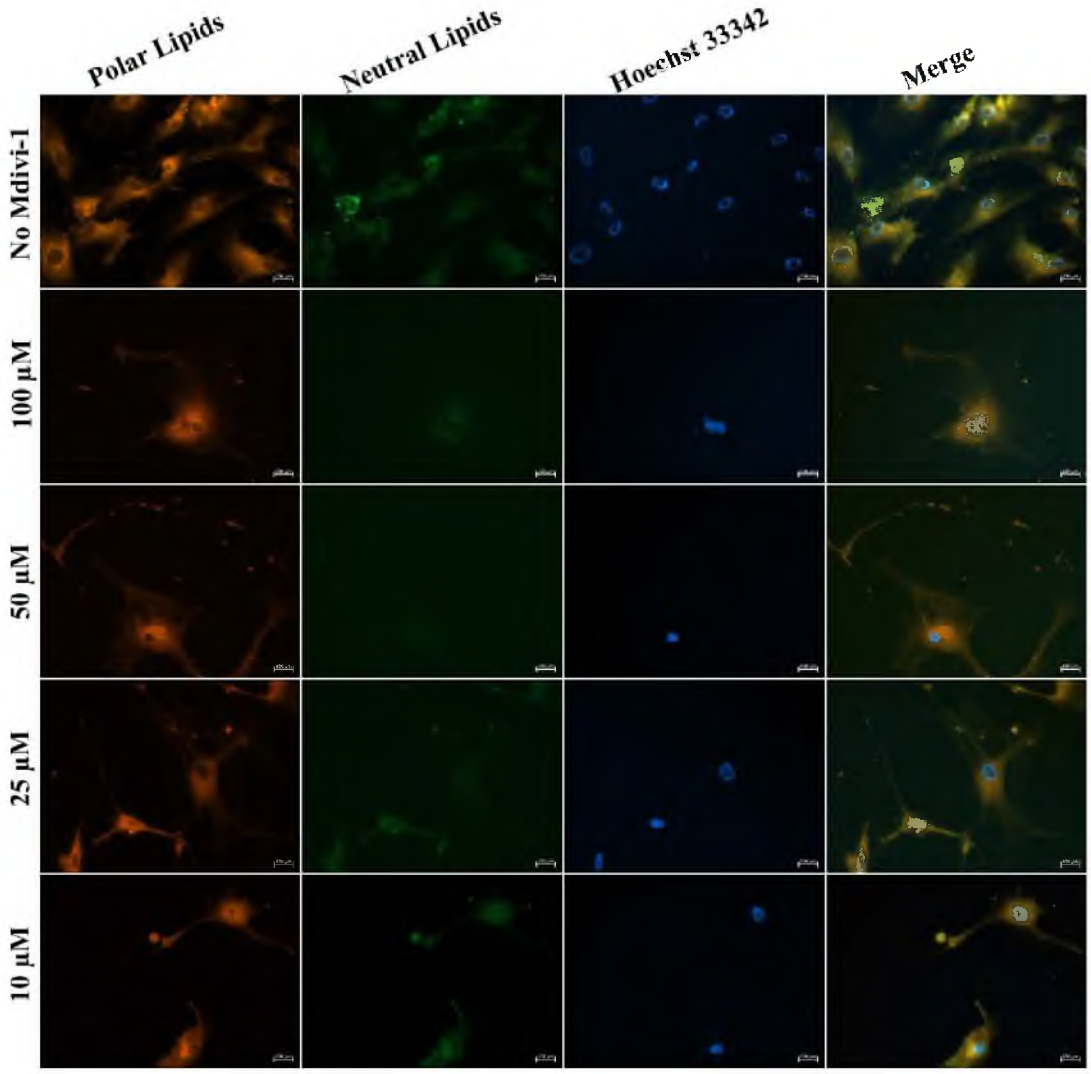


**Figure 3-16. The resulting effects of the mitochondrial fission inhibitor, Mdivi-1, on hMSC-ad cells after 24 hours of exposure.** The hMSC-ad cells were seeded onto a plate and allowed to settle for 24 hours, after which a medium change occurred. The cells were left to grow for an additional 24 hours without the presence of Mdivi-1. The fission inhibitor was then added and the effects were observed after 24 hours. The control represents no Mdivi-1. Images were captured using the Zeiss AxioVert.A1 FL-LED Fluorescence Microscope at 200x magnification. Images shown are representative of multiple images acquired (N = 3) at random locations within the culture vessel. Scale bar = 20 µm.

A control was established by means of the inclusion of untreated hMSC-ad non-differentiating cells; this would serve as the guide line that may aid in the interpretation of the effects that Mdivi-1 may have on undifferentiated hMSC-ad cells. The control consists of human adipose derived mesenchymal stromal cells that exhibit the typical fibroblastic morphologies; as shown throughout this study, the untreated hMSC-ad cells (N = 3) are mainly composed of polar lipids, as exhibited in Figure 3-16, however, they do display some indication of neutral lipids. This, in turn, creates a golden colour when superimposed. Upon the addition of Mdivi-1 to the non-differentiating hMSC-ad cells, an alteration in this fluorescence was observed; with an increase in Mdivi-1 concentration, there was an increase in the resulting superimposed polar lipid fluorescence. This was the result of the decrease in neutral lipids displayed as the Mdivi-1 concentration was increased for non-differentiating hMSC-ad cells. In addition to this observation, it was also noted that there was perinuclear localization of neutral lipids for the 10 μM Mdivi-1 treatment. However, in all instances, the non-differentiating hMSC-ad cells seemed to maintain their fibroblastic morphologies; limited cell death was observed, thereby leading to the conclusion that Mdivi-1 may not have deleterious effects on hMSC-ad cells. Albeit, it must be acknowledged that cell survival may have been maintained due to the proposed half-life of Mdivi-1 within hMSC-ad cells in vitro. Within the panel of 100 μM treatment with Mdivi-1, it is clear that the cell is either undergoing mitosis, due to the presence of the double nuclei; however, this may also be the result of cell-to-cell fusion. Cell-to-cell fusion is a vital process utilized in fertilization, skeletal muscle formation, and bone development (Sottile et al., 2016). Such a process is evident in the generation of regenerative bone marrow-derived hybrids, which are utilized in the restoration of many tissues. Albeit, this restorative process may also be associated with the development of cancers and metastasis formation (Sottile et al., 2016). A form of this interaction comes in the form of entosis; cells actively seek to invade another cell due to a deficit in the cell-matrix adhesive properties. Sottile and colleagues (2016) reported the invasion of mouse embryonic stem cells into mesenchymal stem cells; mesenchymal stem

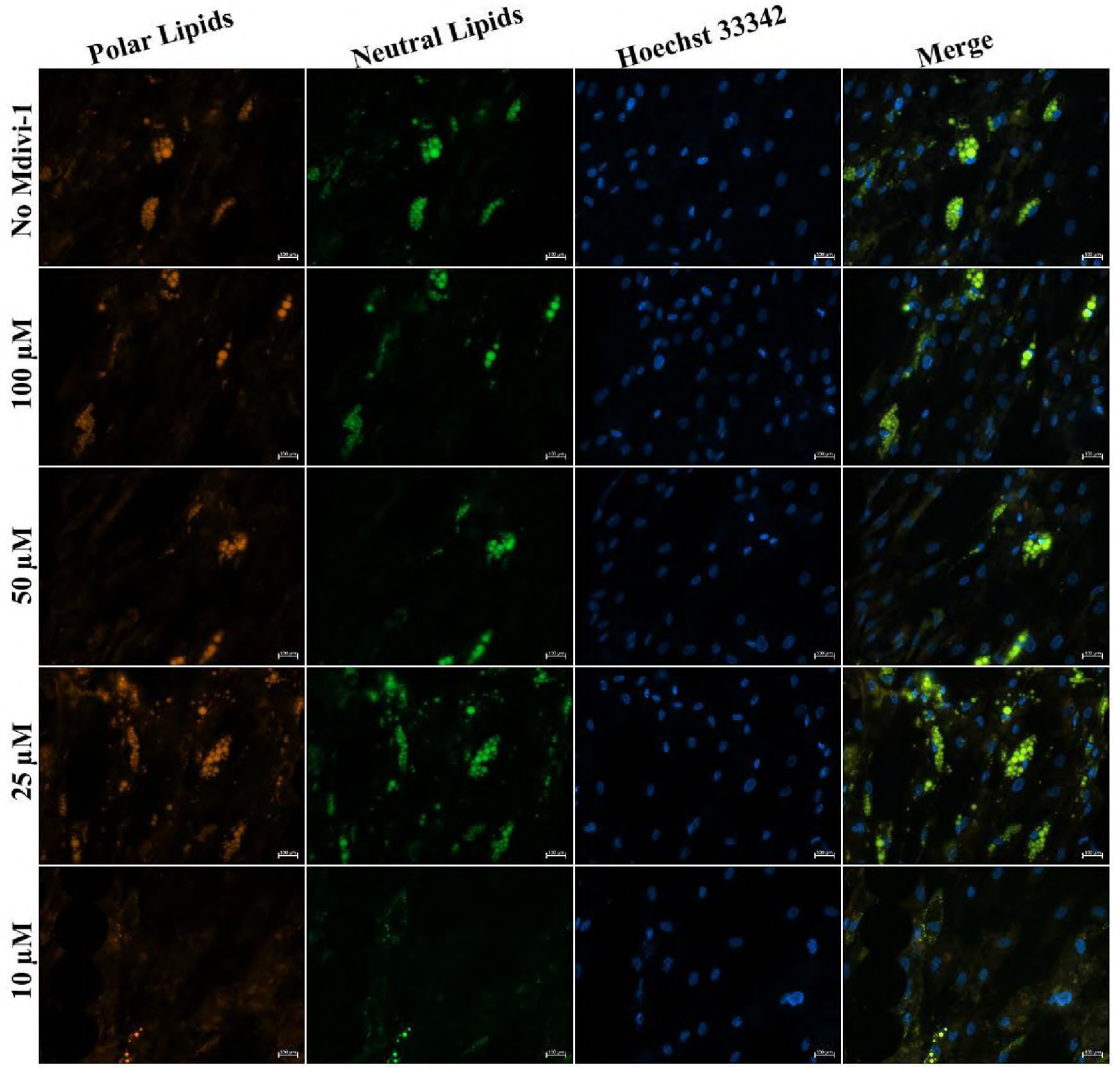


**Figure 3-17. The resulting effects of the mitochondrial fission inhibitor, Mdivi-1, on adipogenic differentiating cells after 12 days of exposure.** The hMSC-ad cells were seeded onto a plate and allowed to settle for 24 hours, after which a medium change occurred. The cells were left to grow until confluent after which the induction medium and concentrations of Mdivi-1 were added. Adipogenic differentiation was permitted to occur over 12 days before observations were recorded. The control represents no Mdivi-1. Images were captured using the Zeiss AxioVert.A1 FL-LED Fluorescence Microscope at 200x magnification. Images shown are representative of multiple images acquired (N = 2) at random locations within the culture vessel. Scale bar = 20 µm.

cells also presented with the ability of fusion, thus, producing heterokaryons. In the aforementioned study, Sottile and colleagues (2016) also noted that nuclear membranes did not undergo fusion, whereas, cytoplasmic membranes underwent fusion.

The hMSC-ad cells were induced for differentiation using the aforementioned differentiation induction medium; excluding the control, this medium was supplemented with varying concentrations of Mdivi-1 mitochondrial fission inhibitor (N = 2). The control was not treated with Mdivi-1 and represented differentiation under general conditions. Figure 3-17 depicts the differentiation of hMSC-ad cells to adipocytes in the presence of the Mdivi-1 compound; the control demonstrated the accumulation of lipid droplets, indicative of lipogenesis, a process commonly associated with the formation of adipocytes. In addition to this, the cells adopted a morphology that was similar to that previously described for adipocytes. The superimposed images provide clear indication that the formation of neutral lipids was successful. The addition of Mdivi-1 to the induction medium (and maintenance medium) provided very little/no deleterious effects on the formation of neutral lipids; this was observed for all concentrations within Figure 3-17, especially that of the 100 μM. This was unexpected due to the effect that Mdivi-1 has on mitochondrial fission, which has been deemed an important trait of differentiation due to the increased requirement of ATP energy throughout the process; however, once again, this result may be attributed to the Mdivi-1 half-life previously discussed. Initial inhibition may have occurred while the compound was still active, however, the resulting damage could have been overcome in order to promote the development of the healthy phenotypes observed throughout Figure 3-17. As an aside, the addition of 25 μM Mdivi-1 throughout adipogenesis provided the largest accumulation of lipid droplets in relation to the untreated control.

### 3-2-3. B. Use of ACEA xCELLigence RTCA system for monitoring the effects of the mitochondrial fission inhibitor, Mdivi-1, on adipocyte differentiation.

As per the ACEA xCELLigence RTCA SP protocols mentioned previously, this system was utilized in order to gain further insight into the effects that the inhibition of mitochondrial fission may have on both non-differentiating and adipogenic differentiating hMSC-ad cell lines. The hMSC-ad cells were seeded using hMSC-ad maintenance medium (MSCM) at a cell density of approximately 5 000 cells per well. As demonstrated previously, the control

consisted of untreated hMSC-ad non differentiating cells, as shown by the red in Figure 3-18, which possessed an increased initial peak and plateau, suggestive of the attachment of the undifferentiated hMSC-ad cells to the culture vessel. The cells were permitted to settle for 24 hours, after which they were subjected to a medium change in order to remove the residual trypsin from previous sub-culturing methods. The general trend of CI experienced a gradual, consistent increase during the additional 44 hours allocated.

Mdivi-1 was added into the medium utilized during the first medium change after the initial 24hour period. The resulting curves generated coincided closely with that provided by the untreated control; looking more closely, it was evident that a slightly increased decline was noted upon the initial addition of Mdivi-1 to the non-differentiating cells. However, the cells were soon able to recuperate and a general increase in trend was experienced, albeit, it remained lower than the control (shown in red), with the exception of the 100 μM Mdivi-1 treated sample (shown in green). The average trend seemed to almost identically mimic that of the untreated control, and upon initial treatment of the mitochondrial fission inhibitor, a slight increase in CI was observed, before the 100 μM Mdivi-1 treated cells responded in a similar trend to that of the control, decreasing slightly in CI at approximately 60 hours into the experiment.

A preliminary $IC_{50}$ was established using the concentrations of Mdivi-1 utilized throughout the course of this study; the resulting $IC_{50}$ value calculated was approximately 15.068 mM. This suggests that the hMSC-ad cells were able to recover quite easily from the initial stress/damage induced by non-lethal concentrations of the mitochondrial fission inhibitor, due to the fact that the concentrations used were considerably lower than the established $IC_{50}$; however, additional experiments and repeated trials would be required in order to confirm this $IC_{50}$ value.

Adipogenesis was induced within the hMSC-ad cells while in the presence of Mdivi-1. Originally, the cells were seeded and cultured as mentioned previously; however, upon induction of adipogenesis, Mdivi-1 was added into the induction medium and fresh Mdivi-1 was maintained in the maintenance medium upon each change. The resulting xCELLigence graphs generated during adipogenesis are shown in Figure 3-20.

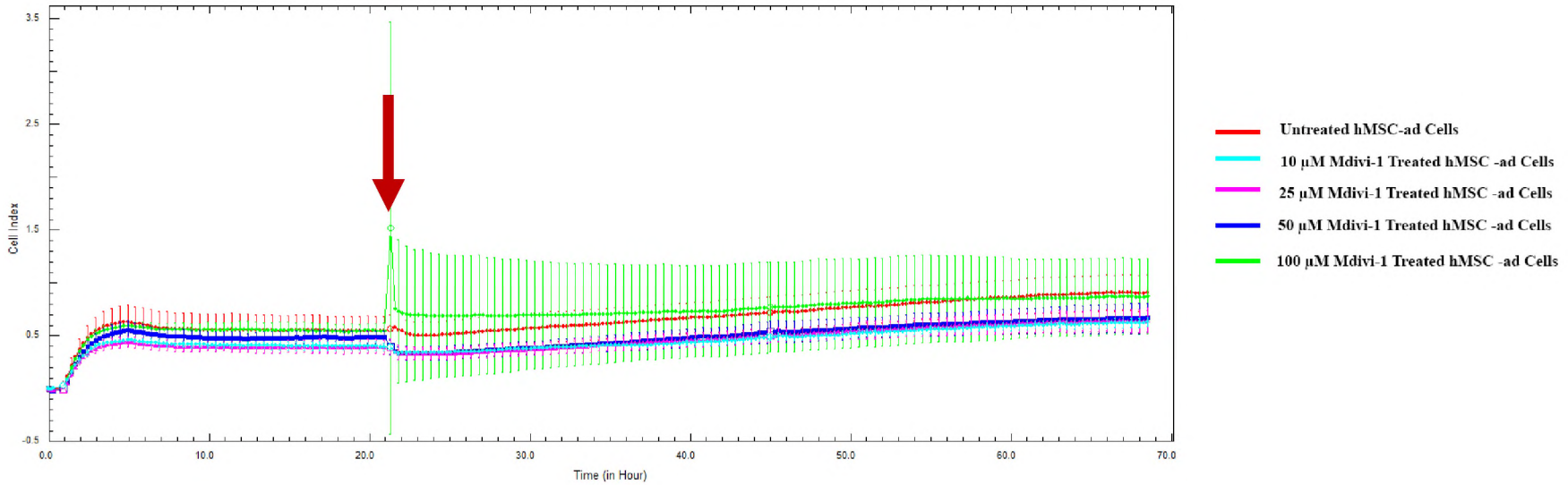


**Figure 3-18. Effects of varying concentrations of Mdivi-1 fission inhibitor on hMSC-ad growth CI curves.** The cells were seeded onto the plate at a density of 5 000 cells/well, and allowed to settle for 24 hours in MSCM, after which a medium change occurred whereby mitochondrial fission inhibitor, Mdivi-1, was added at varying concentrations; this point was indicated with use of an arrow. All curves were plotted as an average of 3 treatments per concentration; graphs were constructed using the ACEA xCELLigence RTCA SP software. (N = 2)

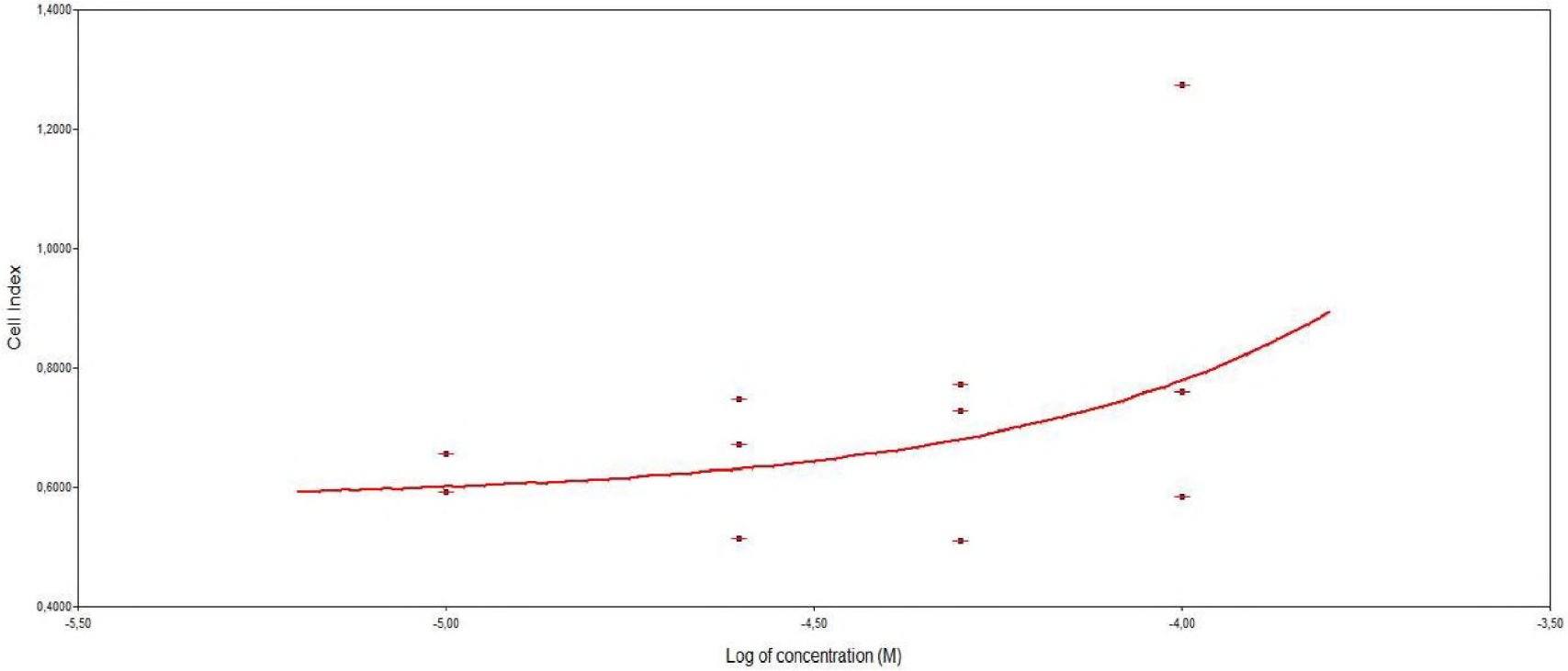


**Figure 3-19. The resulting preliminary $IC_{50}$ value was calculated using the concentrations of Mdivi-1 treatment of non-differentiating hMSC-ad cells.** Using the resulting data acquired upon the addition of the mitochondrial fission inhibitor, Mdivi-1, at varying concentrations, a basic $IC_{50}$ could be established in order to better interpret the effects of Mdivi-1 on non-differentiating and differentiating hMSC-ad cell lines. The $IC_{50}$ generated a value of 15.068 mM using the RTCA SP software provided by the ACEA xCELLigence.

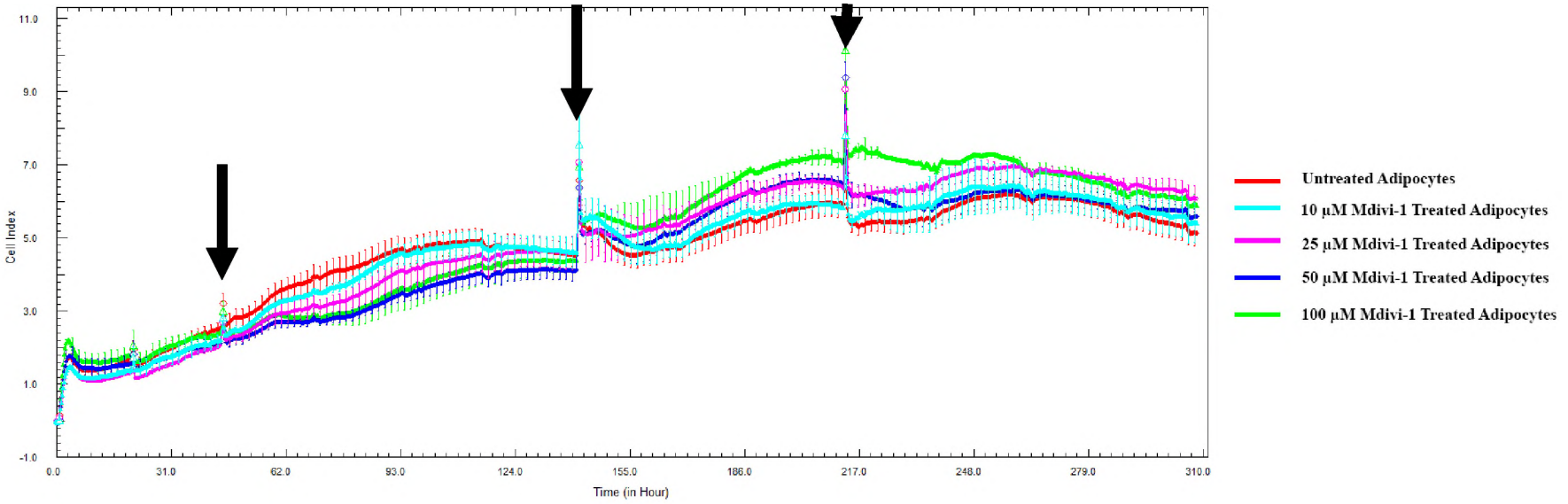


**Figure 3-20. Effects of varying concentrations of the Mdivi-1 fission inhibitor on the adipogenic differentiation growth CI curves.** The cells were seeded onto the plate at a density of 5 000 cells/well, and allowed to settle for 24 hours in MSCM, after which a medium change occurred whereby the mitochondrial fission inhibitor, Mdivi-1, was added at varying concentrations. The regions specified indicate the points at which adipogenesis was induced and maintained with fresh additions of Mdivi-1. All curves were plotted as an average of 3 treatments per concentration; graphs were constructed using the ACEA xCELLigence RTCA SP software. (N = 2)

The control consisted of untreated cells undergoing adipogenesis, and was indicated using red within the graph located in Figure 3-20. An alteration in curve was noted between non-differentiating hMSC-ad cells, and those that had been induced for adipogenesis; within this control sample a clear indication of differentiation was noted via the overall appearance of the CI growth curves established. Plateaus were established during the inhibition of proliferation during differentiation; the peaks indicated the medium change from induction medium to maintenance medium throughout the course of the 12 days during which differentiation was permitted. The general CI trend, established within the control, was commonly observed throughout the course of xCELLigence experiments.

The non-deleterious effects of Mdivi-1 were experienced through the addition of this chemical compound to both induction and maintenance media used throughout differentiation; fresh Mdivi-1 was added into the medium with each change every 3 – 4 days. Using 100 μM Mdivi1, a similar CI growth curve was generated when compared to that of the control sample; albeit, a definite decline in CI was expressed upon initial addition of the induction medium combined with the Mdivi-1. This decrease was rectified as time increased; between 124 and 155 hours, there was a definite increase in CI following the medium change and addition of Mdivi-1. The growth curve generated for 100 μM remained relatively increased for the remainder of the experiment, and was notably higher than that obtained for the control. However, it was not only the 100 μM treatment of Mdivi-1 that exceeded the growth curve generated for the untreated sample; this increased CI was experienced throughout the various concentrations of Mdivi-1 treatment. It must be acknowledged that the overall shape of the CI growth curves remained consistent with those generated for the untreated control, indicating that adipogenesis was occurring within the Mdivi-1 treated cells, thereby suggesting that Mdivi-1 does not, in fact, inhibit adipogenesis altogether. This increase in lipogenesis/adipogenesis reinforced the speculations derived from previous microscopy results. Altogether, the results shown may support speculations that mitochondrial protective properties of Mdivi-1 may play an important role in maintaining and regulating successful adipogenesis, and/or impair signalling that may try to rectify or inhibit adipogenesis. Alternatively, the results shown may simply be indicative of healthy phenotypes being established after undergoing compensation to rectify the previous mitochondrial damage inflicted upon the differentiating cells.

Mdivi-1 treatment during adipogenesis provided surprising results due to the fact that adipogenesis was not inhibited, as originally hypothesized. In fact, it may be speculated that Mdivi-1 treatment enhanced certain aspects of adipogenesis, namely the hereby accumulation of lipid droplets within the cell cytoplasm. These results may, once again, indicate the protective properties of Mdivi-1 against mitochondrial fragmentation, as stated by Jheng and colleagues (2012), whereby inhibition of Drp1 prevents a decrease in mitochondrial membrane potential and blocks the release of cytochrome c, which is used in the signalling of apoptosis. This could further be used to explain any additional advantages of non-lethal amounts of Mdivi-1 in adipogenesis. However, it must be noted that the concentrations used in this study were well below the preliminary $IC_{50}$ established; therefore, should these concentrations increase to more lethal doses, the original hypothesis of adipogenesis inhibition and decreased growth of non-differentiating hMSC-ad cells may still be applicable. Further experiments would be required in order to conclude these results.

### 3-2-4. The validation of adipogenesis while in the presence/absence of certain small molecules within an increased hypoxic environment

#### 3-2-4. A. Morphological Changes During Adipogenesis and Lipogenesis

In addition to the small molecule compounds, as mentioned previously, the non-differentiating and differentiating hMSC-ad cells were exposed to cobalt chloride in order to create a chemical-induced hypoxic environment, which is known to effect various characteristics of stem and progenitor cells, as well as their ability to differentiate into their selected progeny (Grayson et al., 2007; Ren et al., 2006). The cobalt chloride was freshly made upon each administration during the allocated medium changes throughout the course of differentiation and/or cell culture. A consistent concentration of 100 µM was maintained throughout all experiments. This chemically-induced form of hypoxia was mainly paired with the inhibition of STAT3 using S3I-201.

Adipogenesis was permitted to occur utilizing protocols as mentioned previously, with the inclusion of cobalt chloride and the relevant compounds (S3I-201, M1, or Mdivi-1). Figure 3-21 depicts the resulting degree of adipogenesis to occur when differentiating hMSC-ad

cells were exposed to a combination of 100 µM and varying concentrations of S3I-201 (N = 2).

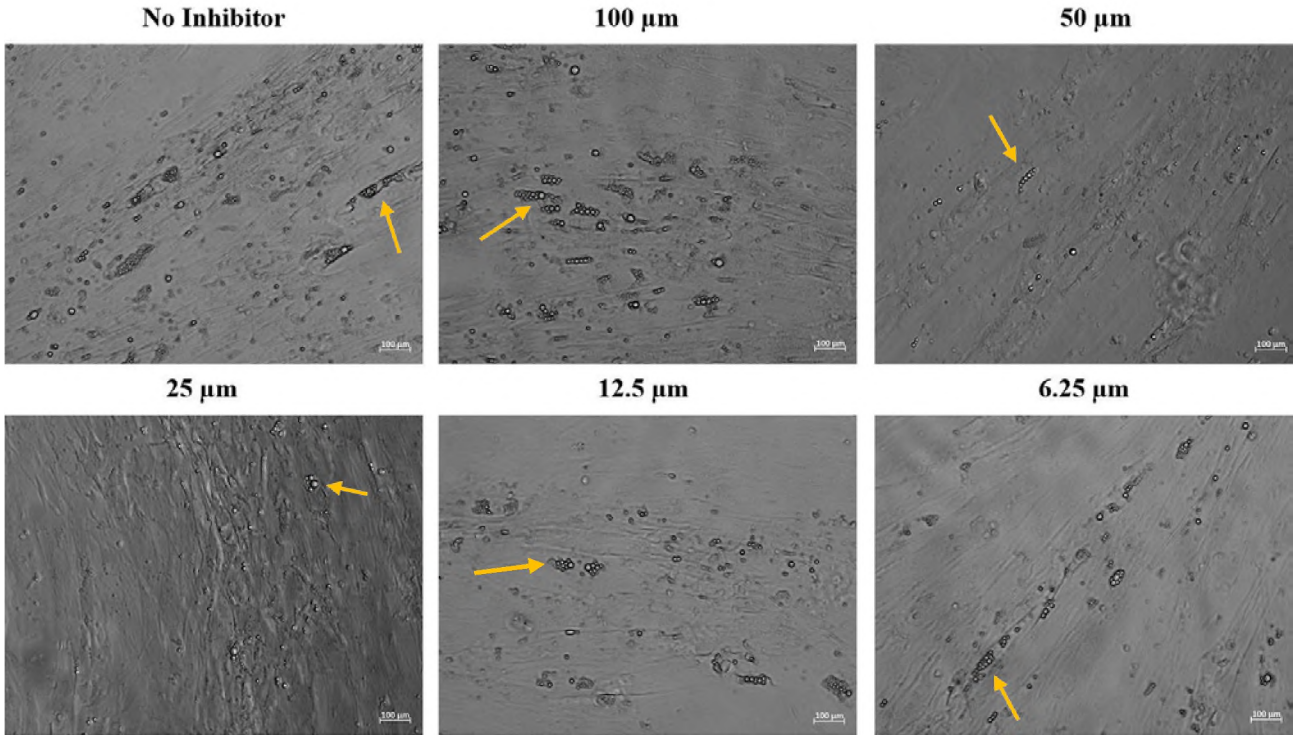


**Figure 3-21. Morphological changes observed during the induction of adipogenesis while in the presence of a STAT3 inhibitor and Cobalt Chloride.** Adipocyte differentiation was captured upon day 6 after adipogenesis was induced in combination with the presence/absence of varying concentrations of a STAT3 inhibitor (S3I-201) in combination with 100 µM cobalt chloride to chemically induce hypoxia. Arrows represent the areas of lipid formation and accumulation observed. Images were obtained using the phase contrast 2 filter on the Zeiss AxioVert.A1 FL-LED Fluorescence Microscope at 200x magnification. Scale bars = 20 µm. Images shown are representative of multiple images acquired (N = 2).

Due to the fact that previous experiments included the differentiating cells untreated with cobalt chloride, the control utilized, in this circumstance, consisted of differentiating hMSC-ad cells treated only with the 100 µM cobalt chloride in order to determine what effect this chemically induced hypoxic environment may have on adipogenic differentiating hMSC-ad

cells. It was hypothesized, using studies performed by Kramer and colleagues (2015), that an increased state of hypoxia would inhibit the rate of adipogenesis due to the fact that the mesenchymal stromal cells would attempt to retain their self-renewing properties. The resulting adipogenesis formed can be compared to that observed in the previous studies that excluded this chemical compound; unlike what was expected, there seemed to be some lipid accumulation indicative of successful adipogenesis, as demonstrated by the arrows highlighted in Figure 3-20. Upon the addition of the varying concentrations of S3I-201 there seemed to be no indication of inhibition of lipogenesis nor adipogenesis, when using light microscopy. In fact, the addition of S3I-201 seemed to promote the development of more 'neatly' clustered, generally smaller, lipid droplets that often presented with a singular lipid droplet that was larger than the surrounding cluster of accumulating fat. In order to further determine the resulting degree of adipogenesis, nile red and Oil Red O staining was performed.

Figure 3-22 depicts the resulting nile red stain performed in which both polar and neutral lipids were stained and viewed using fluorescence microscopy. Here, two controls were utilized; the first (demonstrated in Figure 3-22. A.) consisted of undifferentiated hMSC-ad cells exposed to the treatment of 100 μM cobalt chloride; this provided some indication as to the effects that chemically induced hypoxia may have on the undifferentiated hMSC-ad cells that were utilized for differentiation. The control provided minimal fluorescence of the neutral lipids, which, in contrast to undifferentiated hMSC-ad cells used previously (those that had not been exposed to chemically induced hypoxia), it was evident that there was a significant decrease in neutral lipids naturally produced by the hMSC-ad cells. This was further substantiated by the lack of 'gold' colour formed upon superimposition of the images; the polar lipids underwent greater fluorescence. In addition to this control, another control was established, as shown in Figure 322. B., which included differentiating hMSC-ad cells exposed to the chemically induced hypoxia; however, they were left untreated for S3I-201. Strangely, it was evident that the chemically induced hypoxia had little/no effect on the state of lipogenesis; the cells continued to accumulate lipid droplets, as indicated by the fluorescence of these neutral lipids. This substantiated the data obtained using light microscopy in Figure 3-21.

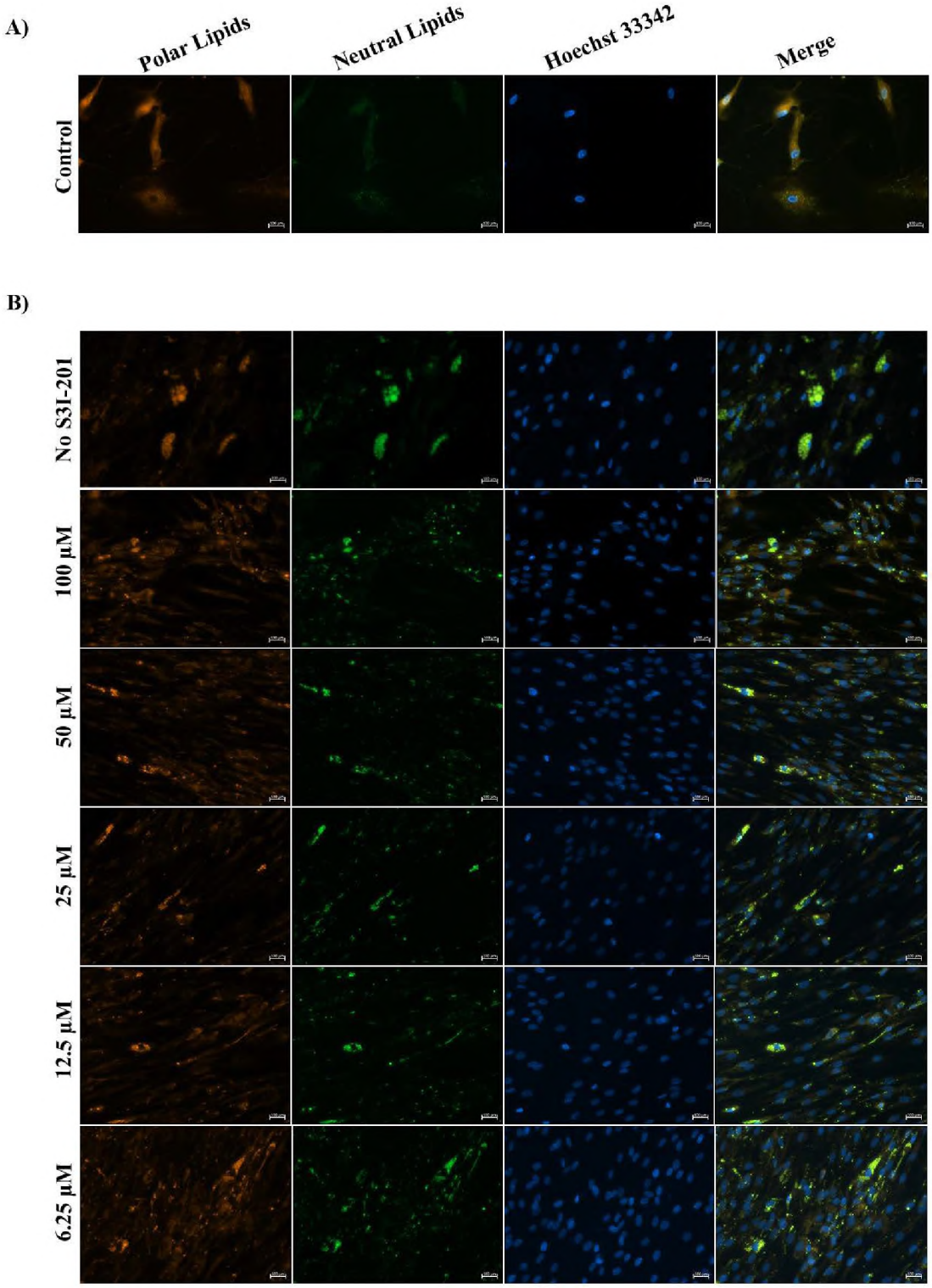


**Figure 3-22. Nile Red staining to confirm the induction of adipogenesis.** The cultures were stained on day 6 post induction in the presence/absence of varying concentrations of S3I-201. A) represents the control non-differentiating hMSC-ad cells exposed to increased hypoxic conditions, whereas B) depicts the resulting effects of S3I-201 treated adipogenic differentiating hMSC-ad cells. Images were captured using the Zeiss AxioVert.A1 FL-LED fluorescence microscope at 200x magnification. Scale Bar = 20 µm. Images shown are representative of multiple images (N = 2).

Furthermore, upon the addition of S3I-201, the differentiating hMSC-ad cells did not display any indication of the inhibition of adipogenesis nor lipogenesis; this was noted by the accumulation of neutral lipid droplets present amongst the cells. A morphology typically associated with adipocytes, as described previously, was also present amongst a population of the cells, suggesting that adipogenesis was occurring to some degree. When compared to previous experiments that excluded cobalt chloride (namely that observed in Figure 3-3), it may be noted that a minimal increase in the formation of lipids was observed for cells treated with cobalt chloride; this was particularly noted with regards to the controls that were left untreated for S3I-201. A minimal increase in lipid accumulation was noted as the S3I-201 concentrations decreased.

In order to justify the observations recorded via fluorescence microscopic methods, an additional validation stain was performed: Oil Red O. Here, the differentiating cells were stained using Oil Red O (N = 2), which is known to provide a stain that is directly proportional to the extent of cell differentiation and, thus, lipid accumulation (Ramirez-Zacarias et al., 1992). Figure 3-23 depicts an overall Oil Red O stain performed on S3I-201 treated cells that were not subjected to the chemically induced hypoxia, and those that had been additionally treated with cobalt chloride. Once again, two controls were ideally used in this scenario; the first is depicted in Figure 3-23. A., whereby the adipocyte differentiating hMSC-ad cells remained untreated for S3I-201 and cobalt chloride. These cells were permitted to differentiate under normal differentiating conditions without any additional disturbance. The resulting stain did not provide a vast collection of lipid droplets, which may have been caused by excessive washing and rough handling throughout the staining process (some of the lipids may have been washed off). The second control is found within Figure 3-23. B.; this consists of adipogenic differentiating hMSC-ad cells that have been subjected to cobalt chloride (100 μM) treatment, but remain untreated for S3I-201. Comparatively, the control observed within Figure 3-23. B. demonstrated an increased accumulation of lipids, in addition to the fact that these notable lipid droplets remained neatly clustered together, as previously described for those witnessed for light microscopy within Figure 3-21.

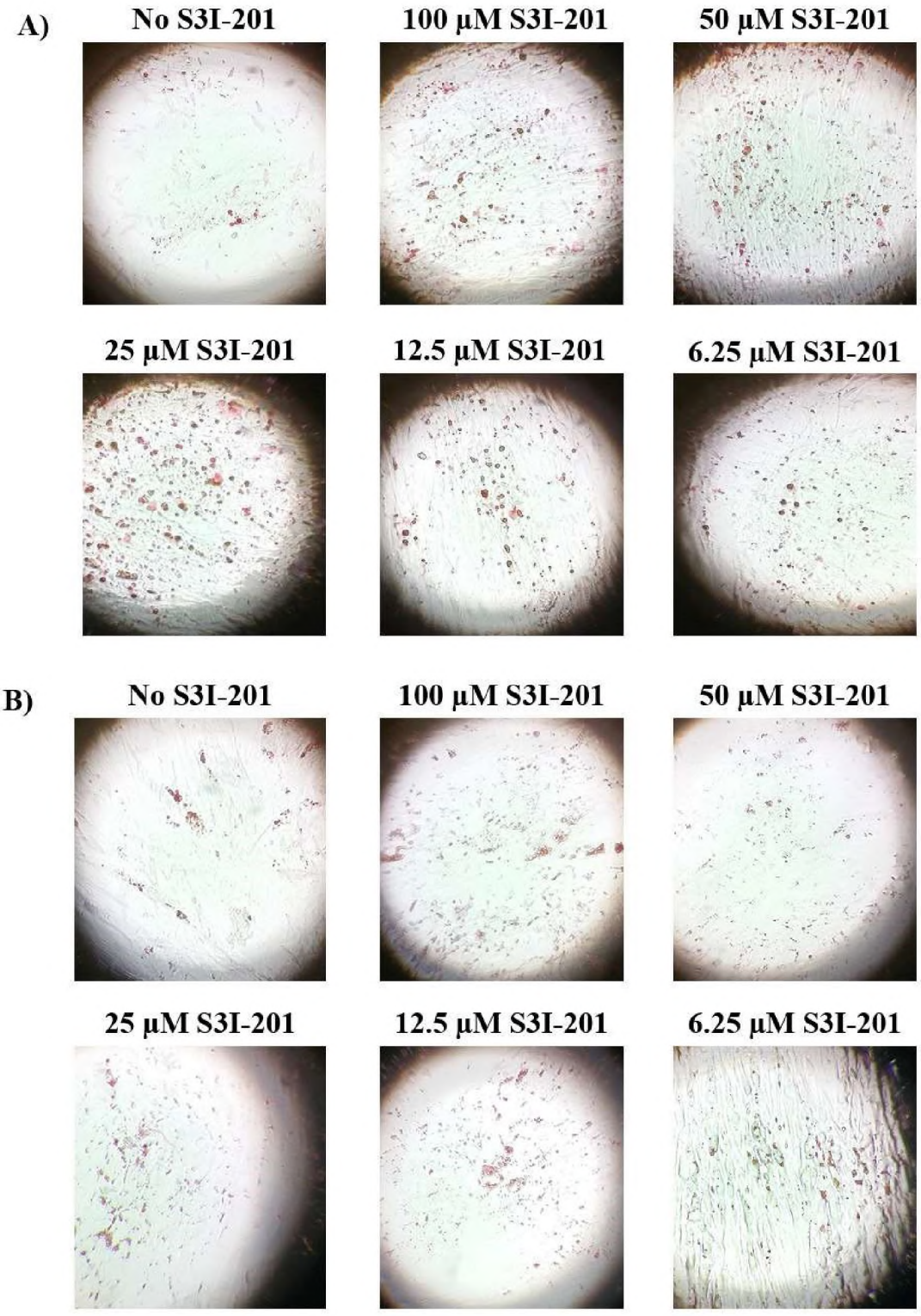


**Figure 3-23. Oil Red O staining to confirm the induction of adipogenesis within hypoxic conditions.** The cultures were stained on day 6 post-induction in the presence/absence of the varying concentrations of STAT3 inhibitor (S3I-201). A) represents normal conditions whereas B) represents an increased hypoxic environment. Images were captured using a Samsung Galaxy Note 4 camera with magnification 2x and the Zeiss AxioVert.A1 FL-LED Fluorescence Microscope at 200x magnification. Images shown are representative of

multiple images acquired (N = 2).

The most notable difference for lipid accumulation was presented with the addition of S3I-201. For cells treated with cobalt chloride (Figure 3-23. B.), the lipids appeared to be considerably smaller and more tightly clustered within multiple groups forming around a larger, singular droplet; whereas, the cells left untreated for cobalt chloride (Figure 3-23. A.) demonstrated larger, more singular, larger lipid droplets, which may be indicative of an increased rate of lipid formation/accumulation as the multiple, smaller droplets merge together to form the larger singular droplet. From this, it can be further speculated that the chemically induced hypoxic environment had little impact on the inhibition of adipogenesis; in some of the cases presented within this study, adipogenesis/lipogenesis seemed to be slightly promoted. The results presented are somewhat in accordance with studies performed by Chandel and colleagues (2000) whom demonstrated that the use of cobalt chloride elicits an increase in the levels of ROS; this increased generation occurs within the mitochondria during the mechanisms of complex III, which result in the production of superoxide anions. Chandel and colleagues (2000) further went on to demonstrate the increased production of ROS formed at complex III (Hamanaka et al., 2009). Increased levels of reactive oxygen species are vital for adipogenesis; STAT3 is responsible for the regulation of this ROS during differentiation, where decreased levels of STAT3 promote adipogenesis (Kramer et al., 2015). Therefore, the combination of STAT3 inhibition and increased ROS production via chemically induced hypoxic conditions would, ultimately, provide grounds for adipogenesis to occur, thereby substantiating the results provided within this study. While adipogenesis may have occurred, the recruitment of lipid droplets may have been decreased within the hypoxic conditions.

In order to successfully inhibit adipogenesis, one may have to consider inhibiting the mechanisms of the mitochondria responsible for the complex III ROS formation and regulation. Additional experiments could include the effects that small molecule compounds and increased hypoxic conditions have on the different lineage potentials of hMSC-ad cells, such as osteogenesis and chondrogenesis.

**3-2-4. B. Use of ACEA xCELLigence RTCA system for monitoring the effects of increased hypoxic conditions on the growth CI curves during adipogenic differentiation.** As per the xCELLigence RTCA protocols previously mentioned, the system was used in order to gain additional insight and greater understanding into the effects that a chemically-induced hypoxic environment may have on non-differentiating and adipogenic differentiating hMSC-ad cell lines. The hMSC-ad cells were seeded at a cell density of approximately 5 000 cells/well using normal maintenance media for both adipogenic differentiating and undifferentiated hMSC-ad cells.

For non-differentiating hMSC-ad cells, the maintenance medium change occurred after the initial 24-hour settling stage; during this medium change, 100 µM cobalt chloride (cobalt chloride) was added into the maintenance medium in addition to the varying concentrations of small molecule compounds (S3I-201, M1, and Mdivi-1). For all non-differentiating hMSC-ad treatments demonstrated for this experiment, a mutual control was established. This control was comprised of two aspects: the first was the inclusion of completely untreated hMSC-ad cells (these cells did not include treatment with the small molecules nor cobalt chloride), while the second involved cobalt chloride treated hMSC-ad cells that remained untreated for the small molecules as previously listed. A comparison between these two controls indicated that a shift in morphology does occur for the hMSC-ad cells subjected to the chemically induced hypoxia. While both demonstrated the initial peak and plateau, suggestive of the cells settling, the first medium change, in which the cobalt chloride was added, provided a larger decrease in CI observed. Instead of the regular general consistent increase of CI as experienced for the untreated hMSC-ad cells (as shown by the red), the cobalt chloride treated cells seem to experience a lower CI overall with a trend shape that indicated a greater 'curve'. In comparison to the hMSC-ad control, the drop in CI was of a reasonable significance; however, the undifferentiating cells were able to adjust to this added increase in hypoxia and continued to proliferate further, albeit, the overall CI was slightly decreased.

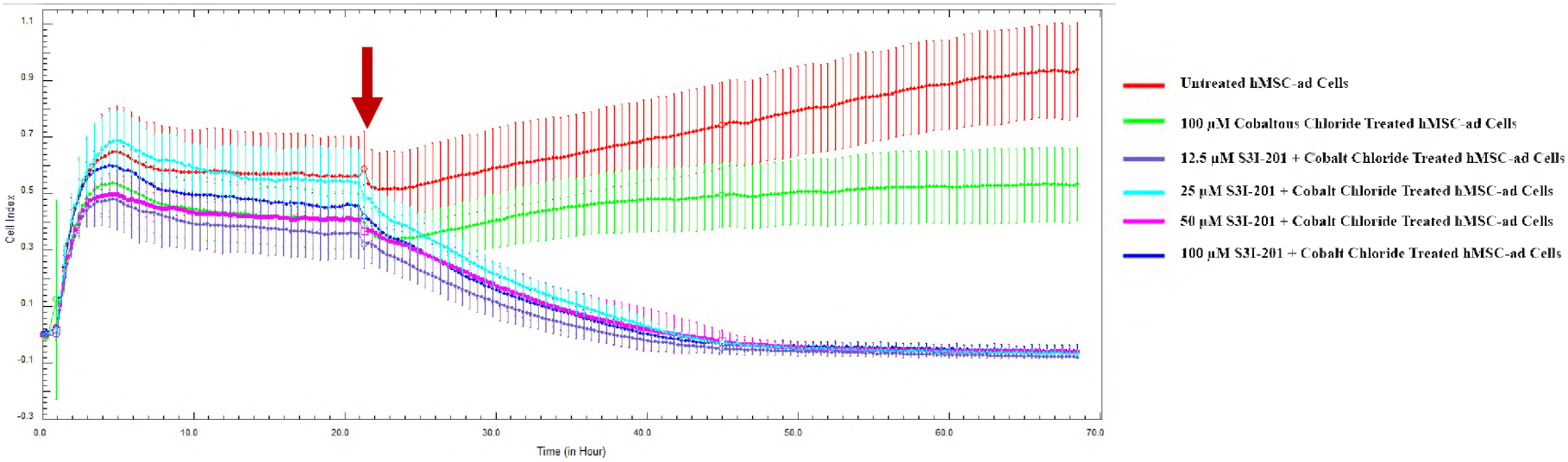


**Figure 3-24. Effects of varying concentrations of S3I-201 and cobalt chloride on hMSC-ad growth CI curves.** The cells were seeded onto the plate at a density of 5 000 cells/well, and allowed to settle for 24 hours in MSCM, after which a medium change occurred whereby S3I-201 and cobalt chloride were added into the maintenance medium; this point has been identified as shown above. All curves were plotted as an average of 3 treatments per concentration; graphs were constructed using the ACEA xCELLigence RTCA SP software. (N = 2)

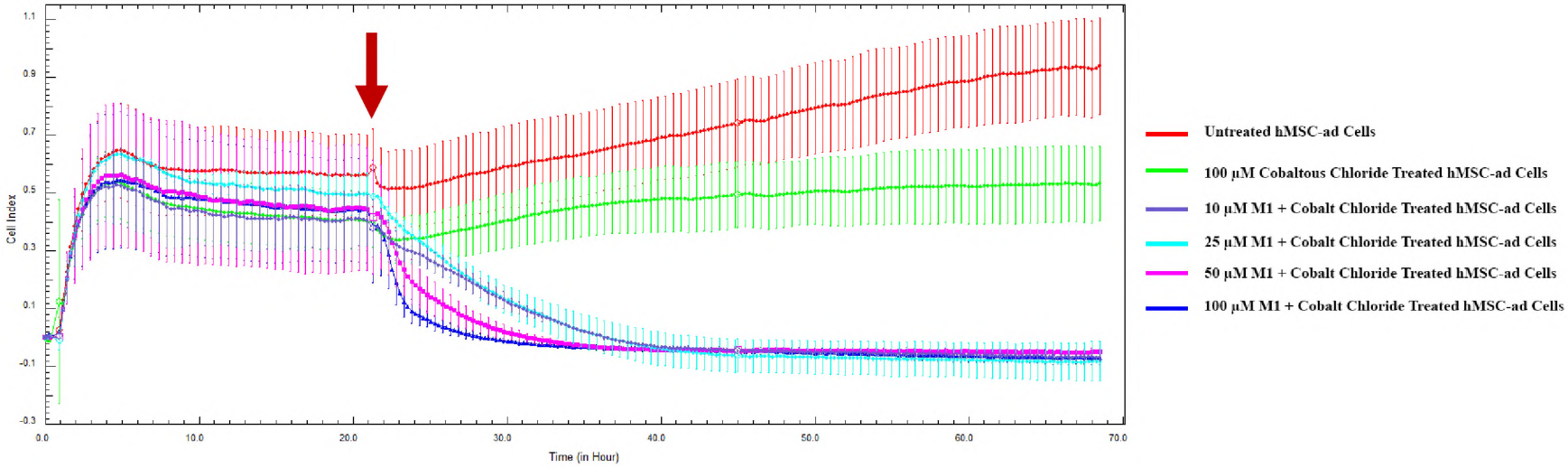


**Figure 3-25. Effects of varying concentrations of M1 fusion promoter and cobalt chloride on hMSC-ad growth CI curves.** The cells were seeded onto the plate at a density of 5 000 cells/well, and allowed to settle for 24 hours in MSCM, after which a medium change occurred whereby M1 fusion promoter and cobalt chloride were added to the maintenance medium. This point has been highlighted above. All curves were plotted as an average of 3 treatments per concentration; graphs were constructed using the ACEA xCELLigence RTCA SP software. (N = 2).

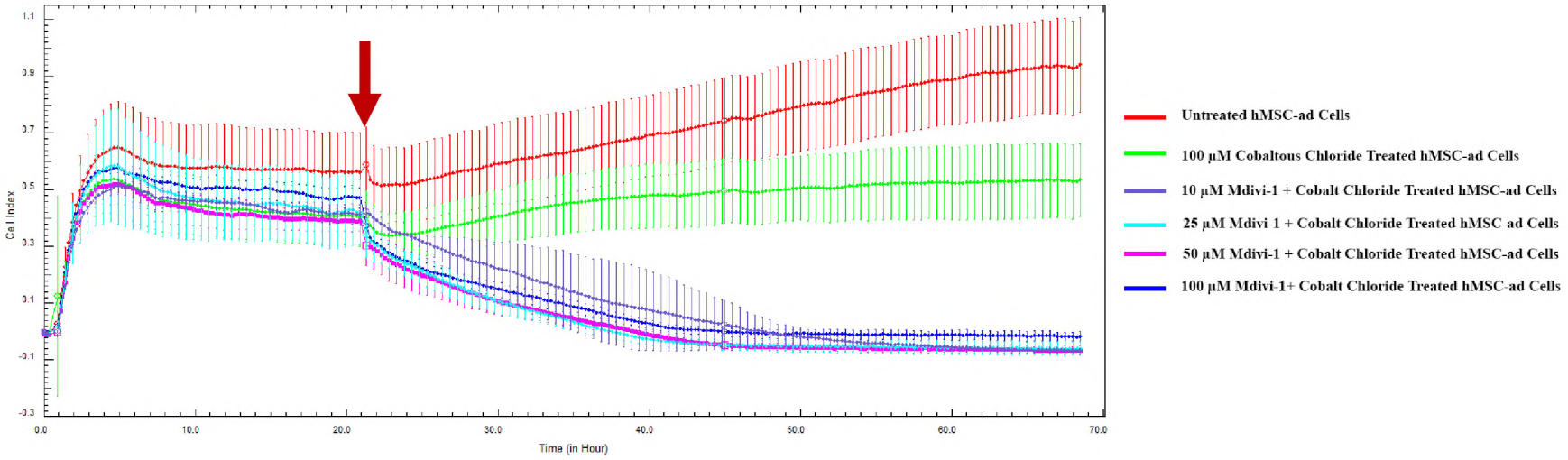


**Figure 3-26. Effects of varying concentrations of Mdivi-1 and cobalt chloride on hMSC-ad growth CI curves.** The cells were seeded onto the plate at a density of 5 000 cells/well, and allowed to settle for 24 hours in MSCM, after which a medium change occurred whereby Mdivi-1 and cobalt chloride were added into the maintenance medium; this point is highlighted above. All curves were plotted as an average of 3 treatments per concentration; graphs were constructed using the ACEA xCELLigence RTCA SP software. (N =2).

When in the presence of different small molecules, a common adverse effect was observed for all non-differentiating hMSC-ad cell lines, regardless of what may have been observed for the same growth curves cultured under normal conditions. S3I-201, M1, and Mdivi-1 (Figure 324, 3-25, and 3-26, respectively) all provided negative effects on the CI growth curves, with minimal cell survival and/or maximal cell detachment. The addition of the small molecules in combination with 100 μM cobalt chloride caused the cells to suffer a drastic drop in the cell index values; this created a decreased linear trend for all compounds, regardless of concentrations utilized. Speculation as to the cause of this decline in cellular health may be attributed to the addition of the cobalt chloride, used to chemically induce hypoxia; this may be justified by the previous experiments performed in which compounds S3I-201 and Mdivi-1 were utilized and did not present with negative effects on the overall growth of the cells. The mitochondrial fusion promoter, M1, is exempt from this as it, alone, was toxic to the cells, thereby resulting in decreased CI growth curves. The combination of the small molecule compounds and cobalt chloride may have induced cellular apoptosis due to the excessive amount of stress within the cellular environment; the stress may have exceeded any attempts of rectifying the damage, or compensation methods, employed by the cells in response to this change in environment. The lowest concentrations of S3I-201, M1, and Mdivi-1 seemed to collectively display the least severe decline in the overall CI curve.

When induced for differentiation, the trends were exceptionally different to that which was found for non-differentiating hMSC-ad cells. Adipogenesis was promoted using the protocol as previously described throughout this study; however, in addition to the small molecules utilized within the induction and maintenance media, 100 μM cobalt chloride was included into the final mixture. Once the hMSC-ad cells had reached 100 % confluency, the induction medium was added, and adipogenesis was left to occur while in the presence of the chemically induced hypoxic environment.

For this experiment, two controls (as shown in Figure 3-27) were maintained throughout; these included an untreated sample of adipogenic differentiating hMSC-ad cells, and those that were treated only with 100 μM cobalt chloride. From this, a basic indication of expected growth curves was established in order for comparisons when the small molecules were combined with the cobalt chloride.

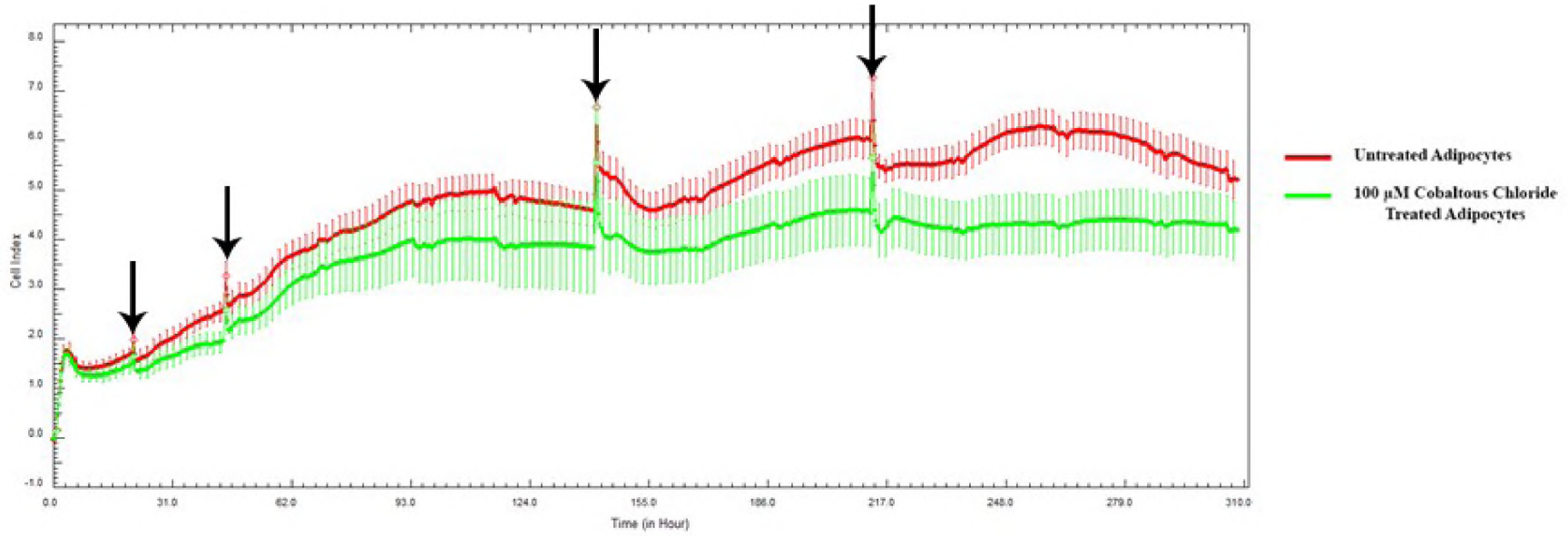


**Figure 3-27. Effects of cobalt chloride on the adipogenic differentiation growth CI curves.** The cells were seeded onto the plate at a density of 5 000 cells/well, and allowed to settle for 24 hours in MSCM, after which a medium change occurred whereby 100 µM cobalt chloride was added to the induction medium, which consisted of INS/ROSI/DEX/IBMX. The points of induction and maintenance media with supplemented with fresh cobalt chloride have been indicated above. All curves were plotted as an average of 12 treatments per concentration; graphs were constructed using the ACEA xCELLigence RTCA SP software. (N = 3).

The resulting curves for the untreated control was as expected in terms of overall shape and general trend; the very first peak was indicative of cells settling onto the culture vessel used, whereas the second peak marks the addition of non-differentiating hMSC-ad maintenance medium without any cobalt chloride or small molecules added. The third peak observed at approximately 58.0 hours was that which marked the induction of adipogenesis, and, in the case of the cobalt chloride control (highlighted in green), the addition of cobalt chloride to the induction medium. It seemed evident that a slight decrease in CI, indicative of cellular detachment and/or death, occurred after the addition of cobalt chloride. This decline in CI may also suggest a lack of lipid droplet accumulation present amongst the differentiating cells. However, the general CI growth curve obtained was almost identical, in shape, to that observed for the untreated differentiating cells, highlighted in red. Therefore, it could be concluded that adipogenesis did occur within the chemically induced hypoxic environment, although the rate of lipogenesis may have been somewhat adversely affected.

The addition of S3I-201 and cobalt chloride to the induction and maintenance media cocktail resulted in the generation of CI curves that substantiated the previous findings obtained via microscopy. Figure 3-28 demonstrated the effects that the combination of S3I-201 and cobalt chloride had on adipogenic differentiating hMSC-ad cells throughout the course of differentiation. In comparison to the untreated control, the cells that were exposed, in general, to the combination of cobalt chloride and S3I-201 seemed to undergo adipogenesis, displaying a general curve shape similar to that obtained for the untreated control; however, while initial induction (after 56.0 hours) seemed notably higher than that observed for the untreated control, the CI seemed to steadily decrease until 112.0 hours, whereby a medium change to the maintenance medium containing fresh S3I-201 and cobalt chloride created an increase in CI once again; this increase continued until a plateau was reached, after which another slight increase was noted upon the following medium change and restoration of S3I201 and cobalt chloride. However, once again, it must be acknowledged that adipogenesis was being maintained within these cells, as shown by comparisons with the untreated control (displayed in red). The rate of adipogenesis was slightly decreased; however, this decline in CI may also be indicative of a decreased rate of lipogenesis. The concentration of 12.5 μM S3I201 and 100 μM cobalt chloride (indicated by the purple) provided a growth curve that maintained the highest CI end result from the S3I-201 concentrations utilized within this experiment.

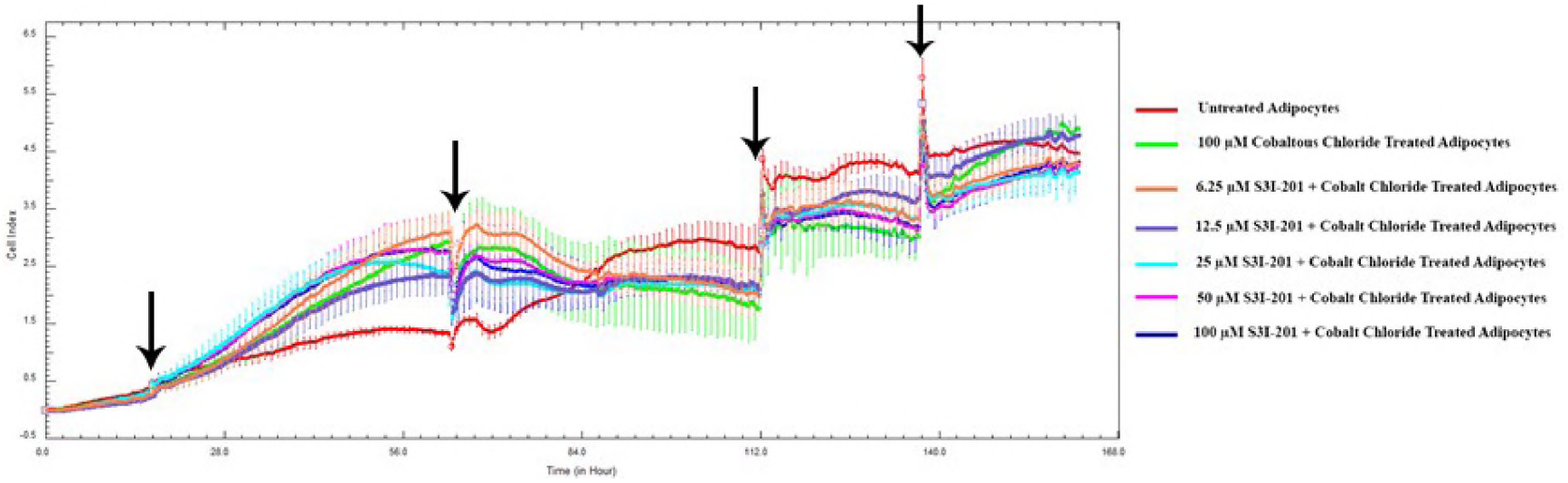


**Figure 3-28. Effects of varying concentrations of the S3I-201 and cobalt chloride (cobalt chloride) on the adipogenic differentiation growth CI curves.** The cells were seeded onto the plate at a density of 5 000 cells/well, and allowed to settle for 24 hours in MSCM, after which a medium change occurred whereby S3I-201 was added at varying concentrations, in addition to 100 µM cobalt chloride. The point where the addition of induction medium and freshly supplemented maintenance medium have been highlighted above. All curves were plotted as an average of 12 treatments per concentration; graphs were constructed using the ACEA xCELLigence RTCA SP software provided. (N = 2)

Concentrations of 100 μM, 50 μM, and 25 μM S3I-201 (represented by dark blue, magenta, and turquoise respectively) provided a CI growth curve that remained constant with one another, generating a similar growth curve throughout the course of differentiation.

In order to establish a preliminary conclusion regarding the ideal conditions for adipogenesis, a comparison of the effects that cobalt chloride may have on S3I-201 treated cells was generated using data previously acquired within this study, and is displayed as Figure 3-29. The resulting adipogenic CI growth curves generated provided indication that cells treated with a combination of cobalt chloride and S3I-201 resulted in a greater overall CI after approximately 6 days of culture. This was evident by the collective S3I-201 CI values observed within the highlighted region of the graph; all S3I-201 concentrations possessed a decreased CI value when compared to that of the S3I-201 and cobalt chloride treated adipogenic differentiating hMSC-ad cells. This comparison may lead to the speculation that adipogenesis, on a whole, is promoted by the addition of a chemically induced hypoxic environment, as previously discussed using microscopy as a means of adipogenesis validation. However, the general increase in linear trend for cells treated with both S3I-201 and cobalt chloride may be indicative of accumulating lipid droplets still being formed within the cells. In addition to this, cells treated with both S3I-201 and cobalt chloride possess differentiation CI curve traits similar to that demonstrated by the untreated adipocytes control, as shown in red on Figure 3-29.

With the corresponding comparisons generated for S3I-201 and S3I-201 + cobalt chloride treatments used throughout adipogenic differentiation, the CI growth curves for the remaining small molecules (M1 and Mdivi-1) while in the presence of cobalt chloride were exhibited. Much like the negative effect that M1 had on non-differentiating hMSC-ad cells and adipogenic differentiating hMSC-ad cells, it was expected that the resulting effect would not be too different regarding the use of this compound throughout differentiation.

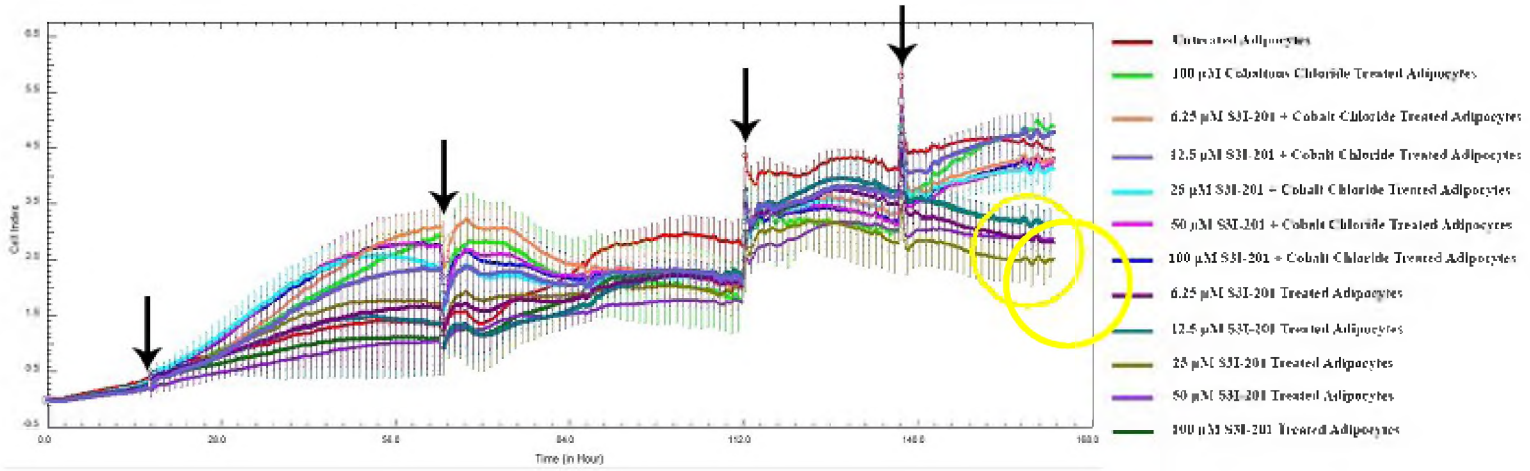


**Figure 3-29. Comparison of the effects of the addition of cobalt chloride to S3I-201 treated adipogenic differentiating hMSC-ad cells.** The overall growth curves of adipogenesis within the presence of cobalt chloride and S3I-201 were compared to those generated for adipogenic differentiating hMSC-ad cells that were treated only with S3I-201 in order to establish the effects that the chemically induced hypoxic environment may have on the product of differentiation. The point where the induction medium and freshly supplemented maintenance medium has been highlighted above. A collective region was identified, which marked the 'end-points' of adipogenesis reached for S3I-201 only treated cells over the course of 6 days; this region was established and all CI curves shown within the region corresponded to those of the S3I-201 only treated cells. Graphs were constructed using the ACEA xCELLigence RTCA SP software provided. (N = 2).

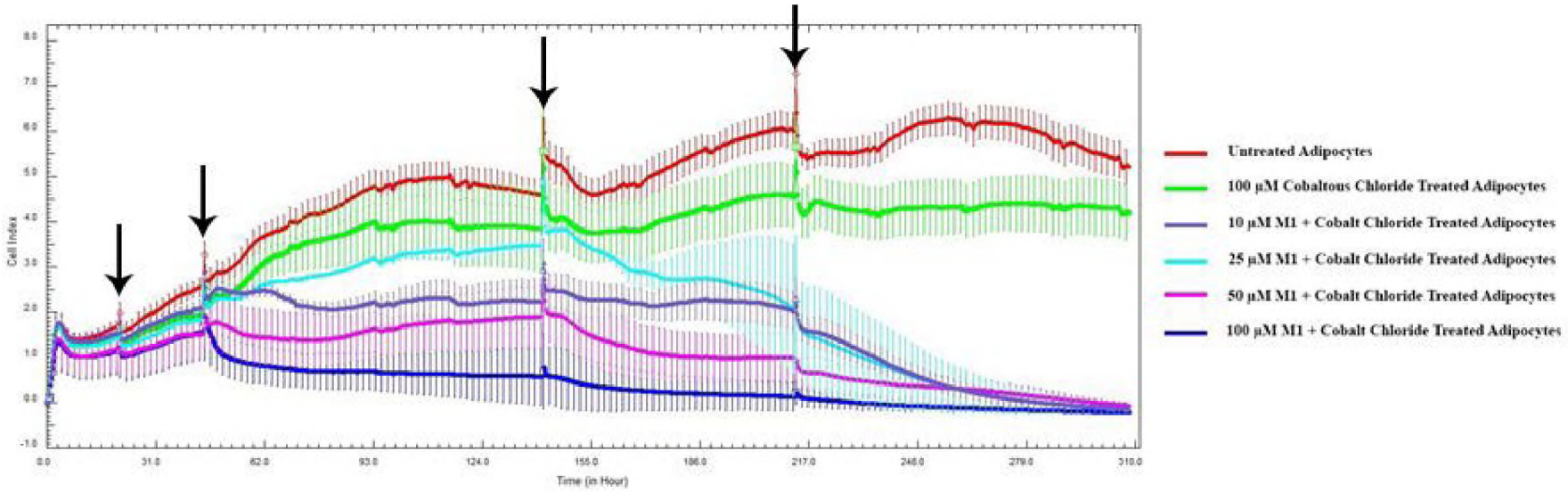


**Figure 3-30. Effects of varying concentrations of the M1 fusion promoter and cobalt chloride on the adipogenic differentiation hMSC-ad cells' growth CI curves**. The cells were seeded onto the plate at a density of 5 000 cells/well, and allowed to settle for 24 hours in MSCM, after which a medium change occurred. The induction medium contained fresh M1, a mitochondrial fusion promoter, as well as 100 µM cobalt chloride. These compounds were added to the maintenance medium and maintained throughout differentiation, where the time of addition have been highlighted above. All curves were plotted as an average of 12 treatments per concentration; graphs were constructed using the ACEA xCELLigence RTCA SP software provided. (N = 2).

As noted throughout the course of xCELLigence experiments performed, the two controls, previously described, were established and superimposed onto the resulting CI growth curves in order to generate a greater comparison of the effects that M1 may have on adipogenesis when in the presence of cobalt chloride, demonstrated in Figure 3-30. As was expected, the overall growth, indicated by CI, suffered a decline as a result of the lethal concentrations of M1 (bearing in mind that the preliminary $IC_{50}$ established was approximately 5.4794 μM). The conclusion that M1 was responsible for the cell death and/or cell detachment may be justified by the resulting curve generated for the control in which the adipogenic differentiating cells were exposed to the 100 μM treatment with cobalt chloride (as shown by the green curve within Figure 3-30), as well as experiments, previously described, in which M1 provided deleterious effects on adipogenic differentiating hMSC-ad cells under normal conditions (without chemical induced hypoxia). It may be noted that an increased concentration of M1 resulted in a greater rate of decline in cellular viability; this was observed by the decreased CI growth curves generated for 100 μM M1 in contrast with that of 50 μM, 25 μM, and 10 μM.

Mdivi-1 previously demonstrated a result that did not suggest inhibition of adipogenesis; Figure 3-31 represents the addition of both cobalt chloride and Mdivi-1 to adipogenic differentiating hMSC-ad cells, and while initial induction and maintenance was as expected (the CI growth curves generated for each concentration remained on par with the two controls, and, in some cases, provided a result greater than that of the 100 μM cobalt chloride control demonstrated in green), the CI seemed to collectively suffer a decline in CI after, approximately 217.0 hours, whereby a routine medium change (supplemented with Mdivi-1 and cobalt chloride) occurred. The general decreasing trends seemed to reach a CI of 0.0, indicating cell death and/or detachment, with the exception of the 10 μM Mdivi-1 and cobalt chloride treated sample, which was undergoing a decline at a 'slower' rate. This decline in adipogenesis, when compared to results previously obtained, may be suggestive of the mitochondrial imbalance that may have, eventually, prevented the formation of complex III ROS responsible for the hypoxic adjustments and the driving factor of adipogenesis (ROS is increased). It must be noted, however, that adipogenesis for concentrations 50 μM, 25 μM, and 10 μM remained consistent until this declining point had been reached; in fact,

adipogenesis was almost on the same level, if not greater, than that achieved by the untreated differentiating hMSC-ad cells cultured under 'normal' conditions.

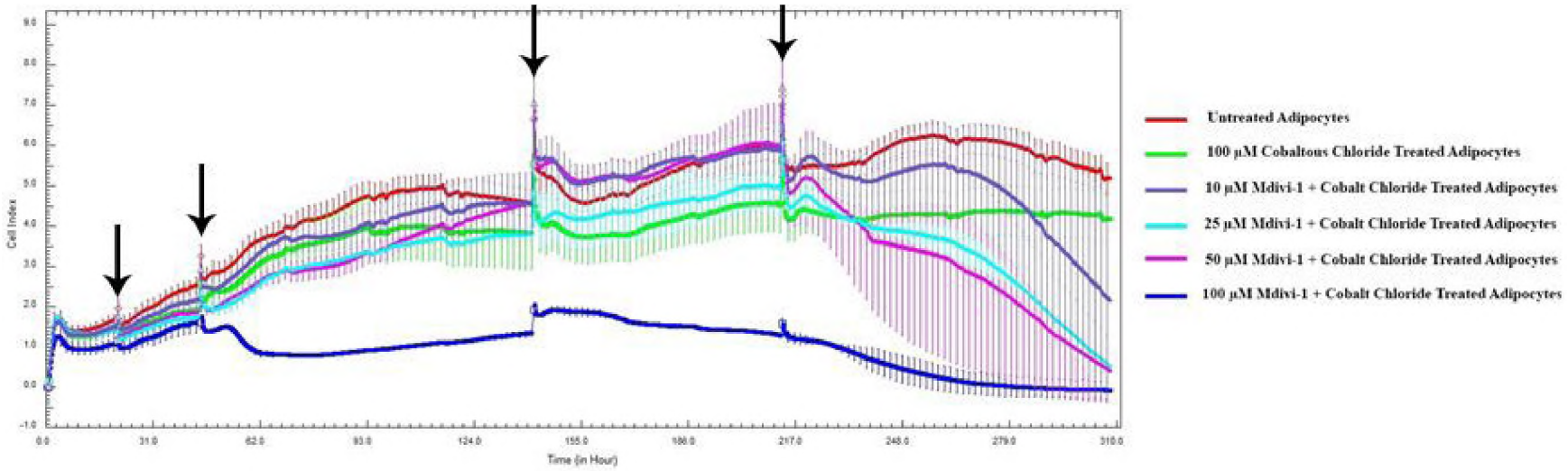


**Figure 3-31. Effects of varying concentrations of Mdivi-1 and cobalt chloride on the adipogenic differentiating hMSC-ad cells' CI curves.** The cells were seeded onto the plate at a density of 5 000 cells/well, and allowed to settle for 24 hours in MSCM, after which a medium change occurred. The induction medium contained fresh Mdivi-1, a mitochondrial fission inhibitor, as well as 100 µM cobalt chloride. These compounds were added to the maintenance medium and maintained throughout differentiation, and the points of addition have been highlighted above. All curves were plotted as an average of 12 treatments per concentration; graphs were constructed using the ACEA xCELLigence RTCA SP software provided. (N = 2).

## 3-3. Conclusion and Complications

Adipogenesis may be validated following several various techniques, including Nile Red staining, Oil Red O staining, as well as taking note of the CI profiles obtained using the ACEA xCELLigence RTCA system.

The effects that certain small molecules and chemical compounds may have on mitochondrial dynamics and overall cellular function must be understood in order to fully determine the differentiating capabilities presented with the hMSC-ad cell line. An intricate balance must be established between fission and fusion in order to promote the maintenance of certain cellular functions, as well as their capabilities of differentiation. As seen with the over-stimulation of mitochondrial fusion, adipogenesis is somewhat inhibited and the cells may be driven maintain their multi-potent morphologies, or acquire spontaneous differentiation into different phenotypes not associated with adipocytes; however, further studies are necessary in order to generate a justifiable statement regarding the true effects that M1 may present on non-differentiating and differentiating hMSC-ad cell lines. For example, further cytotoxicity experiments could be utilized in order to calculate an appropriate $IC_{50}$ value, which may create the grounds for further studies using non-lethal concentrations of this compound; from this, previously describe techniques may be used in the validation of adipogenesis, and/or the differentiating properties present within the hMSC-ad cells. Biomarkers, such as those that target the self-renewal proteins (Sox2) of stem cells, may be used, in conjunction with western Blotting and/or Immunofluorescence, in order to determine whether or not the non-differentiating hMSC-ad cells still hold their capabilities of differentiation. UCP1 could be targeted in order to confirm the formation of adipocytes during adipogenesis while in the presences of M1.

The potentially positive result of Mdivi-1 was demonstrated through the combination of acquired CI profiles and the accompanying microscopy images, which revealed little/no adverse effects on adipogenesis, on the whole. The process was slightly decreased in some aspects; however, differentiation was not inhibited completely and, in some cases, the accumulation of lipid droplets seemed significantly increased. However, a discernible conclusion, regarding any beneficial effects that Mdivi-1 may have on adipogenesis, may not

be decided until additional experimentation occurs due to the fact that, in particular, the half-life of this compound has not truly been taken into effect. As described previously, Mdivi-1 used within in vitro cell lines possessed a half-life of 6 – 24 hours; adipogenic induction occurred over the course of 96 hours and maintenance medium was changed every 72 – 96 hours, which means that Mdivi-1 could have possibly expired thereby resulting in the cells rectifying this damage to further produce healthy phenotypes. Another concept to acknowledge would be the $IC_{50}$ values obtained; perhaps the concentrations used throughout this study were too low to provide a true representation of Mdivi-1 capabilities and effects on hMSC-ad cells.

STAT3 inhibition did not exclusively determine the fate of adipogenesis; STAT3 is an important regulator of differentiation, with increasing STAT3 levels responsible for a decline in ROS, which, in turn, provides an adverse effect on differentiation. In order for adipogenesis to occur, the cells require higher levels of ROS, therefore STAT3 inhibition may be beneficial during adipogenesis to a certain degree. The resulting experiments provided indication that, while adipogenesis does occur, the overall CI curves generated were inferior in comparison to the untreated control; i.e. adipogenesis was decreased to a certain extent. However, the accumulation of lipid droplets remained greater than what was observed for the untreated control.

Hypoxia is essential for stem cells to maintain their self-renewing properties; however, chemically induced hypoxia, using cobalt chloride, did not completely halt differentiation, as shown within this study. While differentiating hMSC-ad cells exposed to this chemically induced hypoxic environment were subjected to a decreased rate of adipogenesis, the combination of cobalt chloride and S3I-201 demonstrated a slight increase in adipogenesis and lipogenesis when compared to S3I-201treated adipogenic differentiating hMSC-ad cells; however, throughout the initial course of differentiation, the cobalt chloride + S3I-201 treated cells remained somewhat lower than that provided by the untreated control, before exceeding CI values for the untreated control. This may be linked to previous studies in which increased ROS was generated through chemically induced hypoxia, whereby increased levels of ROS are vital promoters of adipogenesis, due to their involvement with C/EBPβ, in combination with decreased levels of STAT3, whereby increased levels of STAT3 are known to inhibit ROS (Hamanaka et al., 2009; Chandel et al., 2000; Tormos et al., 2012; Kramer et al., 2015).

The overall increase in ROS may have accounted for the increase in lipid accumulation; this excessive lipogenesis has been attributed to mitochondrial dysfunction, which promotes the generation of ROS as reviewed by Kusminski and colleagues (2012).
Definitive conclusions cannot be drawn until additional experimentation is performed; in addition to adipogenesis, chondrogenesis and osteogenesis could be studied with regards to a chemically induced hypoxic environment and exposure to the several compounds utilized throughout the course of this study. Gene manipulation of mitochondrial phosphorylated serine 727 STAT3 may be utilized, whereby knockout and/or over-expression of this protein may provide greater understanding into the differentiating capabilities within the chemically induced hypoxic environment.

Multiple complications did arise regarding the ectodermal model originally planned for this study, including constant contamination of newly acquired SH-SY5Y cells, senescence of older SH-SY5Y cells, and the cancerous increased growth rate of high passaged SH-SY5Y cells. Therefore, an additional ectodermal cellular model was not provided for comparative studies regarding the effects that the previously described compounds may have elicited on undifferentiated and differentiated cell lines. Additional ectodermal models may have been sought after and utilized instead of SH-SY5Y neuroblastoma cells; alternatively, additional mesodermal models and precursor cells could have been utilized in order to provide a closer comparison of these effects.

These experiments illustrate the resulting advantageous and disadvantageous effects that certain small molecules have on non-differentiating and differentiating hMSC-ad cells. Further experiments that could be performed include more precise time-dependent studies which could monitor the effects that both time and the exposure of the small molecules may have on these cellular models. While the morphological traits of adipogenesis (such as the accumulation of lipid droplets and adipocyte phenotype) were of particular interest in this study, it might be worth investing some time into delving deeper and monitoring the effects that these molecules have on particular genes and proteins; this would involve gene and protein analysis, such as knockouts and over-expressions of particular proteins of interest (such as STAT3), and the effects that these small molecules may have pertaining to these altered states.

From the results acquired for the validation of successful adipogenesis, it can be concluded that mitochondrial dynamics is an important feature to maintain and regulate in order to ensure cell integrity as well as its capability of differentiation. In addition to the health of the mitochondria, environmental factors and additional cellular responses must be met in order for the cells to undergo successful differentiation. Here, it was observed that the over-stimulation of mitochondrial fusion has severely compromising effects and inhibits adipogenesis in human adipose-derived mesenchymal stromal cells; whereas the inhibitor of Drp1, Mdivi-1, provided non-detrimental effects due to the non-lethal concentrations utilized, as well as the half-life of the compound. STAT3 inhibition did not lead to the complete inhibition of adipogenesis, although it decreased the rate of adipogenesis, and provided an increase in lipid accumulation. When combined with chemically induced hypoxia, S3I-201 provided an increase in adipogenesis, when compared to that of S3I-201 under normal conditions. Combined with M1 and Mdivi-1, cobalt chloride posed a negative effect on adipogenesis, in particular for that observed with M1, which resulted in almost instantaneous cell death/cell detachment.

# Chapter 4:

Specific Objectives:

1. The assessment of the overall health of mitochondria present within the hMSC-ad cells and their differentiated progeny.
2. Two-dimensional analysis of the mitochondrial networks present within hMSC-ad cells and their differentiated progeny.
3. The investigation of the effect of various inhibitors and promoters on the differentiated progeny relative to the undifferentiated stem cell population.

# 4: Assessment of the status of mitochondrial networks within HMSC-ad cells and their differentiated progeny after exposure to certain small molecules.

## 4-1. Introduction

Obesity and associated diseases are becoming of increasing concern within the modern population, therefore, increasing interest in the research of adipocytes. While often associated with its energy storage capabilities, white adipose tissue has been classed as a highly active endocrine organ that is essential for the maintenance of overall health (Boudina et al., 2014; De Pauw et al., 2009). White adipose tissue differs from brown adipose tissue: it possesses less mitochondrial density with mitochondria that are smaller in size, located around the rim of the periplasm and is generally associated with a singular, large lipid droplet (Kusminski et al., 2012; Boudina et al., 2014). Brown adipose tissue holds a high mitochondrial content and demonstrates the expression of uncoupling protein I (UCP1), which aids in the regulation of non-shivering thermogenesis responsible for the prevention of hypothermia in mammals (Boudina et al., 2014). Mitochondria located within white adipose tissue have been speculated to play an important role in the co-ordination of the production of energy using nutritional signals that lead to either the oxidation of fatty acids and carbohydrates, or the storage of energy in the form of triglycerides (Kusminski et al., 2012; Boudina et al., 2014).

It is vastly known that the mitochondria are the main energy producers within a living cell, and are responsible for multiple cellular functions, which include: apoptosis and ageing, as well as signalling pathways within the cell. This organelle has been deemed as "dynamic" due to its ability to constantly undergo fission and fusion; thereby allowing it to alter its structure from a fragmented state to a filamentous state, and vice versa (Lihavainen et al., 2012). The mitochondrion's dynamic ability is crucial for the organelle's functional maintenance and tissue homeostasis. Should dysfunction arise, thereby altering the dynamic processes of the mitochondria, degeneration may occur. For example, abnormal mitochondrial fission may result in the eventual loss of mitochondrial function, which may eventually contribute to the development of degenerative diseases (Khacho et al., 2016). Mitochondrial dysfunction is particularly problematic within the tissues that demonstrate a high demand in energy, such as: the brain, muscles, heart, and adipose tissue (De Pauw et al.,

2009; Kusminski et al., 2012). A correlation between decreased mitochondrial density and oxidative metabolism has been established, coinciding with the progression of obesity

During adipogenesis, the mitochondria are heavily affected whereby co-ordination between mitochondrial biogenesis and an energy balance must be maintained. This is seen in the activation of various transcription factors, including peroxisome proliferator-activated receptor γ (PPARγ) and the co-activator PGC-1, and other components used in energy metabolism demonstrated in adipogenesis and mitochondrial biogenesis (De Pauw et al., 2009; Boudina et al., 2014). To substantiate the increase of mitochondrial biogenesis during adipogenesis, an increased rate of oxygen consumption occurs. Lipogenesis consumes vast amounts of energy, ATP, due to processes such as lipogenesis and mitochondrial biogenesis, thereby, the amount of ATP suffers a dramatic decrease as the demand for consumption is increased (Kusminski et al., 2012; De Pauw et al., 2009). Mitochondrial fragmentation due to an excessive mitochondrial fission has been linked to an increase in body mass (Jheng et al., 2011).

Neurodegenerative diseases, such as Alzheimer disease and Parkinson disease, have been attributed to a loss in mitochondrial dynamics; Mfn2 is a crucial mitofusin protein that aids in the maintenance of structure and function within mitochondria, and is a primary protein, along with Mfn1, in mitochondrial fusion (Fang et al., 2016). Alterations in the dynamic ability of the mitochondria negatively impact differentiation and proliferation of stem cells. A decline in Mfn2 results in an impaired mitochondrial transport throughout the cell, as well as mitochondria that possess an abnormal morphology (Fang et al., 2016). Fang and colleagues (2016) have linked a deficit in Mfn2 to the deterioration of dopaminergic neurons. During differentiation, Mfn2 is increased resulting in an acquired elongated mitochondrial morphology. Pathological phenotypes, in neurons, may also be presented within cells that possess an excessive affinity for mitochondrial fission (Jheng et al., 2011). Mitochondrial fragmentation is achieved through the activation of Drp1; this permits the stem cell to maintain its potency (Fang et al., 2016). A decrease in Drp1 will result in a lack of mitochondrial DNA in addition to a decline in mitochondrial membrane potential (Jheng et al., 2011).

### 4-1-1. JC-1: A Mitochondrial Membrane Potential Stain

The mitochondrial probe, 5,5',6,6'-tetrachloro-1,1',3,3'-tetraethylbenzimidazol-carbocyanine iodide, otherwise known as JC-1, has long been associated with the assessment of mitochondrial membrane potential (Salvioli et al., 1997; Garner et al., 1999). This lipophilic cationic monomeric molecule has been used to identify mitochondria that display a low membrane potential, generating a green fluorescence (510 – 520 nm), as well as to differentiate the mitochondria that produce a generally high membrane potential, which display a bright red/orange fluorescence (590 nm). The resulting red/orange fluorescence observed has been deemed as J-aggregates. JC-1 live staining allows for a quantitative and qualitative method of analysis, and permits the observation of varying mitochondrial populations within a cell (Salvioli et al., 1997).

### 4-1-2. Mytoe: Mitochondrial Analysis Software

Mytoe is an easy-to-use automated image analysis tool developed by Lihavainen and colleagues (2012), which permits the study of mitochondrial structural dynamics and kinetics via acquired fluorescence images. This novel software bears an easily understandable user interface and can identify the individual branches present within mitochondria via thresholding and morphological image processing.

Mytoe was developed to combat the restraints that the previous methods of mitochondrial analysis tools possessed. For example, methods to detect mitochondrial motility only provided the mitochondrial motion but did not present with data on directionality; optical flow (OF) estimation is a method employed to assess mitochondrial motility, however, the method strongly relies on human interaction, which may increase the chance for error. Lihavainen and colleagues (2012) have shown that the Mytoe software provides quantifiable properties of the single branches within the mitochondrial network, as well as the resulting macroscopic mitochondrial structure, providing results relatable to mitochondrial thickness, length, tortuosity, and orientation. It also utilizes optical flow during motion analysis, producing the average speed and direction of each of the branches. Mytoe additionally provides insight into the number of branches and the total mitochondrial area extracted from cell-level quantities. Studies using Mytoe further went on to highlight the software's

robustness to noise and insensitivity to saturation, thereby indicating that reliable results may still be acquired from a saturated image, as long as the mitochondrial branches remained distinguishable (Lihavainen et al., 2012). Lihavainen and colleagues (2012) have further stated that future development of the software may include the ability to detect aberrations in the mitochondrial structure as a result of chemical induction and/or disease.

Due to the importance of the mitochondria in regulating multiple cellular processes to maintain a healthy cell, studies into the mitochondrial dynamics and kinetics have become of great value, especially with the development of mitochondrial dysfunction aiding in the pathological procurement of degenerative diseases. Thereby, in combination with the aforementioned methods, a greater understanding of the effects that certain small molecules have on the mitochondria, and, thus, the overall health and well-being of a cell may be acquired.

## 4-2. Results and Discussion

### 4-2-1. The assessment of the membrane potential of non-differentiating hMSC-ad cellular mitochondria when exposed to small molecule treatment and/or increased hypoxic conditions

Non-differentiating hMSC-ad cells were exposed to the small molecules S3I-201, Mdivi-1, and M1, whereby the effects of the small molecules were observed after a total time of at least 48 hours had passed; however, changes in some cellular properties were easily observed after 24 hours. This included changes in the number of cells, in relation to the control sample (which remained clear of any small molecules), morphological alterations, as well as the cell's ability to adhere to the culture vessel. The mitochondria within the non-differentiating hMSC-ad cells possessed a more elongated, tubular network of interconnecting mitochondria; membrane potential seemed to be notable high within untreated hMSC-ad cells. The addition of certain small molecules (S3I-201, M1, and Mdivi-1) had varied effects on the mitochondrial membrane potential; S3I-201 caused a decrease in mitochondrial membrane potential, M1 seemed to indicate little effect on the overall mitochondrial

membrane potential generated, whereas Mdivi-1 seemed to show an adverse effect on the mitochondrial membrane potential.

Mitochondrial membrane potential refers to the cells' ability to produce ATP, energy, through a process known as oxidative phosphorylation; the overall health of a cell may, in fact, be monitored via the resulting mitochondrial membrane potential. Perry and Colleagues (2011) have suggested that an increase in mitochondrial membrane potential polarity will provide a greater fluorescence as more stain is retained within the mitochondria. JC-1, as previously described, is a dual fluorescent dye capable of staining red and green in relation to the formation of aggregation within the mitochondria (Perry et al., 2011). The resulting red fluorescence observed equates to the formation of J-aggregates formed, whereas the green fluorescence is indicative of the J-monomer. Mitochondrial polarisation is indicated by the intensity at which the red/green fluorescence ratio is observed, i.e. mitochondrial polarisation is supported by an increased red/green fluorescence ratio, whereas mitochondrial depolarisation is indicated by a decreased red/green fluorescence ratio. In other words, high mitochondrial polarisation is demonstrated by the red/orange fluorescence, whereas the green fluorescing J-monomers are indicative of depolarized membrane potentials. Another indication of mitochondrial depolarisation pertains to the loss of formed monomers (green fluorescence) localised within the mitochondria, in other words, cytoplasmic monomer formation may be present (Perry et al., 2011).

Figure 4-1 demonstrates the resulting mitochondrial membrane potential obtained for non-differentiating hMSC-ad cells treated with varying concentrations of S3I-201 (N = 3). Initially, the cells were seeded onto the culture vessel and allowed to settle for 24 hours after which a media change occurred, consisting of the general MSCM. The media change included the addition of S3I-201, whereby the cells were maintained in this medium for an additional 48 hours.

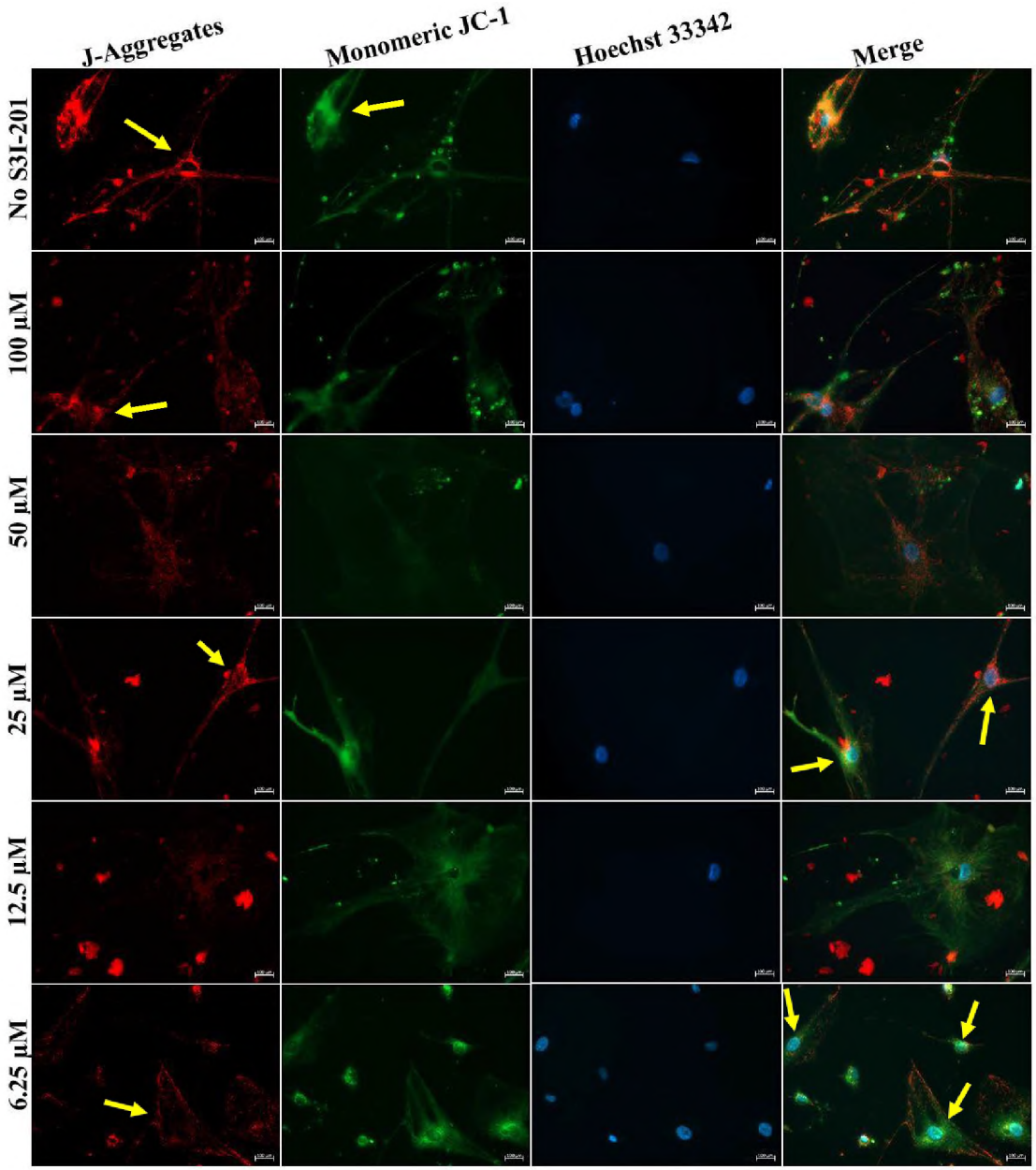


**Figure 4-1. The effects of S3I-201 on the mitochondrial membrane potential in non-differentiating hMSC-ad cells.** HMSC-ad cells were seeded and maintained in MSCM. S3I201 was added into the maintenance media and incubated for 48 hours at 37 °C and 5 % $CO_2$. Images were captured using the Zeiss AxioVert.A1 FL-LED fluorescence microscope at 200x magnification. Scale bar = 20 µm. Images shown are representative of multiple images obtained at random locations within the culture vessel (N = 3).

The results were monitored using fluorescence microscopy and the JC-1 membrane potential live stain as previously discussed. In order to monitor the effects that S3I-201 had on the cells, a control was established in the form of untreated non-differentiating hMSC-ad cells. These cells did not possess any S3I-201 and were cultured under normal conditions. As shown by the arrow for J-Aggregates formed, the untreated hMSC-ad cells retained a highly polarised mitochondrial profile, which is suggestive of stem cells that may undergo differentiation, and, thus, require an increase in energy (Fang et al., 2016). This highly polarised mitochondrial membrane potential was indicated by the high fluorescence intensity of the red/green ratio observed collectively within the Merge panel for untreated hMSC-ad cells.

Upon the addition of S3I-201, there was a significant decrease in J-aggregates formed, i.e. the red fluorescence was decreased quite significantly, in comparison to that observed within the control (panel: No S3I-201); however, this decline in J-aggregates formed did not result in the complete removal of red fluorescence from the images. The concentration-dependent treatments displayed a slight indication of J-aggregates, notably observed for concentrations 100 μM, 50 μM, 25 μM, and 6.25 μM, which, when superimposed with the green fluorescing monomers (merge panels) provided significant indication of resulting red fluorescence with respect to the green fluorescence. In some scenarios, such as that observed for the 6.25 μM, 12.5 μM, 25 μM, and 100 μM S3I-201 concentrations utilized, some cells did not seem to exhibit the red fluorescence of the aggregates, and, instead, only demonstrated the high intensity fluorescence of the monomers. This may indicate that while some cells retained the high mitochondrial polarisation profiles, there were others that suffered from injury and possessed mitochondrial depolarisation to a certain degree. As indicated, concentrations 6.25 μM, 12.5 μM, and 25 μM provided intensely fluorescent monomers localised around the nucleus of the cells, in comparison to the remaining cellular extensions present. Yet, for the 6.25 μM concentration, the merged product still provided indication of mitochondrial polarisation, suggestive of a healthy phenotype.

With regards to the depolarisation evident within the S3I-201 treated cells, this may indicate the cells preparing for apoptosis or mitophagy, as mitochondrial depolarisation does not necessarily result in cell death (Levraut et al., 2003). Mitochondrial permeability transition (MPT) is a process in which the inner mitochondrial membrane undergoes depolarisation in response to perturbance of the outer mitochondrial membrane (Heiskanen et al., 1999; Zorov

et al., 2014). The inhibition of STAT3 may have resulted in the overproduction of reactive oxygen species (ROS), which has been known to activate the MPT pore located within the inner mitochondrial membrane (Levraut et al., 2003; Zorov et al., 2014). The opening of the MPT pore creates mitochondrial depolarisation due to the decrease in mitochondrial membrane potential as the protons within the intermembrane space flow back independent of ATP production within the electron transport chain (Levraut et al., 2003).

It must be noted that there was a large amount of orange/red structures captured within the image. While the precise identification of these was not made, it can be assumed that these 'lumps' coincided with rounding/apoptotic cells or that they were merely the result of the JC1 not dissolving completely in the DMSO.

In order to generate numerical data that may be used to closer evaluate the correlations between the effects of small molecules on non-differentiating hMSC-ad cells and their mitochondria, the fluorescent images obtained via the live JC-1 stains (as shown in Figure 4.1) were input into the Mytoe software, after the green fluorescence channel was altered to display a violet colour. This action was performed due to the finding that the Mytoe analysis software did not necessarily detect the green channel as well as those of a "red" value. It was found that two different results were obtained for the green channel versus the violet channel, with the violet channel providing a more accurate representation of the low mitochondrial membrane potential-stained mitochondria.

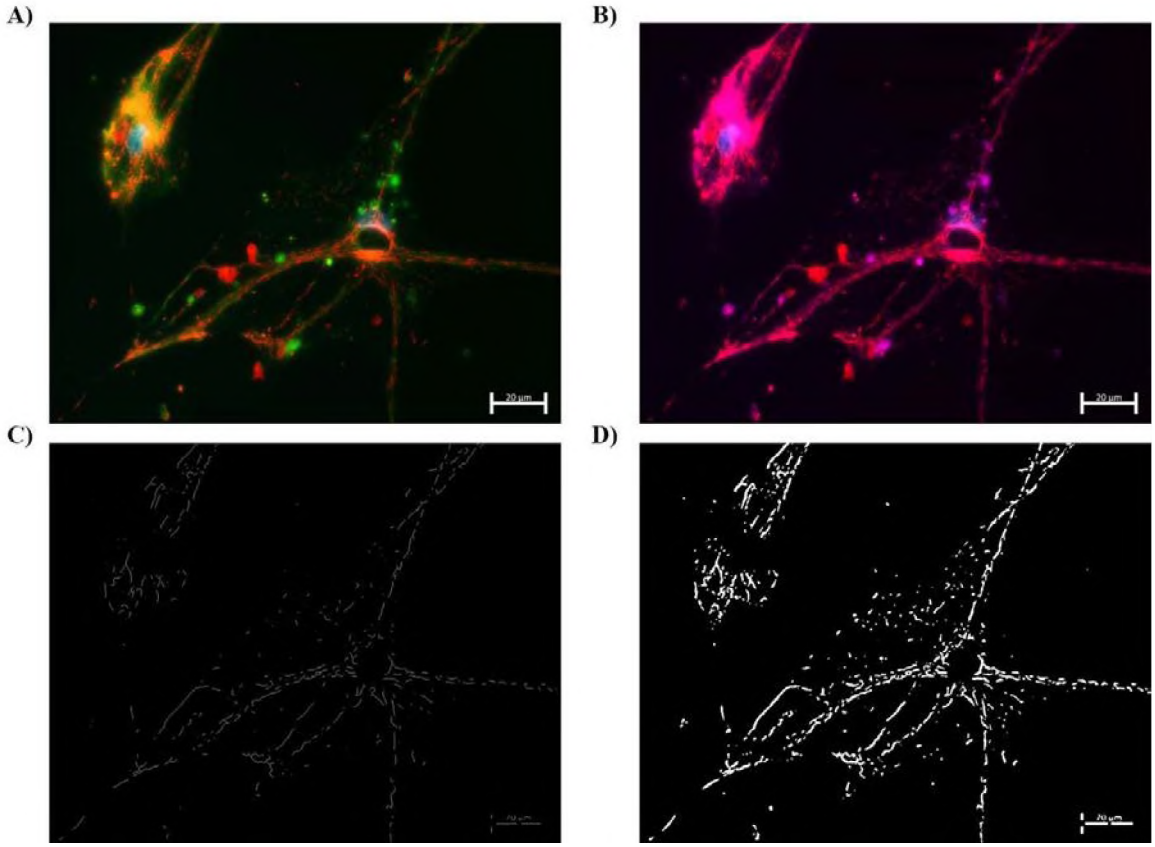


**Figure 4-2. Mitochondrial mask and skeleton generated by Mytoe software**. Examples of mitochondrial masks and skeletons generated using the Mytoe software in order to generate relevant data. A) represents the original image captured, B) is the image with fluorescent colours edited, C) represents the mitochondrial skeleton, and D) indicates the resulting mitochondrial mask generated.

The resulting masks and skeletons, examples found in Figure 4-2, were used to calculate mitochondrial characteristics, such as: the tortuosity (the curvature of the mitochondria); the thickness and the length of the mitochondria; as well as the resulting distances from the cellular membrane and the nucleus membrane, measured in μm. Individual values for each mitochondrial characteristic listed were obtained for each mitochondrion identified by the software. The values for each of the treatments with the small molecules were averaged and the standard deviations were calculated as demonstrated below.

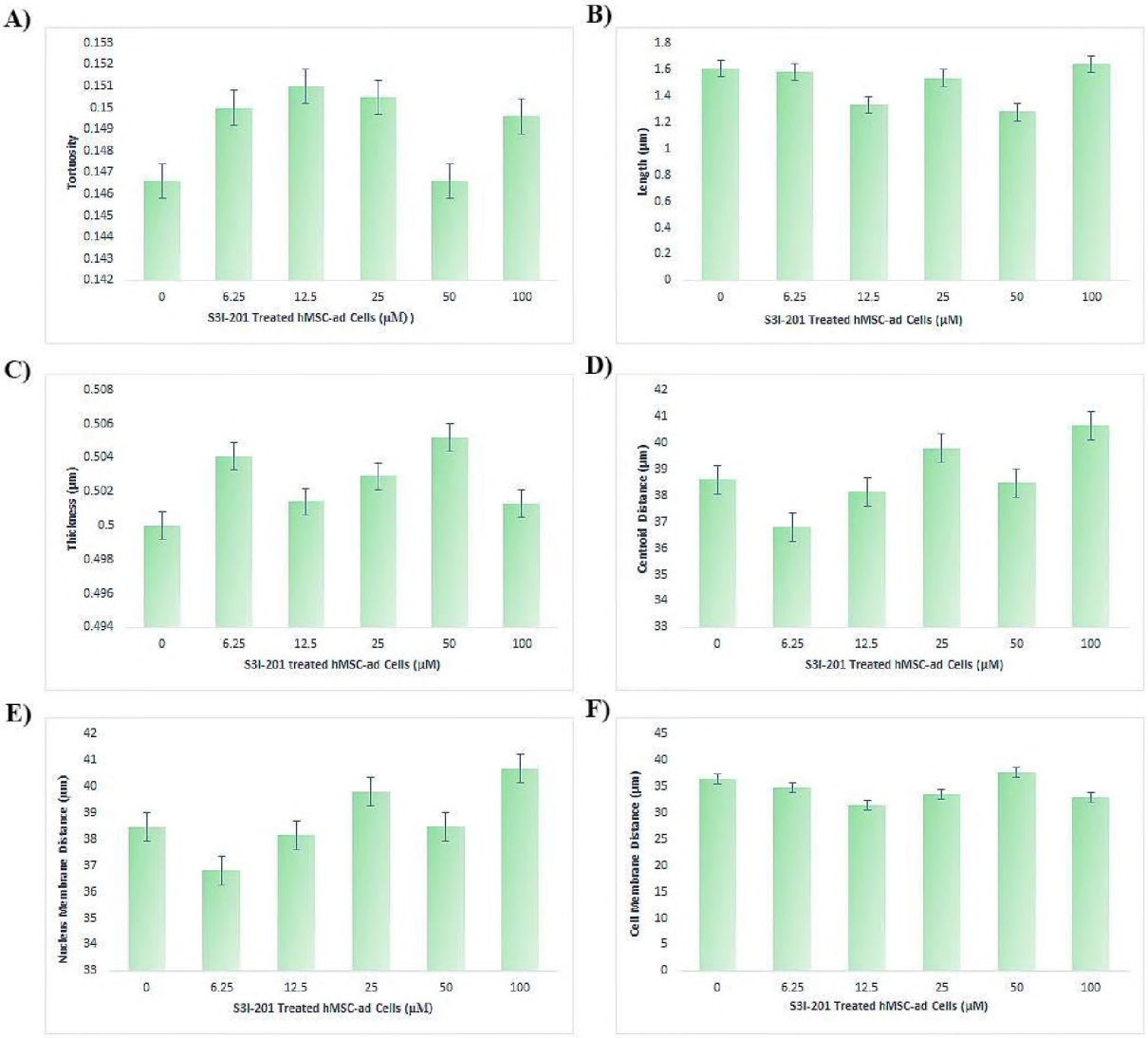


**Figure 4-3. Mitochondrial characteristics observed after the S3I-201 treatment of hMSC-ad non-differentiating cells.** Data was generated using the fluorescent images obtained via live JC-1 staining and the input of these images into the Mytoe software. The values were obtained and the average and standard deviation was calculated. The average values obtained for each characteristic was graphically represented as A) the tortuosity of the mitochondria, B) the length of the mitochondria, C) the thickness of the mitochondria, D) the centroid distance of the mitochondria, E) the distance from the nucleus membrane, and F) the distance from the cell membrane. (N = 3).

**Table 4-1. Numerical values obtained for mitochondrial characteristics observed after S3I-201 treatment of non-differentiating hMSC-ad cells.**

| Sample (μM) | Tortuosity | Length (μm) | Thickness (μm) | Centroid Distance (μm) | Distance Nucleus Membrane (μm) | Distance from Cell Membrane (μm) |
|---|---|---|---|---|---|---|
| 0 | 0.147 ± 0.003 | 1.602 ± 0.025 | 0.500 ± 0.007 | 38.460 ± 0.267 | 38.458 ± 0.264 | 36.347 ± 1.531 |
| 6.25 | 0.150 ± 0.003 | 1.584 ± 0.034 | 0.504 ± 0.002 | 36.805 ± 2.023 | 36.797 ± 2.026 | 34.742 ± 0.288 |
| 12.5 | 0.151 ± 0.007 | 1.327 ± 0.088 | 0.501 ± 0.008 | 38.135 ± 5.620 | 38.139 ± 5.622 | 31.329 ± 2.809 |
| 25 | 0.151 ± 0.001 | 1.534 ± 0.117 | 0.503 ± 0.001 | 39.778 ± 2.012 | 39.784 ± 2.014 | 33.493 ± 7.236 |
| 50 | 0.147 ± 0.004 | 1.276 ± 0.106 | 0.505 ± 0.010 | 38.463 ± 3.275 | 38.463 ± 3.276 | 37.541 ± 4.790 |
| 100 | 0.150 ± 0.003 | 1.640 ± 0.028 | 0.501 ± 0.007 | 40.664 ± 2.295 | 40.663 ± 2.294 | 32.910 ± 0.636 |

From the data generated, as per Figure 4-3 and Table 4-1, it seemed evident that there was no significant impact of S3I-201 treatment on the mitochondrial characteristics of non-differentiating hMSC-ad cells. It can be noted that the length of the mitochondria varied slightly, with 50 μM S3I-201 demonstrating the lowest mitochondrial length; albeit, the 100 μM S3I-201 treated hMSC-ad cells exhibited a similar length to the untreated cells. The thickness of the mitochondria was not significantly affected; this was evident within Table 41 whereby the greatest difference in thickness was between the 0.505 ± 0.010 μm calculated for the 50 μM S3I-201 treatment and the 0.500 ± 0.007 μm calculated for the untreated control. There was little difference observed regarding the overall cellular and nuclear membrane distances; however, it must be acknowledged that a general collective decrease in distance was observed for the distance from the cell membrane. This was evident by the general decrease in distances observed across all concentrations of S3I-201 treatment (including the control). Therefore, this is indicative that, while the mitochondria seem to be

equally dispersed throughout the cell body, the mitochondria are slightly closer to the cellular membrane than the nucleus membrane.

From the data observed above, it may be speculated that S3I-201 does not necessarily affect the STAT3 localised within the mitochondria, and/or inhibition of STAT3 does not necessarily alter the characteristics of the mitochondria that might inhibit/promote adipogenesis, and, thus, lead to degenerative disorders, such as obesity and insulin resistance. The average healthy mitochondrion present within a eukaryotic cell possesses a reported length of approximately 1 – 2 μm, and an approximate diameter of 0.2 – 0.7 μm (Baffou et al., 2014).

The images demonstrated in Figure 4-4 were the result of JC-1 live staining performed on cells treated for cobalt chloride and S3I-201 (N = 2); this was performed in order to observe the effects that chemically induced hypoxia may have on the characteristics of mitochondria exposed to the STAT3 inhibitor within non-differentiating hMSC-ad cells. The control was comprised of untreated hMSC-ad cells that had been treated with 100 μM cobalt chloride. A generally low intensity was observed for both aggregates and monomers formed within the resulting stain; however, the merged ratio of intensity provides an indication that mitochondrial membrane polarization is present within the chemically induced hypoxic cells.

As the concentration of S3I-201 was increased, the ratio of intensity of monomer fluorescence increased, thereby leading to speculation that mitochondrial membrane depolarisation was occurring. Another indication of severe depolarisation is present, in particular, within the 100 μM S3I-201 treated hMSC-ad cells where it appears as though there is some indication of cytoplasmic monomers; and as previously described, cytoplasmic monomer formation is an indication of mitochondrial depolarisation. There were multiple incidences of a greater intensity of monomer fluorescence observed throughout the collection of concentrations of S3I201 utilized; however, for the 50 μM, 12.5 μM, and 6.25 μM S3I-201 treatments, superimposition of the images established the red/green ratio of aggregates and monomers, suggesting that mitochondrial polarisation remained established within these cells.

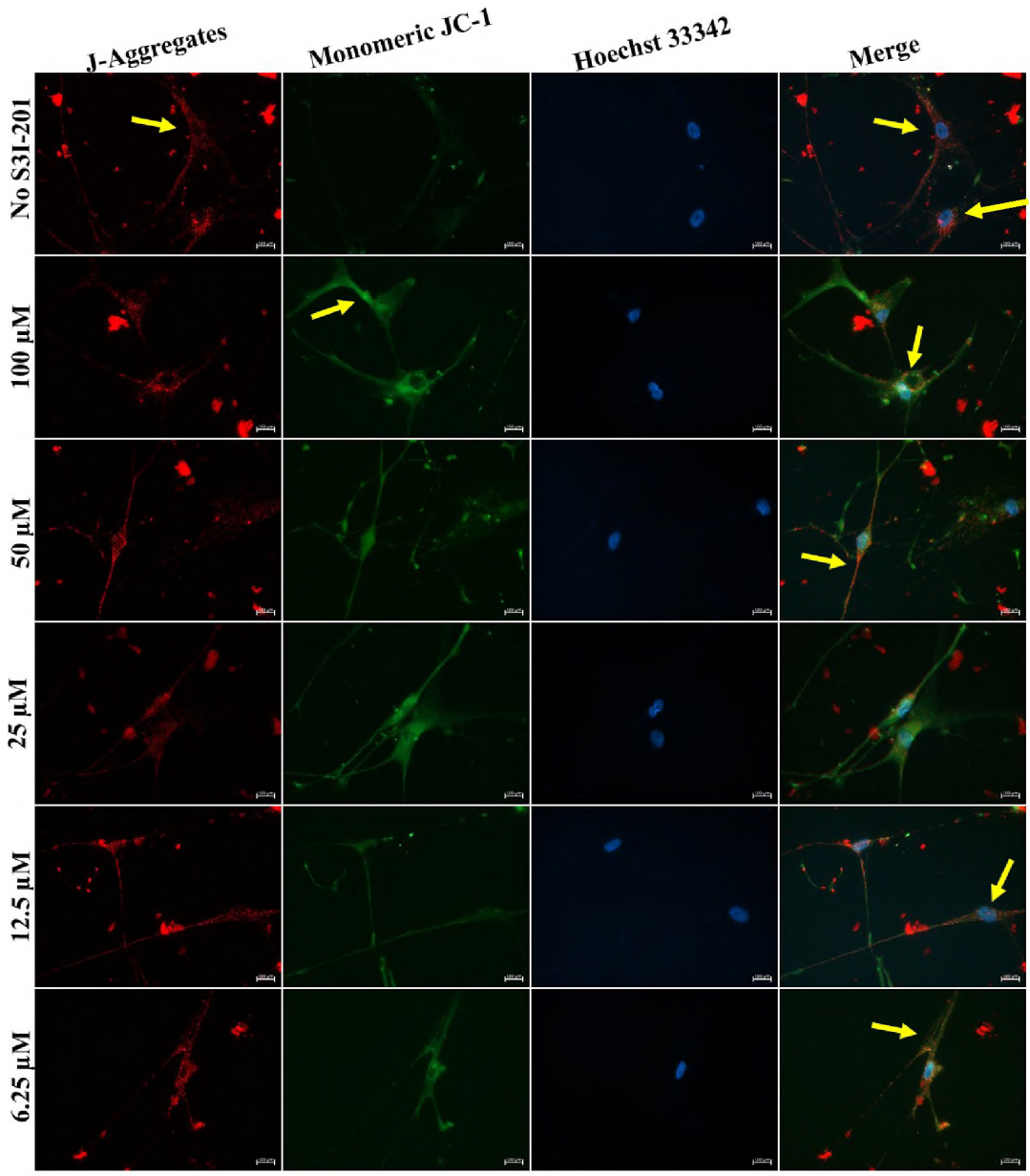


**Figure 4-4. The effects of S3I-201 in a chemically induced hypoxic environment on the mitochondrial membrane potential in non-differentiating hMSC-ad cells.** HMSC-ad cells were seeded and maintained in MSCM. S3I-201 and 100 µM cobalt chloride (CoCl) was added into the maintenance media and incubated for 48 hours at 37 °C and 5 % $CO_2$. Images were captured using the Zeiss AxioVert.A1 FL-LED fluorescence microscope at 200x magnification. Scale bar = 20 µm. Images shown are representative of multiple images obtained at random locations within the culture vessel (N = 2).

It must be noted that cellular morphological differences were observed between the cells exposed to an increased level of hypoxia, and those that were cultured in normal conditions. The hMSC-ad cells shown in Figure 4-4 seemed to demonstrate a more spindle-like/fusiform morphology with long, thin cellular extensions. The cells present within Figure 4-1 possessed a more fibroblastic morphology with, overall, larger bodies that seemed to provide a greater surface area.

When compared to results obtained in Figure 4-1, which represented the effects of S3I-201 on the mitochondrial membrane potential within normal culture conditions (i.e. with the exclusion of cobalt chloride), it was evident that the non-differentiating hMSC-ad cells exposed to chemically induced hypoxia displayed a decreased intensity of fluorescence, therefore mitochondrial depolarisation, overall, as the untreated hMSC-ad cells in Figure 4-1 displayed an increased affinity for a high mitochondrial membrane potential, yet, still showed evidence of some monomeric JC-1 that was not obsolete. The intensity of S3I-201 for monomeric JC-1, in Figure 4-1, seemed to be visually on par with that observed in Figure 4-4.

The resulting data (N = 2) obtained, as shown in Figure 4-5 and Table 4-2, demonstrated little relative difference in tortuosity values generated for each S3I-201 concentration. There was a minimal difference in mitochondrial average thickness throughout the concentrations of the various S3I201 treated cells, with only a slight increase in thickness observed for S3I-201 treatment, with the exception of the 25 μM S3I-201 treated hMSC-ad cells which possessed an average thickness of 0.496 μm, which was equal to that of the control. A slight increase in average mitochondrial length was observed as the concentrations of S3I-201 increased, with the exception of the 12.5 μM S3I-201 treatment, which demonstrated the greatest average length observed with a calculated value of 1.622 μm. However, it must be acknowledged that the overall length demonstrated remained within the reported mitochondrial range, previously described, of 1 – 2 μm. Looking at the slight increase, however, it may be speculated that S3I-201 within a chemically induced hypoxic environment may have an impact on the resulting length of mitochondria.

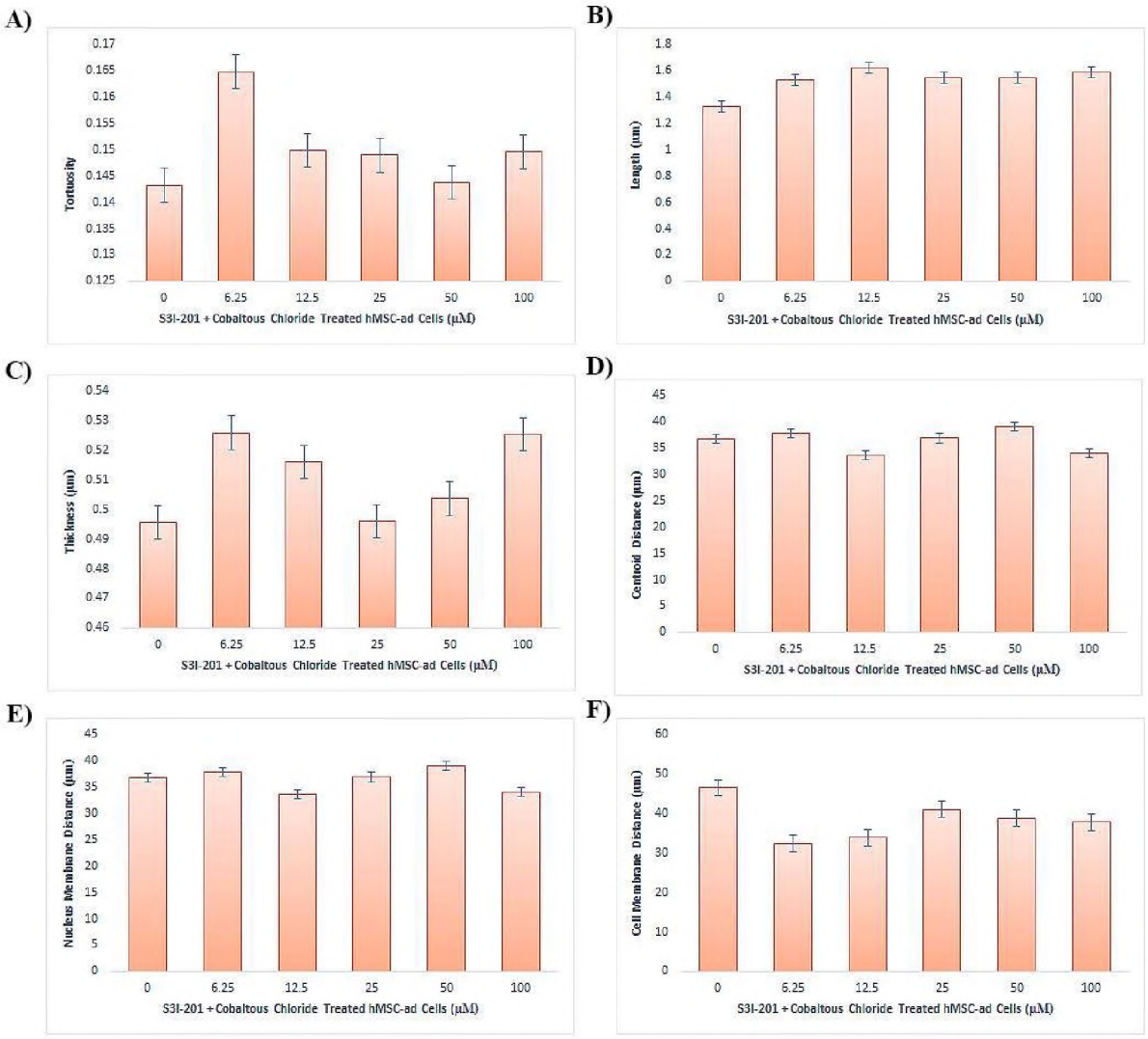


**Figure 4-5. Mitochondrial characteristics of S3I-201 and cobalt chloride treated non-differentiating hMSC-ad cells**. Data was generated using the fluorescent images obtained via live JC-1 staining and the input of these images into the Mytoe software. The values were obtained and the average and standard deviation was calculated. The average values obtained for each characteristic was graphically represented as A) the tortuosity of the mitochondria, B) the length of the mitochondria, C) the thickness of the mitochondria, D) the centroid distance of the mitochondria, E) the distance from the nucleus membrane, and F) the distance from the cell membrane. (N = 2)

**Table 4-2. Numerical values obtained for mitochondrial characteristics observed after S3I-201 and cobalt chloride treatment of non-differentiating hMSC-ad cells.**

| Sample (μM) | Tortuosity | Length (μm) | Thickness (μm) | Centroid Distance (μm) | Nucleus Membrane Distance (μm) | Cell Membrane Distance (μm) |
|---|---|---|---|---|---|---|
| 0 | 0.143 ± 0.003 | 1.327 ± 0.061 | 0.496 ± 0.001 | 36.666 ± 0.100 | 36.663 ± 0.102 | 46.430 ± 9.036 |
| 6.25 | 0.165 ± 0.005 | 1.528 ± 0.046 | 0.528 ± 0.016 | 37.802 ± 2.511 | 37.808 ± 2.512 | 32.370 ± 1.252 |
| 12.5 | 0.149 ± 0.001 | 1.622 ± 0.045 | 0.516 ± 0.007 | 33.615 ± 4.719 | 33.616 ± 4.722 | 33.832 ± 0.345 |
| 25 | 0.149 ± 0.001 | 1.544 ± 0.072 | 0.496 ± 0.001 | 36.819 ± 0.778 | 36.813 ± 0.784 | 40.933 ± 1.481 |
| 50 | 0.144 ± 0.005 | 1.544 ± 0.054 | 0.504 ± 0.005 | 38.933 ± 4.179 | 38.927 ± 4.180 | 38.691 ± 3.312 |
| 100 | 0.150 ± 0.004 | 1.583 ± 0.056 | 0.525 ± 0.007 | 33.949 ± 2.634 | 33.951 ± 2.629 | 37.767 ± 0.281 |

The distance between the nucleus and cell membrane decreased in both perspectives; with an initial value of 36.663 ± 0.102 μm and 46.430 ± 9.036 μm, respectively, for untreated cells (those that remained untreated for S3I-201 but were treated with 100 μM cobalt chloride), these values decreased to 33.951 ± 2.629 μm and 37.767 ± 0.281 μm, respectively, as the concentration of S3I-201 increased to 100 μM. The resulting impact that the addition of cobalt chloride had on the S3I-201 deficit cells may lead to speculations that the mitochondria are drawn closer to the nucleus in the event of chemically induced hypoxia. However; regarding the treatment with S3I-201, it cannot be definitively stated that these conditions resulted in the migration of the mitochondria to the closer proximity to either the nucleus or cell membrane. The addition of increasing concentrations of S3I-201 provided distance values that were relatively similar; for example, 50 μM S3I-201 treatment resulted in a nucleus membrane distance of 38.927 ± 4.180 μm and a cell membrane distance of 38.691 ± 3.312 μm.

When compared to the results previously obtained for cells only treated with S3I-201 under normal culture conditions for hMSC-ad cells, it was found that the cells treated for S3I-201

and cobalt chloride displayed an equivalent overall mitochondrial tortuosity and a similar thickness for each of the aforementioned concentrations; however, there was a minimal difference observed regarding the average mitochondrial length. The cobalt chloride treated cells displayed a slight decrease in mitochondrial length when compared to those that remained untreated; this was evident in values obtained for the cells that were not treated for S3I-201 in both scenarios. For the cobalt chloride-deficit cells, an average length of $1.602 \pm 0.025$ μm was observed, whereas the 100 μM cobalt chloride treated cells possessed an average length of $1.327 \pm 0.061$ μm. This length was almost rectified with the addition of the S3I-201 concentrations to the increased hypoxic environment. This may, in turn, lead to the speculation that the inhibition of STAT3 may be essential when hMSC-ad cells are exposed to a chemically induced hypoxic environment; the restriction of STAT3 production enhances the generation of ROS, which are required, within moderation, for various cell signalling functions. Upon chemical induction of hypoxia, the mitochondria undergo an enhanced production of ROS through complex III of the electron transport chain (Al-Mehdi et al., 2012). Jung and colleagues (2005) demonstrated the potential of hypoxia to activate STAT3 and HIF-1α (hypoxiainducible factor-1α). The continuous activation of STAT3 and HIF-1α has been linked to cancer and tumour development, and angiogenesis.

From this, it may be speculated that during the chemical induction of hypoxia (generated by 100 μM cobalt chloride) ROS content and activation of STAT3 is promoted; however, in contradiction, this increased level of STAT3 may cause an additional inhibition of ROS generated, thereby reducing the cell's capability of regulating cellular functions while in a hypoxic environment. The introduction of S3I-201 depletes this additional STAT3, and promotes the regulation and maintenance of normal cellular function.

The distance relative to the nucleus membrane also differed in the way that cells that were not treated with cobalt chloride had an increased distance from the nucleus membrane, whereas the hMSC-ad cells treated with cobalt chloride bore an increased distance from the cell membrane in comparison to what was observed for those that were not cultured in the presence of cobalt chloride. Due to their dynamic ability of motility, mitochondria may be distributed throughout the cell in accordance to specific conditions; Al-Mehdi and colleagues (2012) have suggested mitochondrial transportation to the proximity of the cytoplasm endoplasmic reticulum controls the release of calcium, whereas perinuclear mitochondrial clustering may be in response to high energy demands, such as cell stress during infection,

as well as embryonic development. Furthermore, Al-Mehdi and colleagues (2012) demonstrated that induced hypoxia results in the clustering of the mitochondria around the nucleus; this action is performed in order to deliver ROS to the nucleus, which, thus, causes various oxidative DNA modifications to occur.

In contradiction, Estrada and colleagues (2012) have indicated that the culture of hMSC cells at 20 % oxygen may lead to an increase in oxidative damage, DNA damage markers, chromosomal abnormalities, as well as telomere shortening; thereby, they performed a study whereby the compared the effects of culture within a 20 % oxygen environment versus a 3 % oxygen environment. It was found that the cells cultured at the lower oxygen environment demonstrated an increased growth rate, as well as a reduced rate of telomere shortening. This increased the lifespan of the cells due to the increased protection from oxidative stress.

Future experiments are vital in order to confirm the above speculation; immunofluorescence microscopy and immunoblotting may be vital techniques to be considered with regards to the determination of STAT3 levels present within non-hypoxic versus hypoxic hMSC-ad cells. This would provide greater insight into the true nature of induced hypoxia and the role it plays upon ROS and STAT3. Antioxidant treatments may also be utilized.

Fusion was originally defined as a mechanism in which intact, functioning mitochondria compensated for a damaged unit, thereby initiating a recovery mechanism in which it would aid in the maintenance of the metabolic activity (Twig et al., 2008). Upon the reduction of the mitochondrial membrane potential, a considerable amount of mitochondrial network fragmentation and the degradation of OPA1 occurs; this leads to the inhibition of fusion. Twig and colleagues (2008) stated that mitochondria unable to undergo fusion exhibit a low mitochondrial potential due to the depletion of OPA1.

As previously described, a control was utilized whereby the cells were not subjected to treatment with M1; only non-differentiating hMSC-ad cells were cultured in normal culture conditions. The control present with a higher intensity fluorescence of monomers formed, indicative of a decreased mitochondrial membrane potential; however, the intensity of fluorescence of the red/green ratio observed within the 'Merge' panel, provided evidence that mitochondrial polarisation was still present.

Much unlike what was observed in the previous chapter, the JC-1 live stain of the mitochondrial fusion promoter, M1, treated cells produced different results in terms of cell survival (N = 2).

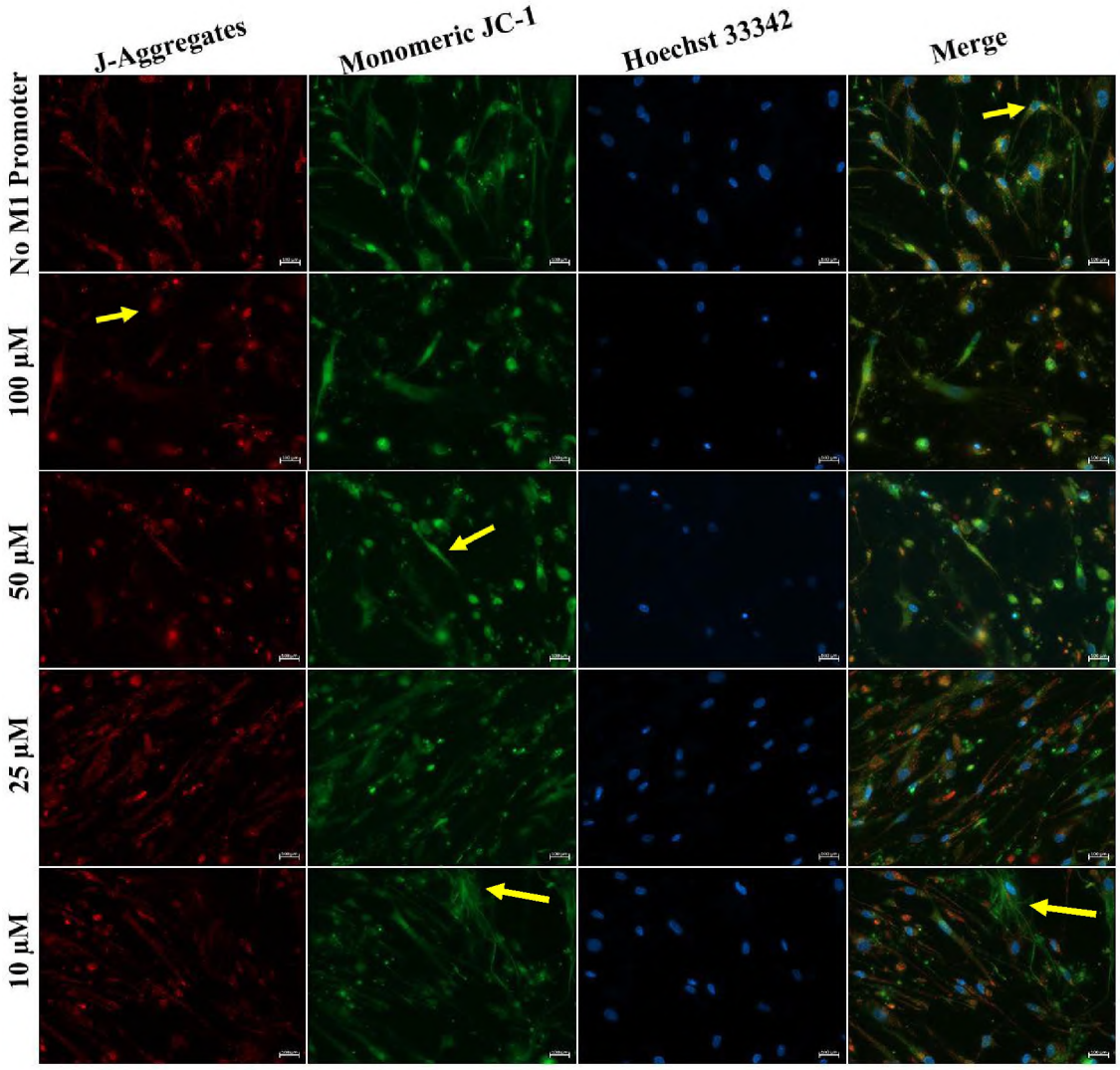


**Figure 4-6. The effects of the mitochondrial fusion promoter, M1, on the mitochondrial membrane potential in non-differentiating hMSC-ad cells.** HMSC-ad cells were seeded and maintained in MSCM. M1 mitochondrial fusion promoter was added into the maintenance media and incubated for 48 hours at 37 °C and 5 % $CO_2$. Images were captured using the Zeiss AxioVert.A1 FL-LED fluorescence microscope at 200x magnification. Scale bar = 20 µm. Images shown are representative of multiple images obtained at random locations within the culture vessel (N = 2).

This may be attributed to several reasons, including a more delicate wash procedure that did not extensively rinse the cells, thus, preserving those that were attached to the culture vessel, as well as the cells might have undergone a more rapid proliferation, thus increasing the confluency more dramatically over the 24 hours. From brief observations, it may be noted that the resulting monomeric JC-1 seemed to be of similar intensity throughout the various concentrations of M1 fusion promoter and the untreated cells. Inspection of the J-Aggregates formed provided evidence that there was an evident decrease in functioning mitochondrial membrane potential upon the increase of the M1 fusion promoter; 100 μM M1 treatment provided the least amount of J-Aggregates in comparison to the monomeric JC-1 formed. A decrease in cell survival must also be noted; some of the cells were undergoing apoptosis and possessed an unhealthy rounded morphology. These 'rounded' cells decreased as the M1 mitochondrial fusion promoter decreased; thereby suggesting that high levels of mitochondrial fusion recruit the damaged mitochondria at an increased rate, whereby they either undergo autophagy or fission promotes additional damaged/altered mitochondria to be produced.

An interesting observation was made in terms of morphology present within the 10 μM concentration of M1. The morphology observed was of a more filamentous form with multiple cellular extensions present; this structure could be identified as a cell due to the presence of the nucleus within the merged image. Interestingly, this filamentous structure seemed to lack the J-Aggregates associated with a high mitochondrial membrane potential; thereby suggesting that this cell held a reduced capacity of ATP production and was the result of either injury or a malfunction in cellular health (Perry et al., 2011). This structure was only observed within the non-differentiating hMSC-ad cells treated with 10 μM M1 fusion promoter, and was noticed on several occasions within the culture vessel at random locations. It may be further speculated that the highlighted figure may have been, in fact, a network of filamentous mitochondria present within the cell, itself; however, it can be concluded that this filamentous structure held an increased mitochondrial depolarisation due to the formation of monomers within the cellular cytoplasm instead of mitochondria, as well as the lack of green/red intensity fluorescence ratio.

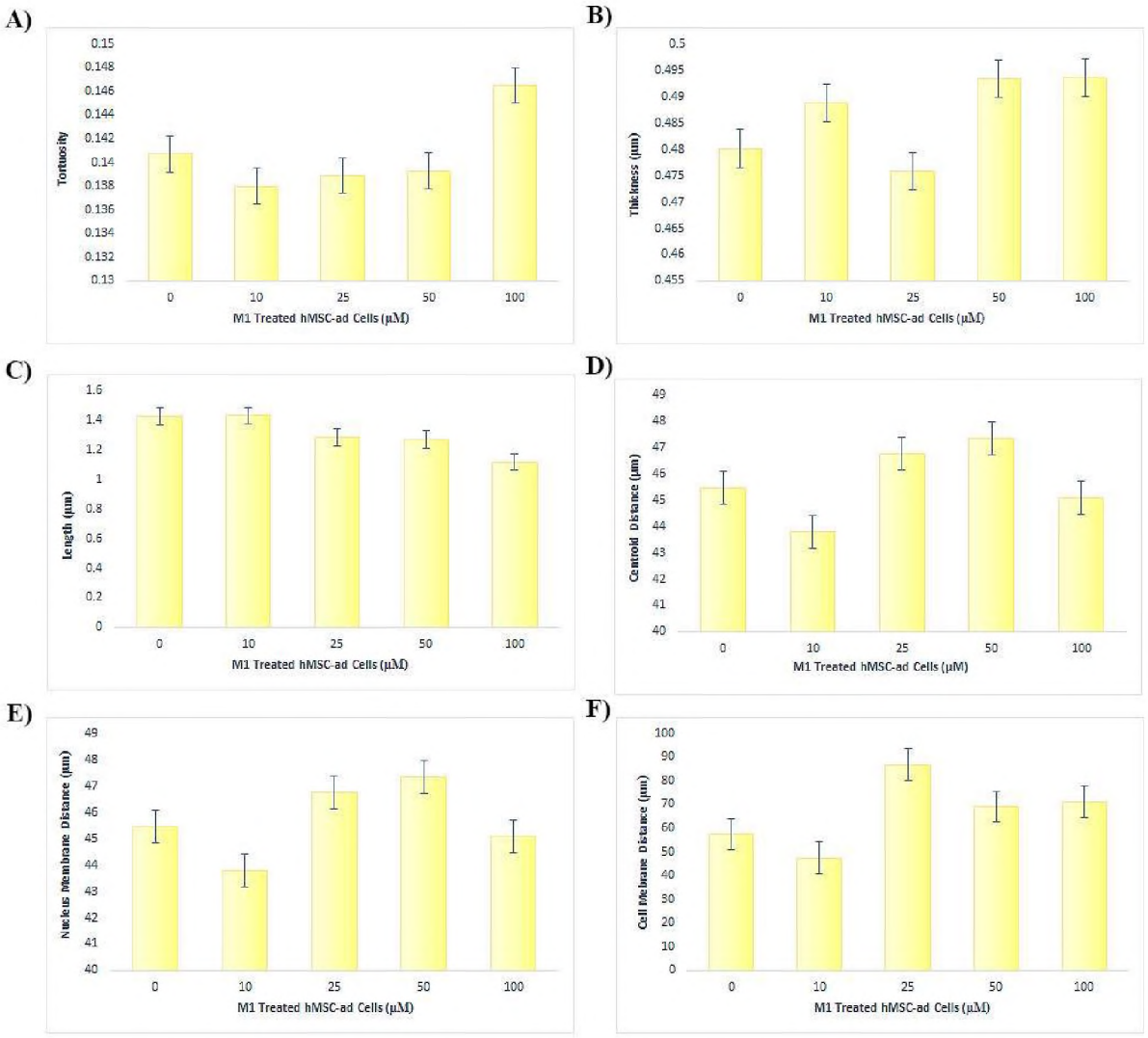


**Figure 4-7. Mitochondrial characteristics obtained after undifferentiated hMSC-ad cells were treated with the mitochondrial fusion promoter, M1, after 48 hours**. Data was generated using fluorescent images obtained via the JC-1 live staining. These images were applied to the Mytoe software, and the resulting values generated for each characteristic were plotted graphically as A) the tortuosity of the mitochondria, B) the thickness of the mitochondria, C) the length of the mitochondria, D) the centroid distance, E) the distance from the nucleus membrane, and F) the distance from the cell membrane. (N = 2)

**Table 4-3. Numerical values obtained for mitochondrial characteristics observed after the treatment of non-differentiating hMSC-ad cells with the mitochondrial fusion promoter, M1.**

| Sample (μM) | Tortuosity | Length (μm) | Thickness (μm) | Centroid Distance (μm) | Nucleus Membrane Distance (μm) | Cell Membrane Distance (μm) |
|---|---|---|---|---|---|---|
| 0 | 0.141 ± 0.003 | 1.422 ± 0.026 | 0.480 ± 0.004 | 45.450 ± 1.092 | 45.450 ± 1.092 | 57.402 ± 0.227 |
| 10 | 0.138 ± 0.001 | 1.428 ± 0.072 | 0.489 ± 0.008 | 43.789 ± 0.969 | 43.794 ± 0.972 | 47.320 ± 3.936 |
| 25 | 0.140 ± 0.003 | 1.284 ± 0.055 | 0.476 ± 0.000 | 46.767 ± 0.043 | 46.762 ± 0.041 | 86.735 ± 19.495 |
| 50 | 0.140 ± 0.001 | 1.269 ± 0.049 | 0.493 ± 0.002 | 47.348 ± 0.534 | 47.346 ± 0.536 | 69.024 ± 3.628 |
| 100 | 0.147 ± 0.000 | 1.114 ± 0.014 | 0.494 ± 0.011 | 45.086 ± 1.431 | 45.082 ± 1.433 | 71.085 ± 6.767 |

The resulting graphical representation and numerical values tabulated (Figure 4-7 and Table 43) provide insight into the effects that the mitochondrial fusion promoter, M1, may have on non-differentiating hMSC-ad cells. Little change was evident regarding these tortuosity and mitochondrial thickness, leading to the speculation that the mitochondrial fusion promoter does not affect the curvature of the mitochondria nor the width. There was a slight decrease in the overall length; this was evident in the decreasing values observed for the M1 treated cells, whereby the highest concentration (100 μM) provided the lowest average length (1.114 ± 0.014 μm) in comparison to the untreated control (1.422 ± 0.026 μm). Treatment of 10 μM M1 held a relatively similar value to that of control, calculated at 1.428 ± 0.072 μm, suggesting that mitochondrial "normalcy" regarding morphological traits are exhibited here, regardless of the strange filamentous structures observed. It was originally speculated that the fusion promoter would enhance both the length and thickness of the mitochondria due to the belief that after mitochondrial division, the cells would fuse together as a result of their dynamic capabilities (Hales, 2010). This hypothesis was substantiated by the claim that a lack of functioning mitofusins resulted in the fragmentation of the mitochondrial network;

therefore, by enhancing the ability of the mitochondria to undergo fusion, long chains of tubular mitochondrial networks would be formed. Parkinson's disease has been correlated with mitochondrial dynamics whereby the excessively damaged mitochondria undergo fusion and are present within the network. These damaged mitochondria are responsible for excess ROS generation. The integrity of the mitochondria is maintained by the segregation techniques associated with mitofusin regulation. A change in the membrane potential of damaged mitochondria is monitored by PINK1, which then recruits Parkin. Parkin is responsible for the ubiquitination of the mitofusins (Hales, 2010). It can, thus, be speculated that damaged mitochondria are constantly being recruited/fused into a 'healthy' mitochondrial network through the excessive promotion of the fusion process.

Future studies may be performed in accordance to the impact that mitochondrial fusion may have on the integrity of the mitochondrial networks; here, a more gene-targeted approach may be adopted whereby direct knockdown and/or expression of mitofusins may be utilized in addition to inhibition/promotion of PINK1.

A greater affinity to the nucleus membrane was demonstrated by the mitochondria within M1 treated cells, as, overall, an increased distance was calculated regarding the nucleus membrane distance, and that of the cell membrane. Comparatively, the 100 μM M1 treated cells demonstrated a mitochondrial localisation of 45.082 ± 1.433 μm nucleus membrane distance, whereas the cellular membrane distance was calculated at approximately 71.085 ± 6.767 μm. It could, therefore, be concluded, that a general increase in cell membrane distance was observed for increasing concentrations of M1, whereas, the nucleus membrane distance remained a bit more consistent throughout the concentration dependent treatments. The affinity to the nucleus membrane was to be expected, especially during the event of injury or a decline in cellular health caused by an imbalance within the mitochondrial dynamic network. It was speculated that the mitochondria would seek to actively protect and recover the nucleus during this time, or transfer ROS across to the nucleus. This hypothesis was substantiated both graphically and numerically throughout the treatment of the cells with the mitochondrial M1 fusion promoter. It may further be substantiated by Al-Mehdi and colleagues' (2012) observation that mitochondrial clustering around the nucleus occurs within an event of injury. Mfn2 is responsible for regulating mitochondrial fusion as well as

regulating the movement of mitochondria around the cell (Misko et al., 2010). It was demonstrated that neurons lacking
Mfn2 provided a decreased rate of mitochondrial transport that led to the clustering of the mitochondria around the nucleus instead of maintaining the movement to the axons. This concept may be applied to the hMSC-ad cells, which may also possess cellular extensions that may be deprived of mitochondria.

As mentioned previously, the M1 fusion promoter is known to restore the mitochondrial tubular network within Mfn1/2 deficient cells; however, there seems to be little evidence into the effects that an overstimulation of fusion may present on human adipose-derived mesenchymal stem cells. However, it may be speculated that an excess of mitochondrial fusion may upset the balance within mitochondrial dynamics as this remains to be a tightly controlled process. This upset may, thus, lead to the development of pathological states whereby the mitochondrial aberrations formed are the culprits.

Mitochondrial fission is governed by a dynamin-related protein (DRP1) and the fission 1 (Fis 1) protein. Drp1 is responsible for the maintenance of apoptosis, mitophagy, as well as the overall survival of the cell. This dynamic process plays an extremely significant role in the proliferation of the mitochondria, as well as the removal of damaged mitochondria from cells (Rosdah et al., 2016). Mdivi-1 is a fission inhibitor that restricts the GTPase activity through the inhibition of Drp1 to self-assemble. Yeon and colleagues (2015) have suggested that the addition of Mdivi-1 presents with netlike mitochondria, depending on the concentrations used, which may be reversible. Extreme ROS production occurs when mitochondrial membrane potential is perturbed in addition to the uncoupling of oxidative phosphorylation (Yeon et al., 2015). As discussed previously, Mdivi-1 (mitochondrial division inhibitor-1)is a chemical compound responsible for the inhibition of Drp1 and bears a half-life of approximately 6 – 24 hours within in vitro cell lines.

For comparative purposes, an untreated control was established, in Figure 4-8, whereby the cells remained untreated for Mdivi-1; a strong fluorescence intensity was observed as demonstrated by the formation of aggregates, which provided a red/green ratio indicative of mitochondrial polarization. As previously described, this mitochondrial polarization is

expected within stem cells capable of differentiation, and is indicative of their plastic properties.

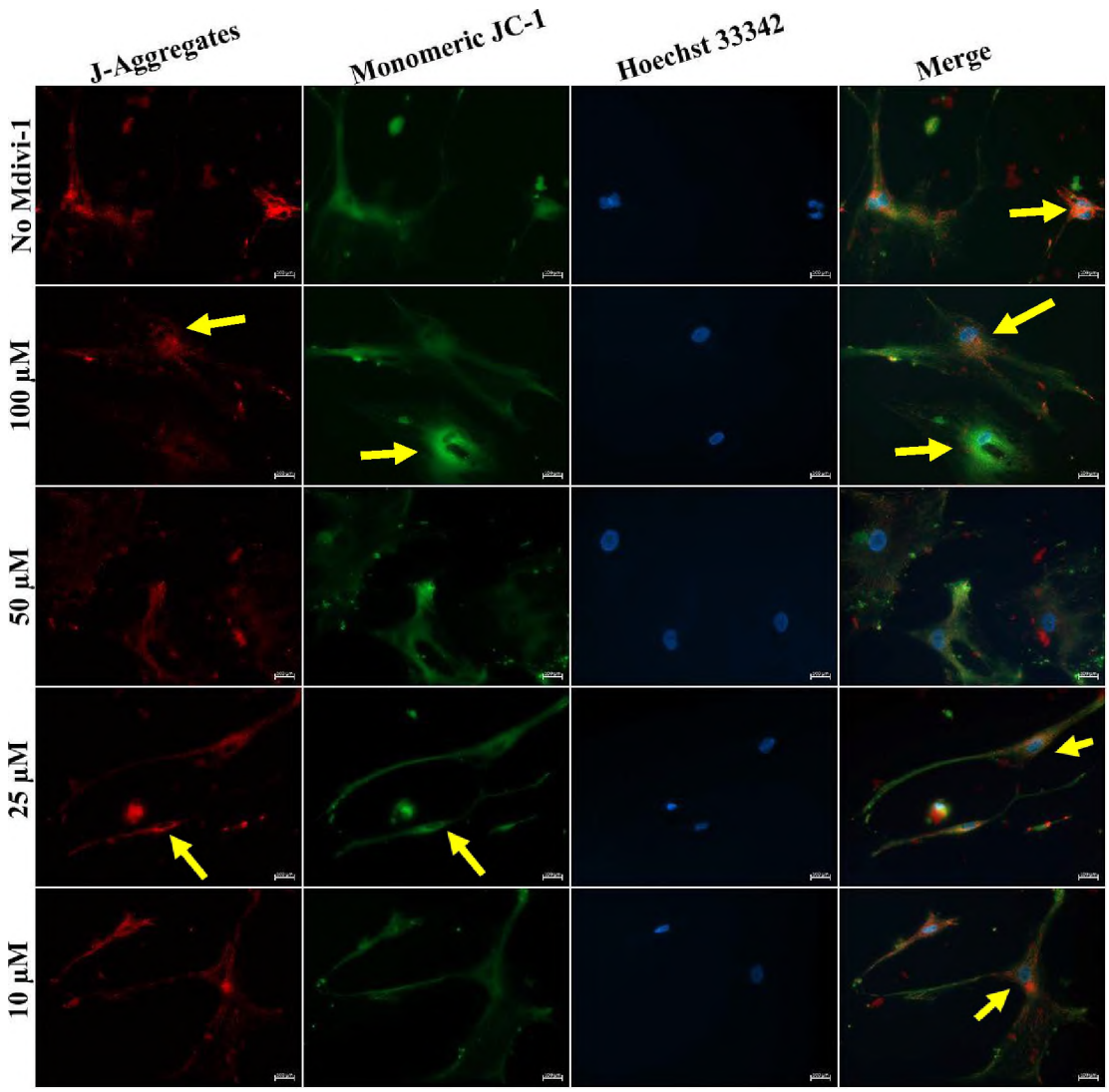


**Figure 4-8. The effects of the mitochondrial fission inhibitor, Mdivi-1, on the mitochondrial membrane potential in non-differentiating hMSC-ad cells**. Human adipose derived mesenchymal stem cells were seeded and maintained using MSCM. The Mdivi-1 fission inhibitor was added into the maintenance media and incubated for approximately 48 hours within a 37 °C and 5 % $CO_2$ humidified environment. Images were captured using the Zeiss AxioVert.A1 FL-LED fluorescence microscope at 200x magnification. Scale bar = 20 µm. Images shown are representative of multiple images obtained at random locations within the culture vessel (N = 3).

When exposed to Mdivi-1, the resulting mitochondrial membrane potential fluorescence intensities (N = 3) provided evidence of an increase in mitochondrial polarization and mitochondrial membrane potential as concentrations of Mdivi-1 were decreased. This was particularly evident for comparisons between the 100 μM Mdivi-1 treatments and the 10 μM Mdivi-1 treatments, whereby the ratio of red/green was more favourable for the 10 μM Mdivi-1 treatments; however, it must be noted that on some occasions, the aggregates were noted in a greater than/equal to manner regarding monomer formation. This observation was highlighted within the 'Merge' panel of 100 μM Mdivi-1 treatment. This may lead to the speculation that, while a general increase in mitochondrial depolarization may be observed for some populations within the culture, there are others that still possess a strong inclination of mitochondrial polarization.

In addition to the mitochondrial membrane potentials observed, it was also evident that perinuclear mitochondrial clustering was observed due to the intensity of fluorescence generated overall; such an event was highlighted in Figure 4-8 for concentrations 100 μM Mdivi-1, and 25 μM Mdivi-1. This correlates with aforementioned studies discussing the characteristics of mitochondrial motility as previously described. This reinforced the previous speculation that an imbalance in mitochondrial dynamics, and/or injury, may result in the consequent clustering of the mitochondria around the nucleus. The decrease in mitochondrial membrane potential, following the exposure to concentrations of Mdivi-1, coincide with results obtained from Yeon and colleagues (2015), who demonstrated the reduction of mitochondrial membrane potential, via JC-1 staining, in 50 μM Mdivi-1 treated porcine embryos in comparison to the non-treated group.

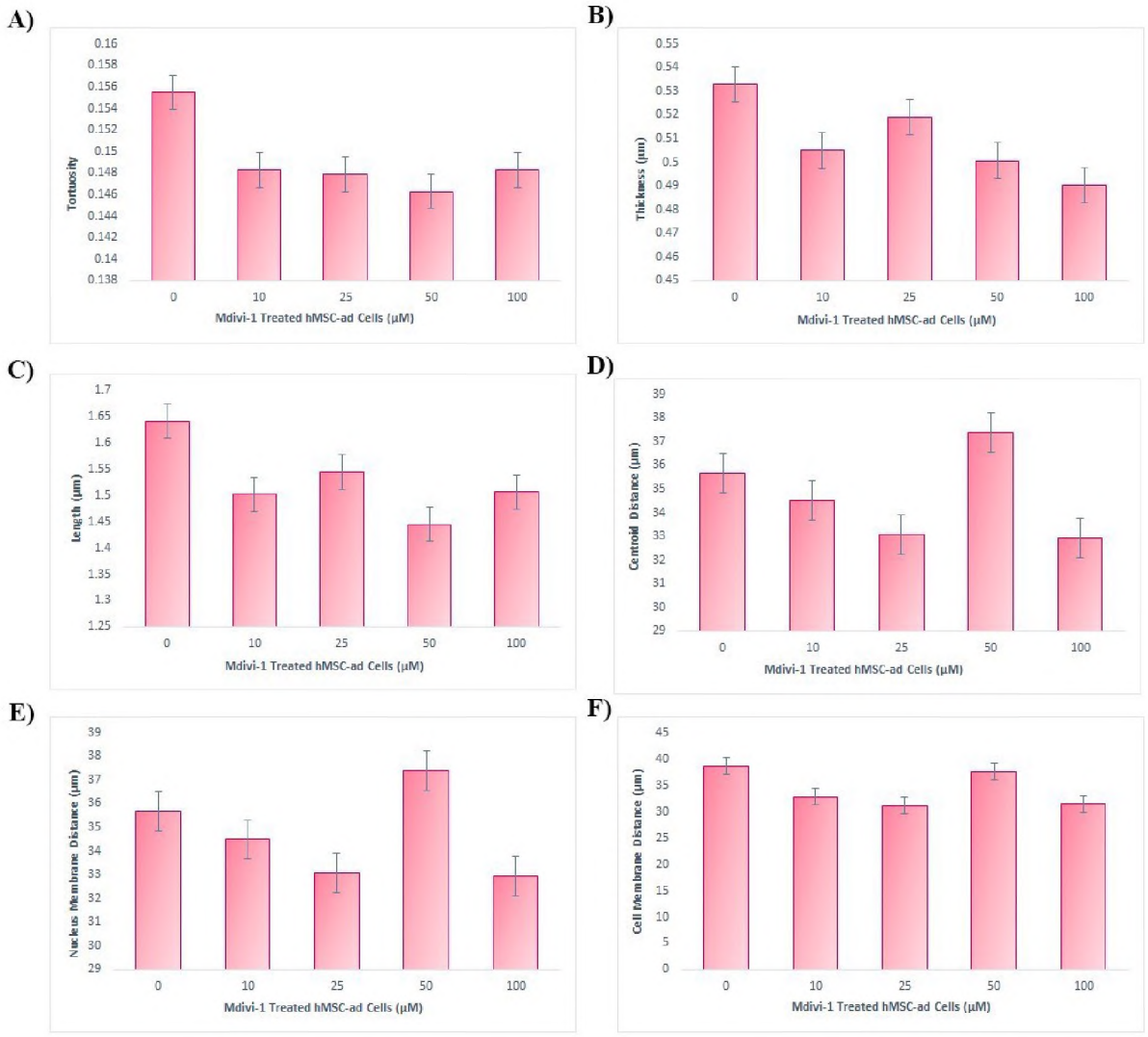


**Figure 4-9. Mitochondrial characteristics obtained after undifferentiated hMSC-ad cells were treated with the mitochondrial fission inhibitor, Mdivi-1, for a total period of 48 hours.** Data was generated using the JC-1 fluorescent images obtained. These images were applied to the Mytoe software; the resulting values generated for each characteristic were shown graphically as A) the tortuosity of the mitochondria, B) the thickness of the mitochondria, C) the length of the mitochondria, D) the centroid distance, E) the distance from the nucleus membrane, and F) the distance from the cell membrane. (N = 3).

**Table 4-4. Numerical values obtained for mitochondrial characteristics observed after the treatment of non-differentiating hMSC-ad cells with the mitochondrial fission inhibitor, Mdivi-1.**

| Sample (μM) | Tortuosity | Length (μm) | Thickness (μm) | Centroid Distance (μm) | Nucleus Membrane Distance (μm) | Cell Membrane Distance (μm) |
|---|---|---|---|---|---|---|
| 0 | 0.156 ± 0.003 | 1.640 ± 0.076 | 0.533 ± 0.010 | 35.682 ± 1.836 | 35.684 ± 1.835 | 38.595 ± 3.899 |
| 10 | 0.148 ± 0.000 | 1.502 ± 0.051 | 0.505 ± 0.004 | 34.496 ± 1.575 | 34.491 ± 1.574 | 32.782 ± 0.937 |
| 25 | 0.148 ± 0.002 | 1.544 ± 0.043 | 0.519 ± 0.007 | 33.086 ± 1.983 | 33.083 ± 1.983 | 31.086 ± 2.961 |
| 50 | 0.146 ± 0.003 | 1.444 ± 0.078 | 0.501 ± 0.007 | 37.372 ± 1.244 | 37.370 ± 1.247 | 37.542 ± 5.970 |
| 100 | 0.148 ± 0.002 | 1.506 ± 0.126 | 0.490 ± 0.008 | 32.950 ± 1.841 | 32.951 ± 1.843 | 31.449 ± 2.949 |

Mitochondrial lengths are believed to be regulated through the intricate balance between fusion and fission (van der Bliek et al., 2013). If these dynamic capabilities are altered in any way, the mitochondrial morphology is subject to undergo an alteration. Fragmentation of mitochondria is the result of an enhanced fission, thereby increasing the susceptibility of the cell to cell death. Mdivi-1 is believed to be a small molecule that can rescue the Drp1-mediated fragmentation of mitochondria, and apoptosis, should the process of fission be promoted (Rosdah et al., 2016). It has been demonstrated that the treatment of cells with Mdivi-1 may promote the formation of interconnected mitochondria, with half maximal concentrations ranging from 1 – 50 μmol/l (Rosdah et al., 2016).

When applied to the non-differentiating hMSC-ad cells, Mdivi-1 demonstrated little evident effect on the physical traits of the mitochondria. It seemed evident that the fission inhibitor did not possess severe deleterious effects on the mitochondrial morphologies that may promote pathological effects, causing cell death; this was observed within Figure 4-9 and Table 4-4, whereby the average length and diameter of the mitochondria remained within the

previously described reported values. It must be noted that a slight decrease in cell length, tortuosity, and thickness, was observed as the concentration of Mdivi-1 was increased; however, this was extremely minimal. This contrasted the observations recorded for the treatment of these cells with the mitochondrial fusion promoter, M1, which seemed to have the greatest effect on the cellular length, providing a value of $1.114 \pm 0.014$ μm for cells treated with 100 μM. Non-differentiating hMSC-ad cells treated with 100 μM of Mdivi-1 provided an average length of
$1.506 \pm 0.126$ μm.

The overall effects observed were not as expected. It was originally hypothesized that the effects of Mdivi-1 on the mitochondria would have significant deleterious effects on the overall state of the cell due to the inhibition of mitochondrial fission. It was also speculated that the total number of mitochondria would be decreased, due to a lack of proliferation, as well as the number of damaged mitochondria would be increased, due to a lack of mitophagy; this would all negatively impact the overall health of the cell, thereby leading to greater cell death. However, when applied to the hMSC-ad cells, Mdivi-1 did not promote cell death. The cells maintained their survival and morphological traits as observed for cells that did not undergo treatment with Mdivi-1. As previously discussed, this lack of cell death could be due to the Mdivi-1 half-life experienced within human adipose-derived mesenchymal stromal cells. Multiple cell lines have been used to determine the Mdivi-1 half-life; these cell lines included cardiomyocytes, vascular cells, neurons, skeletal myoblasts, and cancer cells (Rappold et al., 2014; Rosdah et al., 2016). From in vitro and in vivo experiments, it was demonstrated that Mdivi-1 presented with a half-life of approximately 8.9 hours within the brain, and ranged between 6 – 24 hours for in vitro cell lines. There have been few studies performed that demonstrate an accurate half-life for adipocytes and the hMSC-ad cell lines; however, it may be speculated that the half-life may fall within the in vitro range. With this information in mind, it may be further speculated that while it appeared that Mdivi-1 had little/no deleterious effect on the overall cell growth, mitochondrial compensation may have rectified the damage done in order to produce a healthy mitochondrial progeny once the effects of Mdivi-1 wore off.

It must be noted that the mitochondria were more prone to cluster around the cell nucleus in higher concentrations of Mdivi-1 (100 μM); there was an exception to this observed for the treatment with 50 μM Mdivi-1, which demonstrated an increased distance from the nuclear

membrane in comparison to the untreated control sample. This average value of 37.370 ± 1.247 µm could have been the result of the calculation of an extreme outlier. The outlying values obtained for the treatment of 50 µM Mdivi-1 was also observed within the average distance calculated from the cell membrane. Here, the 50 µM treatment displayed an average value of 37.542 ± 5.970 µm in comparison to the 100 µM treatment average value of 31.449 ± 2.949 µm, whereby, the increase of Mdivi-1 showed a general decrease in the cell membrane distance (shown in Table 4-4).

This general movement of the mitochondria within Mdivi-1 treated hMSC-ad cells may lead to the speculation that the mitochondrial movement within the cell is minimally affected with lower concentrations of Mdivi-1, and that the actively moving mitochondria are still capable of reaching the cellular extensions observed within human adipose-derived mesenchymal stem cells.

### 4-2-2. The assessment of the mitochondrial membrane potential of adipogenic differentiating hMSC-ad cellular mitochondria when exposed to certain small molecules and/or increased hypoxic conditions

Adipogenic differentiation was induced for the hMSC-ad cell line; Napolitano (1963) once stated that non-differentiating precursor cells demonstrated mitochondria that were small in size and resembled spheres, whereas those that were observed within the earlier differentiating stages possessed mitochondria demonstrating a predominantly spherical shape, while some held a more filamentous form. The number of filamentous-shaped mitochondria seemed to increase as differentiation progressed. It was also stated that the number of mitochondria increased throughout differentiation, and mature adipocytes held mitochondria that varied in shape. Kita and colleagues (2009) demonstrated the alterations of mitochondrial morphology during murine 3T3-L1 pre-adipocyte differentiation; filamentous networks of mitochondria adopted a more fragmented, or punctate, morphology during differentiation.

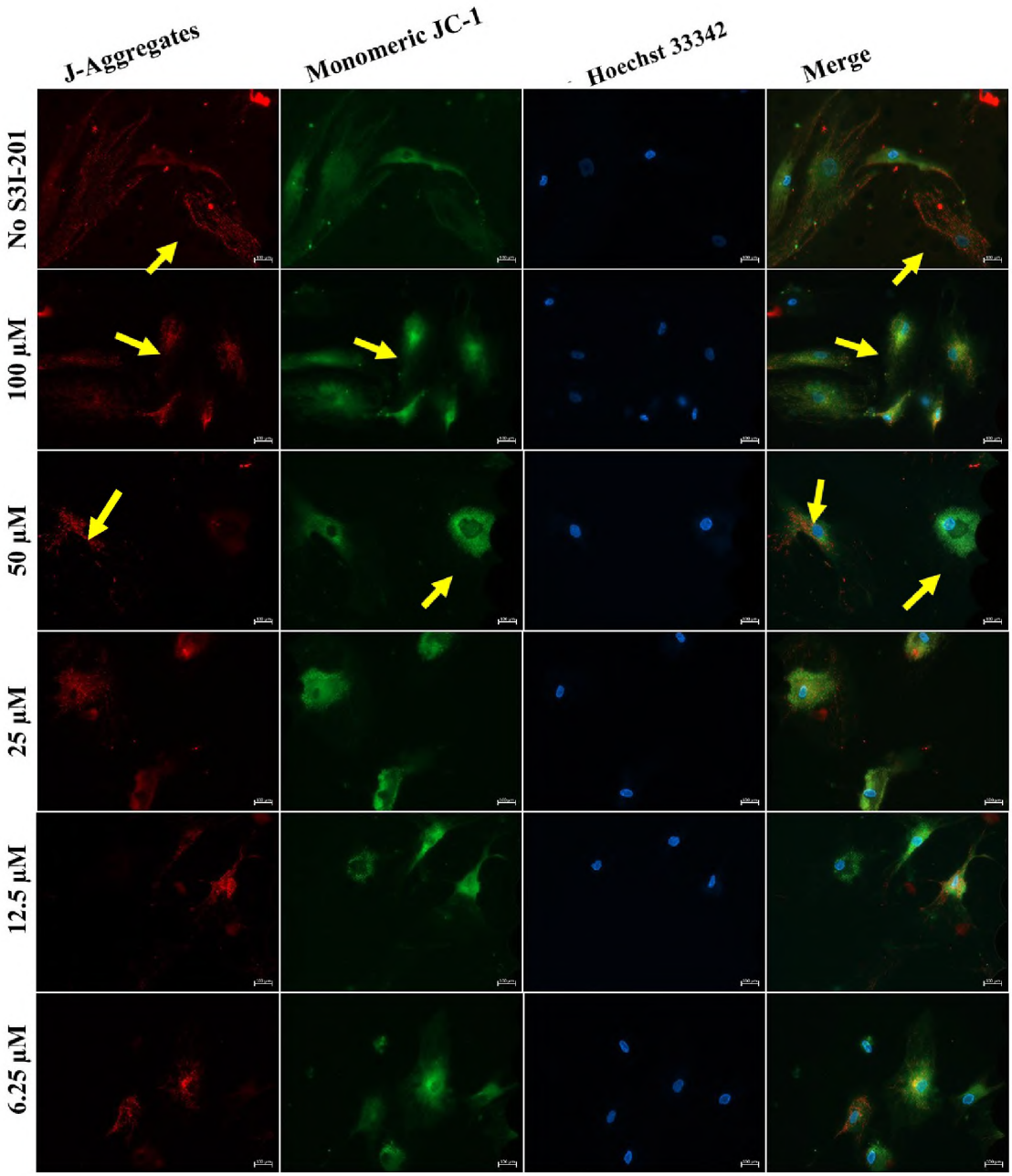


**Figure 4-10. Mitochondrial membrane potential observed for S3I-201 treated adipogenic differentiating hMSC-ad cells after a total period of 12 days.** The hMSC-ad cells were initially seeded into MSCM maintenance media and incubated until at least 100 % confluency was observed. The induction media was treated with varying concentrations of S3I-201 before being added to the confluent hMSC-ad cells. Adipogenesis in the induction medium was maintained for approximately 4 days before the adipogenic maintenance medium treated with S3I-201 was added for the remaining 8 days. Adipogenesis was permitted over the course of 12 days. Images were captured using the Zeiss AxioVert.A1 FL-LED fluorescence microscope at 200x magnification. Scale bar = 100 µm. Images shown are representative of multiple images obtained at random locations within the culture vessel (N = 3).

The resulting JC-1 mitochondrial membrane potential live stain shown in Figure 4-10 presents with the adipogenic differentiation of hMSC-ad cells treated with S3I-201 (N = 3). A control was established in which the adipogenic differentiating hMSC-ad cells were left untreated for S3I201. This would provide a basis for comparisons between adipogenic differentiating hMSC-ad cells under normal conditions and those exposed to S3I-201. With regards to mitochondrial polarization, the red/green fluorescence provided was not as intense as that which was observed for non-differentiating hMSC-ad cells, thereby, indicating that a decrease in mitochondrial membrane potential was present within this stage of differentiation. However, it must be noted that, in some cases the resulting aggregates generated were increased in comparison to the monomers formed.

Upon the induction of differentiation, the cells underwent an additional treatment with varying levels of S3I-201 in order to determine the resulting effect on the mitochondria during adipogenesis. Overall, the cellular morphology provided insight into transformation of the hMSC-ad cells to early/maturing adipocytes. Shown by the mitochondrial membrane potential stain, the resulting cell morphology was established; the cells had grown significantly larger and had developed a more rounded morphology, especially evident for concentrations 50 μM – 12.5 μM S3I-201. However, the morphology could not be exclusively determined in this manner as mitochondria localization could have been reserved for around these specific areas within the cell, with minimal/no mitochondria evident in the remaining cellular cytoplasm. It was hypothesized that the mitochondria would cluster around the nucleus; this was evident in Figure 4-10 which demonstrated large amounts of mitochondria (J-Aggregates and J-Monomers) present around the nucleus. This coincided with aforementioned studies that state that the mitochondria will gather around the nucleus as well as large lipid depots present within the cell; however, the clustering of the mitochondria around these lipid depots was not clearly noticeable for these maturing adipocytes.

The ratio of J-Aggregates to J-Monomers formed (red/orange to green fluorescence) must also be noted. Figure 4-10 clearly demonstrates that as the hMSC-ad cells undergo differentiation to maturing adipocytes, some mitochondrial membrane potential is lost, thereby causing the mitochondria with lower membrane potentials to form a higher number

of J-Monomers. This was speculated via the comparisons between the J-Aggregates and J-Monomers formed, as well as supporting documentation, previously mentioned, that speculates the decrease in mitochondrial membrane potential as the cells reach a more mature adipocyte stage. However, with the notable presence of J-Aggregates, it can further be speculated that the adipogenic differentiating hMSC-ad cells had not yet reached full maturity, or the resulting adipocytes maintained a reasonable level of mitochondrial membrane potential in order to provide energy for specific functions performed by the adipocytes. It may also be assumed that not 100 % of the cell population present within the culture vessel underwent a successful differentiation to adipocytes; some of the cells could have maintained their stem cell morphology/characteristics.

However, it appeared as though the S3I-201 had little/no deleterious effect on adipogenesis, other than causing the cells to obtain a more rounded/cuboidal morphology generally associated with adipocytes. Boudina and colleagues (2014) stated that white adipose tissue possess a decreased number of mitochondria that are smaller in size and are located around the rim of the periplasm, which is demonstrated for some cells in Figure 4-10. Saely and colleagues (2012) reviewed that mitochondria within white adipocytes bore a thin, elongated structure; they also noted that there was an undefined, variable amount present with the white adipocytes. The mention of the thin, elongated structure coincides with previous information provided by Napolitano in 1963, who stated that the mitochondria observed in maturing adipocytes bore a more filamentous form, albeit, spherical mitochondria were also noted. In contrast, Kita and colleagues (2009) demonstrated the alterations of mitochondrial morphology during murine 3T3-L1 pre-adipocyte differentiation whereby the filamentous networks of mitochondria became more fragmented during differentiation.

It was previously discussed that the mitochondria within the hMSC-ad cells demonstrated little difference regarding their tortuosity and thickness over the range of S3I-201 concentrations. This minimal difference was observed within Figure 4-11 and the corresponding Table 4-5 (N = 3); no general trend regarding these characteristics could be conclusively distinguished as the untreated control and the highest concentrations of S3I-201 treatment (100 μM) possessed similar values for both tortuosity and mitochondrial thickness (the control possessed a calculated tortuosity of $0.144 \pm 0.001$ and average thickness of $0.483 \pm 0.005$ μm, in contrast to the 100 μM S3I-201 treatment which demonstrated an average

tortuosity of 0.145 ± 0.010 and average thickness of 0.487 ± 0.011 μm. A slight decrease in the average mitochondrial length was observed upon the treatment of S3I-201; as the concentration of S3I-201 increased, the average length decreased. This general trend was substantiated by the general decline in average length for the S3I-201 treatments (the untreated control possessed an average length of 1.327 ± 0.038 μm, whereas the 100 μM S3I-201 treated adipocytes demonstrated an average length of 1.213 ± 0.126 μm).

With relation to the general localization of the mitochondria within the cellular cytoplasm, there seemed to be an almost equal distribution of mitochondria between the nucleus membrane and the cellular membrane for the untreated differentiating adipocytes. There were noted discrepancies observed when this value was compared to those of the increasing S3I-201 concentrations; however, it may be speculated that this average value calculated does not take into account the overall shape of the cell, as well as any additional cellular extensions present.

It must be acknowledged that an overall difference was observed between the mitochondrial characteristics observed for non-differentiating hMSC-ad cells (Table 4-1) and the differentiating adipocytes (Table 4-5). Here, it is evident that the human adipose derived mesenchymal stem cells possess elongated mitochondria (with an average length of 1.602 ± 0.025 μm for untreated cells) in comparison to the shorter mitochondria observed within the differentiating adipocytes that bore an average length of 1.327 ± 0.038 μm. These lengths further decreased slightly as the concentration of S3I-201 increased, whereas an indeterminate trend was noted for the non-differentiating hMSC-ad cells, whereby the average length randomly varied across the increasing concentrations. In addition to the notable changes in mitochondrial length, the overall thickness was only barely increased within non-differentiating hMSC-ad cells in comparison to the differentiating adipocytes. An average value of 0.500 ± 0.007 μm was obtained for the non-differentiating hMSC-ad cells, whereas an average value of 0.483 ± 0.005 μm was generated for the adipocytes. The tortuosity values were closely related; it can, thus, be speculated that the length of the mitochondria does undergo a slight transformation, acquiring a more punctate morphology, during adipogenesis.

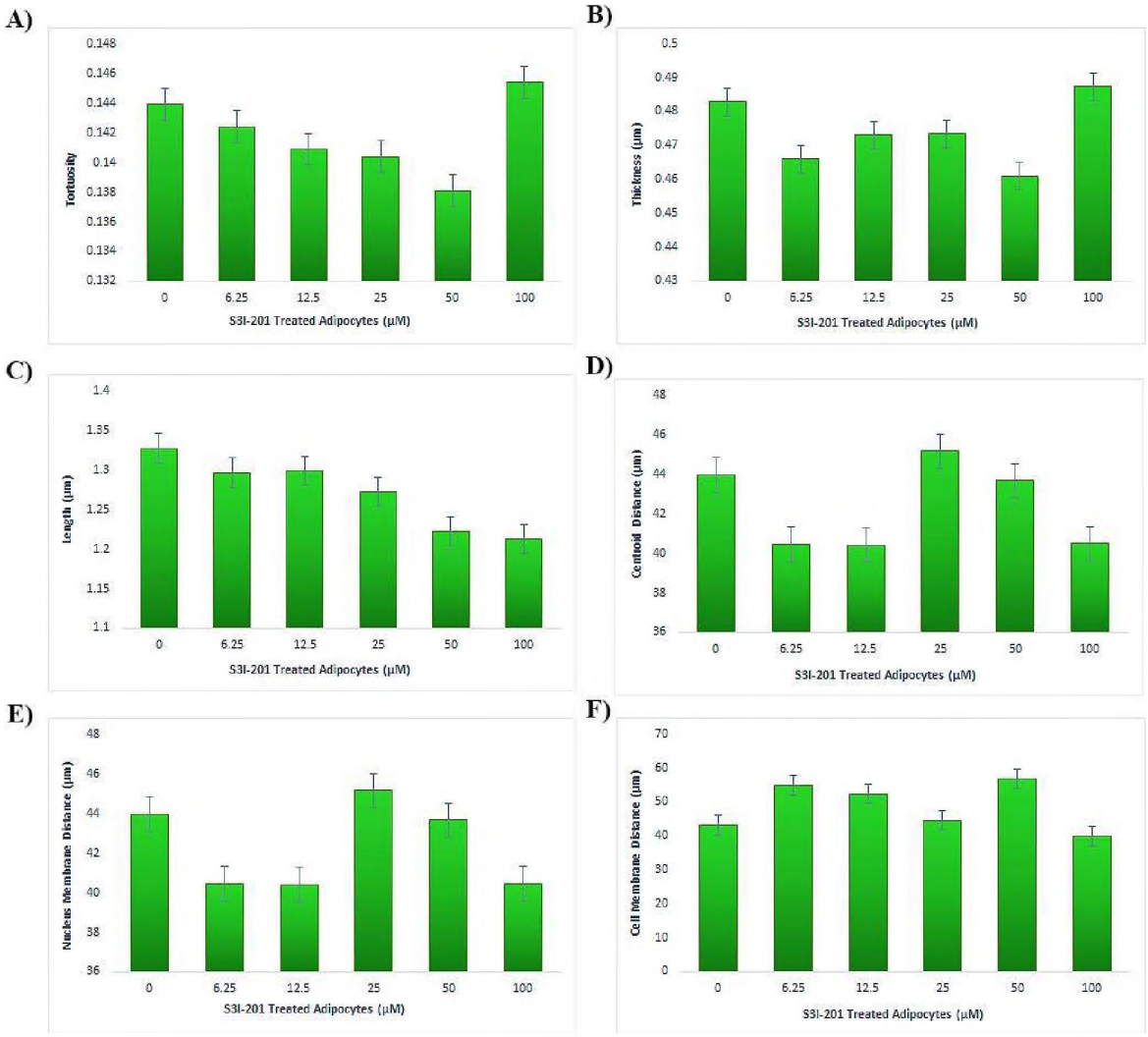


**Figure 4-11. Mitochondrial characteristics generated for adipogenic differentiating hMSC-ad cells treated with S3I-201 for a total period of 12 days.** Data was generated using the JC-1 fluorescent images obtained. These images were applied to the Mytoe software; the resulting values generated for each characteristic were shown graphically as A) the tortuosity of the mitochondria, B) the thickness of the mitochondria, C) the length of the mitochondria, D) the centroid distance, E) the distance from the nucleus membrane, and F) the distance from the cell membrane. (N = 3).

**Table 4-5. Numerical values obtained for mitochondrial characteristics observed after the treatment of adipogenic differentiating hMSC-ad cells with the STAT3 inhibitor, S3I201.**

| Sample (μM) | Tortuosity | Length (μm) | Thickness (μm) | Centroid Distance (μm) | Nucleus Membrane Distance (μm) | Cell Membrane Distance (μm) |
|---|---|---|---|---|---|---|
| 0 | 0.144 ± 0.001 | 1.327 ± 0.038 | 0.483 ± 0.005 | 43.962 ± 0.372 | 43.961 ± 0.373 | 43.065 ± 5.498 |
| 6.25 | 0.142 ± 0.006 | 1.297 ± 0.090 | 0.466 ± 0.014 | 40.436 ± 2.811 | 40.442 ± 2.809 | 54.780 ± 13.624 |
| 12.5 | 0.141 ± 0.007 | 1.299 ± 0.044 | 0.473 ± 0.017 | 40.407 ± 3.133 | 40.407 ± 3.135 | 52.347 ± 14.117 |
| 25 | 0.140 ± 0.005 | 1.272 ± 0.068 | 0.473 ± 0.010 | 45.146 ± 0.306 | 45.147 ± 0.306 | 44.513 ± 11.474 |
| 50 | 0.138 ± 0.003 | 1.222 ± 0.095 | 0.461 ± 0.009 | 43.649 ± 0.800 | 43.645 ± 0.802 | 59.701 ± 6.390 |
| 100 | 0.145 ± 0.010 | 1.213 ± 0.126 | 0.487 ± 0.011 | 40.482 ± 2.327 | 40.450 ± 2.326 | 39.855 ± 4.916 |

The adipogenic differentiation shown in Figure 4-12 demonstrates the mitochondrial membrane potential live stain, JC-1, for differentiating adipocytes treated with S3I-201, a STAT3 inhibitor, as well as cobalt chloride (N = 2), which is known to increase the levels of hypoxia within the *in vitro* environment. Increased levels of hypoxia have been linked to severe inflammation associated with obesity, whereby, this increased level of inflammation impacts glucose, lipid, and energy metabolism (Ye, 2009). Adipose tissue hypoxia correlates with insulin resistance through the inhibition of post-receptor signal transduction. Increased hypoxic conditions are known to inhibit differentiation within pre-adipocyte cells, as well as promote the secretion of leptin and vascular epithelial growth factor within matured adipocytes, in vitro (Ye, 2009). It was hypothesized that an increased hypoxic environment would constrict the level of adipogenesis observed, thereby, preventing significant morphological changes from occurring. Upon inspection of the images obtained in Figure 4-

12, there seemed to be little morphological changes evident when compared to the differentiating hMSC-ad cells shown in Figure 4-10. However, it must be noted that the more evident differences were observed for the concentrations of S3I-201 ranging between 50 μM and 12.5 μM, where the large rounded cells were evident in S3I-201 treated cells devoid of the cobalt chloride. The cells maintained a spindle-like morphology indicative of their mesenchymal stem cell origins; concentrations 6.25 μM and 100 μM seemed to present with the larger phenotypes characteristic of the earlier stages of differentiation. Therefore, it may be speculated that this increased rate of hypoxia significantly decreases the rate of adipogenesis.

Upon the addition of the varying concentrations of S3I-201, it is evident that a decrease in mitochondrial membrane potential was present, especially when compared to Figure 4-12. A, which depicts the S3I-201 untreated differentiating hMSC-ad cells. Here, a significant fluorescence is observed as J-Aggregates are formed; this indicates that the adipogenic differentiating cells still possess a relatively high mitochondrial membrane potential that will either aid in the production of energy to continue adipogenesis and/or maintain vital cellular functions required with this increased level of level of hypoxia. However, it must be noted that some cells also displayed a lower mitochondrial membrane potential. Both images were included for a comparative purpose, as it was observed within the culture vessel that the overall mitochondrial membrane potential seemed to be varied across the multiple cells present. This decrease in mitochondrial membrane potential, observed with the addition of S3I-201, could be indicative of the inhibition of adipogenesis due to a deficit of adipogenesis-driving STAT3 in addition to the differentiation-inhibiting hypoxic conditions; this would have resulted in the cells reaching a stage whereby they are unable to differentiate and/or proliferate further.

Once again it is noted that the mitochondria are localized around the central point of the nucleus; however, it must also be acknowledged that their presence is not only restricted to these areas and extended further downwards into the cellular extensions associated with the spindle-like shape of confluent mesenchymal stem cells. The mitochondria within the larger cells, evident of differentiation, seem to decrease with an increase in the distance from the nucleus membrane.

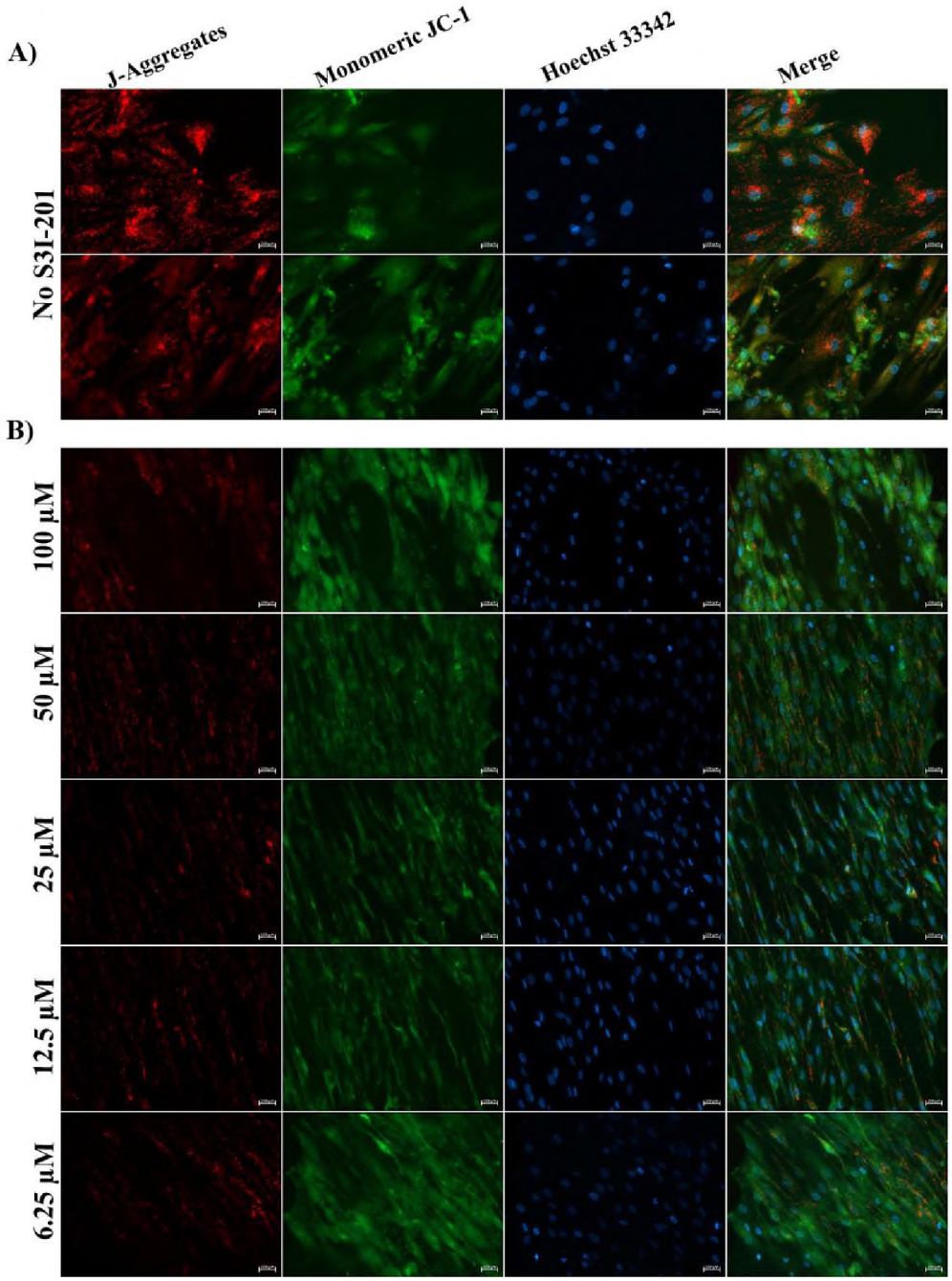


**Figure 4-12. Mitochondrial membrane potential observed for S3I-201 and cobalt chloride treated adipogenic differentiating hMSC-ad cells after a total period of 12 days.** The hMSC-ad cells were initially seeded using MSCM and incubated until at least 100 % confluency was observed. The induction media was treated with varying concentrations of S3I201 and 100 µM cobalt chloride. Adipogenesis in the induction medium was maintained for approximately 4 days before the adipogenic maintenance medium, treated with S3I-201 and cobalt chloride, was added for the remaining 8 days. Adipogenesis was permitted over the course of 12 days. A) represents treatment with cobalt chloride only, B) represents treatment with S3I-201 and cobalt chloride. Images were captured using the Zeiss AxioVert.A1 FLLED fluorescence microscope at 200x magnification. Scale bar = 20 µm.

Images shown are representative of multiple images obtained at random locations (N = 2).

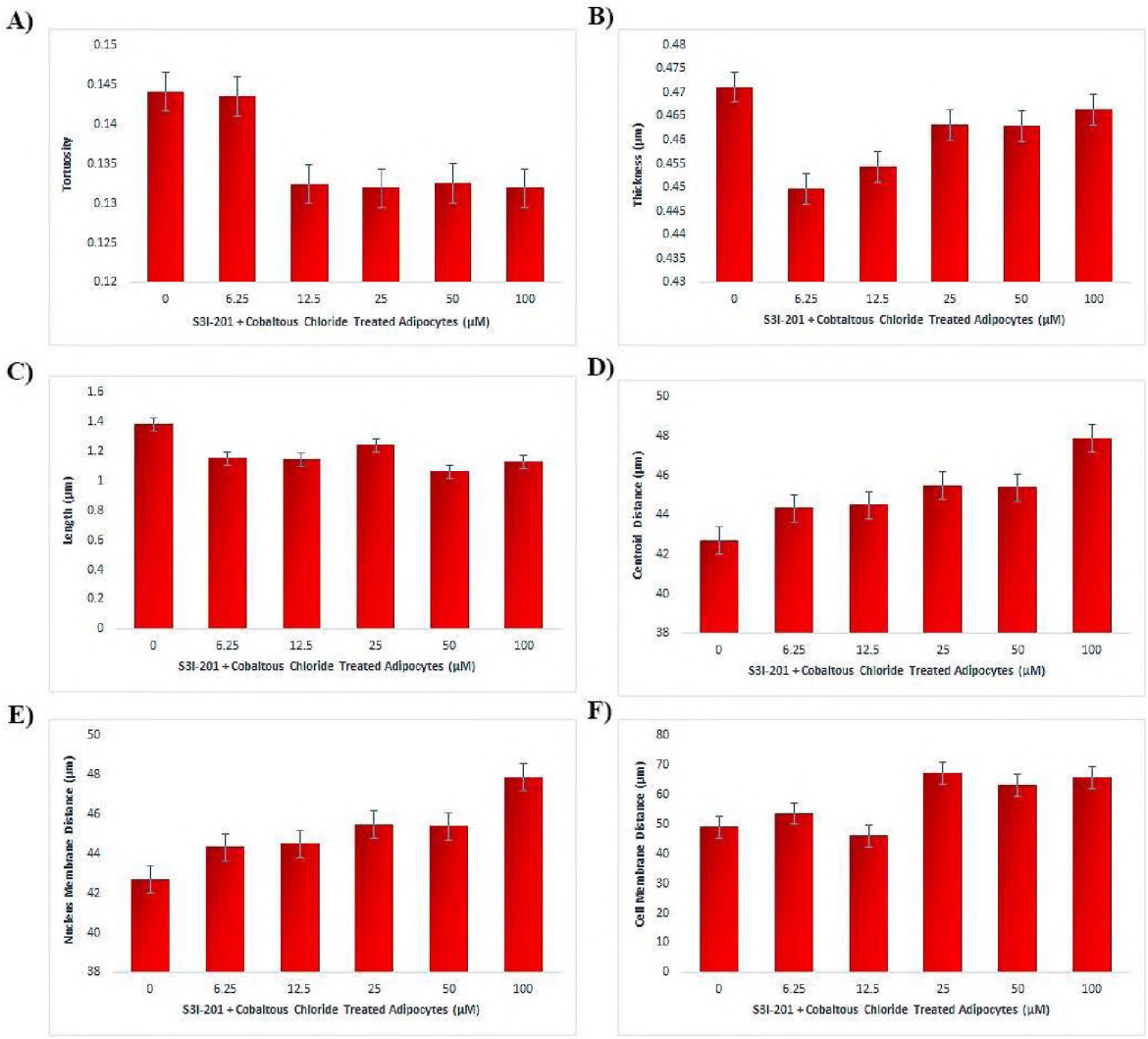


**Figure 4-13. Mitochondrial characteristics generated for adipogenic differentiating hMSC-ad cells treated with S3I-201 and cobalt chloride for a total period of 12 days.** Data was generated using the JC-1 fluorescent images obtained. The images were applied to the Mytoe software; the resulting values were represented graphically as A) the tortuosity of the mitochondria, B) the thickness of the mitochondria, C) the length of the mitochondria, D) the centroid distance, E) the distance from the nucleus membrane, and F) the distance from the cell membrane. (N = 2).

**Table 4-6. Numerical values obtained for mitochondrial characteristics observed after the treatment of adipogenic differentiating hMSC-ad cells with S3I-201 and cobalt chloride.**

| Sample (μM) | Tortuosity | Length (μm) | Thickness (μm) | Centroid Distance (μm) | Nucleus Membrane Distance (μm) | Cell Membrane Distance (μm) |
|---|---|---|---|---|---|---|
| 0 | 0.144 ± 0.007 | 1.377 ± 0.148 | 0.471 ± 0.005 | 42.689 ± 1.188 | 42.688 ± 1.186 | 48.905 ± 6.083 |
| 6.25 | 0.144 ± 0.001 | 1.151 ± 0.028 | 0.450 ± 0.001 | 44.321 ± 1.687 | 44.322 ± 1.678 | 53.544 ± 3.703 |
| 12.5 | 0.132 ± 0.002 | 1.140 ± 0.017 | 0.454 ± 0.000 | 44.494 ± 1.344 | 44.495 ± 1.342 | 45.896 ± 1.619 |
| 25 | 0.132 ± 0.002 | 1.236 ± 0.002 | 0.463 ± 0.001 | 45.460 ± 0.480 | 45.455 ± 0.482 | 67.141 ± 12.427 |
| 50 | 0.133 ± 0.000 | 1.061 ± 0.005 | 0.463 ± 0.002 | 45.392 ± 0.926 | 45.390 ± 0.926 | 63.032 ± 4.527 |
| 100 | 0.132 ± 0.015 | 1.128 ± 0.156 | 0.466 ± 0.001 | 47.844 ± 1.920 | 47.845 ± 1.914 | 65.448 ± 28.146 |

It has been reported that hypoxia inhibits cellular differentiation within precursor cells. Lin and colleagues (2006) state that increased hypoxic conditions coincide with an undifferentiated phenotype observed in solid tumour cells, such as the neuroblastoma. Gao and colleagues (2014) demonstrated STAT3 may inhibit mechanisms adopted by cells under hypoxia, such as cell invasion, generation of cytokines, and migration. Furthermore, it was reported that hypoxia in adipose tissue is associated with insulin resistance and obesity; this is achieved through the inhibition of the signalling pathway specific for insulin (Regazzetti et al., 2009). Regazzetti and colleagues (2009) further went on to suggest that the self-renewal capabilities of mesenchymal stem cells were promoted in the presence of hypoxia, leading to the inhibition of adipogenesis. It can therefore be concluded that hypoxia performs a vital function in the regulation of differentiating within stem cell populations. When the adipogenic differentiating hMSC-ad cells were exposed to cobalt chloride, thereby increasing the amount of hypoxia present, the mitochondrial characteristics seemed to be

consistent with the differentiating cells that were treated with only S3I-201, and those that were treated with both cobalt chloride as well as S3I-201 (Table 4-5 and Table 4-6).

The average length observed for differentiating hMSC-ad cells untreated for S3I-201 was calculated to be 1.327 ± 0.038 μm whereas that which was observed for the differentiating hMSC-ad treated with cobalt chloride bore an average length of 1.377 ± 0.148 μm. This indicates that the increase of hypoxia had little/no deleterious effect on mitochondrial length and phenotypic characteristics. The slight decrease in length may be attributed to the increase in S3I-201 in conjunction with the 100 μM; a minimal decline in mitochondrial length was observed for adipocytes treated with increasing concentrations of S3I-201, as shown in Table 4-5. It may be speculated that this decrease in mitochondrial length may have been increased slightly due to the additional hypoxic conditions.

Due to the maintenance of a more elongated cellular morphology, the mitochondria were able to cover an additional area within the cellular cytoplasm, thereby, increase the distance travelled between the cell membrane and the nucleus membrane. This distance seemed to increase with an increase in S3I-201 concentration.

As previously mentioned, mitochondrial fusion is an important dynamic process that aids in compensation of stress across mitochondria; partially damaged mitochondria are subjected to the mixing of mitochondrial DNA with healthier mitochondria, thereby aiding in the regulation of mitochondrial function and maintaining overall health (Youle et al., 2012). Mitochondrial DNA is subject to mutations and deletions, which may impair mitochondrial function, thus promoting a pathological state. These mutations of mitochondrial DNA can be passed down to future generations, leading to the development of certain pathologies; fusion of this mutant DNA with healthier mitochondria present within the cell aid in the compensation of these defective mitochondria through the sharing of mitochondrial components (Youle et al., 2012). Youle and colleagues (2012) have further described fibroblastic mitochondria to hold a filamentous-like appearance with mitochondrial lengths ranging from 1 – 10 μm and a diameter of approximately 700 nm.

The adipogenic differentiating cells were exposed to these varying concentrations of M1 mitochondrial fusion promoter over the course of 12 days, throughout which the cells

underwent adipogenesis (N = 2). Much like what was observed in Figure 4-6, which depicted the effects of the mitochondrial fusion promoter, M1, on non-differentiating hMSC-ad cells, there was some cell survival observed. This cell survival was decreased as the M1 concentrations were increased; this was noted via the survival of 1 cell observed within the culture vessel treated with 100 μM M1, of which a consistent seeding cell density was utilized throughout. The resulting morphologies seemed a lot thinner and spindle-like with a rounded body wherein the nucleus resided.

The M1 treated adipogenic differentiating hMSC-ad cells seemed to demonstrate a similar ratio between aggregates and monomers formed, suggesting mitochondrial polarization was still in effect regardless of the lethal concentrations of M1 utilized. This was evident predominantly for 50 μM and 25 μM M1 treatment. J-Monomers formed were increased with the addition of the mitochondrial fusion promoter; this was noted throughout the treatments of varying concentrations in comparison to the untreated cells. As seen previously, there were elongated structures present within the culture vessel upon the introduction of the M1 fusion promoter. Traces of these filamentous structures were present within the JC-1 live stains, particularly noted within the concentration of 10 μM M1 mitochondrial fusion promoter. Some morphological alterations associated with adipogenesis were observed for the lower concentrations of M1, namely 10 μM and 25 μM. Upon closer inspection, the mitochondria seemed to have adopted a more rounded, spherical morphology in comparison to that observed for untreated adipogenic differentiating hMSC-ad cells. Mitochondria, however, may differ in morphology within a single cell type; McCarron and colleagues (2013) indicated that two populations of mitochondria exist within skeletal muscle. Therefore, it cannot be definitively determined whether or not these smaller, more rounded, mitochondria are, in fact, diseased state mitochondria. Additional experiments would be required to reach this conclusion.

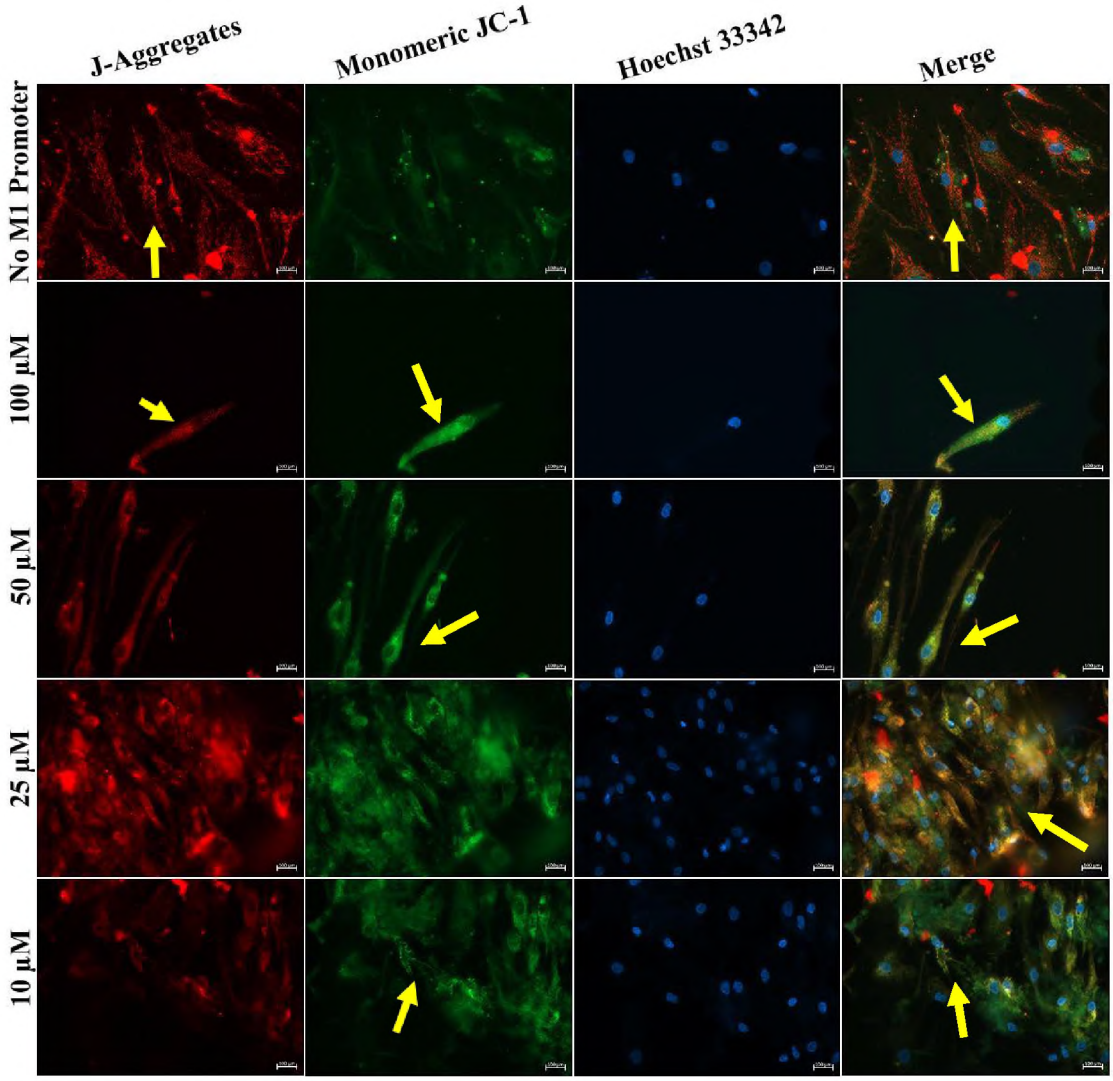


**Figure 4-14. Mitochondrial membrane potential observed for mitochondrial fusion promoter, M1, treated adipogenic differentiating hMSC-ad cells after a total period of 12 days.** The hMSC-ad cells were initially seeded using MSCM and incubated until at least 100 % confluency was observed. The induction media was treated with varying concentrations of M1 mitochondrial fusion promoter. Adipogenesis in the induction medium was maintained for approximately 4 days before the adipogenic maintenance medium, treated with M1 was added for the remaining 8 days. Adipogenesis was permitted over the course of 12 days. Images were captured using the Zeiss AxioVert.A1 FL-LED fluorescence microscope at 200x magnification. Scale bar = 20 µm. Images shown are representative of multiple images obtained at random locations (N = 2).

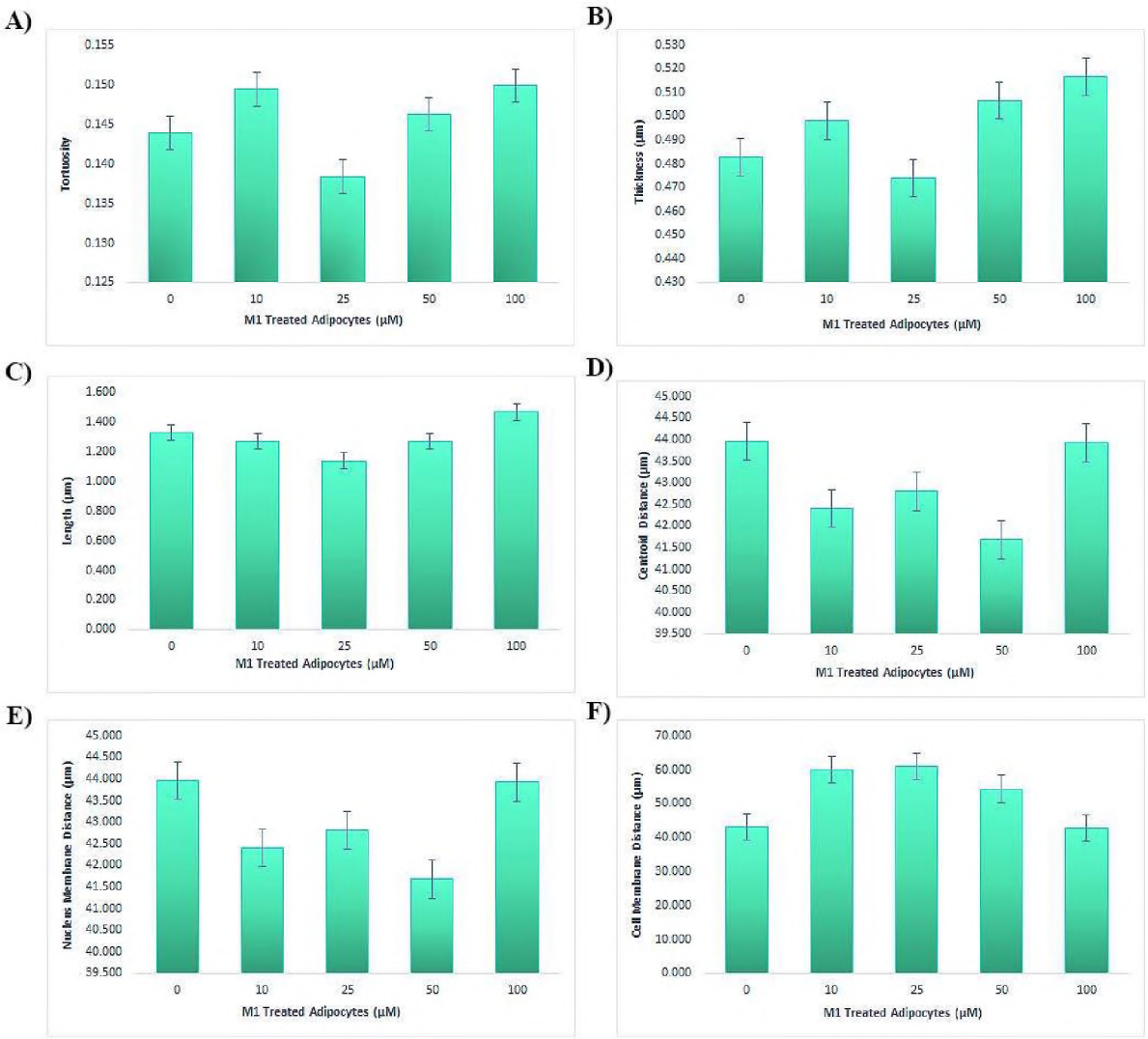


**Figure 4-15. Mitochondrial characteristics generated for adipogenic differentiating hMSC-ad cells treated with the mitochondrial fusion promoter, M1, for a total period of 12 days.** Data was generated using the JC-1 fluorescent images obtained. The images were applied to the Mytoe software; the resulting values were represented graphically as A) the tortuosity of the mitochondria, B) the thickness of the mitochondria, C) the length of the mitochondria, D) the centroid distance, E) the distance from the nucleus membrane, and F) the distance from the cell membrane. (N = 2)

**Table 4-7. Numerical values obtained for mitochondrial characteristics observed after the treatment of adipogenic differentiating hMSC-ad cells with the mitochondrial fusion promoter, M1.**

| Sample (μM) | Tortuosity | Length (μm) | Thickness (μm) | Centroid Distance (μm) | Nucleus Membrane Distance (μm) | Cell Membrane Distance (μm) |
|---|---|---|---|---|---|---|
| 0 | 0.144 ± 0.001 | 1.327 ± 0.038 | 0.483 ± 0.005 | 43.962 ± 0.372 | 43.961 ± 0.373 | 43.065 ± 5.498 |
| 10 | 0.149 ± 0.011 | 1.267 ± 0.030 | 0.498 ± 0.013 | 42.400 ± 4.321 | 42.400 ± 4.316 | 59.955 ± 1.999 |
| 25 | 0.138 ± 0.000 | 1.137 ± 0.037 | 0.474 ± 0.006 | 42.807 ± 0.050 | 42.810 ± 0.047 | 60.903 ± 1.440 |
| 50 | 0.146 ± 0.004 | 1.267 ± 0.019 | 0.507 ± 0.002 | 41.680 ± 1.737 | 41.680 ± 1.741 | 54.261 ± 6.946 |
| 100 | 0.150 ± 0.005 | 1.465 ± 0.283 | 0.517 ± 0.004 | 43.921 ± 0.315 | 43.922 ± 0.318 | 42.707 ± 13.100 |

The JC-1 fluorescent images were applied to the Mytoe software in order to generate numerical values for certain mitochondrial characteristics, tabulated in Table 4-7 and represented graphically in Figure 4-15. There was little/no general differences observed for the tortuosity and thickness of the mitochondria; however, it can be noted that slight mitochondrial swelling was observed with an increase of mitochondrial fusion promoter, M1. The average length initially decreased; however, when the M1 concentration reached 50 μM, the average mitochondrial seemed to increase yet again. This might be a discrepancy regarding the number of mitochondria present within a cell, as well as the number of cells present within the culture vessel at the time; it may also be indicative or the morphologies acquired regarding confluency. The mitochondria seemed to adopt a central localization within the cell; the trend of a general increase in cellular membrane distance was observed until 25 μM after which the value started to decrease with 42.707 ± 13.100 μm being the final value observed for 100 μM M1.

These results were further compared to those obtained for Table 4-3, whereby the mitochondrial fusion promoter, M1, was added to non-differentiating hMSC-ad cells. It was observed that a general increase in mitochondrial tortuosity occurred with 0.141 ± 0.003 representative of the tortuosity in non-differentiating hMSC-ad cells, and 0.144 ± 0.001 was indicative of the tortuosity present within adipogenic differentiating hMSC-ad cells, both of which excluded M1 treated. This slight difference could be indicative of adipogenesis occurring within the cells. The mitochondrial were also minimally more swollen within adipogenic cells treated with M1 than the non-differentiating hMSC-ad cells, with an average thickness of 0.494 ± 0.011 μm observed for non-differentiating cells treated with 100 μM M1 versus an average thickness of 0.517 ± 0.004 μm observed for adipogenic differentiating cells treated with 100 μM M1. This 'balling' of mitochondria may be due to the consequent oxidative stress or a resulting leak of protons (depolarization) associated with increased mitochondrial membrane potentials (Liesa et al., 2013).

As predicted, a decrease in average length was observed for differentiating cells, with an average value of 1.327 ± 0.038 μm observed for untreated adipocytes, versus the average value of 1.422 ± 0.026 μm for untreated non-differentiating hMSC-ad cells. It must be acknowledged that there is a dramatic decrease in mitochondrial length for non-differentiating hMSC-ad cells which correlates closely with values obtained within Table 4-7, which also provided somewhat decreasing values. Therefore, it can be concluded that mitochondrial fusion promoter, M1, may be responsible for the shortening of mitochondria, albeit, the differentiating hMSC-ad cells seem to provide an increase in average mitochondrial length when treated with 100 μM M1. This may also be indicative of a lack of differentiation amongst cells treated with the mitochondrial fusion promoter, M1.

A general distance from the cellular membrane was increased within non-differentiating cells, with an average value of 57.402 ± 0.227 μm being established, whereas the average value calculated was 43.065 ± 5.498 μm within the differentiating progeny. This may be indicative of the mitochondria moving closer towards the nucleus or the change in morphology experienced within differentiating adipocytes. However, these decreased values were maintained throughout the treatment of M1 concentrations; once again, it may be noted that after 25 μM M1 treatment, the cellular membrane distance is decreased with the increasing concentrations of M1; whereas an average increase of cellular membrane distance

was observed within Table 4-3, with the exception of treatment with 10 μM M1, whereby a decrease was observed.

Perhaps the most interesting result was the effects that the mitochondrial fission inhibitor, Mdivi-1, had on adipogenic differentiating hMSC-ad cells. Mitochondrial fission is a dynamic quality that is required for the proliferation and formation of new mitochondria, as well as the removal of dysfunctional mitochondria from the cellular system (Youle et al., 2012). It has been speculated that when cells are put under excessive levels of stress, mitochondrial fission may be over-stimulated, thereby causing cellular death. Previously, it was noted that Mdivi-1 possesses therapeutic properties whereby it suppresses this enhanced mitochondrial fission within overly stressed cells. Mdivi-1 was combined with both induction and maintenance media used throughout the course of adipogenic differentiation, and medium changes occurred every 3 – 4 days. The resulting mitochondrial membrane potential images obtained seemed to demonstrate a higher mitochondrial membrane potential present within cells that had been treated with a higher concentration of Mdivi-1, namely concentrations 100 μM and 50 μM (N = 2). It was also evident that the differentiating hMSC-ad cells underwent a major morphological alteration when treated with 100 μM Mdivi-1. The cells obtained a larger, more rounded/cuboidal appearance with very few cellular extensions, remnants of the mesenchymal stem cell morphology, visible. When the J-Aggregates and J-Monomers were merged together, a bright gold/orange colour was observed, suggesting that these ratios were similar within most of these cells; however, it must be noted that the remaining cells seemed to demonstrate a lower mitochondrial membrane potential. It has been previously discussed as to the reasoning behind this loss of mitochondrial membrane potential, which causes the J-Monomers to be formed: during the course of differentiation mitochondrial membrane potential fluctuates according to the demand of ATP energy. The earlier stages of differentiation require a greater need for energy, thus, display a high mitochondrial membrane potential; whereas, the later stages of differentiation, where mature adipocytes are generated, usually display a low mitochondrial membrane potential. This also impacts the number of mitochondria produced. The untreated maturing adipocytes possess a decreased mitochondrial membrane potential, which coincides with that observed for cells

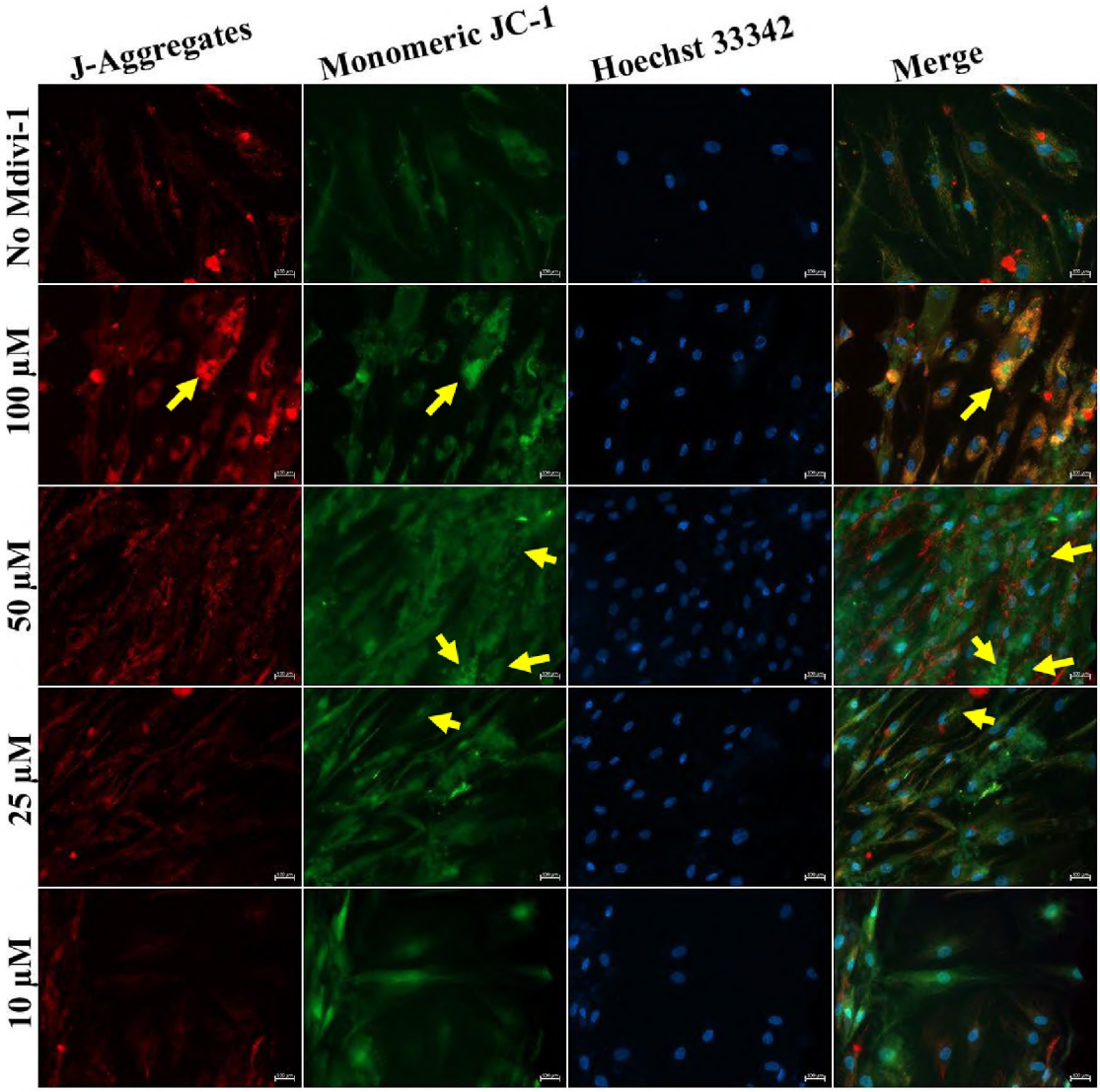


**Figure 4-16. Mitochondrial membrane potential observed for mitochondrial fission inhibitor, Mdivi-1, treated adipogenic differentiating hMSC-ad cells after a total period of 12 days.** The hMSC-ad cells were initially seeded using MSCM and incubated until at least 100 % confluency was observed. The induction media was treated with varying concentrations of Mdivi-1. Adipogenesis in the induction medium was maintained for approximately 4 days before the adipogenic maintenance medium, treated with Mdivi-1 was added for the remaining 8 days. Adipogenesis was permitted over the course of 12 days. Images were captured using the Zeiss AxioVert.A1 FL-LED fluorescence microscope at 200x magnification. Scale bar = 20 µm. Images shown are representative of multiple images obtained at random locations (N = 2).

treated with 10 μM Mdivi-1; albeit, the formation of monomeric JC-1 is still sufficiently higher than what is observed within the untreated cells.

Mitochondrial membrane potential has also been linked to the determination of the overall health of the mitochondria within the network. Mdivi-1 also prevents the loss of mitochondrial membrane potential, therefore, it may be speculated that an increase in Mdivi-1 will lead to a higher mitochondrial polarisation as observed. Lipid vacuoles containing the fat droplets (observed within bright field imaging) became more distinctive with the addition of the Mdivi1 fission inhibitor; this was predominantly observed for concentrations 50 μM and 25 μM. These distinctive lipid vacuoles provided observation of mitochondrial clustering/localization around these droplets whereby the monomer fluorescence was somewhat intensified around these regions.

The resulting output of data obtained (shown in Figure 4-17 and Table 4-8) using the JC-1 fluorescent images depicts the resulting mitochondrial characteristics acquired. These values indicate that there was a minimal change observed between these mitochondrial characteristics, suggesting that Mdivi-1 provided little deleterious effect on the mitochondria regardless of the concentrations used. A minimal decrease in mitochondrial length was observed when the differentiating cells were treated with 100 μM Mdivi-1, obtaining an average length of 1.211 ± 0.109 μm in comparison to that obtained for untreated cells (1.327 ± 0.038 μm). This consistency was observed within the non-differentiating hMSC-ad data generated within Table 4-4, which demonstrated mitochondrial characteristics with close similarities observed amongst the increasing concentrations of Mdivi-1.

A comparison was established between non-differentiating hMSC-ad cells treated with Mdivi1 (Table 4-4) and adipogenic differentiating hMSC-ad cells (Table 4-8) whereby a decrease in mitochondrial length was observed for untreated adipogenic differentiating hMSC-ad cells. An average length of 1.327 ± 0.038 μm was obtained for the adipogenic differentiating hMSC-ad cells, whereas the untreated non-differentiating hMSC-ad cells provided an average length of 1.640 ± 0.076 μm. This decrease in mitochondrial length is indicative of cellular differentiation occurring, as mentioned in previous discussions. A general decrease in average length was maintained throughout both differentiating and non-differentiating cellular models upon the treatment with Mdivi-1.

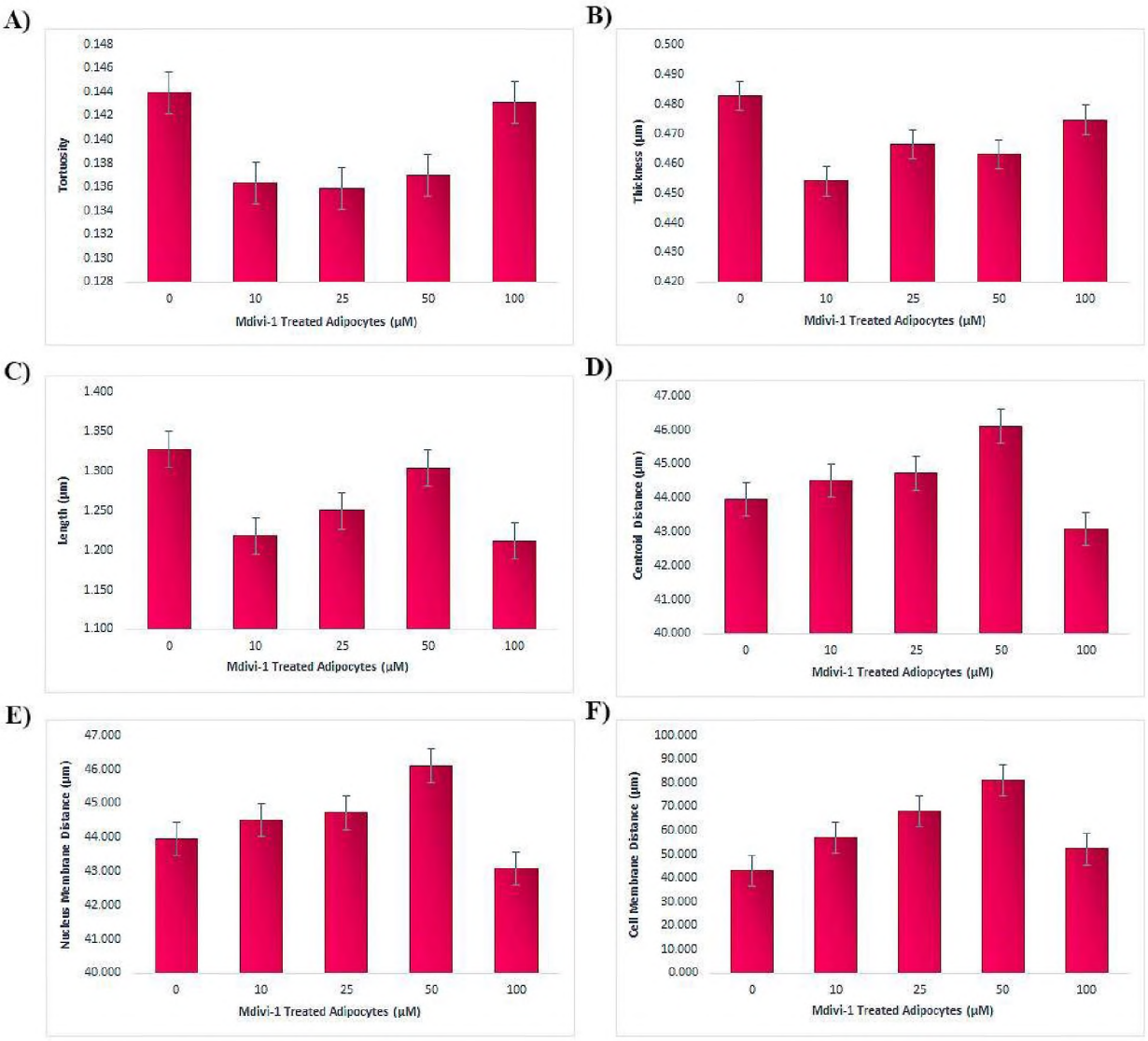


**Figure 4-17. Mitochondrial characteristics generated for adipogenic differentiating hMSC-ad cells treated with the mitochondrial fission inhibitor, Mdivi-1, for a total period of 12 days.** Data was generated using the JC-1 fluorescent images. The images were applied to the Mytoe software; the resulting values were represented graphically as A) the tortuosity of the mitochondria, B) the thickness of the mitochondria, C) the length of the mitochondria, D) the centroid distance, E) the distance from the nucleus membrane, and F) the distance from the cell membrane. (N = 2).

**Table 4-8. Numerical values obtained for mitochondrial characteristics observed after the treatment of adipogenic differentiating hMSC-ad cells with the mitochondrial fission inhibitor, Mdivi-1.**

| Sample (μM) | Tortuosity | Length (μm) | Thickness (μm) | Centroid Distance (μm) | Nucleus Membrane Distance (μm) | Cell Membrane Distance (μm) |
|---|---|---|---|---|---|---|
| 0 | 0.144 ± 0.001 | 1.327 ± 0.038 | 0.483 ± 0.005 | 43.962 ± 0.372 | 43.961 ± 0.373 | 43.065 ± 5.498 |
| 10 | 0.136 ± 0.000 | 1.218 ± 0.045 | 0.454 ± 0.012 | 44.504 ± 2.172 | 44.509 ± 2.171 | 56.856 ± 6.828 |
| 25 | 0.136 ± 0.000 | 1.250 ± 0.025 | 0.466 ± 0.003 | 44.722 ± 0.408 | 44.721 ± 0.411 | 68.115 ± 8.733 |
| 50 | 0.137 ± 0.000 | 1.303 ± 0.025 | 0.463 ± 0.001 | 46.105 ± 0.870 | 46.105 ± 0.869 | 81.062 ± 17.627 |
| 100 | 0.143 ± 0.006 | 1.211 ± 0.109 | 0.475 ± 0.012 | 43.076 ± 0.782 | 43.074 ± 0.785 | 52.153 ± 0.964 |

Both cell membrane and nucleus membrane distances seemed to be increased within the adipogenic differentiating hMSC-ad cells in comparison to that which was generated for the non-differentiating hMSC-ad cells treated with Mdivi-1. A general trend regarding the values obtained for the various concentrations of Mdivi-1 was not definitively established with adipogenic differentiating hMSC-ad cells, nor for the non-differentiating hMSC-ad cells.

As an aside, the adipogenic differentiating hMSC-ad cells were permitted to continue differentiation and treatment with Mdivi-1 over the course of 21 days. The resulting JC-1 stains provided insight into, not only the mitochondrial membrane potentials present, but also the evident change in morphology present. It was previously discussed that mitochondria will localise around the nucleus as well as the lipid droplets within adipocytes; the gathering of the mitochondria was confirmed within the images captured for Figure 4-18, whereby an increase in fluorescence suggested a clustering of mitochondria evident around lipid vacuoles more clearly distinguished after the 21 days differentiation and exposure to Mdivi-1. Arrows have been shown to indicate these lipid vacuoles, whereby lipid droplets were found. In all

scenarios where this is present, a collection of mitochondria may be observed surrounding these vacuoles; albeit, some situations reveal an inclination towards a low mitochondrial membrane instead of the proposed high mitochondrial membrane potential.

This was evident by the ratio of J-monomers formed in comparison to J-aggregates, and the intensity of the resulting fluorescence. It may be speculated that this increasing in low mitochondrial membrane potential is due to the formation of matured adipocytes that no longer need vast amount of energy to continue the differentiating process; it must be noted that the presence of a high mitochondrial membrane potential occurred around the larger lipid vacuoles, as shown for the 50 μM Mdivi-1 treatment.

When compared to untreated adipocytes, the cells observed within Mdivi-1 treatment demonstrated a more elongated, thinner, almost fusiform, morphology, while still presenting with lipid droplet accumulation and vacuoles as indicated within Figure 4-18. It was acknowledged that the morphologies seemed to grow larger and more spaced out with the decrease of Mdivi-1 concentration. This presents with an interesting concept for future studies regarding the effects of Mdivi-1 on adipogenesis; identification of these spindle-shaped fat producing cells may be determined using classical adipogenic markers, thereby providing a conclusion as to whether or not the resulting cells observed within Figure 4-18 are true adipocytes or, perhaps, are pre-adipocyte phenotypes.

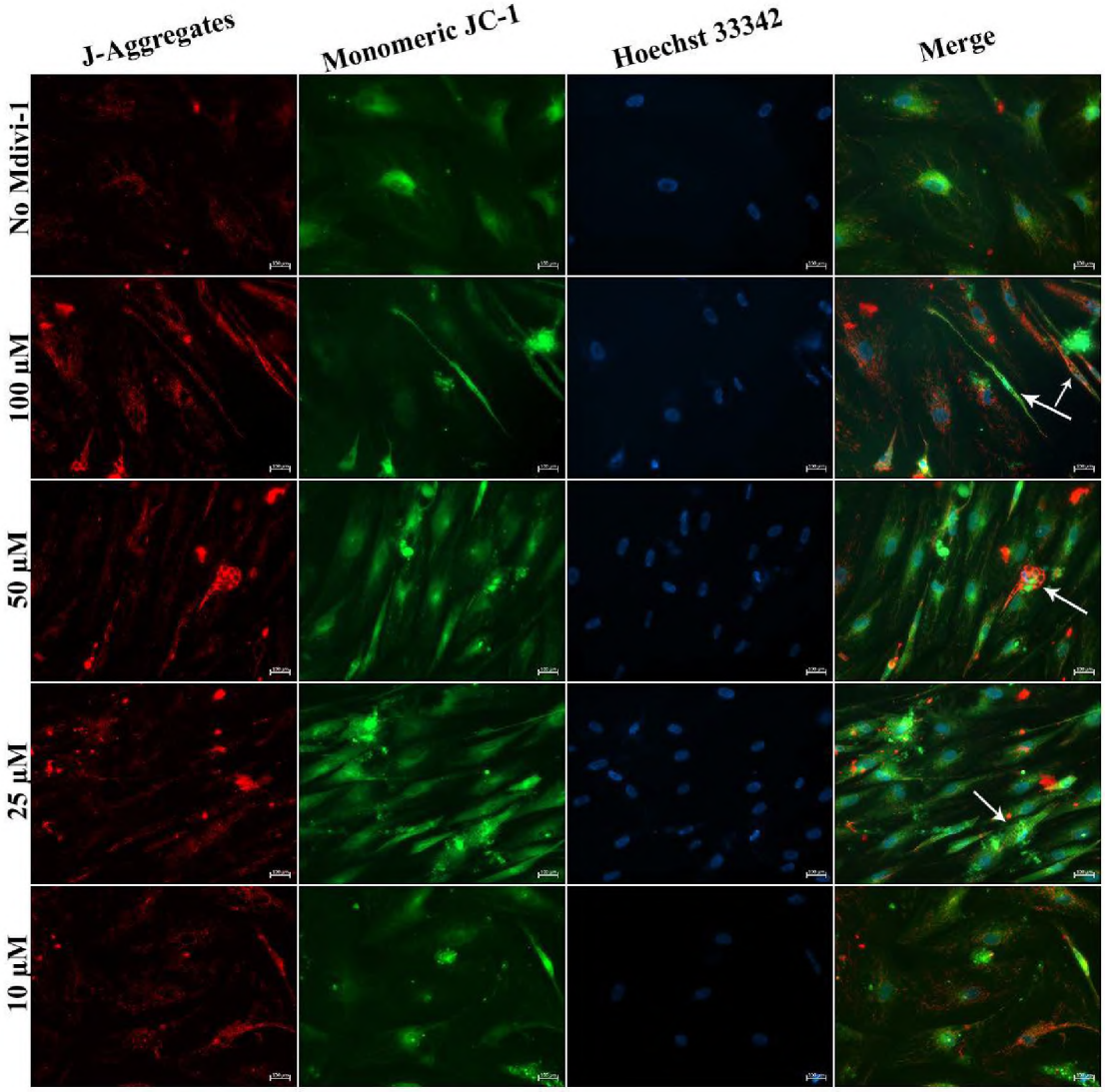


**Figure 4-18. Mitochondrial membrane potential observed for mitochondrial fission inhibitor, Mdivi-1, treated adipogenic differentiating hMSC-ad cells after a total period of 21 days.** The hMSC-ad cells were initially seeded using MSCM and incubated until at least 100 % confluency was observed. The induction media was treated with concentrations of Mdivi-1. Adipogenesis using the induction medium was maintained for approximately 4 days before the adipogenic maintenance medium, treated with Mdivi-1, was added for the remaining 12 days. Adipogenesis was permitted over the course of 21 days. Images were captured using the Zeiss AxioVert.A1 FL-LED fluorescence microscope at 200x magnification. Scale bar = 20 µm. Images shown are representative of multiple images obtained at random locations (N = 2).

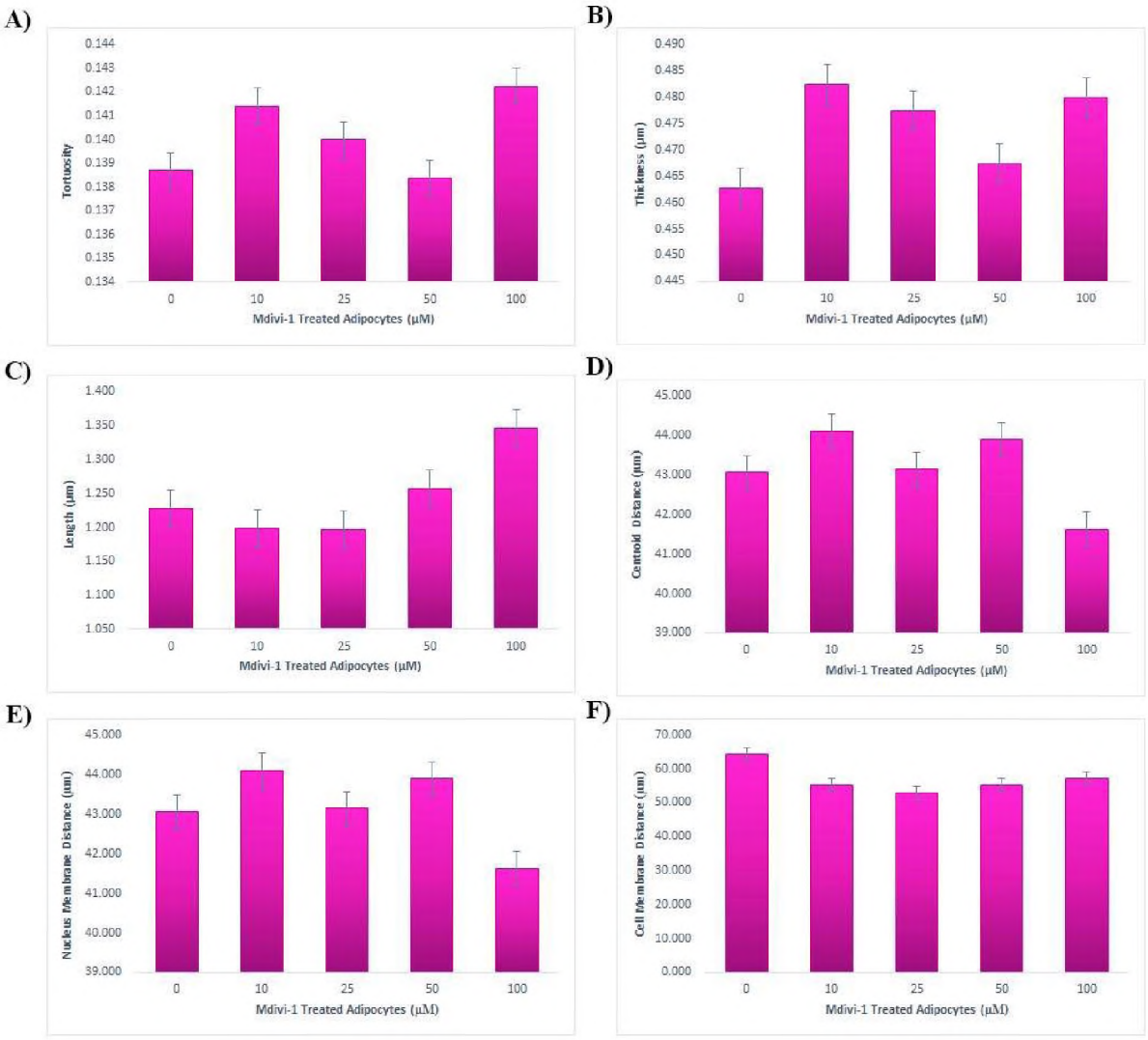


**Figure 4-19. Mitochondrial characteristics generated for adipogenic differentiating hMSC-ad cells treated with the mitochondrial fission inhibitor, Mdivi-1, for a total period of 21 days.** Data was generated using the JC-1 fluorescent images. The images were applied to the Mytoe software; the resulting values were represented graphically as A) the tortuosity of the mitochondria, B) the thickness of the mitochondria, C) the length of the mitochondria, D) the centroid distance, E) the distance from the nucleus membrane, and F) the distance from the cell membrane. (N = 2).

**Table 4-9. Numerical values obtained for mitochondrial characteristics observed after the treatment of adipogenic differentiating hMSC-ad cells with mitochondrial fission inhibitor, Mdivi-1, for a total period of 21 days.**

| Sample (μM) | Tortuosity | Length (μm) | Thickness (μm) | Centroid Distance (μm) | Nucleus Membrane Distance (μm) | Cell Membrane Distance (μm) |
|---|---|---|---|---|---|---|
| 0 | 0.139 ± 0.001 | 1.228 ± 0.017 | 0.463 ± 0.004 | 43.055 ± 1.358 | 43.054 ± 1.359 | 64.265 ± 3.364 |
| 10 | 0.141 ± 0.001 | 1.198 ± 0.021 | 0.482 ± 0.007 | 44.089 ± 0.621 | 44.088 ± 0.621 | 55.186 ± 3.065 |
| 25 | 0.140 ± 0.001 | 1.197 ± 0.009 | 0.477 ± 0.004 | 43.132 ± 0.657 | 43.131 ± 0.657 | 52.965 ± 3.350 |
| 50 | 0.138 ± 0.001 | 1.256 ± 0.027 | 0.467 ± 0.006 | 43.881 ± 0.980 | 43.881 ± 0.982 | 55.184 ± 3.846 |
| 100 | 0.142 ± 0.001 | 1.346 ± 0.013 | 0.480 ± 0.002 | 41.620 ± 1.340 | 41.621 ± 1.340 | 57.175 ± 8.588 |

When added to the Mytoe software, the resulting output of data was tabulated and graphically represented as Table 4-9 and Figure 4-19. The average mitochondrial tortuosity, length, and thickness were indicative of a minimal difference observed between the average values generated; the tortuosity and thickness provided no general trend upon the increase of Mdivi-1 concentrations. The average length underwent a minimal decrease for concentrations 10 μM and 25 μM of Mdivi-1; albeit, an increase in average length was evident for the increasing concentrations. The average mitochondrial length observed for 100 μM treatment was 1.346 ± 0.013 μm in relation to the average mitochondrial length of 1.228 ± 0.017 μm for untreated adipocytes.

A comparison was established between differentiating adipocytes over 12 days and those that were permitted to differentiate for 21 days in the presence of Mdivi-1. It was acknowledged that the average mitochondrial length was increased for the 12 days' differentiating adipocytes (Table 4-8), in comparison to those that differentiated for 21 days (N = 2) (Table 4-9). There was little/no difference calculated between the average thickness of the

mitochondria as well as the tortuosity, leading to the speculation that Mdivi-1 treatment is not necessarily time-dependent and that cells are capable of differentiating and surviving under these conditions.

There was one difference readily observed between the two cellular models; the adipocytes after 12 days possessed a decreased cell membrane distance in comparison to that which was observed for adipocytes after 21 days. An initial average value of 43.065 ± 5.498 μm was obtained for untreated adipocytes after 12 days, whereas an initial average value of 64.265 ± 3.364 μm was obtained for untreated adipocytes after 21 days. This may suggest that mitochondria gather more readily around the nuclei/increasing lipid droplets within the matured adipocytes. The nucleus membrane and centroid distances were of similar values with no significant differences observed.

### 4-2-3. The Conclusion, Complications, and Future Work

The overall number of mitochondria observed within this study seemed to increase during the earlier stages of differentiation where a large amount of ATP-energy is required to maintain this process; the number of mitochondria seemed to decrease during the later stages of differentiation due to the lesser energy requirements once mature adipocytes were formed. This observation coincided with a time dependent study that demonstrates the mitochondrial membrane potential present within Mdivi-1 treated adipogenic differentiating hMSC-ad cells after 12 days and 24 days. Here, the mitochondrial membrane potential also underwent a reduction, indicating that the matured adipocytes no longer required the same amount of energy as what was used during the differentiating process.

Regarding the phenotypical morphology, the mitochondria seemed to possess a more rounded morphology and were of a smaller size, when compared to those observed for non-differentiating hMSC-ad cells. The networks were more tightly clustered, and seemed to localize around the nucleus with a decreasing number extending into the rest of the cytoplasm. The mitochondria displayed in non-differentiating hMSC-ad cells possessed an elongated, tubular network that were less densely clustered together. This observation was substantiated by Wilson-Fritch and colleagues (2003) study whereby they found that the mitochondria present in adipocytes were in densely populated networks that were localized around the lipid droplets as well as the nucleus. In addition to the morphological attributes

observed, the mitochondrial location seemed to be centred around the nucleus, and, in the case of the matured adipocytes, encompassing the lipid droplets, as seen more exclusively in Figure 4-18.

An increase in green fluorescence (the J-Monomer) was observed in the maturing adipocytes, suggesting a decrease in mitochondrial membrane potential. This decrease in mitochondrial membrane potential may be attributed to the resulting mature adipocyte's lack of requirement for high energy processes after differentiation. However, it must be noted that a fluorescence was observed for the J-Aggregates, which indicate that while the maturing adipocyte does not require the same amount of energy as non-differentiating hMSC-ad cells, there is some high mitochondrial membrane potential present to ensure the overall maintenance of specific cellular functions that the adipocytes regulate. The mitochondrial membrane potential seemed to be at its lowest for the Mdivi-1 treated maturing adipocytes.

It is to be noted that a distinctive change in cellular morphology was easily observed when the mitochondria were stained with JC-1. The cells became larger and more cuboidal/oval; however, a clear distinction in morphology was noted for cells treated with S3I-201 and Mdivi1, whereby a mainly cuboidal form was observed lacking the cellular extensions commonly associated with an earlier stage of differentiation where the spindle-shaped/fibroblastic mesenchymal stem cell still maintains a similar morphology to that observed for the non-differentiating cells observed in the previous sub-chapter.

The development of the Mytoe software by Lihavainen and colleagues (2012) provides great fundamental promise to unlocking the traits that the mitochondria may develop throughout the course of a cell's existence. This will help further increase the understanding of mitochondrial mechanisms, dynamics, and the pathologies that may arise due to mitochondrial dysfunction. The results generated provided an insight into some of the mitochondrial characteristics observed under various situations; this included the curvature of the mitochondria (tortuosity), the thickness, the length, as well as localization areas. Further to this, the software was easy to use and generated a rapid output of data for analysis. However, some constraints were noted while using this software; while the mitochondrial parameters were determined, the biological information gained was limited. In addition to this, cell size and shape must also be taken into consideration.

Complications did arise when using this software; at first it was not recognized that the software had difficulty reading the green channel of the JC-1 live stain fluorescent images, therefore, only the J-Aggregates were detected and analysed. It was only later that it was decided to alter the colouring of the channel to a violet colour, which, when run through the Mytoe software, provided a different result to what was generated previously. It may be speculated that the acquired results are not definitive as the number of cells within the fluorescent images varied; therefore, in order to generate an idea of individual cells' mitochondria, individual whole cells would need to be captured and processed in multiple screenings. This would help isolate outliers and gain better insight into the mitochondrial characteristics and networks observed within cells treated with varying small molecules.

Further studies into the effects of Mdivi-1 on adipogenesis and non-differentiating human adipose derived mesenchymal stromal cells should be carried out; additional experiments would have included time-dependent studies that demonstrated the effects of Mdivi-1 on these cell lines during the stages of adipogenesis (i.e. the early stage through to the resulting mature adipocyte), as well as the determination of the Mdivi-1 half-life life within the human adipose-derived mesenchymal stromal cells and adipocytes. Additional cellular stress would have been an additional study to consider. This would have included an induced oxidative stress experiment whereby ROS would be increased within the presence of the small molecules (Mdivi-1, M1, and S3I-201), and the resulting effects on the mitochondria would be observed. Hydrogen peroxide could have been used as a continuous treatment within the presence of the small molecules. Additionally, western blotting could be used to identify key proteins present within differentiating cells, thereby confirming whether or not the resulting cells were true adipocytes, instead of a mixture of cell types or, in fact, another progeny altogether. Flow cytometry is another technique to be considered. Flow cytometry was attempted, however, the machine was available for a limited amount of time that was not sufficient for adipogenic differentiation, as well as certain small molecule compounds had not been delivered. Therefore, data was only captured for mesenchymal stromal cells treated with S3I-201. Additionally, time dependent studies that constantly monitor mitochondrial movement may be beneficial in order to track their motility during the course of differentiation, as well as the treatment with various small molecules. Electron microscopy has long been used to identify mitochondrial structure, therefore, it might be beneficial to use this technique in the determination of the resulting mitochondrial morphologies.

The experiments performed reinforce the advantageous and disadvantageous effects that certain small molecules may have on non-differentiating and differentiating hMSC-ad cells as mentioned in the previous chapter. The combination of JC-1 live fluorescent staining and the technology of the Mytoe software have made it possible to easily distinguish certain mitochondrial characteristics present within hMSC-ad cells and their adipogenic progeny, such as the average mitochondrial length which was observed to decrease in adipocytes, as well as the clustering/gathering of mitochondria around the nucleus when cells were treated with varying small molecules. From these results, it can be concluded that mitochondrial dynamics is an ongoing process that constantly changes to suit certain environmental circumstances and provide as much compensation as possible to regulate mitochondrial function. A disruption of mitochondrial function results in fragmented mitochondrial networks that may inhibit differentiation and/or lead to apoptosis. An over-stimulation of mitochondrial fusion demonstrated a severely detrimental effect on the hMSC-ad cells whereby mitochondrial networks appeared more fragmented. In order to determine the number of mutant genes shared amongst the mitochondria, genetic studies on the mitochondrial DNA would be required; however, from visual speculation it may be assumed that the deleterious effects are caused by healthy mitochondria adopting mutant, dysfunctional genes. Mitochondrial fission inhibition by Mdivi-1, once again, seemed to have no true deleterious effect on adipogenesis or lipogenesis. Treatment with S3I-201 demonstrated little/no deleterious effect on adipogenesis; it led to a grand morphological difference whereby mitochondria were localised around the nucleus and the periplasmic rim. The cells were rounded and bore a morphology associated with adipocytes. When treated with cobalt chloride, differentiation was reduced/inhibited.

# Chapter 5:

Investigation into reactive oxygen species formed within human mesenchymal stromal cells and differentiated adipocytes after treatment with certain small molecules.

**Specific Objectives:**

1. Observation of ROS formed within hMSC-ad cells and their differentiatedprogeny.
2. The investigation of the effect that mitochondrial fission inhibitor, Mdivi-1, has on ROS generated.
3. The investigation of the resulting ROS generated after treatment with mitochondrial fusion promoter, M1.

# 5: Investigation into reactive oxygen species formed within human mesenchymal stromal cells and differentiated adipocytes after treatment with certain small molecules.

## 5-1. Introduction

Initially it was theorized that reactive oxygen species (ROS) were toxic, deleterious oxygen-derived small molecules that caused cellular damage through the oxidation and nitration of cellular elements (Finkel, 2011; Atashi et al., 2015). However, recently it has become widely accepted that, when regulated, ROS is a vital component used within cellular signalling pathways and the maintenance of cellular function, such as proliferation, differentiation, motility, and apoptosis (Finkel, 2011, Li et al., 2011; Atashi et al., 2015; Wang et al., 2015). These oxygen-derived small molecules can further be defined as a heterogeneous group of free radicals formed from diatomic oxygen within living organisms (Wang et al., 2015; Atashi et al., 2015).

Mitochondria have demonstrated the largest production of ROS due to the mitochondrial electron transport chain, whereby ATP production causes a small amount of oxygen to be released. A superoxide anion is formed from complex I and III; complex I results in the superoxide anion being generated within the matrix, whereas complex III generates the superoxide anion within the matrix or intermembrane space (Atashi et al., 2015). The superoxide anion is then stabilized to form hydrogen peroxide within the intermembrane space, which may be either depleted by antioxidants, or converted into water and diatomic oxygen, or utilized as an important signalling molecule within the cytosol (Atashi et al., 2015).

Reactive oxygen species production drives adipogenesis; according to Wang and colleagues (2015), ROS were responsible for the activation of peroxisome proliferator-activated receptor gamma (PPARγ), which aids in the regulation of adipogenesis. In addition to this, N-acetyl-L-cysteine utilizes ROS to decrease the rate of adipogenesis; additional antioxidants lead to the inhibition of adipogenesis. Transcription factors CCAAT/enhancer binding protein (C/EBP) β, PPARγ and C/EBPα are essential for the activation of adipocyte genes, and therefore, are vital to the differentiation process; PPARγ is of importance for the regulation

of mature adipocytes (Castro et al., 2016). White adipocytes are formed utilizing transcription factors PPARγ and C/EBPα (Tormos et al., 2011). Wang and colleagues (2015) demonstrated that the early stages of adipogenesis displayed an increase of intracellular ROS; this concept was reinforced by studies performed by Kramer and colleagues (2015), whereby intracellular ROS levels experienced an increase over the four days of adipogenesis within murine 3T3-L1 pre-adipocytes. Tormus and colleagues (2011) demonstrated that an increase in intracellular hydrogen peroxide was generated upon day 2 of adipogenesis. PPARγ, the initiator of adipogenesis, was also excessively expressed during this stage of differentiation (Wang et al., 2015). Treatment with mitochondrial antioxidants led to a decrease in lipid formation and the protein levels of C/EBPα and PPARγ (Tormus et al., 2011; Wang et al., 2015). Furthermore, Tormus and colleagues observed the effects exogenous hydrogen peroxide, a member of ROS, had on adipocyte differentiation after treatment with mitochondrial antioxidants. It was demonstrated that the reduced adipogenesis could be redeemed with the addition of exogenous hydrogen peroxide.

In order to visualize the resulting ROS formed within the cells, 2',7'-dichlorofluorescin diacetate (DCF-DA) was utilized. This chemiluminescent compound is highly fluorescent and extremely sensitive regarding the detection of reactive oxygen species (Rastogi et al., 2010). DCF-DA is non-specific for certain types of ROS generated, and will only fluoresce when excessive generation of ROS or reduction of antioxidants occurs during oxidative stress. This compound is generally utilized in techniques including: fluorescence microscopy, flow cytometry, and fluorimetry (Rastogi et al., 2010). Reactive nitrogen species (RNS) may also generate a resulting fluorescence due to DCF formation.

Metabolic disorders, such as type II diabetes, and cardiovascular diseases bear an increasing incidence rate throughout Western communities (Castro et al., 2016). Excessive production of white adipose tissue may result in white adipose tissue dysfunction, which is one of the leading factors resulting in obesity; white adipose tissue is responsible for energy storage within the human system, and aids in the regulation of energy and nutrient homeostasis, as well as angiogenesis and blood pressure (Castro et al., 2016).

With the increased incidence of obesity due to adipocyte dysfunction, it is important to gain a greater understanding into the effects that mitochondrial ROS may have on the mechanisms of adipogenesis, in addition to developing any outstanding correlation between mitochondrial

dynamics and dysfunction, and the effects that this may have on mitochondrial and cellular ROS.

## 5-2. Results and Discussion

### 5-2-1. The resulting ROS observed after non-differentiating hMSC-ad cells had been exposed to concentrations of mitochondrial fusion promoter, M1.

The non-differentiating hMSC-ad cells were treated with varying concentrations of mitochondrial fusion promoter, M1, namely: 10 μM, 25 μM, 50 μM, and 100 μM. Untreated non-differentiating hMSC-ad cells were permitted to settle for approximately 24 hours before the addition of the varying concentrations of M1. The cells were left for a further 48 hours after treatment, and the results were observed using a DCF-DA live microscopy stain in order to view the resulting ROS generated.

DCF-DA has become a popular probe in the detection of intracellular reactive oxygen species formation, in particular, hydrogen peroxide (Wang et al., 1999). This probe detects the presence of ROS through oxidation, i.e. upon the interaction with hydrogen peroxide, the fluorescein will oxidize, thereby producing the observed fluorescence (Wang et al., 1999). The intensity of fluorescence observed corresponds to the resulting ROS levels within the cell; the greater the ROS, the greater the fluorescence. However, this fluorescent probe does provide limitations in use with fluorescence microscopy; photo-oxidation is problematic as the total period of exposure to light is relatively difficult to maintain during microscopic methods (Wang et al., 1999). Due to this difficulty in an accurate DCF-DA evaluation, two controls were utilized in the recording of the data below. The first control included non-differentiating hMSC-ad cells that had been left untreated for M1, and had been cultured under normal culture conditions. The results were obtained almost instantly upon removal of the foil cover due to the photosensitivity attributed with DCF-DA. As demonstrated within Figure 5-1. A., these cells did not produce a high intensity fluorescence, indicating that low ROS levels were being maintained throughout the hMSC-ad cells untreated for M1 (N = 2). Throughout the course of repetitive experiments, it was observed that, an increased exposure

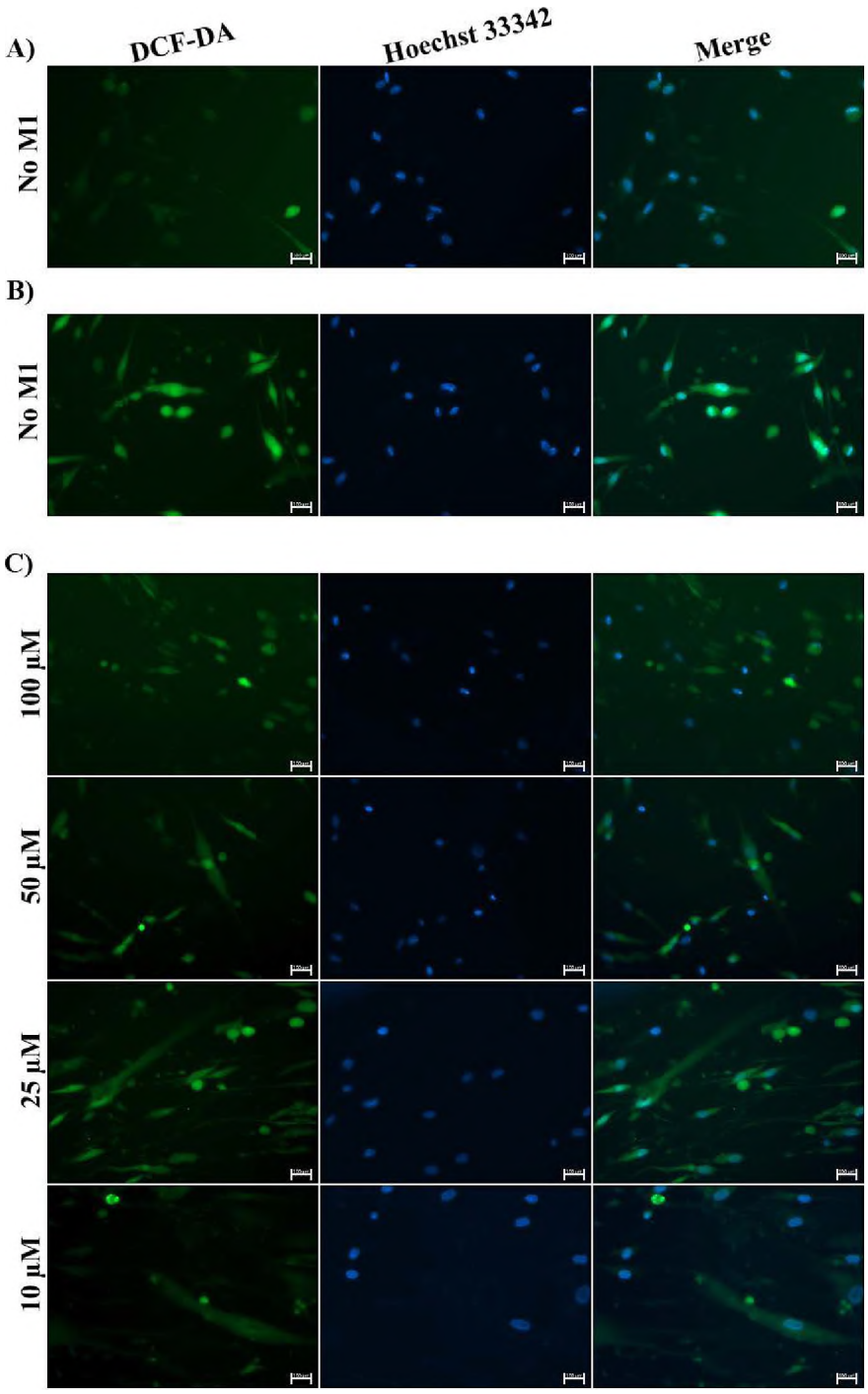


**Figure 5-1. Resulting reactive oxygen species observed for non-differentiating hMSC-ad cells treated with mitochondrial fusion promoter, M1.** The non-differentiating hMSC-ad cells were permitted to rest for 24 hours after which they were treated with varying concentrations of M1 mitochondrial fusion promoter. The resulting ROS was observed using a DCF-DA live stain. A) represents the control (no M1 added); B) is representative of the control captured after an increased period of fluorescent exposure; and C) depicts the resulting DCF-DA stains obtained for each of the M1 concentrations. Images were captured using the Zeiss AxioVert.A1 FL-LED fluorescence microscope at 200x magnification. Scale bar = 20 µm. Images shown are representative of multiple images obtained at random locations within the culture vessel (N = 2).

to the fluorescence light resulted in a greater intensity of resulting fluorescence, due to reasons previously described. Therefore, an additional control (Figure 5-1. B.) was established which captured the relative fluorescence approximately 20 – 30 seconds after initial exposure to the fluorescent LED light emitted. Already it is evident that a greater intensity in fluorescence is observed relative to that which was observed in Figure 5-1. A. With this in mind, the concentrations for M1 treated hMSC-ad cells were acquired as shown in Figure 5-1. C.

Overall, Figure 5-1. C. suggested an increased ROS production throughout concentrations 25 μM, 50 μM, and 100 μM M1, indicating that increased cellular stress combined with the aforementioned resulting effects of perturbance of the outer mitochondrial membrane, may be responsible for this accumulation of ROS, and the associated indications of cellular death. The lowest concentration, 10 μM, seemed to provide the lowest accumulation of ROS, when compared to the higher concentrations of M1 shown in Figure 5-1. C.; however, when compared to the control in Figure 5-1. A., the 10 μM M1 treatment provided a minimal increase in fluorescence. However, these results may not be entirely conclusive due to the nature of DCF-DA and its difficulty with photo-oxidation. Additional experiments, including the use of a fluorescent microplate reader, may have been utilized in order to provide quantitative data regarding ROS generation within these cells.

Unfortunately, the resulting reactive oxygen species generated during adipogenesis in the presence of M1 was not represented below as multiple complications, including complete cell death and detachment, prevented the acquisition of such images. Examples of the attempts are labelled accordingly within the attached appendix.

### 5-2-2. The resulting ROS observed after non-differentiating and adipogenic differentiating hMSC-ad cells had been exposed to concentrations of mitochondrial fission inhibitor, Mdivi-1.

Non-differentiating and adipogenic differentiating hMSC-ad cells were treated with Mdivi-1, a mitochondrial fission inhibitor which acts on Drp1; concentrations included 10 μM, 25 μM, 50 μM, and 100 μM. Initially the hMSC-ad cells were seeded into the culture vessel at

approximately 5 000 cells/well using the general mesenchymal stem cell maintenance medium (MSCM). After 24 hours, the maintenance medium was replaced and the concentrations of Mdivi-1 were added; the non-differentiating hMSC-ad cells were permitted to grow in the presence of Mdivi-1 for approximately 48 hours. The resulting reactive oxygen species were determined using the DCF-DA live staining protocol in which the cells were viewed using fluorescence microscopy; whereby the control sample represented hMSC-ad cells that were left untreated, in addition to cells that were stained only for Hoechst 33342 (as shown in the appendix).

The established control (as shown in Figure 5-2) consisted of untreated hMSC-ad cells that did not possess any Mdivi-1 in the culture medium. The resulting images obtained for DCF-DA fluorescence provides indication that the non-differentiating hMSC-ad cells experienced a decreased level of cellular ROS, indicated by the low intensity of fluorescence obtained (N = 2). Exposure times were kept consistent throughout the experiments; however, in accordance with photo-oxidation of DCF-DA, as previously described, while an attempt at regulating the overall acquisition time was maintained, complete consistency could not be monitored throughout.

As previously described: Mdivi-1, a mitochondrial fission inhibitor, has demonstrated cytoprotective properties that have been considered for therapeutic use; however, this fission inhibitor has also been linked to the acquisition of cytotoxic effects, as well as the inhibition of proliferation (Rosdah et al., 2016). There have been few studies performed that express the effects of Mdivi-1 on human adipose-derived mesenchymal stromal cells and adipocytes, with the main cell types used being cardiomyocytes, vascular cells, neurons, skeletal myoblasts, and cancer cells. Mdivi-1 is said to exhibit a half-life of approximately 8.9 hours within the brain, and may range anywhere between 6 – 24 hours when used on in vitro cell lines as previously mentioned (Rappold et al., 2014; Rosdah et al., 2016). With this in mind, the remaining non-differentiating hMSC-ad cells underwent treatment with varying concentrations of Mdivi-1.

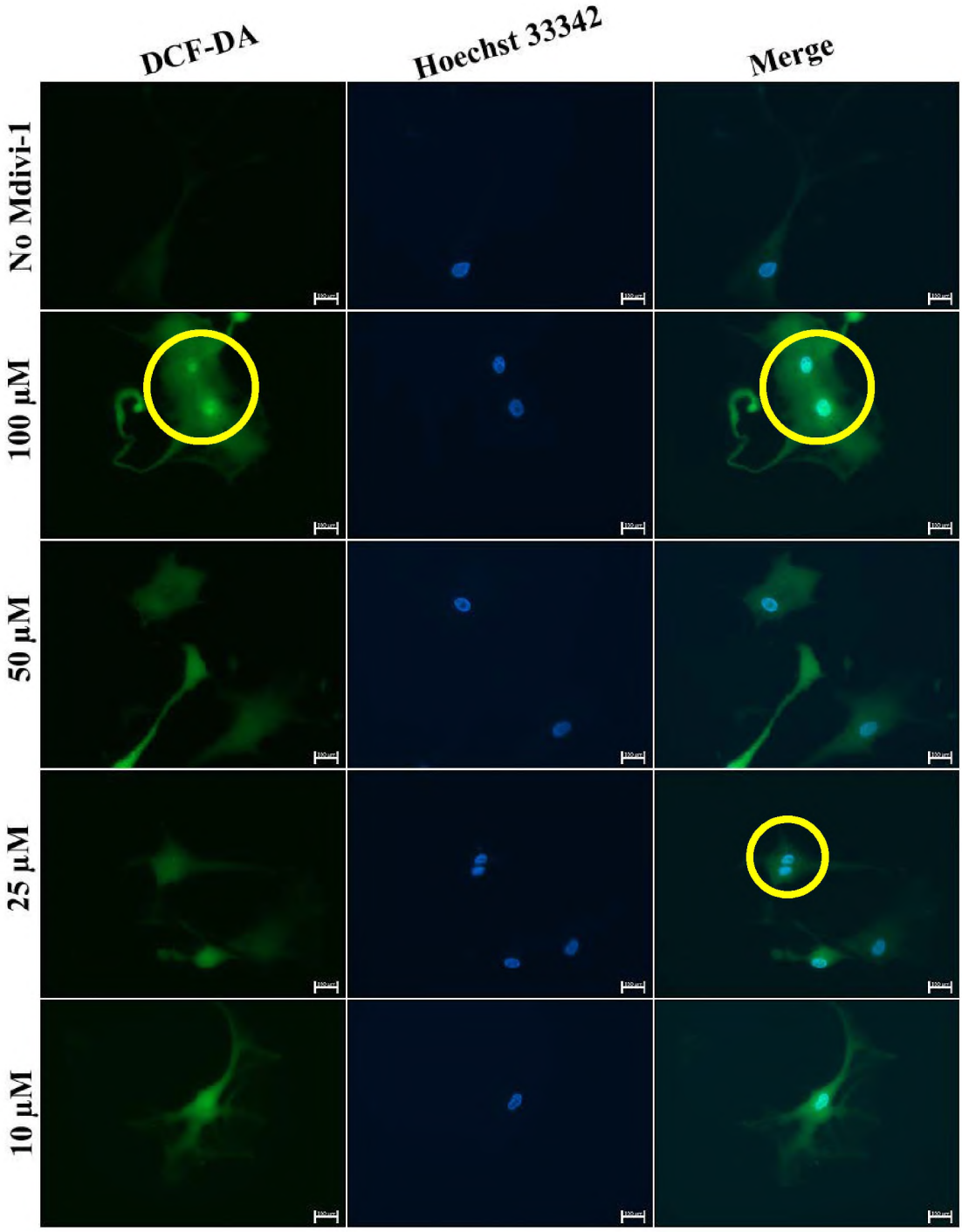


**Figure 5-2. Resulting ROS observed for non-differentiating hMSC-ad cells treated with Mdivi-1, mitochondrial fission inhibitor, for a total period of 48 hours**. The non-differentiating hMSC-ad cells were permitted to settle for 24 hours after which they were treated with varying concentrations of mitochondrial fission inhibitor, Mdivi-1. The resulting ROS was observed using a DCF-DA live stain. Images were captured using the Zeiss AxioVert.A1 FL-LED fluorescence microscope at 200x magnification. Scale bar = 20 µm. Images shown are representative of multiple images obtained at random locations within the culture vessel (N = 2).

An increase in ROS was collectively observed throughout the concentrations of Mdivi-1 (10 μM, 25 μM, 50 μM, and 100 μM), with, seemingly the highest intensity fluorescence occurring at 100 μM Mdivi-1 treatment (N = 2); however, there seemed to be little evident correlation between the concentrations of Mdivi-1 and the relative ROS generated as, while there seems to be a general decrease in ROS present as Mdivi-1 concentrations decreased, the 10 μM Mdivi-1 treatment provided a reasonably intense fluorescence that seemed greater than that observed for cells within 25 μM and 50 μM Mdivi-1 treatments. This, however, may be due to the previously described limitations of photo-oxidation when DCF-DA is utilised within fluorescence microscopy.

Mesenchymal stem cells are generally associated with a hypoxic environment, which, when cultured in vitro, promotes plastic adherent properties as well as maintains the cells' multipotent ability of differentiation. Therefore, it may be speculated that the resulting ROS stains would demonstrate a lower intensity of fluorescence; this would indicate a low ROS production within the mesenchymal stem cells. This low fluorescence is demonstrated within the untreated control sample demonstrated in Figure 5-2, which, in comparison to the Mdivi-1 treated non-differentiating hMSC-ad cells, displayed a relatively low fluorescence. This result coincides with Atashi and colleagues' (2015) review whereby they indicate that mesenchymal stem/stromal cells possess low intracellular levels of ROS, and increased amount of the antioxidant, glutathione. Oxidative stress is constantly regulated through the use of specific enzymes. It has been indicated that reactive oxygen species are essential for the survival of the mesenchymal stem/stromal cells, as well as the proliferative processes and differentiation. It is also important to note that oxidative stress is linked to the aging of the cell; therefore, 'younger' mesenchymal stem/stromal cells may exhibit a lower amount of intracellular ROS when compared to those of a greater age (Stolzing et al., 2008).

It must be acknowledged that, on several occasions noted throughout this study, upon the treatment of hMSC-ad cells with Mdivi-1 an indication of cellular fusion or mitosis occurred. This is evident within the highlighted regions of Figure 5-2, whereby two nuclei are present within a single cell (this was previously documented within Chapter 3, Figure 3-16 at 100 μM Mdivi treatment). Cell-to-cell fusion, as previously described within Chapter 3, is utilized during bone development and skeletal muscle formation in order to produce regenerative

bone marrow derived hybrids used in restoring multiple tissues; however, this mechanism is also associated with cancer formation (Sottile et al., 2016). This cellular fusion, characteristic of hMSC-ad cells recruited to site of injury, has been identified as a potential mechanism of transdifferentiation, indicating the overall potency/plasticity of the mesenchymal stromal/stem cell (Morigi et al., 2004). As previously described, cell-to-cell fusion may be the result of entosis, whereby the cell actively seeks to invade another cell due to a deficit in cell-matrix adhesive properties (Sottile et al., 2016). Spees and colleagues (2003) demonstrated that cellular fusion, utilizing bone marrow derived mesenchymal stem cells, was a common occurrence amongst epithelial cells and adult stem cells by the presence of multi-nucleated cells. This seemed to be a mechanism adopted in order to repair and restore the monolayer of epithelial cells (Spees et al., 2003).

However, within this study, it is uncertain as to whether or not the cells, are, in fact, undergoing cell-to-cell fusion or whether mitosis is occurring. A preliminary speculation may be adopted that indicates Mdivi-1 treatment promotes cell fusion; further experimentation will be required in order to confirm the incidences of cellular fusion. This may be achieved through multiple replicates of Mdivi-1 treatments for fluorescence microscopy and flow cytometry methods whereby multinucleated cells are isolated using immunostaining.

Adipogenesis was permitted for approximately 21 days; initially the hMSC-ad cells were seeded into the culture vessel at approximately 5 000 cells/well using the maintenance medium, MSCM. After 24 hours, the maintenance medium was replaced and the cells were permitted to reach 100 % confluency before induction for adipogenesis, in which the Mdivi-1 was added. The induction medium was replaced with the adipogenesis maintenance medium (insulin and DMEM) approximately 4 days after adipogenesis began; fresh Mdivi-1 was added for each media change. The resulting ROS was observed using DCF-DA and fluorescence microscopy, as demonstrated in Figure 5-3. As previously described, a control was utilized throughout the course of this experiment; this was demonstrated in the form of an untreated differentiating hMSC-ad cell sample. Consisting of no added Mdivi-1, the adipogenic differentiating control provided a reasonable intensity of fluorescence, which was to be expected considering the proposition that differentiation creates a fluctuation in ROS levels. The intensity of DCF-DA fluorescence seemed to be localized predominantly around the central point indicative of nuclear positioning, with a decrease in fluorescence observed the further away from the nucleus travelled.

In comparison to the control, fluorescence intensity seemed to increase upon the increase of Mdivi-1 concentrations; this was observed in relation to the 10 μM, 25 μM, 50 μM, and 100 μM Mdivi-1 treatments observed in Figure 5-3, with 100 μM Mdivi-1 treatment demonstrating the greatest intensity of fluorescence observed. It has been reported that adipogenic differentiating cells exhibit an increase in ROS during adipogenesis, and, thus, play a vital role in the signalling pathways present during adipogenesis (Kramer et al., 2015; Lee et al., 2009). Lee and colleagues (2009) have further stated that increased levels of ROS promote adipogenesis, and is linked to mitotic clonal expansion. However, throughout the course of

Mdivi-1 treatments, displayed in Figure 5-3, showed multiple incidences where low cellular ROS was observed (by indication of intensity of fluorescence) (N = 2). This low ROS formation may have been for several reasons, including the speculation that the entire population of hMSC-ad cells did not undergo adipogenesis, thereby creating this low ROS occurrence, corresponding to what was observed in Figure 5-2, for non-differentiating hMSC-ad cells. In addition to this, it may also be speculated that the cells may not have been on the same plane as that of those that provided a greater intensity; before adipogenesis was induced, the hMSC-ad cells were permitted to grow until at least 100 % confluence. During this period, multiple layers may have been formed, and, upon induction of adipogenesis, this positioning may have been maintained throughout.

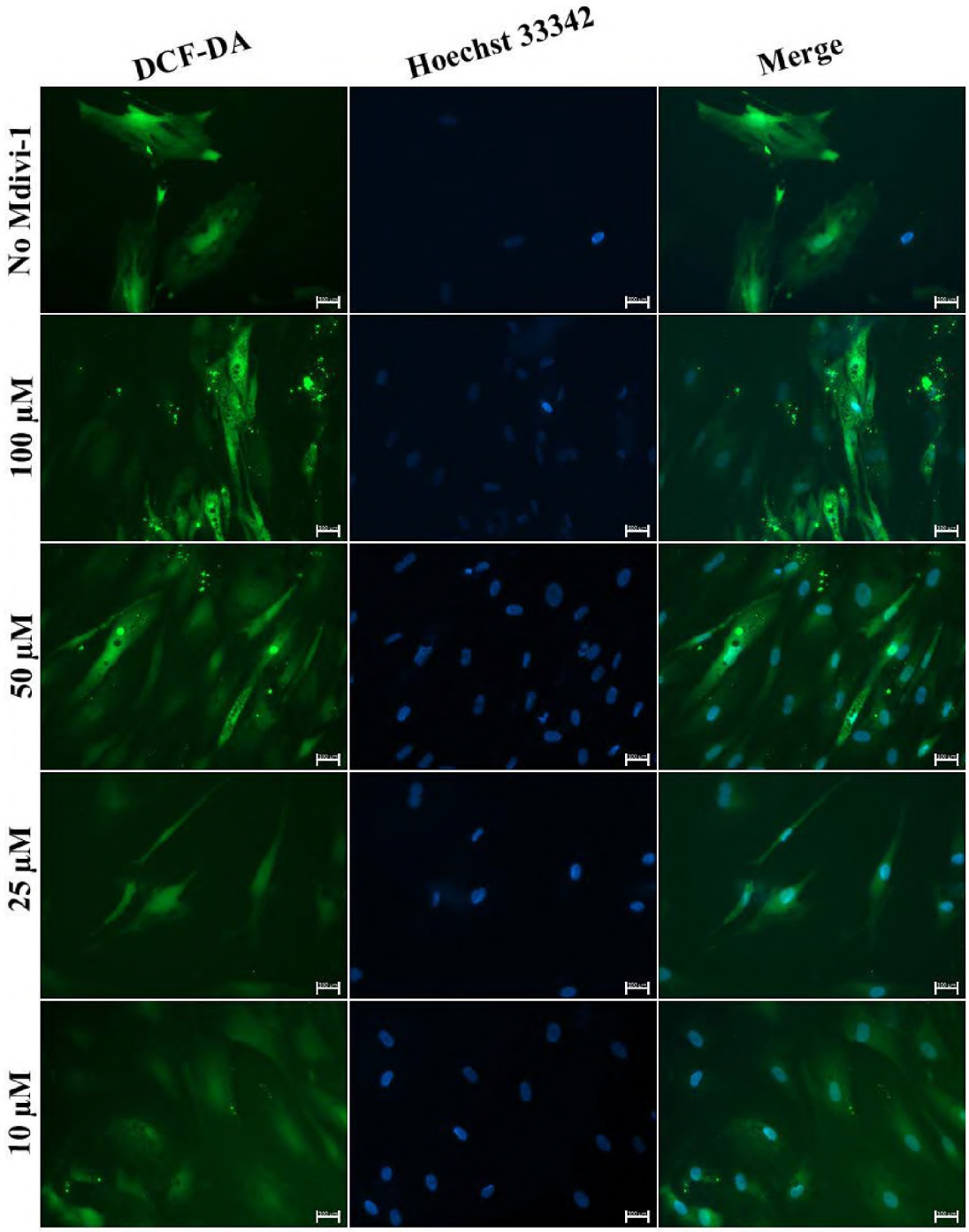


**Figure 5-3. Resulting ROS observed for adipogenic differentiating hMSC-ad cells with Mdivi-1, mitochondrial fission inhibitor, treatment for a total period of 21 days.** The non-differentiating hMSC-ad cells were permitted to reach 100 % confluency before adipogenesis was induced using the induction media in combination with Mdivi-1 concentrations. The adipogenic maintenance media contained fresh Mdivi-1. The resulting ROS was observed using a DCF-DA live stain. Images were captured using the Zeiss AxioVert.A1 FL-LED fluorescence microscope at 200x magnification. Scale bar = 20 µm. Images shown are representative of multiple images obtained at random locations within the culture vessel (N = 2).

The formation of lipid vesicles/droplets was mainly prevalent within adipocytes of 100 μM and 50 μM Mdivi-1 treatment; these cells seemed to present with a higher intensity of DCFDA fluorescence, particularly observed around these vesicles/droplets. This may be related to the high mitochondrial content generally observed around the lipid droplets, as mentioned in the previous chapter, as it has been stated that mitochondria are the primary source of ROS production. This increased lipid vacuole/vesicle/droplet presence was observed over multiple incidences within this study, and may be seen within corresponding images of previous chapters where the adipogenic differentiating hMSC-ad cells were treated with Mdivi-1. Therefore, a preliminary speculation may be formed in that non-lethal concentrations of Mdivi1 may promote lipogenesis. However, such speculation is indeterminate presently until further studies are conducted regarding the correlation between ROS localization and mitochondria using varying staining techniques and mitochondrial isolations. The observation of fusiform morphologies remained prevalent when the adipogenic differentiating hMSC-ad cells were treated with 25 μM, 50 μM, and 100 μM Mdivi-1.

It was acknowledged that the fluorescence intensity decreased slightly as Mdivi-1 concentrations were reduced to 25 μM and 10 μM; however, the untreated control provided an almost visually equivalent intensity when compared to the higher concentrations of Mdivi-1, namely 100 μM and 50 μM. Due to the reported in vitro half-life of this chemical compound, it cannot be definitively concluded that the mitochondrial fission inhibitor, Mdivi-1, had a large deleterious/beneficial effect on adipogenesis throughout the course of differentiation; since fission is inhibited, it may be speculated that the rate of differentiation and other high-energy demanding processes may be reduced or inhibited for the time in which Mdivi-1 remained active. However, due to the half-life and the chosen treatment times, it may be further speculated that the mitochondria were able to compensate for this inhibition of Drp1 and, once Mdivi-1 had become inactive, rectify mitochondrial fission, thereby promoting adipogenesis once again.

Comparatively, the differentiated adipocytes displayed a greater intensity of fluorescence than that of the non-differentiating hMSC-ad cells shown in Figure 5-2, indicating that adipogenesis exhibits a higher level of reactive oxygen species, which coincides with multiple studies in which intracellular ROS levels were shown to increase during

differentiation; this aids in the speculation that ROS plays an important role in adipogenesis (Kanada et al., 2011; Wang et al., 2015; Houstis et al., 2006). When maintained in a hypoxic environment adipogenesis may be inhibited or reduced; Guo and colleagues (2006) exhibited the involvement of ROS in PPARγ activity, which has been linked to the expression of lipogenic genes. Octanoate, a medium-chain triglyceride fatty acid, was utilized and led to the promotion of ROS production within adipocytes, which are responsible for the inhibition of PPARγ activity, and, thus, the formation of lipids (Guo et al., 2006).

## 5-3. Conclusions, Complications, and Future Work

Reactive oxygen species (ROS) have been linked to metabolic diseases, namely obesity, insulin resistance, and diabetes (Tormos et al., 2011; Lee et al., 2009). When exposed to oxidative stress, mature adipocytes exhibit an inhibition of glucose uptake; however, during adipogenesis an increase in ROS may be experienced. Within human mesenchymal stem cells, varying levels of ROS regulate the various lineages of differentiation, with increased intracellular ROS promoting adipogenesis within the mesenchymal stem cells (Wang et al., 2015). Within this study, it was demonstrated that, overall, an increase in intracellular ROS is observed within adipogenic differentiating hMSC-ad cells; reactive oxygen species are also the result of additional oxidative stress, which may be a by-product of mitochondrial dysfunction. This, in turn, may cause an increase in ROS, which was somewhat observed upon the addition of the mitochondrial small molecules, Mdivi-1 and M1.

Complications were experienced with the recording of the ROS fluorescence via microscopy methods as prolonged exposure to LED fluorescence seemed to cause the DCF-DA to become further excited, leading to the saturation of the image. However; it could be speculated that the prolonged exposure resulted in an increase in ROS, thereby causing the resulting DCF-DA fluorescence to over-saturate. Other factors that could lead to this DCF-DA fluorescence increase might include the increased exposure to the atmospheric environment; thereby causing the elevated levels of ROS. In order to provide further conclusions, additional experiments would be required; these might include the utilization of the microplate reader to measure the wavelengths of the resulting fluorescence as well as

flow cytometry techniques that are commonly associated with the use of DCF-DA. Flow cytometry was attempted; however, the machine was only available for a limited amount of time and adipogenesis was not permitted due to these time constraints. Data was obtained for the non-differentiating hMSC-ad cells for S3I-201 concentration treatments, and is shown within the appendix.

The experiments shown within this chapter provide visual evidence to suggest the increase of ROS during adipogenesis, thereby, supporting the claim that a regulated increase in ROS is vital for adipogenesis to occur. Future experiments may exploit the reduction and increase of intracellular ROS, with the resulting effects captured via fluorescence microscopy or via the confocal microscope, which may provide greater analytic value. A speculation that intracellular ROS is increased when mitochondria are placed under stressful circumstances may be vaguely generated, however, localization studies would be required to substantiate this speculation.

# Chapter 6:

# 6: Conclusions, complications and future work

## 6-1: Overall Conclusions.

The aim of this study was to effectively demonstrate the resulting two-dimensional mitochondrial networks within human non-differentiating and differentiating cell lines, and the role that mitochondrial dynamics would play on these cellular models. In addition to this, a comparison of reactive oxygen species (ROS) generated during differentiation was also required.

Mitochondrial dynamics have been implicated in multiple degenerative disorders, including neurodegeneration as well as metabolic degenerative diseases, such as obesity and insulin resistance associated with type II diabetes (Yoon et al., 2011). The balance of mitochondrial dynamics is extremely sensitive, and the slightest alteration may have dire consequences. The data presented provides evidence of this sensitivity due to the treatment of human adipose-derived mesenchymal (hMSC-ad) cells with various small molecule compounds that target these dynamic properties, such as Mdivi-1 (a mitochondrial fission inhibitor) and M1 (a mitochondrial fusion promoter), and a STAT3 inhibitor (S3I-201). The S3I-201 was utilized due to the proposed involvement of mitochondrial STAT3. Using murine pre-adipocytes (3T3L1), Kramer and colleagues (2015) demonstrated the probability of the involvement of STAT3 in the regulation of reactive oxygen species (ROS) levels during adipogenesis; it was noted that ROS levels increased dramatically over the first four days, post-induction, after which ROS levels declined. This study revealed the increase in ROS levels, through microscopy methods; however, the DCF-DA fluoresced more intensely as exposure to the LED fluoresce increased, providing a non-conclusive result.

Initially, it was hypothesized that the treatment of the cells with Mdivi-1 and M1 would result in a decreased/inhibited rate of adipogenesis (for differentiating hMSC-ad cells) and would stunt cell growth. While this remained true for both non-differentiating and differentiating hMSC-ad cells treated with M1, those that underwent treatment with Mdivi-1 provided an unexpected result.

Mdivi-1 was discovered as a small molecule responsible for a selective inhibition of Drp1, a mitochondrial fission protein; it possesses a great potential for therapeutic use, particularly in Parkinson's Disease and cardiac injury patients whereby an over-stimulation of mitochondrial fission has been reported as a potential cause of this degenerative disease (Rosdah et al., 2016; Cui et al., 2010; Sumida et al., 2015; Rappold et al., 2014). It was first demonstrated by Cassidy-Stone and colleagues (2008) that Mdivi-1 treatment led to the decrease in mitochondrial fragmentation and the associated apoptosis. Mdivi-1 has been used for in vitro studies for cell types including: neurons, cardiovascular cells/cardiomyocytes, astrocytes, skeletal myoblasts, and cancer cells (including the human breast carcinoma and SH-SY5Y neuroblastoma cell lines); however, there are very few studies that have been performed that demonstrate the effects that Mdivi-1 may have on human adipose-derived mesenchymal stromal cells and adipocytes (Rosdah et al., 2016). This has made it difficult to speculate an accurate half-life for these cell lines; however, a general idea of 6 – 24 hours may be generated based on data acquired for the in vitro studies of the aforementioned cell lines. Rappold and colleagues (2014) proposed that Mdivi-1 bore a half-life of 8.9 hours when utilized within the brain. When used in this study, Mdivi-1 provided no deleterious effects on the overall cellular growth and/or differentiation capabilities of the hMSC-ad cells. It is to be acknowledged that an initial decline in cell growth was observed upon initial treatment of Mdivi-1; however, the cells were able to rectify the damage done and a healthy progeny of mitochondria were re-established. More importantly, the higher concentrations of Mdivi-1 produced apparent 'fused' cells on repeated occasions; this was either the result of entosis (cell-to-cell fusion) or the cells were captured undergoing mitosis. In addition to this, treatment with Mdivi-1 seemed to promote the generation of lipid vacuoles/droplets in comparison to what was shown for untreated adipogenic differentiating hMSC-ad cells. While Mdivi-1 possesses a half-life of 6 – 24 hours, dependent on the cell line used, it may be assumed that this small molecule did have an advantageous effect on lipogenesis.

The use of the S3I-201 provided an initial prediction that adipogenesis would be inhibited, due to the proposed role that S3I-201 plays on the differentiation capacities. STAT3 levels increase during adipogenesis (Harp et al., 2001). It was found that STAT3 inhibition does not directly block adipogenesis, but does play a role in reducing the rate of lipogenesis.

Non-differentiating and differentiating hMSC-ad cells are proposed to possess mitochondrial networks that differ to one another; non-differentiating hMSC-ad cells have a more elongated, interconnecting network of mitochondria that displayed a notably higher mitochondrial potential, while adipogenic differentiating hMSC-ad cells adopted a more rounded morphology that were slightly smaller in size and more compactly clustered, localizing around the nucleus and the lipid droplets. The resulting two-dimensional networks obtained for adipocytes were substantiated by Wilson-Fritch and colleagues (2003). Regarding the effects that Mdivi-1 and M1, this initial prediction varied according to the compound: For Mdivi-1, shorter, more fragmented mitochondria were expected in comparison to M1-treated cells that would display more elongated, thicker mitochondria. It was demonstrated that treatment with M1 provided shorter mitochondria that remained approximately the same thickness throughout; the decreasing length of mitochondria may have been the product of multiple mutations arising, or the formation of diseased/apoptotic mitochondria. Mdivi-1 treatment produced a decrease in mitochondrial thickness, as concentrations increased, while the average length suffered a minimal decrease. The treatment of S3I-201 provided little/no effect on the mitochondria as there was little difference between resulting average length and thickness observed, for each concentration. This may suggest that the S3I-201 was not, in fact, specific for mitochondria and, instead, may have affected cellular STAT3 on a greater scale. The addition of cobalt chloride to S3I-201 treated cells generated significantly elongated mitochondria that experienced a slight increase in average thickness.

## 6-2: Additional Experiments and Future Work

There are multiple experiments that may be performed to substantiate speculations made, as well as provide a greater understand regarding the impact that mitochondrial dynamics may have on cell survival and phenotype. Various cell lines could have been utilized to reinforce the effects that mitochondrial dynamics plays on cell survival as different compounds react differently within the varying cells. For example, while enhanced mitochondrial fusion had deleterious effects on adipocytes and non-differentiating human adipose-derived mesenchymal stem cells, M1 could have proven to be beneficial in neural progenitor cells,

as Chen and colleagues (2007) provided evidence that mitochondrial fusion may protect the cerebellum from neurodegeneration. Additionally, Mdivi-1 has been shown to have a beneficial effect on cardiomyocytes. Genetic testing and PCR would also be beneficial in order to gain better insight into the mitochondrial mutations generated as the by-product of treatment with M1.

Due to the proposed in vitro half-life for Mdivi-1; the small molecule compound could have been added more frequently within the maintenance medium, thereby promoting an inhibition of fission without permitting cells a "grace period" whereby mitochondria may be able to rectify this deficit. Additionally, the half-life of Mdivi-1 within human adipose-derived mesenchymal stromal (hMSC-ad) cells, as well as the differentiated adipogenic prodigy, may be determined. Kita and colleagues (2009) observed a decrease triacylglycerol generation; however, upon the inhibition of fusion proteins, therefore the increase of fission, an increase in triacylglycerol generation was observed followed by the increased formation of punctate mitochondria. This provides evidence that mitochondrial fission and fusion does play an important role in lipid accumulation, which may lead to increased speculations that the addition of Mdivi-1 promotes lipogenesis, as was demonstrated within chapter 3.

In order to determine the full mechanism of the action of cellular fusion observed for the high concentrations of Mdivi-1 treatment, additional statistically valid experiments may be performed in order to validate the speculation. Two populations of mesenchymal stem cells could be tagged with certain fluorescent dyes, and their movements could be monitored over a selected period of time using a time-lapse microscopy technique whereby cellular movement would be constantly monitored. Flow cytometry is an additional technique that could be utilized in this instance, where cell sorting occurs in order to determine/separate the cells that underwent fusion.

The mitochondrial membrane potential could have been more closely monitored; in other words, more time dependent studies could have been performed, where JC-1 is measured using both microscopy methods and using a microplate spectrophotometer/fluorimeter to gain values of fluorescence, for time intervals of 4 days, 7 days, 12 days, 20 days, and 24

days. This would provide a greater comparison in terms of the resulting mitochondrial membrane potential/activity established throughout the various stages of adipogenesis.

In order to study the three-dimensional network, the confocal microscope was required; multiple attempts were made to view the hMSC-ad cells with a Zeiss LSM780 confocal microscope, however, the resulting live stains (as shown in the appendix) were too granular to determine definite mitochondrial networks and branching. Another complication arose in attempting to view SH-SY5Y cells using the lasers of the confocal microscope; on several occasions the cells detached/died, resulting in free floating rounded cells within the culture vessel. It was speculated that this was the result of the lasers impacting the SH-SY5Y cells; it was further attempted to coat the culture vessel with laminin in order to secure the cells' attachment. However, it was met with the same result.
SH-SY5Y cells were abandoned in this study for several reasons already discussed in the previous chapter.

ROS levels could have been more accurately determined using both flow cytometric methods combined with microscopy and the reading obtained using a microplate spectrophotometer/fluorimeter; this could be performed on all small compounds for a variety of non-differentiating and differentiating cellular models. In addition to this, compounds known to significantly increase/decrease ROS could have been used for comparative purposes, alongside antioxidant treatments.

Furthermore, additional cell lines could have been utilized in order to generate a comparison of the three germ layer models present within the mammalian system: the mesoderm, ectoderm, and endoderm.

# References

Al-Mehdi, A-B., Pastukh, V.M., Swiger, B.M., Reed, D.J., Patel, M.R., Bardwell, G.C., Pastukh, V.V., Alexeyev, M.F., and Gillespie, M.N. (2012). Perinuclear Mitochondrial Clustering Creates and Oxidant-Rich Nuclear Domain Required for Hypoxia-Induced Transcription., Sci. Signal. 5(231): 1 – 20

Atashi, F., Modarressi, A., and Pepper, M.S. (2015). The Role of Reactive Oxygen Species in Mesenchymal Stem Cell Adipogenic and Osteogenic Differentiation: A Review., Stem Cells and Development. 24: 1150 – 1163

Baffou, G., Rigneault, H., Marguet, D., and Jullien, L. (2014). A Critique of Methods for Temperature Imaging in Single Cells., Nature: Methods. 11(9): 899 – 901

Banas, A., Teratani, T., Yamamoto, Y., Tokuhara, M., Takeshita, F., Quinn, G., Okochi, H., and Ochiya, T. (2007). Adipose Tissue-Derived Mesenchymal Stem Cells as a Source of Human Hepatocytes., Hepatology. 46: 219 – 228

Bigarella, C.L., Liang, R., and Ghaffari, S. (2014). Stem Cells and the Impact of ROS Signalling., Development. 141: 4206 – 4218

Caplan, A.I. (1991). Mesenchymal Stem Cells., Journal of Orthopaedic Research, 9: 641 – 650

Cassidy-Stone. A., Chipuk, J.E., Ingerman, E., Song, C., Yoo, C., Kuwana, T., Kurth, M.J., Shaw, J.T., Hinshaw, J.E., Green, D.R., and Nunnari, J. (2008). Chemical Inhibition of the Mitochondrial Division Dynamin Reveals its Role in Bax/Bak-Dependent Mitochondrial Outer Membrane Permeabilization., Dev. Cell. 14(2): 193-204

Castro, J.P., Grune, T., and Speckmann, B. (2016). The Two Faces of Reactive Oxygen Species (ROS) in Adipocyte Function and Dysfunction., Biol. Chem. 397(8): 709 – 724

Cedikova, M., Kripnerová, M., Dvorakova, J., Pitule, P., Grundmanova, M., Babuska, V.,

Mullerova, D., and Kuncova, J. (2016). Mitochondria in White, Brown, and Beige Adipocytes., Stem Cells International. 2016: 1 - 11

Cernkovich, E.R., Deng, J., Bond, M.C., Combs, T.P., and Harp, J.B. (2008). Adipose-Specific Disruption of Signal Transducer and Activator of Transcription 3 Increase Body Weight and Adiposity., Endocrinology. 149: 1581 – 1590

Chandel, N.S., McClintock, D.S., Feliciano, C.E., Wood, T.M., Melendez, J.A., Rodriguez, A.M., and Schumacker, P.T. (2000). Reactive Oxygen Species Generated at Mitochondrial Complex III Stabilize Hypoxia-Inducible Factor-1α during Hypoxia., The Journal of Biological Chemistry. 275 (33): 25130 – 25138

Chen, H., and Chan, D.C. (2009). Mitochondrial Dynamics – Fusion, Fission, Movements, and Mitophagy – in Neurodegenerative Diseases., Human Molecular Genetics. 18: 169 – 176

Chen, H., McCaffery, J.M., and Chan, D.C. (2007). Mitochondrial Fusion Protects Against Neurodegeneration in the Cerebellum., Cell. 130: 548 – 562

De Vos, K.J., Allan, V.J., Grierson, A.J., and Sheetz, M.P. (2005). Mitochondrial Function and Actin Regulate Dynamin-Related Protein 1-Dependent Mitochondrial Fission., Current Biology. 15: 678 – 683

Dominici, M., Le Blanc, K., Mueller, I., Slaper-Cortenback, I., Marini, F.C., Krause, D.C., Deans, R.J., Keating, A., Prockop, D.J., and Horwitz, E.M. (2006). Minimal Criteria for Defining Multipotent Mesenchymal Stromal Cells. The International Society for Cellular Therapy Position Statement., Cytotherapy. 8(4): 315 – 317

Encinas, M., Iglesias, M., Liu, Y., Wang, H., Muhaisen, A., Ceña, V., Gallego, C., and Comella, J.X. (2000). Sequential Treatment of SH-SY5Y with Retinoic Acid and Brain-Derived Neurotrophic Factor Gives Rise to Fully Differentiated, Neurotrophic Factor-Dependent, Human Neuron-Like Cells., Journal of Neurochemistry. 75: 991 – 1003

Estrada, J.C., Albo, C., Benguría, A., Dopazo, A., López-Romero, P., Carrera-Quintanar, L., Roche, E., Clemente, E.P., Enríquez, J.A., Bernard, A., and Samper, E. (2012). Culture of Human Mesenchymal Stem Cells at Low Oxygen Tension Improves Growth and Genetic Stability by Activating Glycolysis., Cell Death and Differentiation. 13: 743 – 755

Finkel, T. (2011). Signal Transduction by Reactive Oxygen Species., Journal of Cell Biology. 194(1): 7 – 15

Fowler, S.D., and Greenspan, P. (1985). Application of Nile Red, a Fluorescent Hydrophobic Probe, for the Detection of Neutral Lipid Deposits in Tissue Sections: Comparison with Oil Red O., Journal of Histochemistry and Cytochemistry. 33: 833 – 836

Garner, D.L., and Thomas, C.A. (1999). Organelle-Specific Probe JC-1 Identifies Membrane Potential Differences in the Mitochondrial Function of Bovine Sperm., Molecular Reproduction and Development. 53: 222 – 229

Gao, W., McCormick, J., Connolly, M., Balogh, E., Veale, D.J., and Fearon, U. (2015). Hypoxia and STAT3 Signalling Interactions Regulate Pro-Inflammatory Pathways in Rheumatoid Arthritis., Annals of the Rheumatic Diseases. 74: 1275 – 1283

Grayson, W.L., Zhao, F., Bunell, B., and Ma, T. (2007). Hypoxia Enhances Proliferation and Tissue Formation of Human Mesenchymal Stem Cells., Biochemical and Biophysical Research Communications. 358: 948 – 953

Greenspan, P., Mayer, E.R., and Fowler, S.D. (1985). Nile Red: A Selective Fluorescent Stain for Intracellular Lipid Droplets., Journal of Cell Biology. 100: 965 – 973

Guo, W., Xie, W., and Han, J. (2006). Modulation of Adipocyte Lipogenesis by Octanoate: Involvement of Reactive Oxygen Species., Nutrition & Metabolism. 3 (30): 1 – 8

Hales, K.G. (2010). Mitochondrial Fusion and Division., Nature Education. 3(9): 12

Hamanaka, R.B., and Chandel, N.S. (2009). Mitochondrial Reactive Oxygen Species Regulate Hypoxic Signalling., Curr Opin Cell Biol. 21 (6): 894 – 899

Harp, J.B., Franklin, D., Vanderpuije, A.A., and Gimble, J.M. (2001). Differential Expression Of Signal Transducers and Activators of Transcription During Human Adipogenesis., Biochemical and Biophysical Research Communications. 281: 907 – 912

Heiskanen, K. M., Bhat, M.B., Wang, H-W., Ma, J., and Nieminen, A-L. (1999). Mitochondrial Depolarization Accompanies Cytochrome C Release During Apoptosis in PC6 Cells., The Journal of Biological Chemistry. 274(9): 5654 – 5658

Houstis, N., Rosen, E.D., and Lander, E.S. (2006). Reactive Oxygen Species have a Casual Role in Multiple Forms of Insulin Resistance., Nature. 440: 944 – 948

Jheng, H-F., Tsai, P-J., Guo, S-M, Kuo, L-H, Chang, C-S., Su, I-J., Chang, C-R., and Tsai, Y. S. (2012). Mitochondrial Fission Contributes to Mitochondrial Dysfunction and Insulin Resistance in Skeletal Muscle., Molecular and Cellular Biology., 32(2): 309 – 319

Jiang, L., Wang, Q., Yu, Y., Zhao, F., Huang, P., Zeng, R., Qi, R.Z., Li, W., and Liu, Y. (2009). Leptin Contributes to the Adaptive Responses of Mice to High-Fat Diet Intake through Suppressing the Lipogenic Pathway., PLoS ONE., 4(9): e6884: 1 – 9

Johnson, A.W., Kinzenbaw, D.A., Modrick, M.L., and Faraci, F.M. (2013). Small Molecule Inhibitors of Signal Transducer and Activator of Transcription 3 Protect Against Angiontensin II-Induced Vasular Dysfunction and Hypertension., Hypertension. 61: 437 - 442

Jones, D.L., and Fuller, M.T. (2004). Hand Book of Stem Cells., 5: Stem Cell Niches. (ed.

Lanza, R.P., Blau, H., Melton, D., Moore, M., Thomas, E.D., Verfailie, C., Weissman, I., and West, M.). Elsevier Inc., 2: 59 – 60

Jung, J.E., Lee, H-G., Cho, I-H., Chung, D.H., Yoon, S-H., Yang, Y.M., Lee, J.W., Choi, S., Park, J-W., Ye, S-K., and Chung, M-H. (2005). STAT3 is a Potential Modulator of HIF-1-Mediated VEGF Expression in Human Renal Carcinoma Cells., The FASEB Journal. 19(10): 1296 – 1298

Kanada, Y., Hinata, T., Kang, S.W., and Watanabe, Y. (2011). Reactive Oxygen Species Mediate Adipocyte Differentiation in Mesenchymal Stem Cells., Life Sciences. 89: 250
– 258

Katajisto, P., Döhla, J., Chaffer, C., Pentinmikko, N., Marjanovic, N., Iqbal, S., Zoncu, R., Chen, W., Weinberg, R.A., and Sabatini, D.M. (2015). Asymmetric Apportioning of Aged Mitochondria Between Daughter Cells is Required for Stemness., Science. 348(6232): 340 – 343

Kim, H., Lee, J.Y., Park, K.J., Kim, W., and Roh, G.S. (2016). A Mitochondrial Division Inhibitor, Mdivi-1, Inhibits Mitochondrial Fragmentation and Attenuates Kainic Acid-Induced Hippocampal Cell Death., BMC Neuroscience. 17(33): 1 - 10

Kim, J., Wei, Y., and Sowers, J.R. (2008). Role of Mitochondrial Dysfunction in Insulin Resistance., Circulation Research. 102: 401 – 414

Kita, T., Nishida, H., Shibata, H., Niimi, S., Hiquti, T., and Arakaki, N. (2009). Possible Role of Mitochondrial Remodelling on Cellular Triacylglycerol Accumulation., J. Biochem. 146(6): 787 – 796

Kolf, C.M., Cho, E., and Tuan, R.S. (2007) Biology of Adult Mesenchymal Stem Cells: Regulation of Niche, Self-Renewal and Differentiation., Arthritis Research and Therapy. 9: 1 - 10

Koopman, W.J., Visch, H-J., Smeitink, J.A.M., and Willems, P.H.G.M. (2005). Simultaneous Quantitative Measurement and Automated Analysis of Mitochondrial Morphology, Mass, Potential, and Motility in Living Human Skin Fibroblasts., Cytometry Part A. 69A: 1 – 12

Krabbe, C., Zimmer, J., and Meyer, M. (2005). Neural Transdifferentiation of Mesenchymal Stem Cells – A Critical Review., Apmis. 113: 831 – 844

Kramer, A.H., Edkins, A.L., Hoppe, H.C., and Prinsloo, E. (2015). Dynamic Mitochondrial Localisation of STAT3 in the Cellular Adipogenesis Model 3T3-L1., Journal of Cellular Biochemistry. 116: 1232 – 1240

Kramer, A.H., Kadye, R., Houseman, P.S., and Prinsloo, E. (2015). Mitochondrial STAT3 and Reactive Oxygen Species: A Fulcrum of Adipogenesis?, JAK-STAT. 4: 1 – 10

Lee, H., Lee, Y.J., Choi, H., Ko, E.H., and Kim, J. (2009). Reactive Oxygen Species Facilitate Adipocyte Differentiation by Accelerating Mitotic Clonal Expansion., The Journal of Biological Chemistry. 284 (16): 10601 – 10609

Lee, Y., Jeong, S., Karbowski, M., Smith, C.L., and Youle, R.J. (2004). Roles of the Mammalian Mitochondrial Fission and Fusion Mediators Fis1, Drp1, and Opa1 in Apoptosis., Molecular Biology of the Cell. 15: 5001 – 5011

Li, Z., Ji, G., and Neugebauer, V. (2011). Mitochondrial Reactive Oxygen Species are Activated by mGluR5 through IP3 and Activate ERK and PKA to Increase Excitability of Amygdala Neurons and Pain Behavior., Journal of Neuroscience. 31(3): 1114 – 1127

Liesa, M., and Shirihai, O.S. (2013). Mitochondrial Dynamics in the Regulation of Nutrient Utilization and Energy Expenditure., Cell Metabolism Review. 17: 491 – 506

Lihavainen, E., Mäkelä, J., Spelbrink, J.N., and Ribeiro, A.S. (2012). Mytoe: Automatic Analysis of Mitochondrial Dynamics., Bioinformatics. 28: 1050 – 1051

Liu, X., Shibata, T., Hisaka, S., and Osawa, T. (2009). Astaxanthin Inhibits Reactive Oxygen Species-Mediated Cellular Toxicity in Dopaminergic SH-SY5Y Cells via Mitochondria-Targeted Protective Mechanism., Brain Research. 1254: 18 – 27

Lennon, D.P., Edmison, J.M., and Caplan A.I. (2001). Cultivation of Rat-Marrow Derived Mesenchymal Stem Cells in Reduced Oxygen Tension: Effects on in vitro and in vivo Osteochondrogenesis., Journal of Cell Physiology. 187: 345 - 355

López-Carballo, G., Moreno, L., Masiá, S., Pérez, P., and Barettino, D. (2002). Activation of the Phosphatidylinositol 3-Kinase/Akt Signaling Pathways by Retinoic Acid Is Required for Neural Differentiation of SH-SY5Y Human Neuroblastoma Cells., The Journal of Biological Chemistry. 277(28): 25297 - 25304

Matsumoto, Y., Iwasaki, H., and Suda, T. (2011). Adult Stem Cells: Biology and Method of Analysis., 2: Maintenance of Adult Stem Cells: Role of the Stem Cell Niche., (ed. Phinney, D.G.)., Springer Science + Business Media, LLC., 35 – 47

Misko, A., Jiang, S., Wegorzewska, I., Milbrandt, J., and Baloh, R.H. (2010). Mitofusin 2 is Necessary for Transport of Axonal Mitochondria and Interacts with the Miro/Milton Complex., Journal of Neuroscience. 30(12): 4232 – 4240

Morigi, M., Imberti, B., Zoja, C., Corna, D., Tomasoni, S., Abbate, M., Rottoli, D., Angioletti, S., Benigni, A., Perico, N., Allison, M., and Remuzzi, G. (2004). Mesenchymal Stem Cells are Renotropic, Helping to Repair the Kidney and Improve Function in Acute Renal Failure., Journal American Society of Nephrology. 15(7): 1794 – 1804

Morino, K., Petersen, K.F., and Shulman, G.I. (2006). Molecular Mechanisms of Insulin Resistance in Humans and their Potential Links with Mitochondrial Dysfunction., Diabetes. 55: S9 – S15

Napolitano, L. (1963). The Differentiation of White Adipose Cells: An Electron Microscope Study., The Journal of Cell Biology. 18: 663 – 679

Panchision, D.M. (2011). Adult Stem Cells: Biology and Method of Analysis., 1: Molecular Mechanisms Regulating Adult Stem Cell Self-Renewal., (ed. Phinney, D.G.)., Springer Science + Business Media, LLC., 2 – 15

Perry, S.W., Norman, J.P., Barbieri, J., Brown, E.B., and Gelbard, H.A. (2011). Mitochondrial Membrane Potential Probes and the Proton Gradient: A Practical Usage Guide., Biotechniques. 50 (2): 98 – 115

Pittenger, M.F., and Marshak, D.R. (2001). 16: Mesenchymal Stem Cells of Human Adult Bone Marrow., Stem Cell Biology., Cold Spring Harbor Laboratory Press., 349 – 373

Pountos, I., and Giannoudis, P.V. (2005). Biology of Mesenchymal Stem Cells., Injury, International Journal of the Care of the Injured. 36S: S8 – S12

Ramirez-Zacarias, J.L., Castro-Muñozledo, F., and Kuri-Harcuch, W. (1992). Quantification of Adipose Conversion and Triglycerides by Staining Intracytoplasmic Lipids with Oil Red O., Histochemistry. 97: 493 – 497

Rappold, P.M., Cui, M., Grima, J.C., Fan, R.Z., de Mesy-Bentley, K.L., Chen, L., Zhuang, X., Bowers, W.J., and Tieu, K. (2014). Drp1 Inhibition Attenuates Neurotoxicity and Dopamine Release Deficits in vivo., Nature Communications. 5:52 44. 1 – 13

Rastogi, R.P., Singh, S.P., Häder, D-P., and Sinha, R.P. (2010). Detection of Reactive Oxygen Species (ROS) by the Oxidant-Sensing Probe 2',7'-Dichlorodihydrofluorescein Diacetate in the Cyanobacterium Anabaena variabilis PCC 7937., Biochemical and Biophysical Research Communications. 397: 603 – 607

Regazzetti, C., Peraldi, P., Grémeaux, T., Najem-Lendom, R., Ben-Sahra, I., Cormont, M., Bost, F., Le Marchand-Brustel, Y., Tanti, J-F., and Giorgetti-Peraldi, S. (2009).

Hypoxia Decreases Insulin Signaling Pathways in Adipocytes., Diabetes. 58: 95 – 103

Ren, H., Cao, Y., Zhao, Q., Li, J., Zhou, C., Liao, L., Jia, M., Zhao, Q., Cai, H., Han, Z.C., Yang, R., Chen, G., and Zhao, R.C. (2006). Proliferation and Differentiation of Bone Marrow Stromal Cells under Hypoxic Conditions., Biochemical and Biophysical Research Communications. 347: 12 – 21

Reva, T., Morrison, S.J., Clarke, M.F., and Weissman, I.L. (2001) Stem Cells, Cancer, and Cancer Stem Cells., Nature. 414: 105 – 111

Rosdah, A.A., Holien, J.K., Delbridge, L.M.D., Dusting, G.J., and Lim, S.Y. (2016). Mitochondrial Fission – a Drug Target for Cytoprotection or Cytodestruction?, Pharmacology Research & Perspectives. 4(3): e00235: 1 – 19

Saely, C.H., Geiger, K., and Drexel, H. (2012). Brown versus White Adipose Tissue: A Mini Review., Gerontology. 58: 15 – 23

Salvioli, S., Ardizzani, A., Franceschi, C., and Cossarizza, A. (1997). JC-1, but not $DiOC_6(3)$ or Rhodamine 123, is a Reliable Fluorescent Probe to Assess $\Delta\Psi$ Changes in Intact Cells: Implications for Studies on Mitochondrial Functionality during Apoptosis., FEBS Letters. 411: 77 – 82

Schust, J., Sperl, B., Hollis, A., Mayer, T.U., and Berg, T. (2006). Stattic: A Small Molecule Inhibitor of STAT3 Activation and Dimerization., Chemistry & Biology. 13: 1235 – 1242

Siddiquee, K., Zhang, S., Guida, W.C., Blaskovich, M.A., Greedy, B., Lawrence, H.R., Yip, M.L.R., Jove, R., McLaughlin, M.M., Lawrence, N.J., Sebti, S.M., and Turkson, J. (2007). Selective Chemical Probe Inhibitor of Stat3, Identified through Structure-Based Virtual Screening, Induces Antitumor Activity., PNAS. 104: 7391 – 7396

Smirnova, E., Griparic, L., Shurland, D., and van der Bliek, A.M. (2001). Dynamin-related

Protein Drp1 Is Required for Mitochondrial Division in Mammalian Cells., Molecular Biology of the Cell., 12: 2245 – 2256

Sottile, F., Aulicino, F., Theka, I., and Cosma, M.P. (2016). Mesenchymal Stem Cells Generate Distinct Functional Hybrids in vitro via Cell Fusion or Entosis., Scientific Reports. 6:36863: 1 – 11

Spees, J.L., Olson, S.D., Ylostalo, J., Lynch, P.J., Smith, J., Perry, A., Peister, A., Wang, M.Y., and Prockop, D.J. (2003). Differentiation, Cell Fusion, and Nuclear Fusion During ex vivo Repair of Epithelium by Human Adult Stem Cells from Bone Marrow Stroma., PNAS. 100(5): 2397 – 2402

Stolzing, A., Jones, E., McGonagle, D., and Scutt, A. (2008). Age-related Changes in Human Bone Marrow-Derived Mesenchymal Stem Cells: Consequences for Cell Therapies., Mechanisms of Ageing and Development. 129: 163 – 173

Terskikh, V.V., Vasiliev, A.V., and Vorotelyak, E.A. (2007). Stem Cell Niches., Biology Bulletin. 34: 211 – 220

Tormos, K.V., Anso, E., Hamanaka, R.B., Eisenbart, J., Joseph, J., Kalyanaraman, B., and Chandel, N.S. (2011). Mitochondrial Complex III ROS Regulate Adipocyte Differentiation., Cell Metabolism. 14: 537 – 544

Trayhurn, P. (2013). Hypoxia and Adipose Tissue Function and Dysfunction in Obesity., Physiol Rev. 93:1 – 21

Trayhurn, P. (2014). Hypoxia and Adipocyte Physiology: Implications for Adipose Tissue Dysfunction in Obesity., Annual Review of Nutrition. 34: 207 – 236

Twig, G., Elorza, A., Molina, A.J.A., Mohamed, H., Wikstrom, J.D., Walzer, G., Stiles, L., Haigh, S.E., Katz, S., Las, G., Alroy, J., Wu, M., Py, B.F., Yuan, J., Deeney, J.T., Corkey, B.E., and Shirihai, O.S. (2008). Fission and Selective Fusion Govern

Mitochondrial Segregation and Elimination by Autophagy., The EMBO Journal. 27: 433 – 446

Vaux, D.L., (2012). Know when your numbers are significant., Nature. 492: 180 – 181

van der Bliek, A.M., Shen, Q., and Kawajiri, S. (2013). Mechanisms of Mitochondrial Fission and Fusion., Cold Spring Harbor Perspectives in Biology. 5:a011072: 1 – 16

Wagegg, M., Gaber, T., Lohanatha, F.L., Hahne, M., Strehl, C., Fangradt, M., Tran, C.L., Schönbeck, K., Hoff, P., Ode, A., Perka, C., Duda, G.N., and Buttgereit, F. (2012). Hypoxia Promoters Osteogenesis but Suppresses Adipogenesis of Human Mesenchymal Stromal Cells in a Hypoxia-Inducible Factor-1 Dependent Manner., PLoS ONE. 9: 1 – 11

Wang, H., and Joseph, J.A. (1999). Quantifying Cellular Oxidative Stress by Dichlorofluorescein Assay Using Microplate Reader., Free Radical Biology & Medicine. 27(5/6): 612 – 616

Wang, D., Zhou, Y., Lei, W., Zhang, K., Shi, J., Hu, Y., Shu, G., and Song, J. (2010). Signal Transducer and Activator of Transcription 3 (STAT3) Regulates Adipocyte Differentiation Via Peroxisome-Proliferator-Activated Receptor γ (PPARγ)., Biology of the Cell. 102: 1 – 12

Wang, W., Zhang, Y., Lu, Q., and Liu, K. (2015). Mitochondrial Reactive Oxygen Species Regulate Adipocyte Differentiation of Mesenchymal Stem Cells in Hematopoietic Stress Induced by Arabinosylcytosine., PLoS ONE. 10(3): e0120629

Watt, F.M., and Hogan, B.L. (2000). Out of Eden: Stem Cells and their Niches., Science. 287: 1427 – 1430

Westermann, B. (2012). Bioenergetic role of mitochondrial fusion and fission., Biochimica et Biophysica Acta. 1817: 1833 – 1838

Wilson, A., and Trumpp, A. (2006). Bone-Marrow Haematopoetic-Stem-Cell Niches., Nature Reviews Immunology. 6: 93 – 106

Wilson-Fritch, L., Burkart, A., Bell, G., Mendelson, K., Leszyk, J., Nicoloro, S., Czech, M., and Corvera, S. (2003). Mitochondrial Biogenesis and Remodeling During Adipogenesis and in Response to the Insulin Sensitizer Rosiglitazone., Molecular and Cellular Biology. 23: 1085 – 1094

Xie, H.R., Hu, L.S., and Li, G.Y. (2010). SH-SY5Y Human Neuroblastoma Cell Line: in vitro Model of Dopaminergic Neurons in Parkinson's Disease., Chinese Medical Journal. 123(8): 1086 – 1092

Ye, J. (2009). Emerging Role of Adipose Tissue Hypoxia in Obesity and Insulin Resistance., International Journal of Obesity. 33: 54 – 66

Yeon, J-Y., Min, S-H., Park, H-J., Kim, J-W., Lee, Y-H., Park, S-Y., Jeong, P-S., Park, H., Lee, D-S., Kim, S-U., Chang, K-T., and Koo, D-B. (2015). Mdivi-1, Mitochondrial Fission Inhibitor, Impairs Development Competence and Mitochondrial Function of Embryos and Cells in Pigs., Journal of Reproduction and Development. 61(2): 81 – 89

Yin, T., and Li, L. (2006). The Stem Cell Niches in Bone., The Journal of Clinical Investigation. 116(5): 1195 – 1201

Youle, R.J., and van der Bliek, A.M. (2012). Mitochondrial Fission, Fusion, and Stress., Science. 337(6098): 1062 – 1065

Zhang, Y., Marsboom, G., Toth, P.T., and Rehman, J. (2013). Mitochondrial Respiration Regulates Adipogenic Differentiation of Human Mesenchymal Stem Cells., PLOS ONE. 8(10): 1 – 12

Zorov, D.B., Juhaszova, M., and Sollot, S.J. (2014). Mitochondrial Reactive Oxygen Species (ROS) and ROS-Induced ROS Release., Physiological Reviews. 94(3): 909 – 950

# Appendix

## A-1. Mycoplasma Staining

The Mycoplasma Staining was conducted as previously described; ideally, uncontaminated samples would provide no indication of the smaller blue specks visible beside the nuclei. Contaminated samples typically present with multiple small blue specks within the field of view.

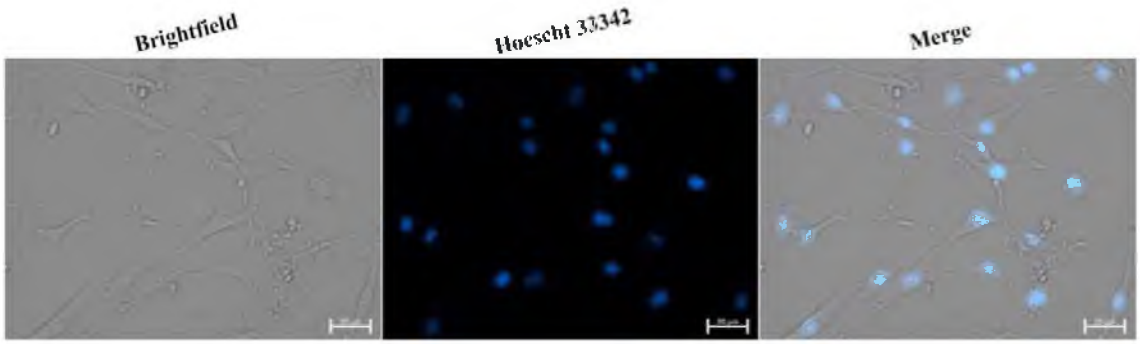


**Figure I. Confirmation of absence of Mycoplasma within human adipose-derived mesenchymal stromal cells.** The human adipose derived mesenchymal stromal cells (hMSCad) were seeded as previously described and permitted to grow within normal culture conditions. Mycoplasma staining, using Hoechst 33342, was performed in order to confirm the lack of contamination within the cells. Images were captured using the Zeiss AxioVert.A1 FLLED fluorescence microscope at 200x magnification. Scale bar = 20 μm. (n = 3).

## A-2. Data Obtained for SH-SY5Y Cell Lines

As previously described throughout this study, complications did arise when attempting to capture data for the SH-SY5Y cell line and its differentiated progeny. While a significant amount of data was inconclusive due to the difficulty with cell death, detachment, and senescence, there remained some data as represented below.

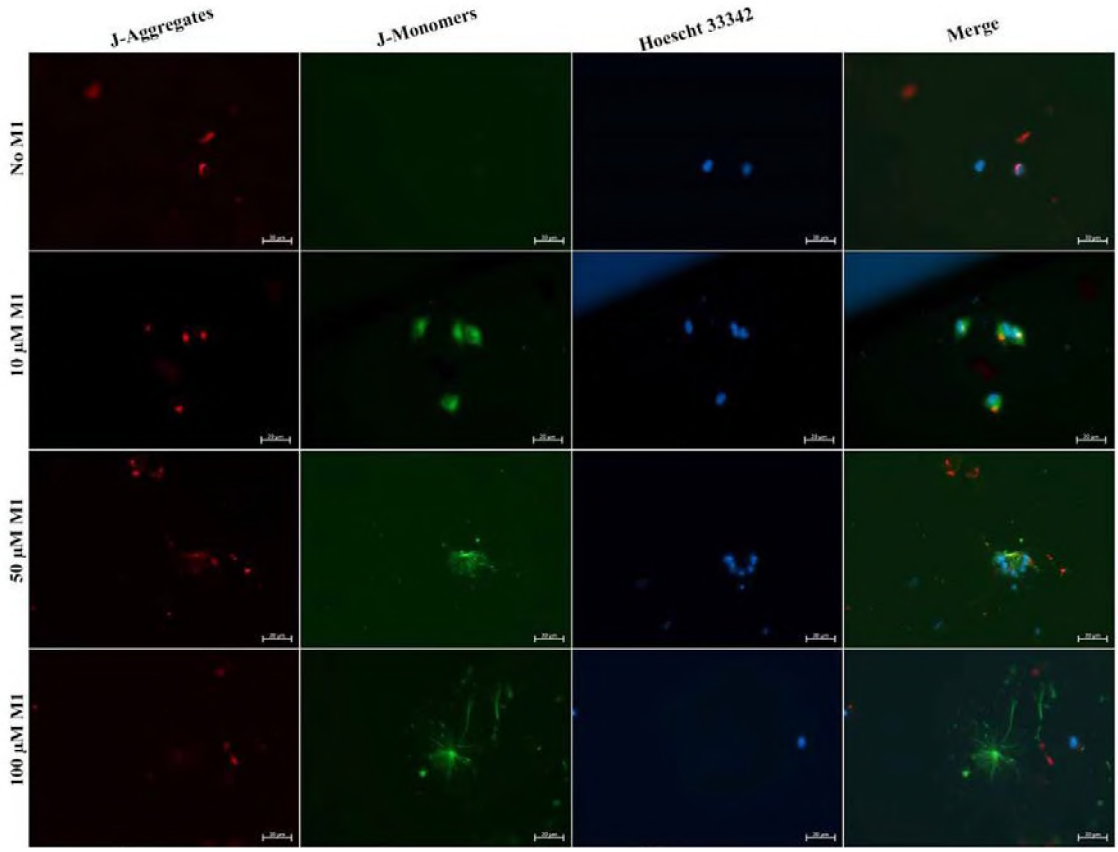


**Figure II. Mitochondrial membrane potentials of undifferentiated SH-SY5Y cells after treatment with mitochondrial fusion promoter, M1.** The cells were cultured as previously described within chapter 2; after 48 hours of treatment with M1, images were captured using Zeiss AxioVert.A1 FL-LED fluorescence microscope at 200x magnification. Scale bar = 20 µm. (N = 2).

## A-3. Evidence of Contamination of SH-SY5Y Cells

As previously discussed, contamination was just one of the many factors that hindered the use of SH-SY5Y cells as an additional cell line model for this study. Multiple experiments were conducted in order to try and source this ongoing issue; as shown below, Figure III, agar plates were prepared on which spread plating, using the culture medium obtained from the culture vessel, was performed.

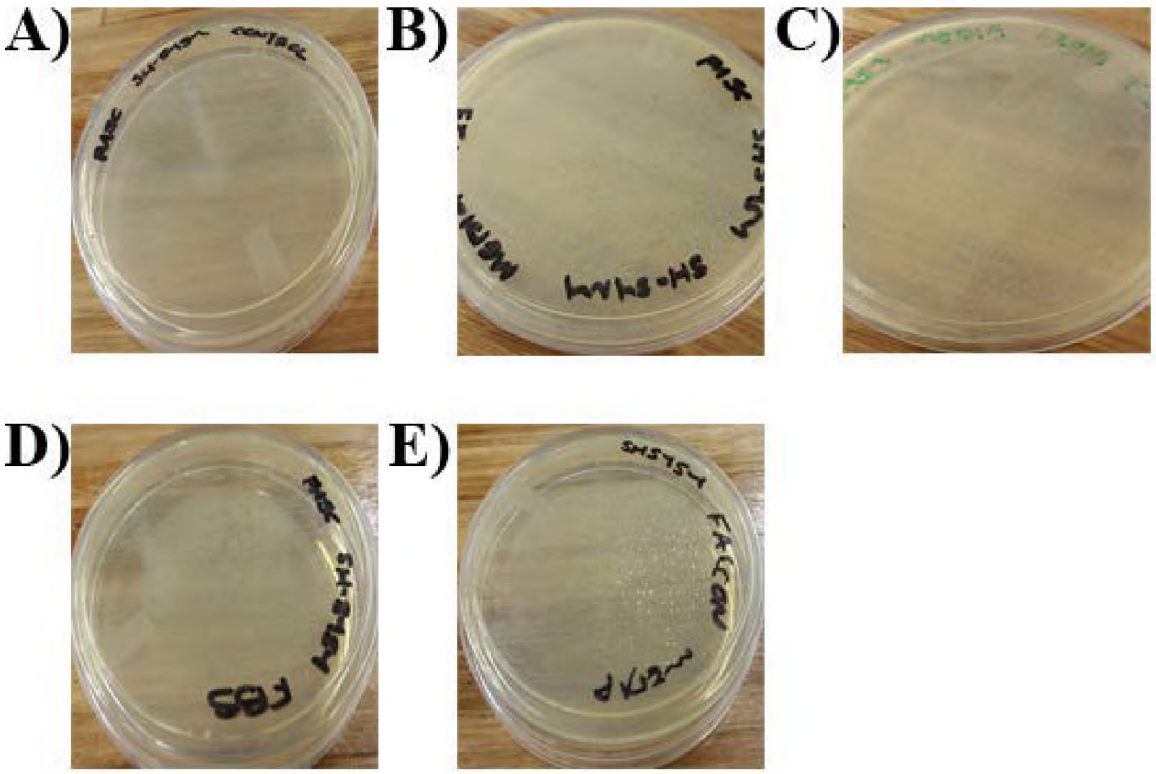


**Figure III: Contamination of SH-SY5Y cells occurred only in the culture vessels that the cells were physically growing in.** Agar plates were prepared in order to provide some explanation into the source of contamination of SH-SY5Y cells. A) A control was established, whereby it was exposed to the same environments as the other plates; the control did not undergo any spread-plating. B and C) A small amount of SH-SY5Y medium was aliquoted from the culture vessel(s) wherein the live cells were present. D) FBS used to make up the medium. E) DMEM F-12 medium used previously to replenish the SH-SY5Y cells. (N = 2).

As seen in Figure III, contamination was confined to the culture vessels and the growing cells. The FBS added into the DMEM F-12 medium, and the DMEM F-12 medium used, provided a result negative for contamination, which provided the conclusion that either the cell lines were contaminated before they were received, or they were contaminated upon arrival and passaging for long term storage.

## A-3. Flow Cytometry Data

Due to time constraints with regard to the utilization of the Guava easyCyte Flow Cytometer (Merk Millipore), limited experiments could be performed, resulting in the acquisition of data pertaining to ROS detection, using DCF-DA, for hMSC-ad cells treated with varying concentrations of S3I-201 (6.25 µM; 12.5 µM; 25 µM; 50 µM; 100 µM).

| ROS low :: Freq. of Parent | ROS intermediate :: Freq. of Paren | ROS high :: Freq. of Parent | Count |
|---|---|---|---|
| 83.8 | 6.28 | 9.60 | 5000 |
| 84.6 | 5.62 | 9.70 | 5000 |
| 84.1 | 6.06 | 9.50 | 5000 |
| 81.1 | 7.86 | 10.4 | 5000 |
| 78.7 | 8.84 | 11.6 | 5000 |
| 80.1 | 6.64 | 13.1 | 5000 |
| 98.7 | 1.18 | 0.040 | 5000 |

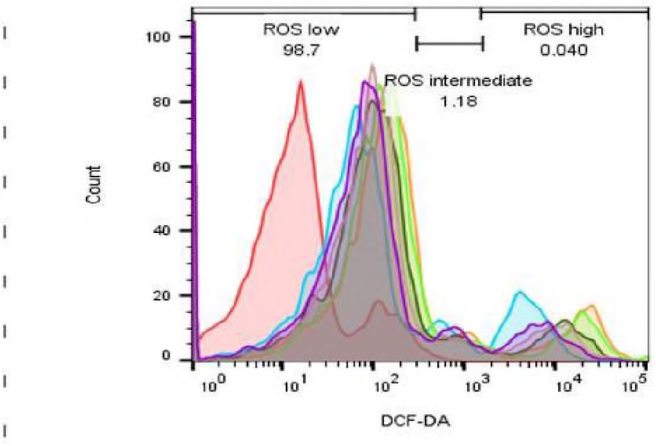


**Figure IV. Flow Cytometric histogram depicting the resulting ROS formation present within S3I-201 treated non-differentiating hMSC-ad cells**. The control was indicated as the red line, representative of a low ROS accumulation; the cells present here remained untreated for S3I-201. The orange and green represents S3I-201 concentrations of 100 µM and 50 µM, respectively, while the brown, purple, and blue are indicative of 25 µM, 12.5 µM, and 6.25 µM S3I-201, respectively.

## A-4. Immunofluorescence Microscopy

Immunofluorescence was attempted for multiple antibodies; however, a clear enough stain, for analytical purposes, was not provided. The following images demonstrate examples of the resulting immunofluorescence for untreated hMSC-ad cells.

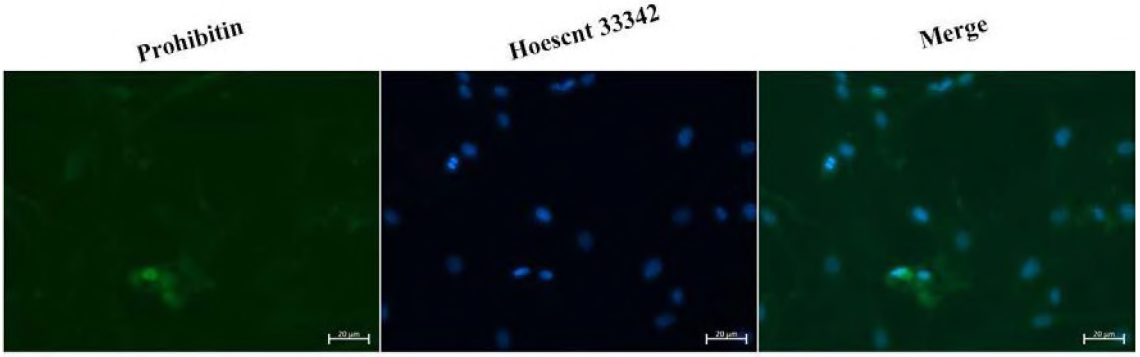


**Figure V: Human adipose derived mesenchymal stromal cells with antibody binding Prohibitin marked fluorescence.** The cells underwent normal culture conditions after which the previously described techniques for immunofluorescence microscopy were performed. The resulting images were captured using the Zeiss AxioVert.A1 FL-LED fluorescence microscope at 200x magnification. Scale bar = 20 µm. (n = 2).

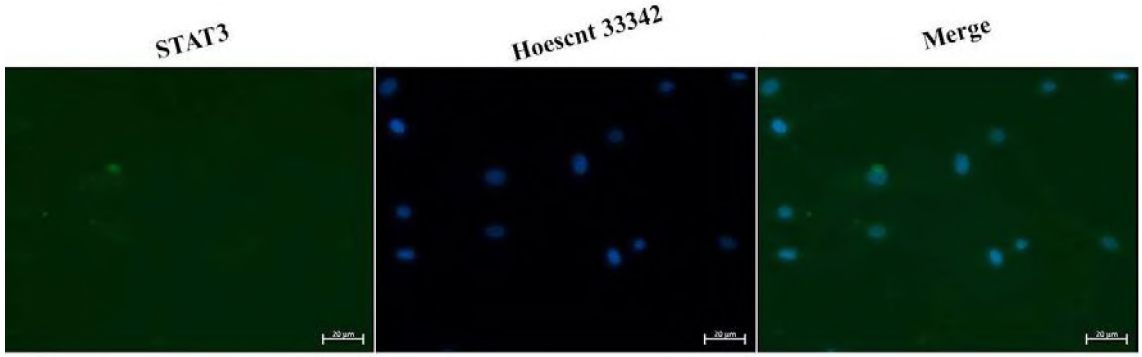


**Figure VI. Human adipose derived mesenchymal stromal cells with antibody STAT3 marked fluorescence.** The cells underwent normal culture conditions after which the previously described techniques for immunofluorescence microscopy were performed. The resulting images were captured using the Zeiss AxioVert.A1 FL-LED fluorescence microscope at 200x magnification. Scale bar = 20 µm. (n = 2).

## A-5. Confocal Images

In an attempt to gain insight into the three dimensional mitochondrial networks present within hMSC-ad cells and adipocytes, the Zeiss LSM780 Confocal microscope was utilized whereby a z-stack was generated in order to obtain multiple layers. An example of the resulting images acquired may be observed within Figure VI.

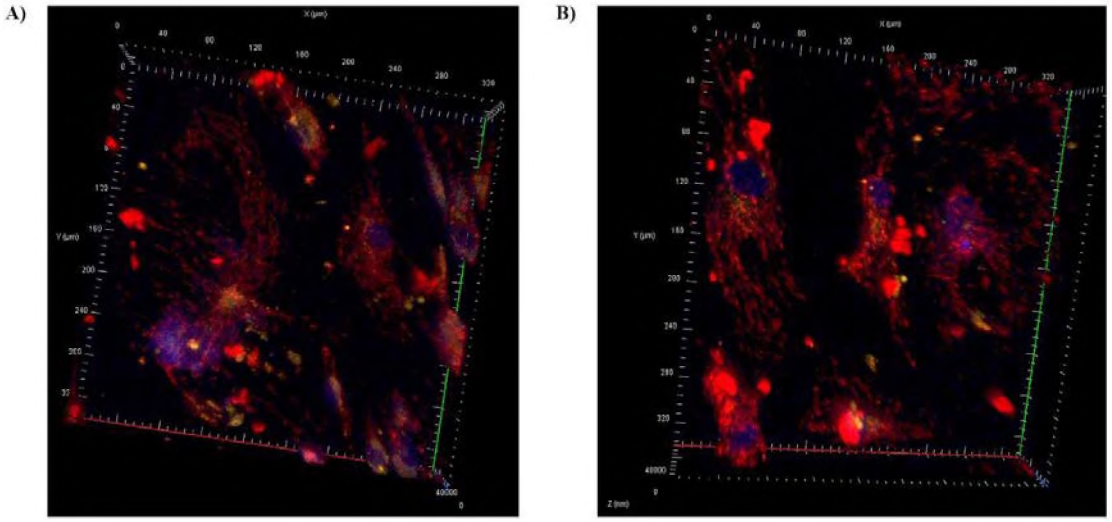


**Figure VII. The resulting z-stack images acquired for adipocytes treated with S3I-201.** The hMSC-ad cells underwent induction for adipogenesis whereby they were permitted 12 days of differentiation. A JC-1 and Hoechst 33342 stain were performed. The cells were captured using Zeiss LSM780 Confocal microscope at 250X magnification. (A) demonstrates adipogenic differentiating hMSC-ad cells that were left untreated for S3I-201; whereas (B) demonstrates adipogenic differentiating hMSC-ad cells that were treated with 100 µM S3I-201.

# Outputs

JAK-STAT

ISSN: (Print) 2162-3996 (Online) Journal homepage: http://www.tandfonline.com/loi/kjks20

# Mitochondrial STAT3 and reactive oxygen species: A fulcrum of adipogenesis?

Adam H Kramer, Rose Kadye, Pascalene S Houseman & Earl Prinsloo

**To cite this article:** Adam H Kramer, Rose Kadye, Pascalene S Houseman & Earl Prinsloo (2015)
Mitochondrial STAT3 and reactive oxygen species: A fulcrum of adipogenesis?, JAK-STAT, 4:2, 1-10, DOI: 10.1080/21623996.2015.1084084

**To link to this article:**
http://dx.doi.org/10.1080/21623996.2015.1084084

JAK-STAT, 4:1–10, 2015

ISSN: 2162-3996 online
DOI: 10.1080/21623996.2015.1084084

REVIEW

# Mitochondrial STAT3 and reactive oxygen species: A fulcrum of adipogenesis?

Adam H Kramer,[#] Rose Kadye, Pascalene S Houseman, and Earl Prinsloo*

Biotechnology Innovation Center; Rhodes University; Grahamstown, South Africa

The balance between cellular lineages can be controlled by reactive oxygen species (ROS). Cellular differentiation into adipocytes is highly dependent on the production of ROS to initiate the process through activation of multiple interlinked factors that stimulate mitotic clonal expansion and cellular maturation. The signal transducer and activator of transcription family of signaling proteins have accepted roles in adipogenesis and associated lipogenesis. Non-canonical mitochondrial localization of STAT3 and other members of the STAT family however opens up new avenues for investigation of its role in the aforementioned processes. Following recent observations of differences in mitochondrially localized serine 727 phosphorylated STAT3 (mtSTAT3-pS727) in preadipocytes and adipocytes, here, we hypothesize and speculate further on the role of mitochondrial STAT3 in adipogenesis.

KEYWORDS. adipogenesis, mitochondria, signal transducer and activator of transcription 3, reactive oxygen species, STAT3

## INTRODUCTION

Adipose tissue (majorly but not solely composed of adipocytes and endothelial cells) as an endocrine organ is vitally important to homeostasis through the release of hormone cytokines like leptin, adiponectin and resistin as well as its involvement in steroid metabolism.[1,2] Imbalances in adipose tissue are largely detrimental to human health e.g. obesity.[3-5] Understanding the developmental and maintenance factors in adipocyte biology are essential.

Reactive oxygen species (ROS), often maligned as in oxidative stress, are generally accepted as required for normal cellular homeostasis through redox signaling.[6-10] The unidirectional process of adipogenesis relies heavily on ROS production to enable a complex cascade mediated by the redox conformation sensitive C/EBPb to upregulate genes associated with the process.[11,12] Mitochondria, the cellular powerhouses, regulate the fine balance of cellular ROS levels through the electron transport chain (ETC) and disproportionation (dismutation).

The Signal Transducers and Activators of Transcription (STAT) family of proteins have well described roles in adipogenesis and the associated process of lipogenesis through canonical activation through phosphorylation, nuclear translocation and gene activation.[13-16] Non-canonical mitochondrial localization, in particular serine 727 phosphorylated STAT3 (hereafter referred to as, mtSTAT3-pS727) have been reported in normal and disease phenotypes to influence cellular respiration through the ETC and associated oxidative phosphorylation through apparent direct interaction with the protein complexes that comprise the ETC.[17,18] Further to this mtSTAT3pS727 has been reported to interact directly with the mitochondrial genome.[19] Recent evidence provided a causal link between mitochondrial STAT3 levels, total cellular ROS and adipogenesis in the gold standard mammalian adipogenesis model 3T3-L1.[20] Here we discuss the potential links and speculate further on the possible mechanisms that mitochondrial STAT3 plays in adipogenesis. in relation to the larger network of the STAT family.[21]

*Correspondence to: Earl Prinsloo; Email: e.prinsloo@ru.ac.za
Received June 9, 2015; Revised August 7, 2015; Accepted August 11, 2015.
[#] Present affiliation: Albert Einstein College of Medicine; Jack and Pearl Resnick Campus; New York, NY USA



## Adipogenesis – a sequential process

Adipogenesis is a process of differentiation and maturation of progenitor stem cells (e.g., mesenchymal stromal stem cells) and preadipocytes (e.g., isolated fibroblast 3T3-L1) to mature lipid accumulating adipocytes. The seemingly stepwise process is regulated by well-coordinated directional signaling through the CCAAT/enhancer binding proteins (C/EBPs), and in turn peroxisome proliferator activated receptors (PPARs) for induction of differentiation programming; C/EBPa, C/EBPb, and C/EBPd exhibit sequential and spatial expression during adipocyte differentiation with C/ EBPb in particular being important by initiating differentiation and required for transcriptional activation of C/EBPa and PPARg.[22-24] The process is highly conserved in mouse and human models allowing for a standard in vitro differentiation cocktail for the differentiation to white adipose tissue (WAT).[25] The differentiation cocktail composed of insulin, dexamethasone and 3-isobutyl-1-methylxanthine (IBMX) promotes differentiation through insulin-like growth factor receptor (IGF-1) stimulation with

concomitant cyclic adenosine monophosphate (cAMP) accumulation, the effects are further enhanced through the glucocorticoid receptor agonist, dexamethasone.[26-28] The cAMP phosphodiesterase inhibitor, 3-isobutyl-1-methylxanthine (IBMX) further increases levels of cAMP resulting in downregulation of Specificity protein 1 (Sp1), a C/EBPa promoter repressor which delays the DNA binding activity of C/EBPb and C/EBPd.[23] The insulin sensitizer and PPARg agonist rosiglitazone is often included to increase differentiation efficiency in the first 3 days of differentiation programming.[29]

## Mitochondria, reactive oxygen species and adipogenesis

### The electron transport chain and ROS

As the double membraned energy powerhouse of the mammalian cell, the mitochondria maintain energy balance through aerobic respiration and adenosine triphosphate (ATP) synthesis through oxidative phosphorylation coupled to the inner membrane located ETC complexes I-IV. Electrons from nicotinamide adenine dinucleotide hydride (NADH) from the citric acid (TCA) cycle in the mitochondrial matrix are oxidized by the ETC complexes (I: NADH:Ubiquinone oxidoreductase, II: Succinate:Ubiquinone oxidoreductase, III: Ubiquinol:Ferricytochrome c oxidoreductase, and IV: Ferrocytochrome c oxygen oxidoreductase) in the mitochondrial cristae to the final acceptor, molecular oxygen at complex IV (to generate water), and concomitantly a proton gradient (through $H^c$ transfer) is established across the inner membrane; the gradient is used to drive the rotary molecular motor component $F_0$ of complex V (ATP Synthase) thereby effecting phosphorylation of adenosine diphosphate (ADP) to ATP through the $F_1$ component. The ETC complexes I and III leak electrons to oxygen and reduces it to a radical ROS superoxide ($O_2^{\cdot}$)[10,30](see Fig. 1). Although radical ROS levels are maintained through spontaneous or enzymatic dismutation [though superoxide dismutase] to the non-radical ROS hydrogen peroxide [$H_2O_2$], this balance can be disturbed leading to cellular senescence or cell death through oxidative stress.[6,9,31] As low molecular weight, easily membrane diffusable reactive species ROS have been described to mediate signal transduction pathways and cell-to-cell communications.[8,32]

### ROS and initiation of adipogenesis

Reactive oxygen species seemingly act as a linchpin of adipogenesis through the redox sensitive CCAAT/enhancer binding protein b (C/ EBPb) which appears to develop a DNA binding conformation in the presence of increased levels of ROS in the gold standard adipogenesis model 3T3-L1 (mouse).[11,12] This results in the transcriptional activation of peroxisome proliferator-activated receptor g (PPARg) which is required for mitotic clonal expansion and terminal adipocyte differentiation.[33] It should be noted that mitotic clonal expansion is not required for adipogenesis in mesenchymal stromal stem cells. High levels of ROS during onset of adipogenesis in mouse and humans have been reported, naturally this should be regulated as fat accumulation is correlated with oxidative stress in both mice and humans.[34] Tormos and co-workers[35] has found that complex III produced ROS regulates adipogenesis in human mesenchymal stem cells through targeted antioxidant inhibition of adipocyte differentiation; the differentiation phenotype was rescued by exogenous hydrogen peroxide. Furthermore knockdown analysis of complex III components confirmed the inhibitory studies. This requirement for ROS in adipogenesis was echoed by Kanda et al. in rat bone marrow derived mesenchymal stromal stem cells.[36] Taken together these studies indicate a strong role for in the activation of C/ EBPb DNA

binding and the induction of adipogenic events through the mediation of PPARg expression; PPARg regulates glucose and fatty acid metabolism.[33]

## STAT3 and adipogenesis

(STAT3-pY705) in proliferating 3T3-L1 preadipocytes with significantly lower levels observed in growth arrested preadipocytes and adipocytes.[14] Interestingly, the group reported a delayed increase in STAT3-pY705 during mitotic clonal expansion following stimulation

FIGURE 1. The mitochondrial electron transport chain, oxidative phosphorylation and sites of superoxide ($O_2^{\cdot}$) ROS production.[19,22] Legend: e , electron; H , proton; Q, co-enzyme Q10; c, cytochrome c. See text for details.

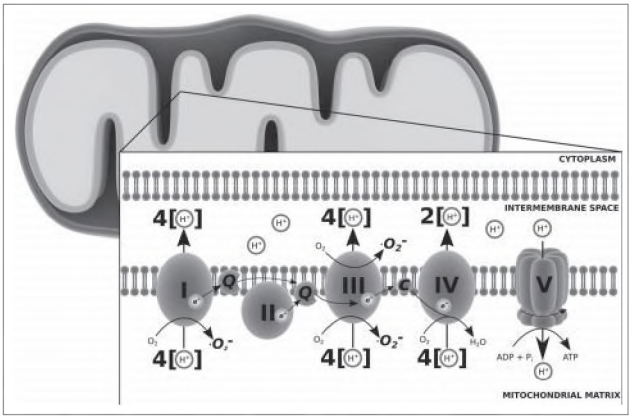


An interplay of STAT1, 3, 5A and 5B and 6 have been described to be functionally expressed in both preadipocytes and adipocytes and seemingly function to enhance or inhibit adipogenesis through up-, downregulation or constitutive expression.[13,21,37] This is discussed in detail elsewhere[21,37] and because of the growing body of knowledge on mitochondrial STAT3,[38] discussed here later, we would like to briefly highlight STAT3 activity in adipogenesis through its canonical localization and activity. However, of particular interest in Stephens et al. are the 2 bands (92 and 84 kDa) observed for STAT3 during differentiation.(in the presence and absence of adipogenesis inhibitor tumor necrosis factor a)[13] which is described as the result of cross reaction with STAT1. The major isoforms STAT3 a and b have molecular weights of 93kDa and 84kDa, respectively, and exhibit highly specific functions with STAT3b exhibiting longer nuclear retention times[39,40]; the effect of the individual isoforms on adipogenesis is still forthcoming. Deng et al. described high levels of tyrosine 705 phosphorylated STAT3 with the differentiation cocktail 3-isobutyl-1-methylxanthine, dexamethasone and insulin; taken together the data pointed to STAT3-pY705 being important in proliferative preadipocytes but not in differentiation. Interestingly, the protein inhibitor of activated STAT3 (PIAS3) was later shown to inhibit adipogenic gene expression and it was shown later that STAT3-pY705 regulated the expression of PPARg through selective inhibition with the JAK2/STAT3 inhibitor AG490.[16,41] This is most likely through STAT3 binding to and activating transcription of CEBP/b through direct interaction with the distal region of the CEBP/b promoter.[15] The importance of phosphorylation of STAT3 at serine 727 (STAT3pS727) in adipogenesis is for the most part undescribed; interestingly serine and tyrosine phosphorylation have been reported to negatively regulate each other and it is known that insulin reduces tyrosine phosphorylation and increases serine phosphorylation of STAT3 thereby reducing nuclear targeting of STAT3 in 3T3-.[42,43]

## The mitochondrial STAT family – non-canonical localization/function

The seven genes that encode the STAT family (STAT1, STAT2, STAT3 STAT4, STAT5a, STAT5b and STAT6) mediate cellular differentiation, proliferation, survival and metabolism through well described specific receptor stimulation i.e. Janus Kinase mediated phosphorylation followed by nuclear targeting in canonical JAK-STAT signaling. Mitochondrial localization of STAT2, STAT3, STAT5 and STAT6 have been described in literature; with STAT1 seemingly following suit.[38] Mitochondrial STAT proteins are still hotly debated with respect to whether it is an actual phenomenon with respect to translocation, DNA binding, and effect on the ETC. While Wegzryn et al.,[17] described a wide tissue distribution in mice for mitochondrial STAT3, Chueh and coworkers' description of STAT5 translocation (through sub-cellular fractionation and fluorescence microscopy) to the mitochondria in cytokine stimulated mammalian cells showed no presence of STAT1 or STAT3.[44] Khan et al. used quantitative confocal laser scanning microscopy to identify STAT6 mitochondrial localization (co-localized with Cytochome Oxidase IV, COXIV) but not STAT3 in Hep3B hepatocytes.[45] Work by our group provided evidence of STAT3-pS727 in mouse 3T3-L1 mitochondria by quantitative confocal laser scanning microscopy and subcellular fractionation which indicated no cytoplasmic or endosomal contamination.[20] Mitochondrial STAT3 remains the best described with respect to mitochondrial localization and associated function in regulation of mitochondrial activity specifically in cellular respiration and associated production of ROS.

## Mitochondrial STAT3 – a modulatory cog in the wheel

Beyond the canonical nuclear targeting of activated STAT3, the reports of endosomal targeting[46] as well as the reported nuclear activity of unphosphorylated and therefore traditionally unactivated STAT3,[47] have further highlighted the complexity of this protein beyond being a simple transcriptional activator. Wegrzyn et al. were the first to describe the strong role in mitochondrial metabolism through the maintenance of the electron transport chain basal activity by maintenance of mitochondrial membrane potential[17] through modulation of complex I and II activity; this was subsequently confirmed in multiple cellular phenotypes and appears that up or down modulation of activity is related to stoichiometric ratios of mitochondrial STAT3 to ETC proteins.[38] It should be noted that STAT3 does not have a clear mitochondrial targeting sequence/signal. Furthermore it has been suggested that it may be a negative regulator of the Mitochondrial Permeability Transition Pore (MPTP).[48] STAT3 activity in the mitochondria appears to be mediated by the complex I subunit GRIM-19 (Genes associated with Retinoid-IFN-induced Mortality-19).[49] GRIM-19 has previously been reported to interact with and act as a negative regulator of STAT3[50,51] and appears to act as a chaperone to recruit STAT3 into mitochondria and enhance STAT3 association with complex I[39]. Mitochondrial STAT3 has also been shown to play an important role in ischemic pre- and post-conditioning in myocardial cells. Boengler et al. showed the presence of STAT3 in cardiomyocyte mitochondria found a positive correlation with reduced cell death after ischemia through the regulation of MPTP.[48] As mentioned, it is still unknown how STAT3 is targeted to the mitochondria but Boengler and co-workers have suggested following co-immunoprecipiation that STAT3 may be imported into the mitochondria via the mitochondrial presequence receptor Tom20.[48] Gough et al., have described that serine 727 phosphorylation of STAT3 was required for mitochondrial localization this was evident in the promotion of cellular transformation by the H-Ras oncogene by mitochondrial STAT3 by sustaining altered glycolysis and oxidative phosphorylation (through increased complex V

activity), further strengthening the fact that STAT3 regulates mitochondrial metabolism.[18] The importance of the phosphorylation at serine 727 was reiterated by Zhang et al. through site directed mutagenesis [SDM] and consequently the group showed the effects of mtSTAT3-pS727 on promoting breast cancer tumor growth, the increased activity of complex I and the accumulation of ROS in the cell.[52] In addition to this, site directed mutagenesis experiments conducted by Tammineni et al. showed that a S727A mutation reduced the import and assembly into complex I of STAT3 by GRIM-19.[49] Combined these data further highlight the role of mtSTAT3-pS727 in ETC activity and consequently ROS production.

Recently, work by our group showed the defined changes in levels of mtSTAT3-pS727 in relation to total cellular STAT3[20] and STAT3-pY705 (Unpublished data AH Kramer). The effect on ETC activity by mtSTAT3-pS727 in adipogenesis is however unknown and currently under investigation. The changes in mtSTAT3-pS727 levels observed between preadipocyte and adipocyte mitochondria may contribute to potential modulation of ETC activity and hence the presence of relatively low ROS levels in preadipocytes as opposed to the differentiated progeny. Large stoichiometric shifts may be important when considering that 3T3-L1 derived adipocytes appear to generate a large amount of lactate through aerobic glycolysis (with the concomitant although not shown generation of ATP).[53,54] Although argued by the authors to be a non-Warburg effect and a potential mechanism of the cells to dispose of excess glucose, this may be a method of the adipocyte to ensure production of sufficient ATP considering the potential that low mtSTAT3-pS727 may result in decreased ATP production.[18,53] Unpublished data by our group further shows that total cellular levels of STAT3-pY705 decrease during differentiation after mitotic clonal expansion, but expression levels remain relatively high in preadipocytes this concurs with previous findings indicating the importance of STAT3pY705 in proliferating 3T3-L1 cells.[13,14] Overall stoichiometric ratios of mtSTAT3-pS727 to cytoplasmic pools of STAT3/STAT3-pY705/ STAT3-pS727 in preadipocytes/stem cells and adipocytes need quantitative evaluation to further mechanistic understanding of the contribution of STAT3 to adipogenesis. As mentioned, Andersson et al. described that insulin decreases the total cellular levels of STAT3pY705 but this results in an increase in STAT3-pS727 levels.[42] This results in reduced nuclear targeting and an increased cytoplasmic pool of STAT3-pS727, this was confirmed by our findings.[20] Relative to this the levels of serine phosphorylated STAT3 decreased during the progress of differentiation. It may be speculated that insulin plays a key role in signaling the "release" of mtSTAT3-pS727 into the cytoplasm, this however requires quantitative confirmation. As mentioned earlier the importance of complex III ROS in mesenchymal stromal stem cell adipogenesis; as the ETC is sequential it may be possible that mitochondrial STAT3 may play an important role in controlling the overall flux of electrons in the chain through its interaction with complex I, i.e., one effective bottleneck of the ETC.[35,36]

## Mitochondria, the Warburg effect and a potential interplay between STAT3-pY705 and mtSTAT3-pS727 in vivo?

STAT3 has been implicated in activating and maintaining the Warburg effect in cancer through down regulation of mitochondrial activity.[55] The Warburg effect, also known as aerobic glycolysis, is when mitochondrial activity is seemingly decreased and glycolytic activity is increased to ensure sufficient ATP production. This has been shown to be essential for survival of cancer cells as well as for stem cells.[56-58] In vivo stem cell niches exhibit a propensity for hypoxia resulting in decreased mitochondrial activity, decreased ROS and increased selfrenewal (therefore decreased differentiation). The in vivo niche of adipose derived mesenchymal stem cells remains largely unknown but hypoxia culture adipose derived mesenchymal stromal stem cells do exhibit normal phenotypes, undergo self-renewal and the ability to differentiate into adipose tissues indicating the potential activation of the Warburg effect.[59,60] This is pure speculation but both canonically active STAT3pY705, through downregulation of mitochondrial protein expression, and non-canonically active mtSTAT3-pS727, through stabilization of the mitochondrial membrane potential and hence stability as well as decreased ROS production, may play a strong role in the regulation of a Warburg effect in vivo and therefore aid in maintaining a non-differentiated phenotype (Fig. 2).

## CONCLUSION

The contribution of STAT3 to mitochondrial metabolism either as directly localized mtSTAT3-S727, nuclear targeted STAT3pY705 as well as individual isoforms in cellular differentiation requires further investigation and clarification. Furthermore, studies need to be expanded beyond 3T3-L1, where adipogenic variability is well characterized, to other cell and in vivo models before any definitive conclusions may be drawn. However, in light of Phillips and coworkers findings on the stoichiometric ratios of mitochondrial STAT3 to other mitochondrial proteins, and considering the substantial fraction of mtSTAT3-pS727 observed relative to loading controls in mitochondrial isolates from 3T3-L1 cells it be that the preadipocyte phenotype may provide an ideal model to quantitatively investigate mitochondrial STAT3 in vitro. The hormone and cytokine signals that control the molecular switches that regulate the balance between cytoplasmic, nuclear and mitochondrial pools of STAT3 however require

FIGURE 2. The interplay between canonical and non-canonical pools of STAT3 in maintenance of an undifferentiated (preadipocyte) phenotype. This graphical representation assumes that total STAT3 expression levels remain constant, irrespective of STAT3a or b. We speculate on the potential of the nuclear targeted STAT3-pY705 and mtSTAT3-pS727 maintaining a Warburg like effect with respect to downregulation of mitochondrial biogenesis and activity through STAT3-pY705 activity and stabilization of mitochondrial membrane potential and decreased ROS production through mtSTAT3-pS727. See text for further details.

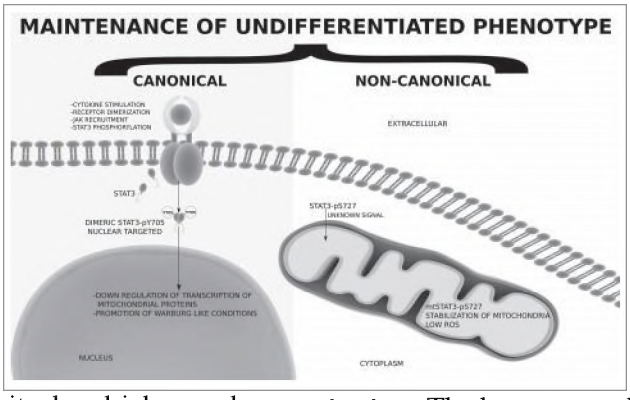

elucidation. Further to this the presence and role of mitochondrial STAT1, STAT5a and b and STAT6 in adipogenesis needs to be investigated. Many questions remain regarding the overall role of these proteins in the mitochondria first and foremost being, what the trigger mechanism is that targets the proteins to the organelle? Is there a specific trigger at all? With respect to STAT3 and its role in mitochondrial activity, it should be evident that there must be a signaling event that regulates the levels in the mitochondria. Furthermore, how do these proteins enter the mitochondria? The potential role of molecular chaperones, as discussed by Meier and Larner should be clear in the mediation of import into the mitochondria.[38] Beyond the interaction with the ETC, is the question of to what extent the STATs interact with the mitochondrial genome and regulate transcription.[19] The exact mechanism, function and activity of the STAT family and notably STAT3 remains to be described in the mitochondria and for example in the case of unphosphorylated nuclear STAT3 in the nucleus as well. The global network of this family however needs description as it is clear that no single event linked to localization (and activity) controls the process of adipogenesis.

## DISCLOSURE OF POTENTIAL CONFLICTS OF INTEREST

No potential conflicts of interest were disclosed

## ACKNOWLEDGMENTS

The authors would like to thank www.somersault1824.com for their Library of Science Illustrations

## FUNDING

The authors would like to acknowledge Rhodes University and the National Research Foundation of South Africa for funding support.

## REFERENCES

1. Li J, Papadopoulos V, Vihma V. Steroid biosynthesisin adipose tissue. Steroids 2015; http://dx.doi.org/10.1016/j.steroids.2015.03.016
2. Kershaw EE, Flier JS. Adipose tissue as an endocrineorgan. J Clin Endocrinol Metab 2004; 89:2548-56; PMID:15181022; http://dx.doi.org/10.1210/jc.20040395
3. Weisberg SP, McCann D, Desai M, Rosenbaum M,Leibel RL, Ferrante AW Jr. Obesity is associated with macrophage accumulation in adipose tissue. J Clin Invest 2003; 112:1796-808; PMID:14679176; http://dx.doi.org/10.1172/JCI200319246
4. Hotamisligil GS, Arner P, Caro JF, Atkinson RL,Spiegelman BM. Increased adipose tissue expression of tumor necrosis factor-alpha in human obesity and insulin resistance. J Clin Invest 1995; 95:2409-15; PMID:7738205; http://dx.doi.org/10.1172/JCI117936
5. Nishimura S, Manabe I, Nagai R. Adipose tissueinflammation in obesity and metabolic syndrome. Discov Med 2009; 8:55-60; PMID:19788868
6. Ray PD, Huang B-W, Tsuji Y. Reactive oxygen species (ROS) homeostasis and redox regulation in cellular signaling. Cell Signal 2012; 24:981-90; PMID:22286106; http://dx.doi.org/10.1016/j.cellsig.2012.01.008
7. D'Autreaux B, Toledano MB. ROS as signalling molecules: mechanisms that generate specificity in ROS homeostasis. Nat Rev Mol Cell Biol 2007; 8:813-24; PMID:17848967; http://dx.doi.org/10.1038/nrm2256
8. Finkel T. Signal transduction by reactive oxygen species. J Cell Biol 2011; 194:7-15; PMID:21746850; http://dx.doi.org/10.1083/jcb.201102095
9. Schieber M, Chandel NS. ROS function in redox signaling and oxidative stress. Curr Biol 2014; 24:R45362; PMID:24845678; http://dx.doi.org/10.1016/j.cub.2014.03.034
10. Murphy MP. How mitochondria produce reactiveoxygen species. Biochem J 2009; 417:1-13; PMID:19061483; http://dx.doi.org/10.1042/BJ20081386
11. Su W-C, Chou HY, Chang CJ, Lee YM, Chen WH,Huang KH, Lee MY, Lee SC. Differential activation of a C/EBP beta isoform by a novel redox switch may confer the lipopolysaccharide-inducible

expression of interleukin-6 gene. J Biol Chem 2003; 278:51150-8; PMID:14530280; http://dx.doi.org/10.1074/jbc.M305501200

12. Lee H, Lee YJ, Choi H, Ko EH, Kim J-W. Reactiveoxygen species facilitate adipocyte differentiation by accelerating mitotic clonal expansion. J Biol Chem 2009; 284:10601-9; PMID:19237544; http://dx.doi.org/10.1074/jbc.M808742200
13. Stephens JM, Morrison RF, Pilch PF. The expressionand regulation of STATs during 3T3-L1 adipocyte differentiation. J Biol Chem 1996; 271:10441104449; PMID:8631837; http://dx.doi.org/10.1074/jbc.271.18.10441
14. Deng J, Hua K, Lesser SS, Harp JB. Activation ofsignal transducer and activator of transcription-3 during proliferative phases of 3T3-L1 adipogenesis. Endocrinology 2000; 141:2370-6;PMID:10875236
15. Zhang K, Guo W, Yang Y, Wu J. JAK2/STAT3 pathway is involved in the early stage of adipogenesis through regulating C/EBPb transcription. J Cell Biochem 2011; 112:488-97; PMID:21268070; http://dx. doi.org/10.1002/jcb.22936
16. Wang D, Zhou Y, Lei W, Zhang K, Shi J, Hu Y, ShuG, Song J. Signal transducer and activator of transcription 3 (STAT3) regulates adipocyte differentiation via peroxisome-proliferator-activated receptor gamma (PPARgamma). Biol Cell 2010; 102:1-12; http://dx.doi.org/10.1042/BC20090070
17. Wegrzyn J, Potla R, Chwae YJ, Sepuri NB, Zhang Q,Koeck T, Derecka M, Szczepanek K, Szelag M, GornickaA,et al.FunctionofmitochondrialStat3incellular respiration. Science 2009; 323:793-7; PMID:19131594; http://dx.doi.org/10.1126/science.1164551
18. Gough DJ, Corlett A, Schlessinger K, Wegrzyn J,Larner AC, Levy DE. Mitochondrial STAT3 supports Ras-dependent oncogenic transformation. Science 2009; 324:1713-6; PMID:19556508; http://dx.doi. org/10.1126/science.1171721
19. Macias E, Rao D, Carbajal S, Kiguchi K, DiGiovanniJ. Stat3 binds to mtDNA and regulates mitochondrial gene expression in keratinocytes. J Invest Dermatol 2014; 134:1971-80; PMID:24496235; http://dx.doi.org/10.1038/jid.2014.68
20. Kramer AH, Edkins AL, Hoppe HC, Prinsloo E.Dynamic Mitochondrial Localisation of STAT3 in the Cellular Adipogenesis Model 3T3-L1. J Cell Biochem 2015; 116:1232-40; PMID:25565605; http:// dx.doi.org/10.1002/jcb.25076
21. Zhao P, Stephens JM. Identification of STAT targetgenes in adipocytes. JAKSTAT 2013; 1-7; PMID:24058802
22 Gregoire FM, Smas CM, Sul HS. Understanding adipocyte differentiation. Physiol Rev 1998; 78:783-809; PMID:9674695
23. Otto TC, Lane MD. Adipose development: from stemcell to adipocyte. Crit Rev Biochem Mol Biol 2005; 40:229-242; PMID:16126487; http://dx.doi.org/ 10.1080/10409230591008189
24. Tang Q-Q, Otto TC, Lane MD. Mitotic clonal expansion: a synchronous process required for adipogenesis. Proc Natl Acad Sci 2003; 100:44-49; PMID:12502791; http://dx.doi.org/10.1073/pnas. 0137044100
25 Janderova L, McNeil M, Murrell AN, Mynatt RL, Smith SR. Human mesenchymal stem cells as an in vitro model for human adipogenesis. Obes Res 2003; 11:65-74; PMID:12529487; http://dx.doi.org/10.1038/oby.2003.11
26. Green H, Kehinde O. An established preadipose cellline and its differentiation in culture.II. Factors affecting the adipose conversion. Cell 1975; 5:19-27; PMID:165899; http://dx.doi.org/10.1016/0092-8674(75)90087-2
27. Rubin CS, Hirsch A, Fung C, Rosen OM. Development of hormone receptors and hormonal responsiveness in vitro. Insulin receptors and insulin sensitivity in the preadipocyte and adipocyte forms of 3T3-L1 cells. J Biol Chem 1978; 253:7570-7578; PMID:81205
28. Russell TR, Ho RJ. Conversion of 3T3 fibroblastsinto adipose cells: triggering of differentiation by prostaglandin F2alpha and 1-methyl-3-isobutyl xanthine. Proc Natl Acad Sci 1976; 73:4516-4520; PMID:188043; http://dx.doi.org/10.1073/pnas.73.12.4516
29. Zebisch K, Voigt V, Wabitsch M, Brandsch M. Protocol for effective differentiation of 3T3-L1 cells to adipocytes. Anal Biochem 2012; 425:88-90; PMID:22425542; http://dx.doi.org/10.1016/j.ab.2012.03.005
30. Brand MD. The sites and topology of mitochondrialsuperoxide production. Exp Gerontol 2010; 45, 46672; PMID:20064600; http://dx.doi.org/10.1016/j. exger.2010.01.003
31. Kobayashi CI, Suda T. Regulation of reactive oxygenspecies in stem cells and cancer stem cells. J Cell Physiol 2012; 227:421-30; PMID:21448925; http:// dx.doi.org/10.1002/jcp.22764
32. Finkel T. Signal transduction by mitochondrial oxidants. J Biol Chem 2012; 287:4434-40; PMID:21832045; http://dx.doi.org/10.1074/jbc. R111.271999

33. Lefterova MI, Haakonsson AK, Lazar MA, MandrupS. PPARg and the global map of adipogenesis and beyond. Trends Endocrinol Metab 2014; 25:293-302; PMID:24793638; http://dx.doi.org/10.1016/j.tem. 2014.04.001
34. Furukawa S, Fujita T, Shimabukuro M, Iwaki M,Yamada Y, Nakajima Y, Nakayama O, Makishima M, Matsuda M, Shimomura I. Increased oxidative stress in obesity and its impact on metabolic syndrome. J Clin Invest 2004; 114:1752-61; PMID:15599400; http://dx.doi.org/10.1172/JCI21625
35. Tormos KV, Anso E, Hamanaka RB, Eisenbart J,Joseph J, Kalyanaraman B, Chandel NS. Mitochondrial complex III ROS regulate adipocyte differentiation. Cell Metab 2011; 14:537-44; PMID:21982713; http://dx.doi.org/10.1016/j.cmet.2011.08.007
36. Kanda Y, Hinata T, Kang SW, Watanabe Y. Reactiveoxygen species mediate adipocyte differentiation in mesenchymal stem cells. Life Sci 2011; 89:250-8; PMID:21722651; http://dx.doi.org/10.1016/j.lfs. 2011.06.007
37. Xu D, Yin C, Wang S, Xiao Y. JAK-STAT in lipidmetabolism of adipocytes. Jak-Stat 2013; 2:e27203; PMID:24498541; http://dx.doi.org/10.4161/jkst. 27203
38. Meier JA, Larner AC. Toward a new STATe: Therole of STATs in mitochondrial function. Semin Immunol 2014; 26:20-28; PMID:24434063; http://dx.doi.org/10.1016/j.smim.2013.12.005
39. Huang Y, Qiu J, Dong S, Redell MS, Poli V, ManciniMA, Tweardy D. J Stat3 isoforms, alpha and beta, demonstrate distinct intracellular dynamics with prolonged nuclear retention of Stat3beta mapping to its unique C-terminal end. J Biol Chem 2007; 282:34958-34967; PMID:17855361; http://dx.doi.org/10.1074/jbc.M704548200
40. Ng IHW, Ng DCH, Jans DA, Bogoyevitch MA. Selective STAT3-a or –b expression reveals spliceform-specific phosphorylation kinetics, nuclear retention and distinct gene expression outcomes. Biochem J 2012; 447:125-36; PMID:22799634; http://dx.doi.org/10.1042/BJ20120941
41. Deng J, Hua K, Caveney EJ, Takahashi N, Harp JB.Protein inhibitor of activated STAT3 inhibits adipogenic gene expression. Biochem Biophys Res Commun 2006; 339:923-31; PMID:16329991; http://dx. doi.org/10.1016/j.bbrc.2005.10.217
42. Andersson CX, Sopasakis VR, Wallerstedt E, SmithU. Insulin antagonizes interleukin-6 signaling and is anti-inflammatory in 3T3-L1 adipocytes. J Biol Chem 2007; 282:9430-5; PMID:17267401; http://dx.doi.org/10.1074/jbc.M609980200
43. Chung J, Uchida E, Grammer TC, Blenis J. STAT3 serine phosphorylation by ERK-dependent and -independent pathways negatively modulates its tyrosine phosphorylation. Mol Cell Biol 1997; 17:6508-16; PMID:9343414
44. Chueh FY, Leong KF, Yu, CL. Mitochondrial translocation of signal transducer and activator of transcription 5 (STAT5) in leukemic T cells and cytokine-stimulated cells. Biochem Biophys Res Commun 2010; 402:778-783; PMID:21036145; http://dx.doi.org/10.1016/j.bbrc.2010.10.112
45. Khan R, Lee JE, Yang Y-M, Liang F-X, Sehgal PB.Live-cell imaging of the association of STAT6-GFP with mitochondria. PLoS One 2013; 8:e55426; PMID:23383189; http://dx.doi.org/10.1371/journal.pone.0055426
46. Xu F, Mukhopadhyay S, Sehgal PB. Live cell imaging of interleukin-6-induced targeting of 'transcription factor' STAT3 to sequestering endosomes in the cytoplasm. Am J Physiol Cell Physiol 2007; 293:C1374-82; PMID:17670892; http://dx.doi.org/10.1152/ajpcell.00220.2007
47. Timofeeva OA, Chasovskikh S, Lonskaya I, Tarasova NI, Khavrutskii L, Tarasov SG, Zhang X, Korostyshevskiy VR, Cheema A, Zhang L, et al. Mechanisms of unphosphorylated STAT3 transcription factor binding to DNA. J Biol Chem 2012; 287:14192-200; PMID:22378781; http://dx.doi.org/10.1074/jbc.M111.323899
48. Boengler K, Hilfiker-Kleiner D, Heusch G, Schulz R.Inhibition of permeability transition pore opening by mitochondrial STAT3 and its role in myocardial ischemia/reperfusion. Basic Res Cardiol 2010; 105:771-85; PMID:20960209; http://dx.doi.org/10.1007/s00395-010-0124-1
49. Tammineni P, Anugula C, Mohammed F, AnjaneyuluM, Larner AC, Sepuri NB. The import of the transcription factor STAT3 into mitochondria depends on GRIM-19, a component of the electron transport chain. J Biol Chem 2013; 288:4723-32; PMID:23271731; http://dx.doi.org/10.1074/jbc. M112.378984
50. Lufei C, Ma J, Huang G, Zhang T, Novotny-DiermayrV, Ong CT, Cao X. GRIM-19, a death-regulatory gene product, suppresses Stat3 activity via functional interaction. EMBO J 2003; 22:1325-35; PMID:12628925; http://dx.doi.org/10.1093/emboj/cdg135

51. Zhang J, Yang J, Roy SK, Tininini S, Hu J, BrombergJF, Poli V, Stark GR, Kalvakolanu DV. The cell death regulator GRIM-19 is an inhibitor of signal transducer and activator of transcription 3. Proc Natl Acad Sci U S A 2003; 100:9342-7; PMID:12867595; http://dx.doi.org/10.1073/pnas.1633516100
52. Zhang Q, Raje V, Yakovlev VA, Yacoub A, Szczepanek K, Meier J, Derecka M, Chen Q, Hu Y, Sisler J, et al. Mitochondrial localized Stat3 promotes breast cancer growth via phosphorylation of serine 727. J Biol Chem 2013; 288:31280-8; PMID:24019511; http://dx.doi.org/10.1074/jbc.M113.505057
53. Phillips D, Reilley MJ, Aponte AM, Wang G, Boja E,Gucek M, Balaban RS. Stoichiometry of STAT3 and mitochondrial proteins: Implications for the regulation of oxidative phosphorylation by protein-protein interactions. J Biol Chem 2010; 285:23532-6; PMID:20558729; http://dx.doi.org/10.1074/jbc.C110.152652
54. Sabater D, Arriaran S, Romero Mdel M, Agnelli S, Remesar X, Fernandez-Lopez JA, Alemany M. Cultured 3T3L1 adipocytes dispose of excess medium glucose as lactate under abundant oxygen availability. Sci Rep 2014; 4:3663; PMID:24413028; http://dx.doi.org/10.1038/srep03663
55. Demaria M, Giorgi C, Lebiedzinska M, Esposito G,D'Angeli L, Bartoli A, Gough DJ, Turkson J,Levy DE, Watson CJ, et al. A STAT3-mediated metabolic switch is involved in tumour transformation and STAT3 addiction. Aging (Albany. NY) 2010; 2:82342; PMID:21084727
56. Lopez-Lazaro M. The warburg effect: why and how do cancer cells activate glycolysis in the presence of oxygen? Anticancer Agents Med Chem 2008; 8:30512; PMID:18393789; http://dx.doi.org/10.2174/187152008783961932
57. Ruckenstuhl C, B€uttner S, Carmona-Gutierrez D, Eisenberg T, Kroemer G, Sigrist SJ, Fr€ohlich KU, Madeo F. The Warburg effect suppresses oxidative stress induced apoptosis in a yeast model for cancer. PLoS One 2009; 4:e4592; PMID:19240798; http://dx.doi.org/10.1371/journal.pone.0004592
58. Ito K, Suda T. Metabolic requirements for the maintenance of self-renewing stem cells. Nat Rev Mol Cell Biol 2014; 15:243-56; PMID:24651542; http://dx.doi.org/10.1038/nrm3772
59. Baer PC, Geiger H. Adipose-derived mesenchymalstromal/stem cells: tissue localization, characterization, and heterogeneity. Stem Cells Int 2012; 2012:812693; PMID:22577397; http://dx.doi.org/ 10.1155/2012/812693
60. Feng Y, Dangelmajer S, Lee YM, Wijesekera O,Castellanos CX, Denduluri A, Chaichana KL, Li Q, Zhang H, Levchenko A, et al. Hypoxia-cultured human adipose-derived mesenchymal stem cells are non-oncogenic and have enhanced viability, motility, and tropism to brain cancer. Cell Death Dis 2014; 5: e1567; PMID:25501828; http://dx.doi.org/10.1038/cddis.2014.521